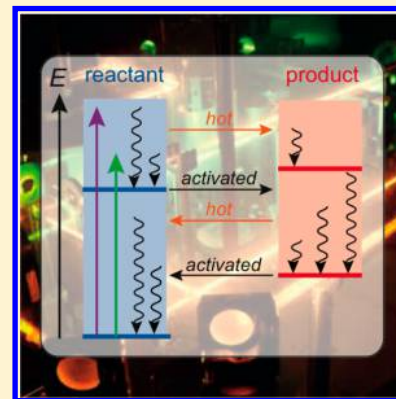


## Ultrafast Elementary Photochemical Processes of Organic Molecules in Liquid Solution

Tatu Kumpulainen, Bernhard Lang, Arnulf Rosspeintner, and Eric Vauthey\*

Department of Physical Chemistry, Sciences II, University of Geneva, 30 Quai Ernest Ansermet, CH-1211 Geneva 4, Switzerland

**ABSTRACT:** Ultrafast photochemical reactions in liquids occur on similar or shorter time scales compared to the equilibration of the optically populated excited state. This equilibration involves the relaxation of intramolecular and/or solvent modes. As a consequence, the reaction dynamics are no longer exponential, cannot be quantified by rate constants, and may depend on the excitation wavelength contrary to slower photochemical processes occurring from equilibrated excited states. Such ultrafast photoinduced reactions do no longer obey the Kasha–Vavilov rule. Nonequilibrium effects are also observed in diffusion-controlled intermolecular processes directly after photoexcitation, and their proper description gives access to the intrinsic reaction dynamics that are normally hidden by diffusion. Here we discuss these topics in relation to ultrafast organic photochemical reactions in homogeneous liquids. Discussed reactions include intra- and intermolecular electron- and proton-transfer processes, as well as photochromic reactions occurring with and without bond breaking or bond formation, namely ring-opening reactions and cis–trans isomerizations, respectively.



### CONTENTS

1. Introduction	10827	2.3.5. Charge Recombination	10867
1.1. Preliminary Remarks and Scope	10827	3. Proton-Transfer Reactions	10869
1.2. Solvent Relaxation	10828	3.1. Introduction	10869
1.3. Vibrational Relaxation	10829	3.2. Intramolecular Proton Transfer	10871
2. Electron-Transfer Reactions	10829	3.2.1. Methyl Salicylate and Related Compounds	10871
2.1. Theory	10829	3.2.2. Hydroxyflavones	10872
2.1.1. Classical Marcus Theory	10829	3.2.3. Benzoazoles	10875
2.1.2. Quantum and Semiclassical Electron-Transfer Theories	10830	3.2.4. Concluding Remarks	10877
2.1.3. Zusman Theory and Solvent-Controlled Electron Transfer	10831	3.3. Intermolecular Proton Transfer	10878
2.1.4. Two-Dimensional Models and Non-Equilibrium Electron Transfer	10832	3.3.1. Naphthols	10879
2.2. Intramolecular Electron Transfer	10833	3.3.2. Hydroxypyrenes	10882
2.2.1. Introduction	10833	3.3.3. Hydroxyquinolines	10886
2.2.2. Direct Optical Charge Transfer in Strongly Coupled Systems	10834	3.3.4. Cyanine Photoacids	10890
2.2.3. Strongly Coupled Systems: Direct Optical CT or CT from a Locally Excited State?	10837	3.3.5. Concluding Remarks	10893
2.2.4. Strongly Coupled Systems with a LE → CT Transition	10839	4. Photochromic Reactions	10893
2.2.5. Charge Separation in Moderately to Weakly Coupled Systems	10846	4.1. Photoisomerization	10893
2.3. Intermolecular Electron Transfer	10852	4.1.1. Stilbene	10893
2.3.1. Diffusional Effects	10852	4.1.2. Azobenzene	10896
2.3.2. Charge-Transfer Dynamics of Excited Donor–Acceptor Complexes	10853	4.1.3. Cyanine Dyes	10898
2.3.3. Bimolecular Charge Separation in Pure Donating Solvents	10858	4.1.4. Concluding Remarks	10901
2.3.4. Diffusion-Assisted Charge Separation	10863	4.2. Conical Intersections	10901
		4.3. Nonreactive Processes	10902
		4.4. Photochromic Systems Undergoing Bond-Rupture	10904
		4.4.1. Diarylethenes	10904
		4.4.2. Fulgides/Fulgimides	10909
		4.4.3. Spiro-Compounds and Chromenes	10911

**Special Issue:** Ultrafast Processes in Chemistry

**Received:** July 27, 2016

**Published:** December 13, 2016

4.4.4. Concluding Remarks	10913
5. Final Remarks	10913
Author Information	10914
Corresponding Author	10914
ORCID	10914
Notes	10914
Biographies	10914
Acknowledgments	10914
Abbreviations and acronyms	10914
References	10914

## 1. INTRODUCTION

### 1.1. Preliminary Remarks and Scope

Direct real-time visualization of the progress of a chemical reaction has been one of the holy grails in chemistry.<sup>1</sup> To reach this goal, two major issues had to be solved: (i) how to initiate the chemical reaction efficiently and quickly enough and (ii) how to identify the various chemical species involved in the process and follow their temporal evolution. These issues were solved, at least partially, more than 60 years ago by pioneers such as Eigen, Norrish, and Porter, who used short pulses of energy (i.e., either a temperature jump or a flash of light) to bring a chemical system out of equilibrium and then applied optical spectroscopy to monitor its relaxation back to equilibrium.<sup>2,3</sup> With the invention of the laser and the development of ever shorter optical pulses, photochemical reactions proved to be ideal for kinetic and mechanistic investigations. Since the seminal work of Norrish and Porter,<sup>3</sup> tremendous progress in the time-resolution and the probing techniques was achieved. Nowadays, laser pulses of a few tens of femtoseconds are routinely available at wavelengths corresponding to the valence electronic transitions. Moreover, the temporal evolution of the photoinduced processes can be monitored in spectral domains ranging from the X-ray to the THz regions. Thanks to these powerful tools, processes that were considered as quasi-instantaneous can now be investigated in detail. Consequently, our understanding of the dynamics of chemical reactions, especially those occurring from an electronic excited state, improved remarkably.

As stated in the title, we will focus on the dynamics of ultrafast photochemical processes of organic molecules in liquids. The definition of an “ultrafast process” evolved in parallel with the availability of ever shorter optical pulses. Here, we will consider a reaction as ultrafast not according to its absolute time scale, but rather according to its relative time scale with respect to those of other processes, such as solvent and vibrational relaxation, or diffusion in the case of intermolecular reactions. According to the Franck–Condon principle, optical excitation of a solute prepares its excited state out of equilibrium. Indeed, in the Franck–Condon excited state, the surrounding solvent molecules are still in the orientation of the ground state. Similarly, the intramolecular nuclear coordinates are also the same as in the ground state. Equilibration of the excited state involves the relaxation of both these solvent and nuclear coordinates and takes place on time scales ranging from a few tens of fs to several tens of ps or longer, as briefly discussed below. We will consider a reaction as ultrafast when it occurs on a shorter or a similar time scale as the time scales of these relaxation phenomena. In this case, the chemical reaction does not take place from an equilibrated excited-state population. Consequently, it no longer follows

simple kinetics, characterized by a rate constant, but rather exhibits nonexponential dynamics with a time-dependent rate coefficient. Moreover, the dynamics depend on the initial location of the population on the excited-state surface. Consequently, it also depends on the excitation wavelength, in contradiction with the Kasha–Vavilov rule. The latter states that both emission and photochemistry take place from the lowest electronic excited states (i.e., the  $S_1$  and the  $T_1$  states for closed-shell molecules) and, consequently, are independent of the excitation wavelength.<sup>4</sup>

We will limit ourselves to organic molecules, which, in most cases, have closed shells. We will thus not address inorganic molecules, particularly transition metal complexes, whose photophysics differ substantially from those of organic molecules, and for which departures from the Kasha–Vavilov rule are not exceptional. We will also only consider processes occurring in homogeneous liquid environments and, therefore, will not discuss photobiological or interfacial processes. Room-temperature ionic liquids (RTILs) represent a new class of liquid solvents that have attracted strong attention over the past decade. These solvents are generally highly viscous and their structure and dynamics are still not fully understood. As the dynamics of photochemical reactions in these RTILs were reviewed recently,<sup>5</sup> ultrafast processes in these liquids will only be marginally mentioned.

In the following, we will discuss some of the most elementary photochemical reactions, where the above-mentioned nonequilibrium effects can be observed. We will start with electron-transfer and continue with proton-transfer reactions. As these two processes involve the transfer of an electric charge, solvent modes may contribute strongly to the reaction coordinate. On the other hand, intramolecular modes, especially those affecting the relative position of the accepting and donating sites can play a crucial role in proton-transfer reactions. Consequently, the dynamics of these chemical reactions can be substantially entangled with the relaxation dynamics of these reactive modes. We will distinguish between intra- and intermolecular electron- and proton-transfer processes. The latter require the diffusion of the reactants to a distance/orientation at which the electron or proton transfer can take place. Therefore, the rate of these processes should not exceed that of diffusion. However, nonequilibrium effects associated with the reactant-pair distribution can be observed in such diffusion-limited processes, especially at a short time after excitation. A proper account of this nonequilibrated stage of the reaction gives access to the intrinsic reaction dynamics that are normally hidden by diffusion. On the other hand, the neglect of these early dynamics, which can extend into the tens of nanoseconds time scale in viscous environments, can lead to erroneous conclusions.

We will then discuss photochromic reactions, distinguishing isomerization processes from those reactions where bonds are broken and/or formed such as ring-opening reactions. In general, these processes involve substantial structural changes, which can, in turn, strongly affect the potential energy landscape of the electronic states and the energy gap between the relevant states. These distortions give access to conical intersections between the potential energy surfaces, which can often be reached without an intervening energy barrier. As a result, these reactions are generally ultrafast and their dynamics often depend on the excitation wavelength.

Before going into the details of these reactions, we briefly discuss the most important aspects of solvent and vibrational relaxation.

## 1.2. Solvent Relaxation

Elementary chemical reactions, like electron and proton transfer, as well as electronic excitation of nonsymmetric molecules, involve substantial charge redistribution and, thus, changes of the local electric field. As a consequence, the orientation of the surrounding solvent molecules, especially the dipolar ones, has to change to minimize the overall free energy of the product. This process is usually called solvation or solvent relaxation. As shown in the next section, its dynamics play a key role in the dynamics of electron and proton transfer reactions. Access to the solvent dynamics was first obtained using dielectric spectroscopy in the microwave region.<sup>6</sup> The measured frequency-dependent complex dielectric constant was analyzed using different line shape functions originating from dielectric continuum theories,<sup>7</sup> the simplest being the Debye equation, which contains a time constant, the so-called Debye relaxation time,  $\tau_D$ , in the denominator. This quantity is related to the longitudinal dielectric relaxation time,  $\tau_1$ :<sup>8</sup>

$$\tau_1 = \frac{\varepsilon(\infty)}{\varepsilon(0)} \tau_D \quad (1)$$

where  $\varepsilon(0)$  and  $\varepsilon(\infty)$  are the static and optical dielectric constants, respectively. Some solvents are characterized by a single Debye relaxation time, like acetonitrile with  $\tau_D = 3.4$  ps, whereas alcohols are described by a sum of several Debye functions and several  $\tau_D$ , for example around 1, 7, and 50 ps for methanol.<sup>6,9</sup>

According to the continuum model, the longitudinal dielectric relaxation time reflects the relaxation of the solvation free energy after a prompt change of the local field and is thus the quantity of interest. Therefore, the solvation time of acetonitrile should be of the order of 200 fs. In general, these measurements were performed at frequencies up to  $\sim 100$  GHz, and therefore relaxation components shorter than  $\sim 1$ – $2$  ps could not be resolved.

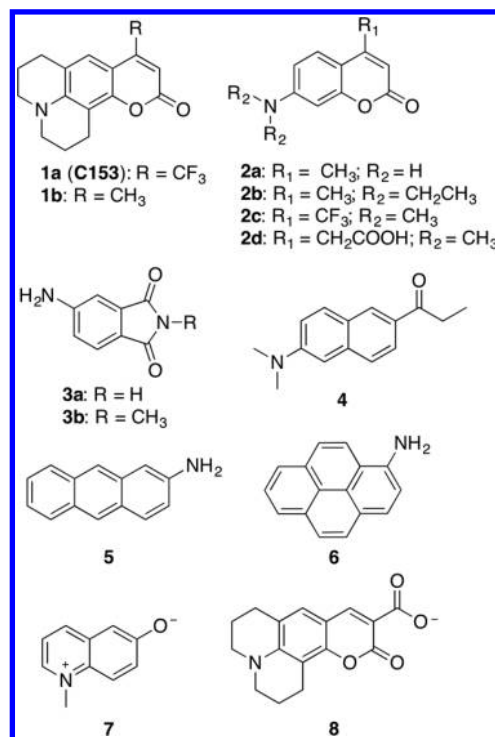
More direct information on the relaxation dynamics of the solvent around a solute was obtained from measurements of the dynamic Stokes shift, i.e., the frequency down shift of the fluorescence spectrum of a probe molecule following optical excitation. This approach, based on pioneering works in the 60s,<sup>10–12</sup> started to be really exploited at the end of the 80s<sup>13–17</sup> and is probably the most used method now. The quantity obtained from this measurements is the spectral response function,  $C(t)$ :

$$C(t) = \frac{\nu(t) - \nu(\infty)}{\nu(0) - \nu(\infty)} \quad (2)$$

where  $\nu(0)$ ,  $\nu(t)$ , and  $\nu(\infty)$  are either the peak or mean (first moment) frequencies of the fluorescence band at time 0, time  $t$  and infinite time, respectively. This function directly reflects the time evolution of the solvation free energy, as long as the measured Stokes shift is only due to solvation and not due to vibrational or structural relaxation following optical excitation. The first studies, with a resolution of a few picoseconds, resulted in solvation times consistent with the  $\tau_1$  values from dielectric spectroscopy.<sup>16,17</sup> However, subsequent investigations with better time resolution revealed that a large fraction of solvent relaxation takes place within 100 fs via inertial motion of the solvent molecules. This contribution, already predicted

by molecular dynamics simulations,<sup>18,19</sup> was first experimentally evidenced in acetonitrile<sup>20</sup> and subsequently in many other solvents.<sup>21–23</sup> Thus, dipolar solvation involves both ultrafast inertial motion and slower diffusive motion with the latter depending on the solvent viscosity. A detailed investigation of the solvation dynamics of coumarin 153 (**1a**, Chart 1) in 24

**Chart 1. Solvation Probes Used in Fluorescence Dynamic Stokes Shift Measurements**



solvents using fluorescence up-conversion with a 100 fs instrument response function (IRF) was reported by Horng and Maroncelli.<sup>22</sup> The solvation times reported there are still used as references.

Apart from dielectric spectroscopy and dynamics Stokes shift, deep insight into solvent dynamics was also obtained using other techniques, such as photon-echo, spectral hole burning, 2D-IR spectroscopy, or the optical Kerr effect.<sup>24–35</sup> The equivalence between all these methods is based on the linear response approximation, which states that solvent relaxation does not depend on how far from equilibrium it starts from, and that it involves the same motion as solvent fluctuations around the equilibrium. There are presently very few reports of a breakdown of this approximation. Most of them concern electron transfer reactions between atoms.<sup>36,37</sup> From transient two-dimensional infrared measurements on a transition metal complex, Hamm and co-workers have shown that solvent fluctuations around equilibrium occur on a different time scale than nonequilibrium solvent relaxation,<sup>30</sup> in contradiction with the linear response approximation.

Another implication of this approximation is that the solvation dynamics should be independent of the probe, unless specific solute–solvent interactions are operative. At the moment, there are only few systematic studies on the probe dependence of dipolar solvation dynamics. Maroncelli and co-workers compared the solvation dynamics of 16 organic fluorescent probes (e.g., 1–6 in Chart 1) in 1-propanol at



253 K, using time-correlated single photon counting (TCSPC) with a 50–60 ps instrument response function (IRF) and did not detect significant probe dependence as long as H-bonding interactions between the solute and the solvent were absent.<sup>38</sup> More recently, Ernstring and co-workers measured the solvation dynamics of four probes in water (among them **2d**, **7** and **8** in Chart 1) and five probes in methanol (among them **1a**, **2a** and **7** in Chart 1) using broadband fluorescence up-conversion spectroscopy with a 85 fs IRF.<sup>39</sup> Whereas no probe dependence of the relaxation dynamics was found in water, the slower part of the dynamic Stokes shift in methanol was found to vary by a factor of  $\sim 2$  depending on the probe. This dependence was ascribed to the effect of solute motion on the solvent relaxation, which strongly varies with the size of the solute. The authors suggested to determine the solvation dynamics of the immobile solute by dividing the experimentally measured solvation correlation function by  $r(t)^\alpha$ , where  $r(t)$  is the anisotropy decay of the solute and  $\alpha$  is a solute-dependent empirical parameter. With an  $\alpha$  value varying between 0.6 and 1.4 according to the solute, the solvation dynamics of the immobile probe was found to be essentially solute independent. More recently, the substantial probe dependence of the dynamics Stokes shift found in RTILs was shown to be still present even after correction for the reorientation of the solute.<sup>40</sup>

This question deserves more systematic investigation. With the advent of broadband fluorescence up-conversion spectroscopy,<sup>41,42</sup> determination of the dynamic Stokes shift has become much faster and more reliable than with the spectral reconstruction method. Therefore, better understanding of the solute dependence of solvation relaxation and of the limit of validity of the linear response approximation can be expected in the near future.

### 1.3. Vibrational Relaxation

In many cases, optical excitation of an organic molecule does not only involve the purely electronic 0–0 transition but is often accompanied by the population of a vibronic excited state. The vibrational energy initially concentrated in Franck–Condon active modes spreads into other intramolecular vibrational modes of the molecule via so-called intramolecular vibrational redistribution (IVR) or dissipates into the environment via vibrational cooling. IVR occurs via anharmonic coupling and results in the establishment of a vibrational temperature of the molecule. Depending on the amount of excess energy accompanying the optical excitation, an electronic excited state can in principle reach relatively high temperatures upon IVR. For example, the vibrational temperature of perylene in the  $S_1$  state after vibronic excitation with an excess energy of  $\sim 0.2$  eV at room temperature and subsequent IVR can be estimated to be of the order of 370 K.<sup>43,44</sup>

The dynamics of a photochemical reaction occurring before the IVR takes place can be expected to depend substantially on the amount of vibrational energy, especially if the Franck–Condon active modes populated upon photoexcitation are also coupled to the reaction.

On the other hand, if the photochemical reaction is slower than the IVR, but faster than the vibrational cooling, excess vibrational energy should have a similar effect to a temperature rise. If the reaction is thermally activated, such a vibrational excitation should lead to a strong acceleration of its dynamics.

The dynamics of IVR were mostly investigated in the gas phase.<sup>45</sup> It was found to occur sequentially: the vibrational energy flowing first into relatively high frequency doorway

modes, from which it is further redistributed into lower frequency modes. As a consequence, the efficiency of this process depends dramatically on the size of the molecule. For small molecules in the electronic ground state, IVR takes place on a 10 to 100 ps time scale.<sup>45,46</sup> It was found to be faster in the solution phase due to the so-called solvent-assisted IVR.<sup>47,48</sup> For example, the slower part of the IVR dynamics of benzene upon excitation of an overtone of the CH stretch mode was found to change from 50 to 4 ps upon going from gas phase to  $\text{CF}_2\text{ClCCl}_2\text{F}$  solution.<sup>47</sup> However, for many small molecules in solution, vibrational cooling takes place before IVR is complete.<sup>49</sup> In the case of larger molecules, IVR and vibrational cooling have often been considered to take place on relatively separate time scales and consequently to occur sequentially. Indeed, IVR time constants ranging from 10 fs to several hundreds of fs were reported for molecules in an electronic excited state,<sup>50–54</sup> whereas vibrational cooling times between  $\sim 1$  ps to several tens of ps were published.<sup>52,54–62</sup>

Such a clear separation between IVR and vibrational cooling is not fully consistent with the typical width of vibrational absorption bands of similar molecules in the electronic excited state, which is of the order of  $10\text{--}20\text{ cm}^{-1}$ ,<sup>63</sup> suggesting 0.5 to 1 ps dephasing times, thus somewhat slower IVR. Moreover, time-resolved studies of perylene and substituted perylenes in a wide variety of solvents pointed to a sub-picosecond cooling component and yielded evidence that IVR and vibrational cooling share common time scales.<sup>44,60</sup>

Whereas it is well established that the thermal equilibration of an excited molecule upon vibration relaxation can take several tens of ps, there is still no general understanding of the solvent dependence of this process, despite several studies. A correlation between the cooling rate constant and the thermal diffusivity of the solvent was reported by several groups.<sup>57,59,64</sup> Kovalenko et al. did not observe such a correlation but measured faster cooling dynamics of various solutes in protic than in aprotic solvents.<sup>52</sup> Pigliucci et al. investigated the influence of solute–solvent interactions on the vibrational cooling dynamics of several perylene derivatives.<sup>44</sup> Whereas no clear effect of nonspecific interactions, such as the dipole–dipole interaction, could be established, an unambiguous acceleration of the cooling dynamics was observed when the solute could form H-bonds with the solvent. Such an enhanced efficiency of the vibrational cooling via H-bond interaction was also observed in subsequent studies.<sup>65,66</sup>

## 2. ELECTRON-TRANSFER REACTIONS

### 2.1. Theory

Electron transfer (ET) can be viewed as the simplest chemical reaction and it has thus been considered a benchmark in the development of theories of reaction dynamics. The aim of this section is not to review ET theories but to focus on the models that are mostly used to rationalize experimental data, and to illustrate the evolution from the classical Marcus theory to multidimensional models that account for ultrafast processes. More thorough discussions on ET theories can be found in several reviews.<sup>67–81</sup>

**2.1.1. Classical Marcus Theory.** Although theories of ET reactions were already developed in the first part of the 20th century,<sup>82</sup> the theory formulated by Marcus in the 50s was a major breakthrough,<sup>83,84</sup> and the Marcus model is at the basis of most theoretical descriptions of charge-transfer processes.

In this model, the free energies of the reactant and product states along the reaction coordinate, which comprises both solvent and intramolecular modes, are described by two parabolas with identical curvature, that are displaced horizontally and vertically (Figure 1). The horizontal displacement,

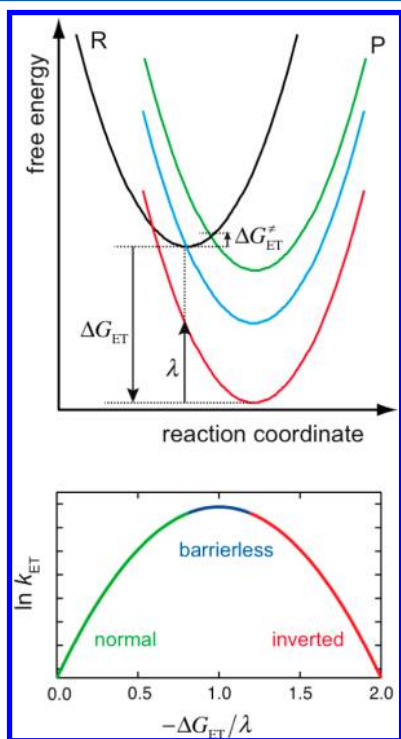


**Figure 1.** (top) Free-energy curves of the reactant (R) and product (P) states for ET in the normal (green), barrierless (blue), and inverted (red) regions. (Bottom) Driving-force dependence of the ET rate constant according to the classical Marcus theory, eq 3.

that accounts for the difference of equilibrium geometries of the two states, is quantified by the reorganization energy,  $\lambda$ . This energy is partitioned into the contributions from the solvent,  $\lambda_s$ , and from intramolecular modes,  $\lambda_i$ . The vertical displacement corresponds to the driving force of the reaction,  $-\Delta G_{ET}$ . The driving force is usually calculated using the redox potentials of the reactants, and for photoinduced processes, the energy of the excited state.<sup>85</sup> The identical curvature of the two parabolas is a crucial aspect of the Marcus model, which is based on the linear response approximation. The original Marcus theory is purely classical and therein, ET is a thermally activated process with a rate constant,  $k_{ET}$ , expressed in an Arrhenius-type form. As the two parabolas have the same shape, the activation free energy,  $\Delta G_{ET}^\ddagger$ , can be expressed as a function of  $\lambda$  and  $\Delta G_{ET}$ , and the ET rate constant is given by

$$k_{ET} = A \exp \left[ -\frac{\Delta G_{ET}^\ddagger}{k_B T} \right] = A \exp \left[ -\frac{(\Delta G_{ET} + \lambda)^2}{4\lambda k_B T} \right] \quad (3)$$

where  $k_B$  is the Boltzmann constant and  $T$  is temperature.

This model predicts a Gaussian dependence of the ET rate constant on the driving force at constant  $\lambda$  and thus three regimes can be distinguished (Figure 1):

- (1) The normal region at  $-\Delta G_{ET} < \lambda$ , where  $k_{ET}$  increases with driving force;

- (2) The barrierless region at  $-\Delta G_{ET} \approx \lambda$  where  $k_{ET}$  reaches its maximum value;
- (3) The inverted region at  $-\Delta G_{ET} > \lambda$  where  $k_{ET}$  decreases with increasing driving force.

In this model, the inverted regime is due to the presence of an activation barrier and thus the ET rate constant is predicted to significantly increase with temperature like in the normal regime.

**2.1.2. Quantum and Semiclassical Electron-Transfer Theories.** A quantum-mechanical description of ET, where the transition probability from the reactant to product states is formulated in a Golden-Rule form, was originally proposed by Levich and Dogonadze.<sup>86</sup> Later on, a similar Golden-Rule treatment was carried out by Jortner and co-workers,<sup>87,88</sup> as well as by Marcus and co-workers,<sup>89</sup> who showed the key role of high-frequency intramolecular vibrations of the product as energy accepting modes in highly exergonic reactions. As a consequence, ET in the inverted regime bears a strong similarity with nonradiative transitions between two electronic states. The Golden-Rule expression of the ET rate is

$$k_{ET} = \frac{2\pi}{\hbar} V^2 \text{FCWD} \quad (4)$$

where  $V$  is a matrix element accounting for the electronic coupling between the initial and final states and FCWD is the Franck–Condon weighted density of states.

In the semiclassical description of ET, the low frequency modes, mostly associated with the solvent, are treated classically, while a single high-frequency intramolecular mode ( $\hbar\omega \gg k_B T$ ) is described quantum mechanically. Assuming that the process occurs from the lowest vibrational level of the initial state, the ET rate constant can be expressed as a summation of the ET rate constants for the transition from the reactant state with the vibrational quantum number  $\nu = 0$  to various  $\nu$  values of the product (Figure 2):

$$k_{ET} = \sum_{\nu=0}^{\infty} k_{ET}^{0 \rightarrow \nu} \quad (5)$$

with

$$k_{ET}^{0 \rightarrow \nu} = \frac{2\pi V_{0 \rightarrow \nu}^2}{\hbar (4\pi\lambda_s k_B T)^{1/2}} \exp \left[ -\frac{(\Delta G_{ET}^{0 \rightarrow \nu} + \lambda_s)^2}{4\lambda_s k_B T} \right] \quad (6)$$

Here, the electronic coupling for each individual transition,  $V_{0 \rightarrow \nu}$ , is calculated by multiplying the coupling for the  $0 \rightarrow 0$  transition by the corresponding Franck–Condon factor:

$$V_{0 \rightarrow \nu}^2 = V^2 | \langle 0 | \nu \rangle |^2 = V^2 \frac{S^\nu}{\nu!} \exp(-S) \quad (7)$$

where  $S$  is the Huang–Rhys factor, also called electron–vibration coupling constant. The intramolecular reorganization energy is equivalent to  $\lambda_i = S\hbar\omega$ ,  $\omega$  being the frequency of the intramolecular mode of the product.

The formation of the ET product in a vibrational excited state leads to a smaller effective driving force:

$$\Delta G_{ET}^{0 \rightarrow \nu} = \Delta G_{ET} + \nu\hbar\omega \quad (8)$$

Consequently, the inverted region is less pronounced than predicted by the classical expression (3) (Figure 2) and is equivalent to the energy-gap law for nonradiative transitions.<sup>90</sup>

In general, the quantum mechanical treatment of vibrational modes allows for nuclear tunneling. As the width of the

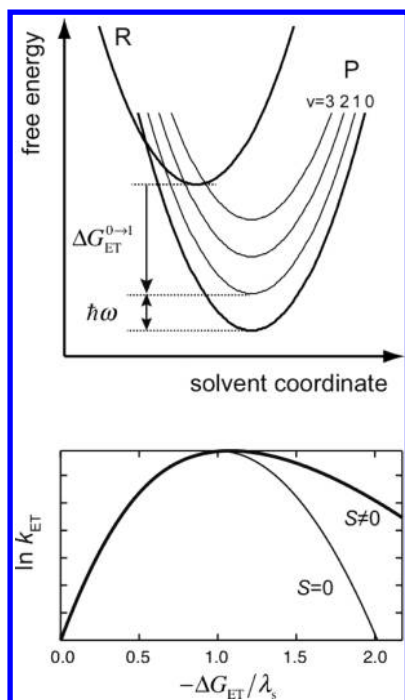


**Figure 2.** (Top) Free-energy curves of the reactant state at  $\nu = 0$  (R) and of the product at different vibrational states (P,  $\nu = 0 \rightarrow 3$ ) for an ET in the inverted regime. (Bottom) Driving-force dependence of the ET rate constant according to the classical (eq 3) and semiclassical treatments (eq 5).

potential energy barrier is much narrower in the inverted than in the normal regime, ET in the inverted region is no longer a thermally activated process but is dominated by nuclear tunneling. Consequently, it is much faster than predicted by the classical Marcus expression and is only weakly affected by temperature.

The classical result, eq 3, with the pre-exponential factor:

$$A = \frac{2\pi V^2}{\hbar(4\pi\lambda_s k_B T)^{1/2}} \quad (9)$$

can be recovered from the Golden-Rule expression in the high-temperature or low-frequency limit, if  $k_B T \gg \hbar\omega$  and  $(\lambda k_B T)^{1/2} \gg \hbar\bar{\omega}$ , where  $\bar{\omega}$  is averaged over all modes.

eqs 5 and 6 are only valid for small  $V$ , i.e., in the nonadiabatic limit, where the transition probability at the crossing region is much smaller than unity.

In the adiabatic limit, the electronic coupling and, thus, the transition probability at the crossing region, are large. In this case, the reaction proceeds entirely on the lower energy surface and its rate constant does not directly depend on  $V$  but rather depends on the probability to reach the crossing region. If the system maintains a quasi-equilibrium distribution as it evolves along the reaction coordinate, i.e., if the response of the solvent and intramolecular modes is faster than ET itself, its motion over the barrier is uniform and the rate constant can be calculated within the framework of transition state theory. If this is not the case, barrier crossing is diffusive and the dynamics can be discussed within the framework of Kramers' theory.<sup>91</sup>

**2.1.3. Zusman Theory and Solvent-Controlled Electron Transfer.** The finite response time of the modes that contribute to the reaction coordinate can influence the ET dynamics even if the adiabatic limit is not reached. This

situation was first treated by Zusman, who modeled the process as a stochastic motion along the reaction coordinate toward the crossing region between the diabatic energy curves, where the transition can take place with a probability proportional to  $V^2$ .<sup>92</sup> In this model, only the solvent modes were considered. The equations of motion of the populations of the reactant and product states,  $\rho_r$  and  $\rho_p$ , are expressed as

$$\frac{\partial \rho_r(Q, t)}{\partial t} = \frac{2\pi}{\hbar} V^2 [\rho_p(Q, t) - \rho_r(Q, t)] \delta(U_r - U_p) + \hat{L}_r \rho_r(Q, t) \quad (10a)$$

$$\frac{\partial \rho_p(Q, t)}{\partial t} = -\frac{2\pi}{\hbar} V^2 [\rho_p(Q, t) - \rho_r(Q, t)] \delta(U_r - U_p) + \hat{L}_p \rho_p(Q, t) \quad (10b)$$

where  $Q$  is the reaction coordinate,  $U_i(Q)$  ( $i = r, p$ ), is the free energy of the reactant and product state along  $Q$ ,  $\delta$  is the delta function and  $\hat{L}_i$  is a diffusion operator:

$$\hat{L}_i = \frac{2\lambda_s}{\tau_1} \left( \frac{\partial^2 U_i}{\partial Q^2} + \frac{\partial U_i}{\partial Q} \frac{\partial}{\partial Q} + k_B T \frac{\partial^2}{\partial Q^2} \right) \quad i = r, p \quad (11)$$

with  $\tau_1$  the longitudinal dielectric relaxation time of the solvent. The second term on the r.h.s. of eq 10 describes the evolution of the system along the reaction coordinate, whereas the first term accounts for the transitions between the reactant to product states at the crossing region.

The ET rate constant derived by Zusman for this case has a similar form as the classical Marcus eq 3, but with the pre-exponential factor:

$$A_z = \frac{2\pi V^2}{\hbar(4\pi\lambda_s k_B T)^{1/2}} \frac{1}{1+g} = \frac{A_{na}}{1+g} \quad (12)$$

with

$$g = \frac{2\pi V^2 \tau_1}{\hbar} \left[ \frac{1}{|\Delta G_{ET} + \lambda_s|} + \frac{1}{|\Delta G_{ET} - \lambda_s|} \right] \quad (13)$$

As only solvent modes are considered, the reorganization energy is entirely due to the solvent. Subsequently, Zusman also addressed solvents with two relaxation times.<sup>93</sup> For large values of  $\tau_1$ , i.e., in slow relaxing solvents,  $g$  is much larger than 1 and eq 12 reduces to

$$A \simeq \left( \frac{\lambda_s}{16\pi k_B T} \right)^{1/2} \tau_1^{-1} \quad (14)$$

In this limit, the ET rate constant is no longer a function of the electronic coupling  $V$  but is only determined by the probability to reach the crossing region, which itself depends on  $\tau_1$ . The same inverse relationship between the ET rate constant and  $\tau_1$  is predicted by Kramers theory in the high friction limit. In both cases, ET is said to be in the solvent-controlled regime.<sup>94</sup>

The Zusman result was also obtained using different approaches.<sup>94,95</sup> Rips and Jortner discussed the transition between the nonadiabatic and the solvent-controlled adiabatic regimes with the ET rate constant defined as

$$k_{ET} \simeq \frac{k_{na}}{1 + \mathcal{H}_A} \quad (15)$$



where  $k_{\text{na}}$  is the classical ET rate constant in the nonadiabatic limit as given by eq 3 with the pre-exponential factor, eq 9, and  $\mathcal{H}_A$  is the adiabatic parameter:

$$\mathcal{H}_A = \frac{4\pi V^2 \tau_1}{\hbar \lambda_s} \quad (16)$$

and is equivalent to the factor  $g$  in the Zusman expression, eq 12, for  $\Delta G_{\text{ET}} = 0$ .

Eq 13 and eq 16 show that, depending on the magnitude of  $V$  and  $\tau_1$ , ET can range from a purely nonadiabatic ( $\mathcal{H}_A \ll 1$ ) to a fully solvent-controlled process ( $\mathcal{H}_A \gg 1$ ). Here again, the inverse dielectric relaxation time,  $\tau_1$ , sets the upper limit of the ET rate constant.

Zusman's model only includes solvent modes, whereas in the subsequent treatments, intramolecular modes were first treated classically.<sup>94,95</sup> As a consequence, eq 15 predicts an important slowing down of the ET at driving forces larger than  $\lambda_s$ . To account for the effect of high-frequency vibrations of the product as energy accepting modes, Jortner and Bixon modified eq 15 with  $k_{\text{na}}$  expressed in terms of the semiclassical ET rate constant (eq 5):<sup>96</sup>

$$k_{\text{ET}} = \sum_{\nu=0}^{\infty} \frac{k_{\text{ET}}^{0 \rightarrow \nu}}{1 + \mathcal{H}_A^{0 \rightarrow \nu}} \quad (17)$$

where  $k_{\text{ET}}^{0 \rightarrow \nu}$  is given by eq 6 and with the adiabatic parameter for the  $0 \rightarrow \nu$  transition:

$$\mathcal{H}_A^{0 \rightarrow \nu} = \mathcal{H}_A \frac{S^\nu}{\nu!} \exp(-S) \quad (18)$$

For a given value of  $\tau_1$ , eq 17 predicts larger ET rate constants than eq 15 at  $-\Delta G_{\text{ET}} > \lambda_s$ , the difference increasing with the Huang–Rhys factor,  $S$ . This is due to the decrease of the effective driving force upon population of the vibrationally excited product. However, ET cannot be faster than the solvent dielectric relaxation in this case either.

**2.1.4. Two-Dimensional Models and Non-Equilibrium Electron Transfer.** Sumi and Marcus investigated the possibility of ET occurring faster than dielectric relaxation by splitting the reaction coordinate into a fast and a slow coordinate,  $q$  and  $X$ , respectively.<sup>97,98</sup> The former is associated with the fast relaxing intramolecular modes, whereas the latter is related to the solvent. The free energies of the reactant and product state along  $X$  and  $q$  are represented by two surfaces, whose intersection corresponds to a line (Figure 3). In such a two-dimensional representation, the minimum free-energy path from the reactant to the product states is identical to the reaction coordinate in the one-dimensional Marcus model. If the system would maintain a quasi-equilibrium distribution along both  $q$  and  $X$  during the reaction, it would follow this path (dashed line in Figure 3). Here, however, the reaction can occur along a path that differs from the minimum free-energy path if it leads more rapidly to the product. Indeed, the reaction can follow a path where the free energy is not minimal, but for which the barrier toward the product is sufficiently low to make ET faster than further evolution along  $X$ . Therefore, in this model, an activation free energy and an ET rate constant can be defined for each value of  $X$ :

$$k_{\text{ET}}(X) = A \exp\left(-\frac{\Delta G_{\text{ET}}^\ddagger(X)}{k_B T}\right) \quad (19)$$

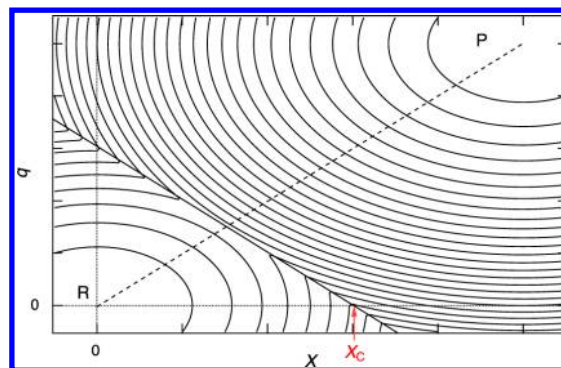


**Figure 3.** Free-energy surfaces of the reactant (R) and product (P) states along the fast intramolecular coordinate,  $q$ , and the slow solvent coordinate,  $X$ . The solid black line is the intersection of the two surfaces, and the dashed line represents the reaction coordinate for an ET much slower than the equilibration along  $q$  and  $X$ .  $X_c$  is the position along  $X$  where the reaction barrier along the  $q$  coordinate vanishes.

with

$$\Delta G_{\text{ET}}^\ddagger(X) = \frac{1}{2}(X - X_c)^2 \frac{\lambda_s}{\lambda_i} \quad (20)$$

where  $X_c$  is the value of  $X$  where the barrier vanishes (Figure 3):

$$X_c = \frac{\Delta G_{\text{ET}} + \lambda}{(2\lambda_s)^{1/2}} \quad (21)$$

The temporal evolution of the reactant state population,  $\rho_r$ , is described in terms of a diffusion-reaction equation:

$$\frac{\partial \rho_r(X, t)}{\partial t} = D \frac{\partial}{\partial X} \left[ \frac{\partial}{\partial X} + \frac{1}{k_B T} \frac{dU_r(X)}{dX} \right] \rho_r(X, t) - k_{\text{ET}}(X) \rho_r(X, t) \quad (22)$$

where  $D = k_B T / (\lambda_s \tau_1)$  is the diffusion coefficient and  $U_r(X)$  is the free energy of the reactant and is quadratic along  $X$ .

Sumi and Marcus considered several cases, assuming that the process starts from the thermally equilibrated reactant state distributed around  $X = 0$ .

- (1) Slow reaction limit: if the ET process is much slower than the relaxation of  $X$ , the survival probability of the reactant population follows an exponential decay with a time constant independent of  $\tau_1$ . In this case, the ET rate constant can be calculated with eq 3.
- (2) Wide reaction window limit ( $\lambda_i/\lambda_s \gg 1$ ): if the process occurs over a wide range of  $X$  values,  $k_{\text{ET}}(X)$  can be approximated by a value independent of  $X$  and averaged over the  $X$  distribution on  $U_r(X)$ . As a consequence, the survival probability decays exponentially with a time constant independent of  $\tau_1$ .
- (3) Narrow reaction window limit ( $\lambda_i/\lambda_s \ll 1$ ): the process occurs as soon as  $X$  reaches values where ET is as fast as further diffusion along  $X$ . Consequently, the decay of the survival probability is strongly nonexponential but depends on  $\tau_1$ , on a way that varies according to the particular case.
- (4) Nondiffusing limit: the reaction occurs very rapidly along  $q$  without any motion along  $X$ . The initial distribution along  $X$  translates into a distribution of the ET rate

constant and the decay of the survival probability is nonexponential but independent of  $\tau_1$ .

Nadler and Marcus investigated some of these limits numerically and showed that, in some cases, an approximate analytical solutions for the survival probability can be derived.<sup>99</sup>

In the Sumi-Marcus model, both solvent and intramolecular modes are treated classically and ET results in the vibrational ground state of the product only. As a consequence, its validity is limited to the normal and barrierless regimes. At high exergonicity, this treatment underestimates the ET rate constant and overestimates its decrease with driving force.

This problem was addressed by Barbara and co-workers,<sup>100</sup> who tried to reproduce the measured solvent dependence of the charge-transfer dynamics of a betaine dye in terms of the Sumi-Marcus model (see section 2.2.2). Here, the initial conditions differed from those considered by Sumi and Marcus as the reactant state is initially populated out of equilibrium via optical excitation in the charge-transfer band of the dye. Consequently, the initial value of  $X$  is not distributed around 0. Whereas the overall variation of the average survival probability with  $\tau_1$  could be qualitatively reproduced with this model, the calculated values were orders of magnitude too slow.

To solve this discrepancy, Barbara and co-workers modified the Sumi-Marcus model by introducing a high-frequency vibration of the product state as the energy accepting mode (Figure 4).<sup>100</sup> The resulting model is called the hybrid model as

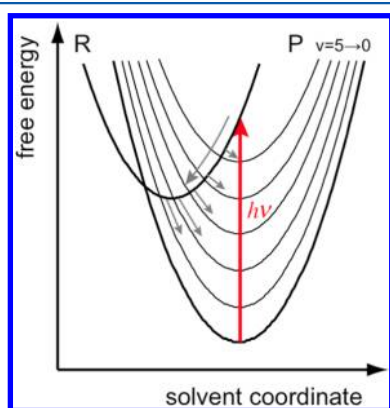


**Figure 4.** Free-energy cuts of the reactant (R) and product (P) surfaces along the solvent coordinates. Optical population prepares R out of equilibrium and ET can occur to vibrational states of P before R is equilibrated.

it combines the classical Sumi-Marcus approach, eq 19, with the semiclassical expression for the ET rate constant, eqs 5–8:

$$k_{\text{ET}}(X) = \sum_{\nu=0}^{\infty} k_{\text{ET}}^{0 \rightarrow \nu}(X) \quad (23)$$

where the ET rate constant to the  $\nu^{\text{th}}$  vibrational state of the product is

$$k_{\text{ET}}^{0 \rightarrow \nu}(X) = \frac{2\pi V_{0 \rightarrow \nu}^2}{\hbar(4\pi\lambda_{\nu}k_{\text{B}}T)^{1/2}} \exp\left[-\frac{(\Delta G_{\text{ET}}^{0 \rightarrow \nu} + \lambda_s - 2X\lambda_s + \lambda_{\nu})^2}{4\lambda_{\nu}k_{\text{B}}T}\right] \quad (24)$$

where  $V_{0 \rightarrow \nu}$  and  $\Delta G_{\text{ET}}^{0 \rightarrow \nu}$  are given by eqs 7 and 8, and  $\lambda_{\nu}$  is the reorganization energy associated with classical low-frequency intramolecular modes.

The introduction of the high-frequency accepting modes of the product has a strong impact on the decay of the survival probability and leads to much faster ET than the Sumi-Marcus model. This hybrid model is well suited for the description of nonequilibrium photoinduced ET processes, as it allows ET to take place before the optically populated reactant state has reached equilibrium. Several variants of the Sumi-Marcus and hybrid models, including multiple solvent relaxation times or more than one high-frequency vibrational modes, were developed afterward.<sup>101–106</sup>

As discussed in more detail below, this is the level of theory that has to be used when discussing ET processes occurring on a similar time scale as the solvent and the vibrational relaxation.

All the theoretical models discussed in this section can in principle be directly applied to discuss intramolecular electron transfer processes. However, as they do not account for the diffusion of the reactants, they cannot be readily used to describe intermolecular reactions. In this case, they have to include diffusion equations and the distance-dependence of the ET rate has to be explicitly taken into account, as discussed in more detail in section 2.3.1.

## 2.2. Intramolecular Electron Transfer

**2.2.1. Introduction.** Photoinduced intramolecular electron transfer (ET) reactions have been and are still very intensively investigated. Two main motivations can be distinguished. The first is to increase the basic understanding of ET as one of the simplest chemical reactions.<sup>107–119</sup> Compared to intermolecular processes, intramolecular ET offers the advantage that the distance and mutual orientation of the electron donating (D) and accepting (A) units can be unique and controlled, at least in some cases. Therefore, the reaction takes place without diffusion of the reactants and the experimentally observed dynamics can be directly compared with theoretical ET models.

A second motivation to study photoinduced intramolecular ET is the potential use of these compounds in various applications, such as photovoltaics, artificial photosynthesis, photocatalysis, molecular electronics, or sensing. Over the past few decades, an impressive number of systems, containing one or several chromophores (as well as donors and acceptors) arranged according to different motifs, were developed. Many of these multichromophoric systems were investigated in liquid solution by time-resolved spectroscopy to determine the various ET pathways and their dynamics. Several reviews have been dedicated to this research.<sup>120–132</sup> In most of these systems, all the ET steps, comprising the initial photoinduced charge separation (CS), the charge recombination (CR) of the ensuing charge-separated state, and, in some cases, the charge shifts leading to different charge-separated states and the CR of the latter, occur on slower time scales than those of the above-discussed relaxation processes. Consequently, their dynamics can be rationalized within the framework of semiclassical ET theory (section 2.1.2).

Here, we will only address a more limited number of cases where intramolecular ET is ultrafast, in the sense that it occurs on a shorter or similar time scale compared to thermal equilibration of the initial state.

These different systems will be sorted according to the electronic coupling,  $V$ , between the D and A units. A large electronic coupling favors ultrafast ET and, thus, the occurrence of nonequilibrium dynamics. It should be noted that, as a nonvanishing  $V$  requires some overlap between the molecular orbitals of the D and A units, full CS can in principle not be



achieved in a dyad with fixed distance and mutual orientation of the D and A units. Therefore, when  $V$  is large, the ET product state should be considered as an excited state with a large electric dipole moment rather than as a covalently linked ion pair. In such case, one usually refers to a charge-transfer (CT) state rather than to a charge-separated state.

**2.2.2. Direct Optical Charge Transfer in Strongly Coupled Systems.** When the D and A units are sufficiently coupled, the electronic absorption spectrum of the DA dyad exhibits a band associated with an optical transition from the ground state to the CT excited state. The coupling  $V$  is directly related to the transition dipole moment,  $\bar{\mu}_{\text{CT} \leftarrow \text{S}_0}$  or alternatively to the molar absorption coefficient at the band maximum,  $\epsilon_{\text{max}}$  (in  $\text{M}^{-1} \text{cm}^{-1}$ ):<sup>133–135</sup>

$$V(\text{cm}^{-1}) = \frac{\bar{\nu}_{\text{max}} \bar{\mu}_{\text{CT} \leftarrow \text{S}_0}}{\bar{\mu}_{\text{IP}}} = 2.06 \cdot 10^{-2} \frac{\bar{\nu}_{\text{max}} \epsilon_{\text{max}} \Delta \bar{\nu}^{1/2}}{d_{\text{DA}}} \quad (25)$$

where  $\bar{\mu}_{\text{IP}}$  is the permanent dipole moment of the fully charge-separated state,  $\bar{\nu}_{\text{max}}$  and  $\Delta \bar{\nu}$  are the maximum and width of the absorption band in wavenumbers, and  $d_{\text{DA}}$  is the center-to-center distance between D and A in Å. This equation shows that a CT band with a large transition dipole moment or absorption coefficient is associated with a large electronic coupling and thus, as mentioned in the previous paragraph, results in an incomplete CS, i.e., the permanent dipole moment of the CT state,  $\bar{\mu}_{\text{CT}}$ , is substantially smaller than  $\bar{\mu}_{\text{IP}}$ . This is typically the case in molecules such as coumarins or other push–pull molecules, whose  $\text{S}_1 \leftarrow \text{S}_0$  absorption band is generally broad and structureless and whose fluorescence is characterized by a strong solvatochromism. According to the analysis of this solvatochromism and to quantum chemical calculations, the excited dipole moment of a standard coumarin like **C153** (**1a**, Chart 1) was reported to be around 14 D,<sup>22,136,137</sup> whereas  $\bar{\mu}_{\text{IP}}$  can be estimated to be of the order of 25–30 D. Consequently, optical excitation in the CT band of such compounds cannot be really considered as an electron transfer but rather as a substantial redistribution of the electronic density.

A substantial number of ultrafast spectroscopic studies have been devoted to such systems, because they allow direct investigation of the relaxation dynamics of the optically populated CT state. This allows better understanding of the relaxation phenomena occurring upon full CS, without the complication from a convolution of the relaxation and the CS dynamics. Indeed, if CS is not fast enough, these relaxation processes are not experimentally accessible. Most of our current understanding on solvent relaxation is based on such investigations, performed mostly by time-resolved fluorescence, as discussed in section 1.2.<sup>14,23,24,138–141</sup>

The determination of the dynamic Stokes shift requires molecules with a sufficiently long-lived CT excited state and a substantial radiative rate constant, i.e., molecules with a large fluorescence quantum yield. This is generally the case for rigid push–pull molecules, where the nonradiative decay, which can be viewed as a CR process, is relatively slow, mostly because of the large energy gap between the CT and the ground state.

The presence of a CT absorption band does not necessarily imply an increase of dipole moment upon excitation. Indeed, such band can also be present in the absorption spectrum of molecules that are strongly dipolar in the ground state and weakly polar in the excited state. This is the case of the zwitterionic DA biaryls, among which betaine-30 (**B30**, **9**,

Figure 5) is probably the most investigated representative. The  $\text{S}_1 \leftarrow \text{S}_0$  absorption band of **B30** exhibits one of the largest

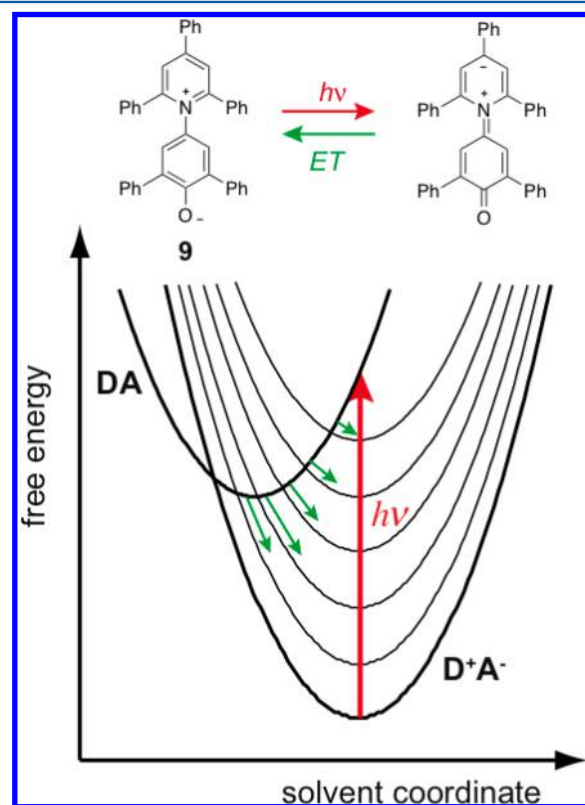


**Figure 5.** Free-energy curves of the ground and first electronic excited state of betaine-30 (**9**) along the classical solvent coordinate. The thin parabolas represent vibrational excited levels and the green arrows possible ET pathways.

solvatochromic shift known. For this reason, the  $\text{S}_1 \leftarrow \text{S}_0$  transition energy has become an empirical measure of polarity, the  $E_{\text{T}}(30)$  scale.<sup>142,143</sup> The negative solvatochromism exhibited by this molecule is due to the zwitterionic nature of its ground state ( $\bar{\mu}_{\text{S}_0} = 15 \text{ D}$ )<sup>144</sup> and to the smaller dipolar nature of its  $\text{S}_1$  state ( $\bar{\mu}_{\text{S}_1} = 6.2 \text{ D}$ ), resulting in a strong CT character of this transition. Consequently, contrary to the cases discussed above, the population of the  $\text{S}_1$  state corresponds to a CR process and its decay to the ground state to a CS process.

Another major difference with the above-mentioned molecules is that **B30**, like several other biaryl betaines, does not fluoresce, pointing to the existence of a very efficient nonradiative decay of the  $\text{S}_1$  state. Because of this and of its unusual dipolar properties, the excited-state dynamics of **B30** were intensively investigated over the past three decades.

The first ultrafast spectroscopic studies of betaines were reported by Barbara and co-workers.<sup>100,145–148</sup> As shown in Figure 5, the nonradiative decay of the  $\text{S}_1$  state of **B30** was considered as a CS from DA to  $\text{D}^+\text{A}^-$ . The dynamics of this process were initially measured by a single color pump–probe measurement at 792 nm, which, in the most polar solvents, corresponds to the red side of the  $\text{S}_1 \leftarrow \text{S}_0$  absorption band. The temporal evolution of the absorption change at this wavelength reflects the recovery of the ground-state population as well as its thermalization by vibrational relaxation. As the absorption spectrum of the vibrationally hot ground state,  $\text{S}_{0,\text{hot}}$  is red-shifted with respect to that of the equilibrated ground

state, the contribution of vibrational relaxation to the transient absorption signal depends on the probe wavelength within the  $S_1 \leftarrow S_0$  absorption band. The fast ground-state recovery component was interpreted to be due to ET from the weakly polar  $S_1$  state to the zwitterionic ground state. In rapidly relaxing solvents like acetonitrile and acetone, the obtained ET time constant was found to be similar to the diffusive solvation time, pointing to a quasi-barrierless and solvent-controlled process.<sup>145</sup> However, in slowly relaxing solvents like glycerol triacetate and alcohols, ET time constants substantially shorter than those of diffusive solvation were measured. The authors also measured the effect of the temperature and observed a small acceleration of the ET dynamics with increasing temperature following an Arrhenius behavior with an activation energy of the order of 0.1 eV.<sup>100</sup> In glycerol triacetate at 228 K, i.e., about 50 K below the melting point of the solvent, ET was still ultrafast with a time constant of 5.5 ps.

To account for such electron transfer occurring faster than solvation, Barbara and co-workers applied first the Sumi-Marcus model.<sup>145</sup> As discussed in section 2.1.4, both slow and fast modes are treated classically, and therefore, this model strongly overestimates the decrease of the ET rate constant in the inverted regime. Consequently, the ET rate constants predicted by the Sumi-Marcus model were orders of magnitude smaller than the measured ones. To solve this problem, Barbara and co-workers developed the hybrid model which includes a quantum mechanical high-frequency vibration of the product as energy accepting mode, eq 23.<sup>100</sup> Application of this model resulted in an excellent agreement with the experimental rate constants as well as with their temperature dependence in glycerol triacetate.<sup>100,147</sup> Consequently, as illustrated in Figure 5, ET in **B30** follows nonequilibrium dynamics. Optical excitation prepares the initial ET state far from equilibrium and, as relaxation along the slow solvent coordinate takes place, electron transfer can take place to vibrational excited states of the product,  $S_{0,\text{hot}}$  before equilibrium is reached.

Unambiguous evidence for the formation of the ET product in a vibrational excited state was obtained from time-resolved anti-Stokes Raman spectroscopy measurements by Elsaesser and co-workers.<sup>149–151</sup> The authors monitored the temporal evolution of the amplitude of anti-Stokes bands associated with vibrational modes of various frequencies after  $S_1 \leftarrow S_0$  excitation of **B30** in propylene carbonate, glycerol triacetate, and ethanol (Figure 6). In the two former solvents, where ET to the ground state is the fastest, with 1 and 3.8 ps time constants, respectively, a high-frequency band of the electronic ground state at  $1603\text{ cm}^{-1}$  was found to rise with the same time

constant (Figure 6), whereas lower-frequency bands showed a 5–7 ps rise. In ethanol, where ET was slower ( $\tau_{\text{ET}} = 6\text{ ps}$ ), all bands rose with a time constant similar to  $\tau_{\text{ET}}$ . All these anti-Stokes bands decayed with a time constant between 5 to 8 ps, depending on the solvent.

This behavior was explained by assuming that the  $1603\text{ cm}^{-1}$  mode, assigned to a pyridinium ring stretch, is directly coupled to the reaction and is therefore directly populated. On the other hand, the lower frequency modes are excited indirectly via IVR. Vibrational cooling occurs afterward and is responsible for the decay of the anti-Stokes Raman bands. Elsaesser and co-workers identified the vibrational modes coupled to the electron transfer using resonance Raman spectroscopy, with the incident beam in resonance with the CT transition.<sup>150</sup> McHale and co-workers performed resonance Raman measurements to determine the mode-dependent reorganization energy associated with ET in **B30**.<sup>152,153</sup> More recently, Chen developed the Functional Mode ET theory, which allows the contribution of each intramolecular mode to the process to be determined.<sup>154</sup> The author found that only 7 among the 210 vibrational modes of **B30** were essential to the ET. All these modes were characterized by a high frequency, in agreement with the experimental findings of Elsaesser and co-workers.<sup>149–151</sup>

The ultrafast excited-state dynamics of **B30** were subsequently investigated by other groups. Schmuttenmaer and co-workers could directly detect the electromagnetic field generated by **B30** upon photoexcitation in the CT band.<sup>155,156</sup> To this end, the authors had first to orient the dye molecules in solution. This was done by using a high-voltage electric field pulse and by exploiting the large permanent dipole moment of the dye in the ground state. The solution was then excited with a femtosecond optical pulse polarized parallel to the high-voltage field, and the field radiated upon ET was detected by electro-optical sampling.<sup>156,157</sup> From the temporal shape of this field, the authors were able to extract the time constants associated with both the population of the excited state and its decay back to the zwitterionic ground state. The former was found to be very short, pointing to a quasi-instantaneous process, whereas the latter was consistent with the time constant found by Barbara and co-workers.

More recently, Kubarych and co-workers measured the electric fields associated with the CT in **B30** by probing the solvent with time-resolved vibrational spectroscopy.<sup>158</sup> They used NaSCN as infrared active solvent, dissolved in ethyl acetate. The dielectric enrichment around the highly polar dye ensured that NaSCN was mostly located in close vicinity to **B30**. Upon excitation of **B30**, the authors measured transient spectra in the CN stretching region consisting of a negative band and a positive band downshifted by  $19\text{ cm}^{-1}$  (Figure 7, left). The intensity of this transient was found to decay exponentially with a time constant similar to that of the excited state (Figure 7, right). The transient spectrum was ascribed to the Stark effect on the CN stretch associated with the change of the local field generated by **B30** upon photo excitation.

The first transient electronic absorption measurements of **B30** with broadband detection and with  $\sim 20\text{ fs}$  resolution after deconvolution were reported by Ernsting and co-workers.<sup>159</sup> The authors could monitor the time evolution of the stimulated emission, of the excited-state absorption and of the ground-state bleach of the dye in several polar solvents. Their investigation confirmed that in slowly relaxing solvents, such as ethanol and ethylene glycol, ET occurs faster than the

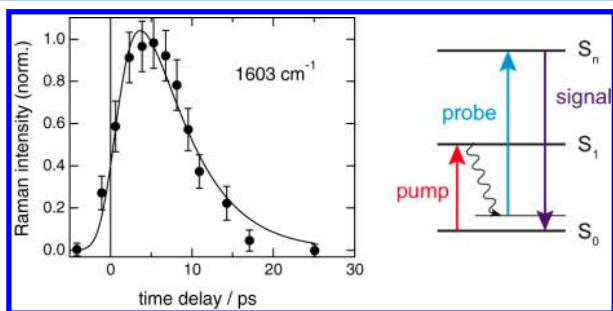


**Figure 6.** Rise and decay of the intensity of the anti-Stokes Raman intensity of the vibrational mode at  $1603\text{ cm}^{-1}$  measured with betaine-30 in propylene carbonate<sup>150</sup> and energy level scheme of the experiment.

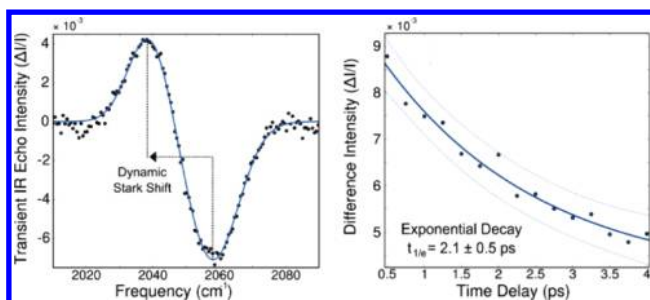


**Figure 7.** (Left) Transient vibrational spectrum measured at zero time delay after excitation of betaine-30 showing the  $19\text{ cm}^{-1}$  red-shift of the solvent  $\text{C}\equiv\text{N}$  stretching frequency induced by the change in the local electric field. (Right) Time evolution of the difference amplitude (induced signal–bleach) with best single-exponential fit (solid) and 90% confidence bounds (dashed). Reprinted from ref 158. Copyright 2010 American Chemical Society.

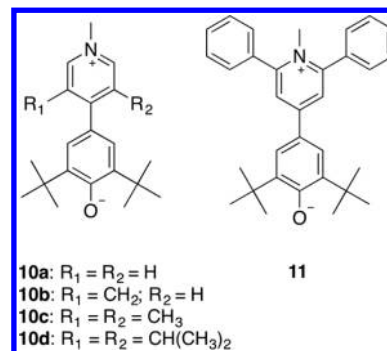
slowest component of solvent relaxation. However, their data indicated that low-frequency intramolecular modes of **B30**, probably associated with the dihedral angle between the pyridinium and the phenolate rings, which were not taken into account in the previous studies, play an important role in the ET dynamics.

The role of the dihedral angle as a relevant CT coordinate was confirmed by quantum-chemistry calculations. Lobaugh and Rossky performed mixed classical/quantum molecular dynamics (MD) simulations, treating **B30** with the semi-empirical Pariser–Parr–Pople method.<sup>160</sup> An ultrafast decrease of the  $S_1$ – $S_0$  energy gap on a 100 fs time scale due to the inertial motion of the solvent was observed, as expected from the model of Barbara and co-workers. Additionally, their simulations pointed to the presence of a slower, picosecond time scale, component in the temporal evolution of  $S_1$ – $S_0$  gap associated with twisting about the central bond between the two betaine rings. According to their calculations, the equilibrium dihedral angle of **B30** changes from  $52^\circ$  to  $90^\circ$  when going from the ground to the  $S_1$  state. More recent quantum-chemistry calculations at the CASSCF level of a betaine analog, with H atoms instead of the phenyl substituents, were reported by Ishida and Rossky.<sup>161</sup> They pointed to a dihedral angle around  $47^\circ$  in the ground state and of  $90^\circ$  in the  $S_1$  state in the gas phase. Very similar results were obtained later at the DFT level of theory.<sup>162</sup> In polar solvents, the  $S_1$  state potential energy surface was found to be mostly flat for torsion angles  $>50^\circ$ . From this, the authors concluded that the early excited-state dynamics of **B30** involves deplanarization as suggested previously and that it is strongly linked with the dynamics of the solvent.<sup>161</sup>

Some experimental insight into the structural changes accompanying charge transfer in **B30** was obtained from femtosecond stimulated Raman spectroscopy (FSRS) measurements in methanol.<sup>163</sup> The authors observed several Raman bands between  $1300$  and  $1700\text{ cm}^{-1}$ , which they assigned to CC and CN stretching modes of the dye in the  $S_1$  state. All bands exhibited frequency shifts during the first 500 fs after excitation, before decaying entirely within a few ps. Based on quantum-chemistry calculations of the vibrational frequencies of the betaine in the ground state at different dihedral angles, the authors assigned the observed frequency shifts to the evolution of the excited-state population along the twist coordinate.

In order to obtain a deeper understanding of the role of the twist coordinate in the ET dynamics of zwitterionic biaryls, a series of pyridinium phenolates with different torsional angles between the rings was investigated by Duvalnet et al. (10, Chart 2).<sup>164</sup> These molecules differ from **B30** by the position of the

**Chart 2. Zwitterionic Pyridinium Phenolates**



phenolate ring on the pyridinium. The ground-state dihedral angle was varied from about  $10^\circ$  (**10a**) to  $50^\circ$  (**10d**) by adding alkyl substituents of different sizes at the meta positions of the pyridinium group. The increasing torsion in this series of compounds was shown to substantially increase their second-order nonlinear optical response.<sup>165</sup> Like **B30**, these molecules exhibit a negligibly small fluorescence quantum yield, indicative of an ultrafast nonradiative decay of the  $S_1$  state. Their excited-state dynamics were investigated using a combination of fluorescence up-conversion and electronic transient absorption (Figure 8). The overall excited-state dynamics were found to slow down when going from **10a** to **10d**, i.e., upon increasing

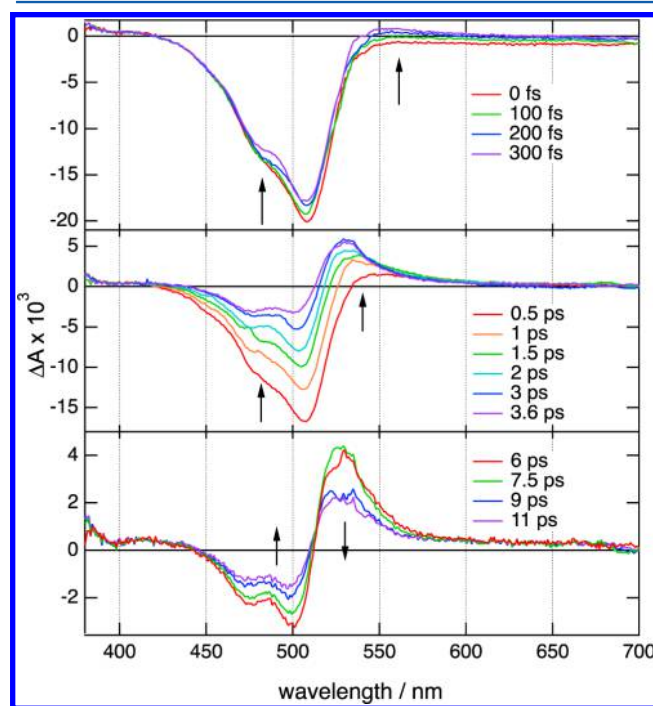


**Figure 8.** Transient absorption spectra recorded with **10a** in ethanol at various time delays after 530 nm excitation. The negative band is the bleach of the  $S_1 \leftarrow S_0$  absorption and the positive band around 525 nm is due to the hot ground state. Reprinted from ref 164 with permission from the PCCP Owner Societies.



the dihedral angle. A slowing down was also observed upon increasing solvent viscosity. The data were rationalized with a three-step model, including relaxation of the Franck–Condon  $S_1$  state, ET to the hot ground state and thermalization of the latter. Relaxation of the Franck–Condon excited state was proposed to mostly involve the increase of the dihedral angle toward close to a perpendicular geometry, resulting in a quasi-nonfluorescent equilibrium  $S_1$  state. Similarly, the relaxation dynamics of the hot ground state populated upon ET was suggested to be mostly controlled by the back-twist toward the equilibrium geometry. The deceleration of the ET dynamics from 0.4 ps for (10a) to 1.5 ps (10d) in acetonitrile was explained by a decrease of the electronic coupling,  $V$ , with increasing twist angle between the rings. A more recent study showed that the overall excited-state dynamics of these dyes can also be slowed down by adding bulky substituents such as phenyl groups on the meta position of the pyridinium ring (11). In this case the torsional dynamics, which involve larger amplitude motion, become substantially slower.<sup>166</sup>

According to these results, ET dynamics in these zwitterionic biaryls is even more complex than initially suggested by Barbara and co-workers,<sup>100,145–148</sup> who did not include slow intramolecular modes in their model, in particular neglecting the change of the dihedral angle between the pyridinium and phenolate rings. Whereas the solvent coordinate  $X$  affects the activation free energy,  $\Delta G_{ET}^\ddagger$  (eq 20), this slow torsional mode should mostly influence the electronic coupling,  $V$ . Therefore, a theoretical description of the excited-state dynamics of B30 and similar zwitterionic biaryls should account for both solvation and structural nonequilibrium dynamics.

**2.2.3. Strongly Coupled Systems: Direct Optical CT or CT from a Locally Excited State?** In the cases discussed above, the first absorption band is associated with a CT transition, and consequently, the intramolecular CT (ICT) process takes place directly upon optical excitation. However, in several other cases, the exact pathway to the CT state is more ambiguous:<sup>140,167–176</sup> is the CT state populated directly upon optical excitation or indirectly via a locally excited (LE) state (Figure 9)?

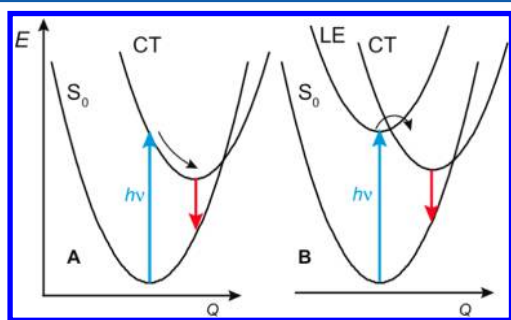


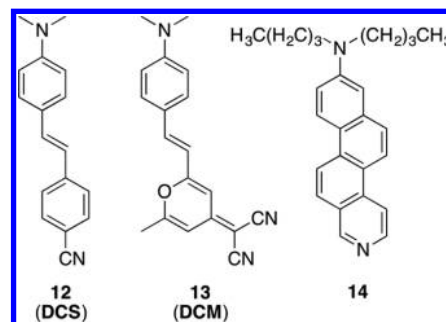
**Figure 9.** Potential energy curves along a generalized coordinate including intramolecular and solvent modes for (A) direct optical population of the CT state or (B) local excitation followed by LE  $\rightarrow$  CT transition.

In principle, this question does not need ultrafast spectroscopy to be answered. If the photophysics of the molecule involves two states (ground and CT states), the transition dipole moments for absorption ( $CT \leftarrow S_0$ ) and emission ( $CT \rightarrow S_0$ ) must be the same. Moreover, in such a case, the solvatochromism of absorption and emission should be consistent with a unique set of ground- and excited-state

dipole moments. A value of the fluorescence anisotropy substantially smaller than 0.4 would also point to an emission originating from a different state than that populated by photoexcitation and would thus be indicative of a three-state system (ground, LE and CT states). Unambiguous evidence of such a three-state system can be obtained by time-resolved spectroscopy through the direct observation of the LE  $\rightarrow$  CT transition. As both population transfer and relaxation (solvent, vibration) phenomena result in spectral dynamics, the interpretation of the transient spectra can sometimes be delicate and prone to confusion.

An illustrative example is given by the push–pull molecule *trans*-4-dimethylamino-4'-cyanostilbene (DCS, 12, Chart 3),

**Chart 3. Molecules with Debated Excited-State CT Dynamics**



whose excited-state dynamics have been highly debated for almost two decades. The first sub-nanosecond investigation of DCS was reported in ethanol by Safarzadeh-Amiri.<sup>177</sup> The observed dynamics was interpreted in terms of a two-state model, with direct optical population of the CT state.

This molecule was reinvestigated a few years later by Rullière and co-workers using a Kerr-gate fluorescence spectrometer with a 80 ps temporal resolution.<sup>178</sup> In apolar solvents, a single emission band peaking around 450 nm and showing no spectral dynamics was measured. By contrast, the emission band in polar solvents, initially around 480 nm, decreased within few tens of ps, while another band around 540 nm showed a concomitant rise. As the temporal evolution of these bands followed a precursor-successor relationship, they were assigned to the LE and CT emission, respectively. Moreover, the CT state was suggested to have a twisted equilibrium structure and was thus called TICT (twisted ICT) state.

Later on, this group performed similar measurements on DCS derivatives, for which the rotation around the various single bonds was inhibited, and found that the dual fluorescence vanishes if rotation of the dimethylaniline group is blocked.<sup>179</sup> Moreover, they observed that the dual fluorescence also vanishes for all the other DCS derivatives if dilute sample solutions and moderate excitation intensities are used. From this, the authors concluded that the long-wavelength fluorescence band was due to a complex consisting of two molecules in the TICT state, a so-called bicimer. Similar conclusions on the nature of the excited state and the formation of bicimers at high excitation intensities were drawn in subsequent studies from the same group with other DCS derivatives using transient electronic absorption, in addition to the time-resolved emission spectroscopy.<sup>180,181</sup>

The bicimer hypothesis was challenged by Schroeder and co-workers, who performed femtosecond fluorescence up-con-

version and transient electronic absorption measurements of DCS in acetonitrile and methanol.<sup>182</sup> Dual emission with precursor-successor relationship was observed at relatively low excitation intensity. The short-wavelength emission band was assigned to the LE state and the other band to the more polar CT state.

A few years later, Ernstring and co-workers showed that the dual fluorescence observed by time-resolved emission was spurious.<sup>183</sup> The authors performed broadband fluorescence up-conversion spectroscopy with sub 100 fs time resolution and found that the presence of two emission bands depended on excitation intensity and dye concentration, in agreement with the measurements by the Rullière group.<sup>179</sup> At low intensity and concentration, the time evolution of the fluorescence consisted of a simple red shift of the fluorescence band, going from ~478 to 547 nm in acetonitrile. Using transient electronic absorption, the authors measured an intense band around 520 nm due to excited-state absorption which exhibited a blue shift on the same time scale as the red shift of the fluorescence. The authors could show that the presence of the two emission bands was artificial and due to the reabsorption of the fluorescence by this strong excited-state band. Once this effect was eliminated by using low concentration and/or very thin samples, the time evolution of the fluorescence was fully consistent with the direct optical population of the CT state and with the dynamic Stokes shift of the emission band due to solvent relaxation.

A conclusive investigation of the nature of the excited state of DCS was presented by Maroncelli and co-workers, who found that the transition dipole moment for emission is essentially the same as that for absorption.<sup>184</sup> Moreover, they showed that the solvatochromism of the absorption and emission of DCS is consistent with a two-state model. They also measured the fluorescence dynamics of DCS in 11 polar solvents using a combination of Kerr-gate spectroscopy and TCSPC and found a continuous red shift of the emission band, in agreement with Ernstring and co-workers (Figure 10).<sup>183</sup> Finally, they showed that this dynamic Stokes shift was identical, within the limit of experimental error, to that measured with the standard solvation probe C153. The authors thus concluded that the fluorescence dynamics of DCS are fully consistent with the two-state model with direct optical excitation of the CT state, and that DCS is a very valuable probe of solvation.

The red laser dye 4-dicyanomethylene-2-methyl-6-(*p*-dimethylamino-styryl)-4-pyran, better known as DCM, is another molecule for which the nature of the emitting state is still debated (13, Chart 3). This molecule contains a stilbene-like core with a dimethylaniline push group and a dicyanomethylene pull group. Solvatochromic investigations pointed to a CT emissive state with a dipole moment of 26 D.<sup>185</sup>

The first ultrafast investigation of DCM was reported by Easter et al., who monitored the temporal evolution of its stimulated emission in methanol and ethylene glycol at several wavelengths using sub-picosecond pump-probe spectroscopy.<sup>186</sup> The temporal changes of the fluorescence intensity measured during the first 100 ps after excitation were ascribed to the dynamic Stokes shift of the emission from the CT state following its direct optical excitation.

A subsequent transient absorption study by Martin and co-workers pointed to the presence of two stimulated emission bands with both an opposite temporal evolution and an isosbestic point, indicative of a precursor-successor relationship.<sup>187</sup> The time constant associated with these changes was

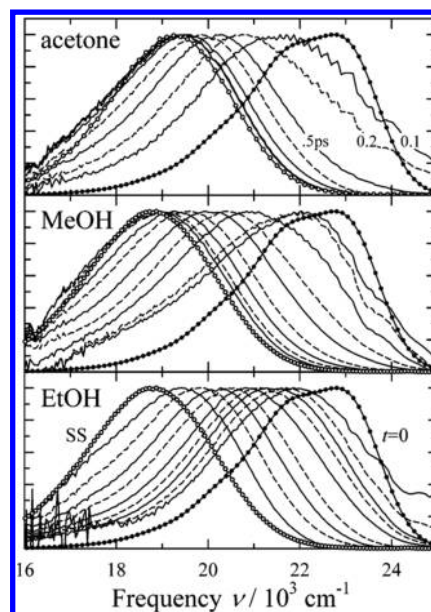


**Figure 10.** Intensity-normalized time-resolved emission spectra of DCS (12) in acetone, methanol, and ethanol measured using the Kerr-gate technique. The time-zero spectra were determined as explained in ref 184, the steady-state spectra (SS) are also shown for comparison. Reprinted from ref 184. Copyright 2006 American Chemical Society.

found to depend on the solvent and to vary from 2 ps in acetonitrile to 8 ps in methanol. These spectral dynamics were interpreted as a transition from the optically populated LE state to the CT state. No evidence of the twisted nature of this CT state, as suggested earlier,<sup>188</sup> could be inferred from these results.

This result was at odds with a fluorescence up-conversion study of DCM in chloroform and methanol with <100 fs time resolution.<sup>189</sup> No change of the integrated spectral intensity, as would be expected for a LE → CT transition, was observed during the first 25 ps after excitation. Moreover, the reconstructed transient emission spectra consisted of a single band. The authors of this study concluded that DCM has a single emitting state, which is directly populated upon photoexcitation.

Other fluorescence up-conversion measurements on DCM in various polar solvents pointed to a biphasic nature of the dynamic Stokes shift with the faster component being due to inertial solvent motion.<sup>190</sup> Additionally, the authors suggested, from the initial rise of the integrated fluorescence intensity, that the emissive CT state is populated within the first 300 fs after excitation from another state with a smaller CT character.

Around the same time, Kovalenko et al. published a transient absorption investigation of DCM in methanol with 40 fs time resolution and found, similar to the findings of Martin et al.,<sup>187</sup> two stimulated emission features with distinct maxima and an isosbestic point that they assigned to the LE and CT states.<sup>191</sup> However, the LE → CT transition was found to be much faster than suggested by Martin et al. and to take place within 300 fs, in agreement with the conclusion of Glasbeek and co-workers.<sup>190</sup>

This conclusion was challenged in a combined experimental and theoretical study by Painelli, Terenziani and co-workers, who showed that both the absorption and emission bands of DCM in solvents varying from hexane to dimethyl sulfoxide could be well reproduced using a two-state model accounting

for the coupling to intramolecular vibrations and to an effective solvent coordinate (Figure 11).<sup>192</sup> They also stressed that a

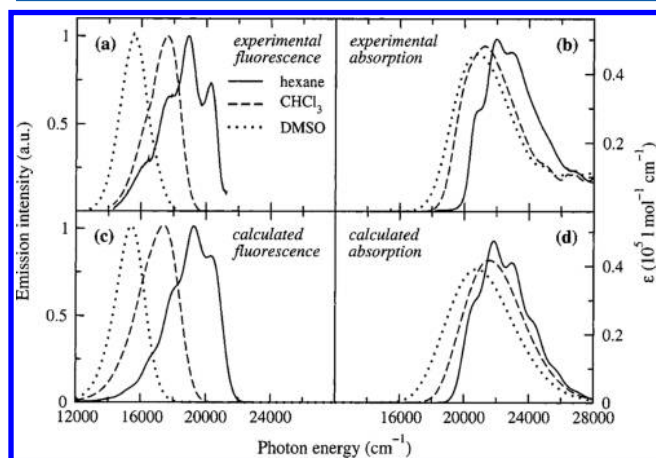


**Figure 11.** Comparison of the experimental and emission (a) and absorption (b) spectra of DCM (13) in various solvents with those calculated assuming a two-level model (c, d). Reprinted from ref 192. Copyright 2002 American Chemical Society.

change of band shape upon varying solvent polarity cannot be considered as an evidence of different emitting states and can be perfectly accounted for in terms of a two-state model.

A few years later, Fleming and co-workers reported on a time-resolved IR study of DCM in acetonitrile and dimethyl sulfoxide.<sup>193</sup> Both the fingerprint region between 1440 and 1620  $\text{cm}^{-1}$  and the CN stretching region were probed. The authors observed excited-state absorption bands in the fingerprint region with different temporal evolutions: one around 1440  $\text{cm}^{-1}$  showing no shift and others between 1490 and 1600  $\text{cm}^{-1}$  exhibiting a frequency upshift and/or changes in band shape on a few ps time scale. The data were explained by a LE  $\rightarrow$  CT transition occurring within the 100 fs IRF of the experiment followed by solvent and structural relaxation toward a TICT state. Occurrence of the twist around the C–N(CH<sub>3</sub>)<sub>2</sub> bond was justified by the time evolution of the 1490–1600  $\text{cm}^{-1}$  band ascribed to the change of C–C bonding character throughout the molecule.

Later on, the nature of the emissive state of DCM in gas phase and in solution was investigated by quantum-chemistry calculations at the DFT and time-dependent (TD) DFT levels of theory.<sup>194</sup> The molecule was found to be planar in both the S<sub>0</sub> and S<sub>1</sub> states, the latter being characterized by a substantial CT from the dimethylaniline to the pyran group. No evidence of a TICT state was found and the authors concluded that the fluorescence dynamics of DCM can be well accounted for by a two-state model.

The 2D electronic-vibrational (2D-EV) spectroscopy recently demonstrated by Fleming and co-workers seems to be a promising technique for obtaining deep insight into the nature of the emitting state.<sup>195</sup> A 2D-EV spectrum at a given pump–probe delay consists of the transient absorption measured as a function of the vibrational probe frequency and of the electronic pump frequency. 2D-EV spectra give rich insight into the nature of the vibrational modes coupled to the electronic excitation and, as shown by Terenziani and Painelli,<sup>196</sup> should allow differentiating between the direct optical population of the CT state or the LE  $\rightarrow$  CT transition.

2D-EV spectroscopy was applied on DCM,<sup>197</sup> but the results finally turned out to be inconclusive.<sup>198</sup>

**2.2.4. Strongly Coupled Systems with a LE  $\rightarrow$  CT Transition.** We consider now strongly coupled DA systems, where full CS is not realized but where a LE  $\rightarrow$  CT transition can be unambiguously observed. These systems are generally characterized by dual fluorescence, one band originating from the LE state and another at lower energy arising from the CT state. A prototypic molecule belonging to this family is dimethylaminobenzonitrile (DMABN, 15, Figure 12). Despite

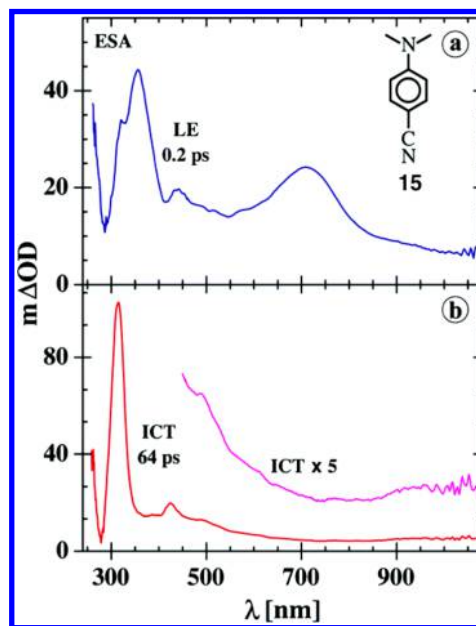


**Figure 12.** Transient absorption spectra recorded at two different time delays after 290 nm excitation of DMABN (15) in acetonitrile. The 0.2 ps (a) and 64 ps (b) spectra were assigned to the LE and ICT state, respectively. Reprinted from ref 209. Copyright 2006 American Chemical Society.

the simplicity of this molecule, the excited-state dynamics of DMABN have been debated for several decades. Whereas everybody agrees on the presence of dual luminescence of DMABN originally reported in 1961,<sup>199</sup> the structure of the state responsible for the CT emission is highly controversial. At least four different structures were proposed: a TICT state with the amino group perpendicular to the benzene plane,<sup>171,200</sup> a planar ICT (PICT) state,<sup>201–203</sup> a wagged ICT (WICT) state with a pyramidal sp<sup>3</sup> hybridized amino group,<sup>204,205</sup> and a rehybridized ICT (RICT) with the rehybridization of the CN carbon from sp to sp<sup>2</sup> and the bending of the CN group.<sup>206,207</sup>

These structures were inferred mostly from the effect of the environment on the photophysical properties of DMABN and of many of its derivatives, as well as from quantum-chemistry calculations. This has resulted in an impressively large number of studies aiming at a conclusive and unambiguous answer to this debate. We will not describe all these efforts, which were thoroughly reviewed in 2003 by Grabowski, Rotkiewicz, and Rettig,<sup>171</sup> who are at the origin of the TICT hypothesis. Before this review, most of the time-resolved studies had been carried out using time-resolved fluorescence with a resolution of a few picoseconds, at best. We will limit ourselves to the most relevant ultrafast spectroscopic studies, which were performed subsequently and give an overview of the current status of this debate.



The first ultrafast spectroscopic investigation of **DMABN** was performed in acetonitrile by Chudoba et al., who used time-resolved IR absorption to monitor the time evolution of the *N*-phenyl and CN stretching bands.<sup>208</sup> The most striking result was the absence of a CN stretching band of the LE state at early time delays and the rise of a band at  $2112\text{ cm}^{-1}$  with a time constant of 4 ps. This band, downshifted by  $103\text{ cm}^{-1}$  with respect to the CN stretching band of **DMABN** in the ground state, was ascribed to the CN vibration of the CT state, and the 4 ps rise time to the LE  $\rightarrow$  CT transition. Whereas these results did not support the RICT hypothesis, they did not allow unambiguous validation of either the TICT or the PICT models.

The first ultrafast transient electronic absorption measurements of **DMABN** were reported by Druzhinin et al.<sup>209</sup> Very clear spectral features of the LE and CT states could be observed in the 300–400 nm region (Figure 12), and the LE  $\rightarrow$  CT time constant of 4.1 ps in acetonitrile was confirmed. As the sharp absorption band of the CT state at 320 nm did not show any temporal shift from 0.2 ps after excitation, the authors concluded that large amplitude motion to a TICT state does not occur.

This conclusion is consistent with a previous study from the same group on fluorinated aminobenzonitrile derivatives.<sup>210</sup> Fluoro-substitution has a major impact on the redox properties of the molecules and was found to lead to a strong acceleration of the LE  $\rightarrow$  CT transition. This process was found to take place even in the apolar *n*-hexane with a time constant of the order of 100 to 300 fs. In acetonitrile, ET was even faster with a  $\sim 90$  fs time constant for all the fluorinated aminobenzonitriles irrespective of the amino substituents. This time constant is substantially shorter than the average solvation time of acetonitrile (260 fs)<sup>22</sup> but matches the time constant reported for inertial solvent motion. The authors thus concluded that the stabilization of the CT state brought about by the inertial component of solvation is enough to make ET ultrafast. This extremely short ET time constant was also considered as strong evidence that this process does not require a twist of the amino group to take place.<sup>210</sup>

The excited-state dynamics of **DMABN** in methanol were examined a few years later using FSRs.<sup>211</sup> Several vibrational modes of the excited state (aromatic ring breathing stretch, CH bending, C=C and CN stretches) were monitored using Raman probe wavelengths at 330 and 400 nm. The integrated intensity of these bands was found to rise with a  $\sim 6$  ps time constant, in agreement with the LE  $\rightarrow$  CT transition in this solvent. Additionally, these bands underwent a frequency up- or downshift by about  $10\text{ cm}^{-1}$  on a similar time scale. By combining these results to those obtained from transient electronic absorption, the authors proposed that the transition from the LE state to the vibrationally hot CT state takes place in 2 ps and is followed by vibrational relaxation in 6 ps. However, the FSRs data did not allow firm conclusion on the structure of the relaxed CT state to be drawn.

More recently, Joo and co-workers reported on a fluorescence up-conversion study of **DMABN** in acetonitrile.<sup>212</sup> Whereas fluorescence up-conversion investigations of **DMABN** had already performed previously, confirming the 4 ps LE  $\rightarrow$  CT transition in acetonitrile,<sup>213</sup> Joo and co-workers measured the time evolution of the whole emission spectrum by scanning the emission wavelength during the measurement, thus avoiding the laborious spectral reconstruction from single-wavelength time profiles. Access to the temporal evolution of

the whole spectrum allowed the distinction between population and solvent/vibrational relaxation dynamics. The decay of the integrated LE emission was dominated by 160 fs and 3.3 ps components. It was accompanied by a red shift attributed to the solvation of the LE state. Surprisingly, a nearly instantaneous ( $<30$  fs) rising component was also observed throughout the whole CT emission band. Additionally, a band with a maximum at 450 nm was found to rise in 160 fs and to decay and shift to the red on a few ps time scale. The integrated fluorescence intensity above 500 nm exhibited the 30 fs rise and a slower 2.7 ps component. Furthermore, the whole CT band red-shifted with a 4.8 ps time constant, i.e., much slower than the slowest component of solvation.

These data were explained with a scheme summarized in Figure 13. Optical excitation populates predominantly the  $S_2$

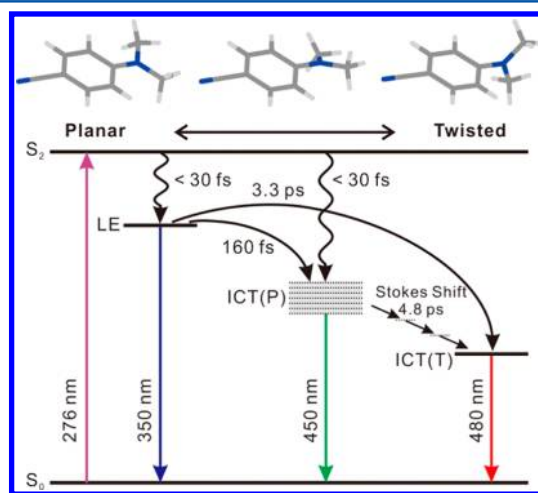


**Figure 13.** Energy-level scheme illustrating the charge-transfer pathways of **DMABN** (**15**) in acetonitrile after 276 nm excitation. Reprinted from ref 212. Copyright 2013 American Chemical Society.

state which, at the equilibrium geometry of the ground state, is a CT state and is characterized by distribution of the twisted angle of the amino group around 0 deg. In agreement with quantum-chemistry calculations by Robb and co-workers which indicate the presence of a  $S_2/S_1$  CI accessible from a large distribution of twist angles,<sup>214</sup> the population residing on the  $S_2$  surface undergoes ultrafast internal conversion via the CI to the lower excited state surface. Depending on the torsional angle and the value of other relevant intramolecular coordinates, the latter corresponds either to a LE state, to a PICT state or to a partial TICT state. It was suggested that this pathway accounts for the  $<30$  fs rising component of the CT emission. The 450 nm band of the CT emission was ascribed to the fluorescence from the PICT populated via the CI and from the LE state. Finally, the long wavelength part of the CT emission band originates from the relaxed CT state, which, according to the 4.8 ps dynamic Stokes shift, corresponds most probably to a TICT state.<sup>212</sup>

This interpretation was supported by a subsequent fluorescence up-conversion investigation by the same group of 1-*tert*-butyl-6-cyano-1,2,3,4-tetrahydroquinoline (**NTC6**, **16**, Chart 3), a rigid analogue of **DMABN**.<sup>215</sup> In this case, internal conversion from the  $S_2$  state was found to take place in 140 fs and to populate both the LE state and a CT state emitting at short wavelength (380 nm) and ascribed to a quasi PICT state. Afterward, this band shifted to 420 nm with a 1.2 ps time

constant, assigned to the equilibration of the CT state via solvation and structural relaxation. This shorter relaxation time compared to **DMABN** (4.8 ps)<sup>212</sup> was ascribed to a partial twist of the amino group, full torsion being hindered in **NTC6**. A LE  $\rightarrow$  CT transition with a 800 fs time constant could also be identified.

Additionally, a periodic oscillation of the fluorescence intensity was observed in the time profiles of the LE emission of **NTC6** in both acetonitrile and in tetrahydrofuran (Figure 14). In tetrahydrofuran the same oscillation, but  $\pi$  out of phase,

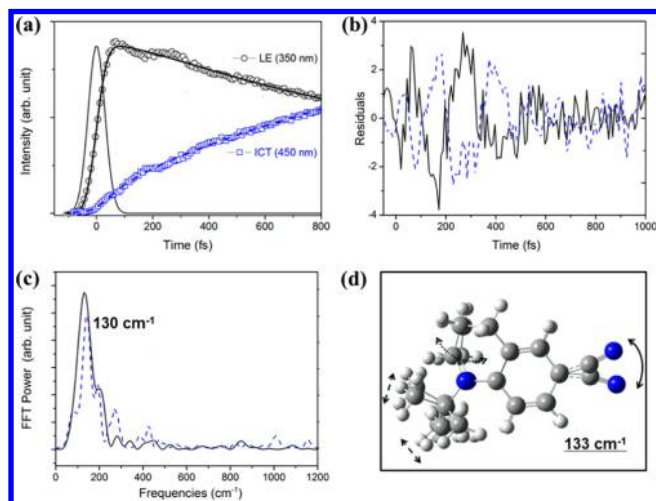


**Figure 14.** (a) Time profile of the LE (black) and CT (blue) emission of **NTC6** in tetrahydrofuran and (b) residuals from an exponential fit illustrating the phase difference of  $\pi$ . (c) Fourier transform spectrum of the residuals and (d) vibrational mode assigned to the observed coherent oscillation. Reprinted from ref 215. Copyright 2014 American Chemical Society.

was also observed with the CT emission. This oscillation was assigned to a vibrational wavepacket generated upon coherent excitation of a low frequency mode around 130 cm<sup>-1</sup>. This mode was found to mostly involve the bending of the CN group. The phase shift of the oscillation measured with the CT emission was explained by a coherent population transfer from the LE to the CT state, with about 5% of the population transferred at each period. The absence of oscillation in acetonitrile was ascribed to the limited signal-to-noise ratio of the data and to the smaller relative contribution of the LE  $\rightarrow$  CT pathway to the overall population of the CT state in acetonitrile, namely 22% vs 100% in tetrahydrofuran.

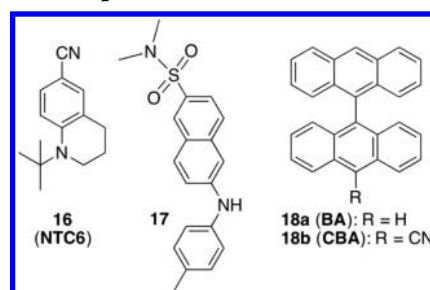
From the preceding discussion, it appears that although our understanding of the excited-state dynamics of **DMABN** has strongly progressed over the past years, thanks to the combination of ultrafast spectroscopy and quantum-chemistry calculations,<sup>216</sup> the question about the equilibrium structure of the CT state in solution still needs an unambiguous answer. However, the ensemble of experimental and theoretical data indicates that the twist of the amino group is probably not required for CT to take place, contrary to the original TICT model,<sup>200</sup> where torsion was the main CT coordinate. Therefore, if **DMABN** is indeed twisted in the equilibrated CT state, this twist should rather be viewed as structural relaxation. Considering the current progress in ultrafast spectroscopy, one should hopefully not have to wait too long for a definitive answer to this question.

TICT states were invoked for many other DA or push–pull molecules, most of these cases having already been reviewed in detail in ref 171. Therefore, we will not address the question about the twisted or not twisted nature of the CT state any further.

One of the main reasons to investigate the ET dynamics in these push–pull molecules was to test the current ET models, to determine the modes most relevant to the reaction and to find out how fast ET can be. The theoretical developments that evidenced the key role of the solvent dynamics (see section 2.1.3) stimulated substantial experimental efforts to observe solvent-controlled ET processes.

The first experimental evidence was reported by Kosower and Huppert, who investigated the fluorescence dynamics of an *N*-aryl-aminonaphthalenesulfonate (**17**, Chart 4) in a series of

**Chart 4.** Molecules Undergoing Ultrafast Intramolecular Charge-Transfer upon Photoexcitation



linear alcohols and found that the LE fluorescence lifetime was almost the same as the longitudinal dielectric relaxation time of the solvent,  $\tau_l$ , in agreement with the theoretical models of solvent controlled ET.<sup>217,218</sup>

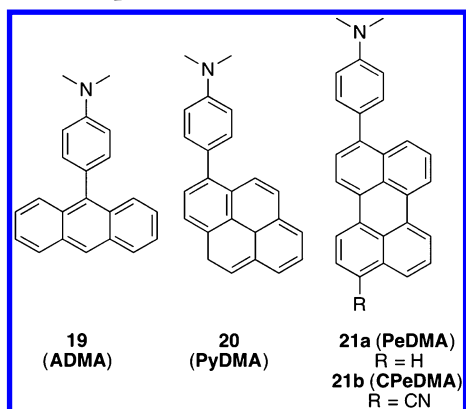
The influence of the finite response time of the solvent was also detected by a temperature dependence of the ET rate constant larger than that predicted for conventional non-adiabatic ET.<sup>219</sup> A transition from a nonadiabatic to a solvent-controlled adiabatic regime was also shown to be feasible upon lowering temperature, and slowing down dielectric relaxation.<sup>220</sup> Additionally, the fluorescence decay of the LE state of *N*-aryl-aminonaphthalenesulfonates in pentanediol was found to be nonexponential and to be reproducible using a stretched exponential function with a time constant equal to  $\tau_l$ .<sup>221</sup> This nonexponential character was ascribed to a distribution of effective solvation times due to specific H-bond solute–solvent interactions.

However, Simon and co-workers proposed that, in the case of flexible molecules, intramolecular modes involving large amplitude motion (such as the twist of a phenyl group) could also control the ET dynamics.<sup>222,223</sup> Therefore, the determination of whether structural changes or solvation is the rate determining parameter could be ambiguous from a viscosity dependence of the ET rate.

Among the various molecules used to address these questions on the role of solvent and intramolecular modes, bianthryl (**BA**, **18a**, Chart 4) and 4-(9-anthryl)-dimethylaniline (**ADMA**, **19**, Chart 5), attracted large attention.

The case of **BA** is intriguing, because this molecule cannot be considered as a push–pull compound. **BA** is apolar in the ground state with the two anthryl units forming a  $\sim 60^\circ$  dihedral angle. However, the fluorescence spectrum of **BA** was shown to strongly depend on solvent polarity, and to be characterized by an increase of the solvatochromic slope when

**Chart 5. Molecules Undergoing Ultrafast Intramolecular Charge-Transfer upon Photoexcitation**



going from weakly to more polar solvents.<sup>224</sup> This was assigned to the presence of two emitting states, a LE state with the excitation localized on one anthryl and a symmetry-broken CT state, with partially positive and negative charges on the two anthryl units.

The ultrafast excited-state dynamics of **BA** were first measured by Barbara and co-workers using fluorescence up-conversion with an IRF of  $\sim 1$  ps.<sup>225,226</sup> In alkanenitriles of varying length, the fluorescence decay observed on the blue side of the emission band was assigned to the LE  $\rightarrow$  CT transition. It was found to be ultrafast and to correlate with the longitudinal dielectric relaxation of the solvents. However, the ET time constants,  $\tau_{ET}$ , were systematically longer than  $\tau_1$  by a factor 3–5. Much better agreement was obtained using the solvation time,  $\tau_s$ , determined experimentally from the dynamic Stokes shift of a coumarin. It was concluded that the microscopic solvation dynamics are not well described by continuum dielectric theory. As discussed in section 1.2, it was shown later on that the molecular nature of the solute and solvents, neglected in the continuum model, plays a crucial role in solvation, via, e.g., the inertial motion of the molecules.<sup>21,227</sup> For this reason, the solvent relaxation does not follow a simple exponential kinetics, contrary to the predictions of the dielectric continuum model for solvents like acetonitrile or dimethyl sulfoxide, which are characterized by a single dielectric relaxation time.

Later on, the fluorescence dynamics of **BA** were simulated using a model similar to that of Zusman,<sup>92</sup> (section 2.1.3) but with several important differences:<sup>228</sup> (1) the temporal evolution of the population on the excited-state surface was calculated using the generalized Langevin equation instead of the Smoluchowski equation; (2) the excited-state free energy along the reaction coordinate was constructed within the adiabatic limit from the zero-order free-energy curves of the LE and CT states using parameters obtained from stationary absorption and emission spectra; (3) the solvent relaxation function, determined experimentally from dynamic Stokes shift measurements with a coumarin, was used as a time-dependent friction kernel. In general, an excellent agreement between the simulated and the experimental fluorescence decay of **BA** was obtained, confirming the essential role of solvation in the excited-state dynamics of **BA**.

The role of solvent fluctuation on the symmetry breaking CT in **BA** was further investigated by Mataga and co-workers, who performed the first ps transient electronic absorption measurements of **BA** in polar and apolar solvents.<sup>167</sup> The early transient

spectrum in pentanol was found to be similar to that in hexane and was dominated by positive band around 550 nm ascribed to the LE state. This spectrum evolved on a  $\sim 200$  ps time scale to a spectrum with a band around 700 nm, also observed in acetonitrile, and assigned to the CT state. The authors also investigated a **BA** derivative with one Cl atom on one of the anthryl unit and measured a faster CT, with a time constant of 140–150 ps compared to 180–200 ps for **BA**. This acceleration was assigned to the breaking of the symmetry of the molecule and of the orientation of the surrounding solvent brought about by the Cl substituent.

A few years later, the same group reported on new transient absorption measurements of **BA** with an improved time resolution and found that the rise of the CT population in alkanenitriles contains components 5 to 10 times as long as  $\tau_1$ .<sup>229</sup> This was considered as an evidence of the involvement of the torsion around the single bond between the anthryl units in the CT process.

Torsion was also invoked by Martin and co-workers, who performed transient absorption measurements of **BA** and its derivatives in ethanol and butanol. They found that the ET time constants of **BA** and anthryl-carbazole were similar to the time constant associated with the slowest component of solvation.<sup>230</sup> Additionally, they observed a loss of structure of the stimulated emission band from the LE state on a 1 ps time scale which they attributed to an “inertial contribution of the intramolecular twisting relaxation on the  $S_1$  state surface out of the Franck–Condon twist angle”. A strong acceleration of the ET dynamics was found with the cyano derivative (**CBA**, **18b** Chart 4), with the CT taking place within the 500 fs IRF of the experiment. This difference with **BA** was ascribed to the more favorable driving force upon CN substitution.

A subpicosecond loss of the structure of the LE emission of **BA** was also observed by fluorescence up-conversion.<sup>231</sup> This process was then followed by a red shift of the emission on the 20 ps time scale in ethanol. The first step was assigned to a partial planarization of **BA** through inertial motion and a partial delocalization of the excitation over the two anthryl units, whereas the second step was ascribed to the ET process, in agreement with the interpretation of Martin et al.<sup>230</sup>

The excited-state dynamics of **BA** and of its cyano derivative were revisited by Kovalenko et al. using transient absorption with 50 fs time resolution.<sup>232</sup> In addition to the band above 500 nm, the TA spectrum of the CT state was found to contain an intense band peaking at 315 nm and partially overlapping with an LE band. Global analysis of the data pointed to a LE  $\rightarrow$  CT transition in acetonitrile with a time constant of 330 fs, close to the diffusive solvation time (Figure 15). The loss of the structure of the stimulated emission spectrum, reported by Martin et al.,<sup>230</sup> was also observed, but it was shown to arise from the LE  $\rightarrow$  CT transition and to the overlap of the bands associated with these two states. In alcohols, the decay of the LE state was multiexponential with time constants very similar to those of solvent relaxation.

Upon CN substitution, the transient band of the CT state was already observed at the earliest time delay and was found to increase with a 150 fs time constant in acetonitrile. Like **BA**, the decay of the LE state in alcohols was multiexponential, with time constants similar to those of solvation, apart from the slowest component of solvation, which was absent. A new model for the ET in **BA** and **CBA** was proposed from these results. The intrinsic LE  $\rightarrow$  CT transition was suggested to take place on the 10 fs time scale. When the CT state is not low



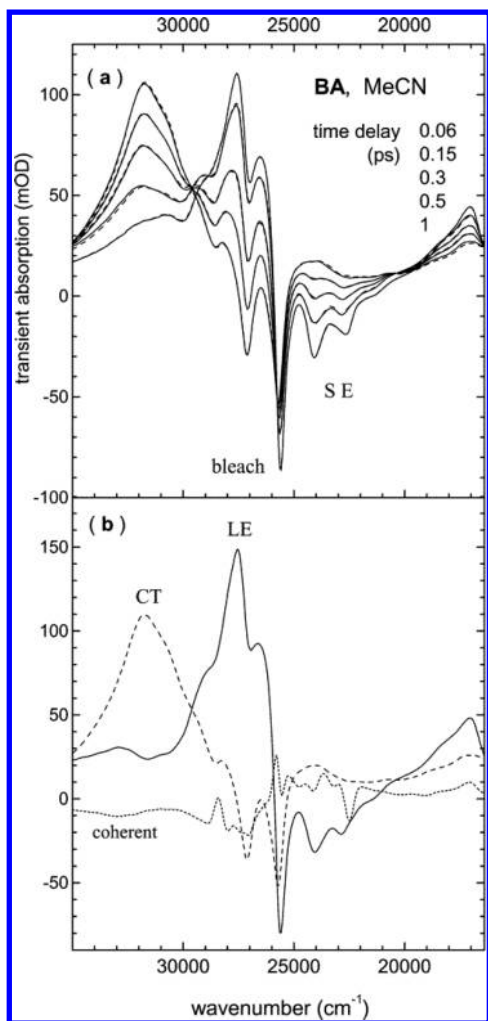


**Figure 15.** (a) Transient absorption spectra recorded at different time delays after 393 nm excitation of **BA** in acetonitrile. The dashed lines are best-fit spectra obtained by a global analysis assuming LE  $\rightarrow$  CT transition with a 330 fs time constant. (b) Species-associated difference absorption spectra obtained from the global analysis. Reprinted from ref 232. Copyright 2003 American Chemical Society.

enough relative to the LE state, this process is reversible, and both states are in equilibrium. As solvent relaxation sets in, the CT state is stabilized and the LE-CT equilibrium shifts toward the CT state. This shift increases to reach a final equilibrium value once relaxation is complete. In the more polar solvents, about 80% of the excited population is in the CT state. Therefore, according to the authors, the ET dynamics of **BA** and **CBA** are entirely determined by solvent modes and no significant contribution of the twist coordinate could be evidenced.

The excited-state dynamics of **BA** were also investigated using near-IR transient electronic absorption spectroscopy by Iwata and co-workers.<sup>233</sup> The LE and CT states were found to absorb around 1050 nm and between 1000 and >1500 nm, respectively. A 380 fs decay time of the LE band was measured in acetonitrile, in agreement with Kovalenko et al.<sup>232</sup> Later, the same group showed that the broad near-IR band observed with **BA** is absent with nonsymmetric derivatives, like **CBA** and anthryl-carbazole.<sup>234</sup> This band was attributed to a charge-resonance transition between the two states that results from the resonance interaction between the  $A^--A^+$  and  $A^+-A^-$  states.

More recently, the same group performed polarization anisotropy measurements to circumvent the complication due to the overlap of the LE and CT bands in the near-IR.<sup>235</sup> The anisotropy of the LE band was  $-0.2$ , whereas that of the CT band was  $0.4$ . In acetonitrile, this band with  $0.4$  anisotropy was found to shift from  $\sim 1500$  nm to about  $1250$  nm with a 600 fs time constant (Figure 16). The 1500 nm band was assigned to

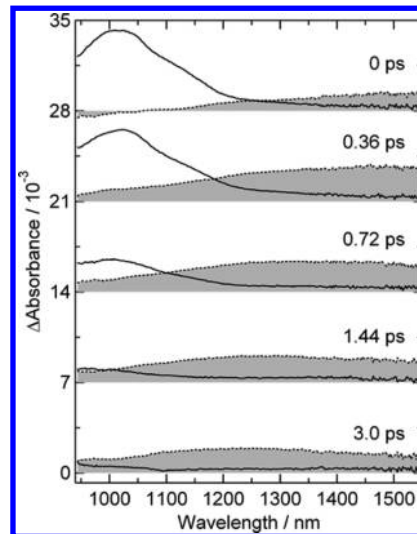


**Figure 16.** Transient absorption bands with an initial anisotropy values of  $0.2$  (LE state, solid line) and  $0.4$  (CT state, dotted line) measured with **BA** (18a) at several time delay after 393 nm excitation. Reprinted with permission from ref 235. Copyright 2009 American Institute of Physics.

a state with partial charge transfer, PCT, in fast equilibrium with the LE state. The 1250 nm band was attributed to the fully solvated CT state and the 600 fs time constant to the PCT  $\rightarrow$  CT transition, mostly through diffusive solvent motion. Overall, this interpretation is in good agreement with the model proposed by Kovalenko et al.<sup>232</sup>

Apart from bianthryl, photoinduced symmetry-breaking ICT between identical units was also reported with other systems,<sup>236–241</sup> as described in a recent review.<sup>242</sup> Ultrafast spectroscopic investigations pointed to the role of the environment as the origin of the symmetry breaking. At a given time, the instantaneous orientation of solvent molecules around the two identical chromophoric units is not the same. This is sufficient to make CT in one direction energetically more favorable than in the opposite direction. Markovic et al. demonstrated that, if the two chromophoric units are apolar, the probability that the excited unit acts as a donor or an acceptor is the same.<sup>240</sup> In this case, the asymmetry of the solvent orientation around the molecule is totally random and its direction alternates according to solvent fluctuations. The situation might be different if the chromophoric moieties had a permanent dipole that changes upon excitation.

Anthracene and *N,N*-dimethylaniline (**DMA**) represent a prototypic fluorophore/quencher or A/D pair in bimolecular photoinduced ET studies. In 4-(9-anthryl)-*N,N*-dimethylaniline (**ADMA**, 19), both units are directly connected, offering the advantage of investigating the ET dynamics without the complications arising from diffusion. This is why **ADMA** and its close derivatives were intensively studied to obtain a deeper insight into ultrafast ICT processes. The first subnanosecond investigation of **ADMA** was performed by Mataga and co-

workers, who observed a strong solvent dependence of the transient absorption spectrum measured 200 ps after excitation.<sup>243</sup> This effect was ascribed to the existence of two nearby excited states differing in their polarity, in agreement with previous investigations by Grabowski et al. using stationary electronic spectroscopy, where dual fluorescence associated with an LE and a CT emission was reported.<sup>244</sup>

Huppert and Rentzepis measured the LE fluorescence decay of **ADMA** using a streak camera with 5 ps time resolution and found nonsingle exponential dynamics that could be reproduced using a biexponential function, with the slow component correlating well with  $\tau_i$ .<sup>245</sup> However, the origin of the fast component could not be established. The authors concluded that ET in **ADMA** is mostly controlled by solvation and not by internal motion like the twist of the **DMA** unit, for example, as suggested earlier by Grabowski et al.<sup>244</sup>

A few years later, the fluorescence dynamics of **ADMA** were reinvestigated using fluorescence up-conversion with a time resolution of  $\sim 100$  fs after deconvolution.<sup>246</sup> Using spectral reconstruction, the authors could monitor the temporal evolution of the emission spectrum from the LE to the CT band. The results revealed that, in dimethylformamide, the LE band is no longer present after  $\sim 300$  fs and that the ensuing spectral dynamics are very similar to those due to solvent relaxation. The LE fluorescence decay was found to be nonexponential with an average decay time significantly shorter than the average solvation time measured with a coumarin. To simulate the observed LE dynamics, the authors applied a similar theoretical model as that developed for **BA** based on the generalized Smoluchowski equation for the diffusion of the probability distribution on the excited-state potential.<sup>228</sup> The latter was constructed assuming adiabatic coupling between the LE and CT potentials, with their main parameters determined from the stationary absorption and emission spectra. Finally, the solvent correlation function,  $C(t)$ , eq 1, was used to calculate the diffusion coefficient. With this model, the authors could successfully reproduce the absorption spectrum of **ADMA**, the temporal evolution of the emission spectrum as well as the LE fluorescence decay and its nonexponential character. Furthermore, an excellent agreement between the measured and simulated average LE fluorescence lifetimes was found.

In previous experimental investigations of the intramolecular ET dynamics in such highly coupled DA systems, the ET rate constant was taken as the inverse decay time of the LE fluorescence. In these cases, however, the lower excited states,  $S_1$  and  $S_2$ , are neither purely LE or CT states but can be described as adiabatic mixtures:<sup>246</sup>

$$|S_n\rangle = C_{LE}^{(n)}(Q)|LE\rangle + C_{CT}^{(n)}(Q)|CT\rangle, (n = 1, 2) \quad (26)$$

where  $Q$  is the position along the reaction coordinate. The relationship between experimental observables and the ET rate constants was addressed by Barbara, Fonseca and co-workers.<sup>247</sup> They showed that, in this case, the ET rate is time dependent,  $k_{ET}(t)$ , and can be expressed by

$$k_{ET}(t) = \frac{d \ln[S_G(t) - S_G(\infty)]}{dt} \quad (27)$$

where  $S_G$  is the generalized survival of the electronic charge on the donor unit divided by the charge of an electron. It was approximated as

$$S_G(t) = \frac{\vec{\mu}_{LE \leftarrow S_0}[B(t)]^{1/2} - \vec{\mu}_{CT \leftarrow S_0}[\vec{\mu}_{LE \leftarrow S_0}^2 + \vec{\mu}_{CT \leftarrow S_0}^2 - B(t)]^{1/2}}{(\vec{\mu}_{LE \leftarrow S_0}^2 + \vec{\mu}_{CT \leftarrow S_0}^2)^2} \quad (28a)$$

with

$$B(t) \propto \frac{A(t)}{A(\infty)} \quad (28b)$$

where  $\vec{\mu}_{LE \leftarrow S_0}$  and  $\vec{\mu}_{CT \leftarrow S_0}$  are the  $LE \leftarrow S_0$  and  $CT \leftarrow S_0$  transition dipole moments, respectively, and  $A$  is the fluorescence intensity integrated over the whole spectrum.

In the nonadiabatic limit, where the coupling between the D and A units is small and the reactant and the product states are separated by a well-defined barrier,  $S_G(t)$  is well described by the LE fluorescence decay measured at a single wavelength,  $I(\lambda, t)$ . This is also the case in the adiabatic limit in the case of a high activation barrier. In other cases, the ET dynamics is reflected by the temporal evolution of the emission band area. The time dependence of the ET rate is due to three main factors: (i) the dependence of the  $C_{LE}$  coefficients on the reaction coordinate,  $Q$ , (ii) the shape of the excited-state potential at the  $Q$  position where the excited-state population is initially prepared, and (iii) the time dependence of the diffusion coefficient  $D(t)$ .

The authors also showed that, in the case of **ADMA**, the long-time limit of the ET rate,  $k_{ET}(\infty)$ , in dimethylformamide is equal to the inverse of the longer solvation time constant. For **ADMA**, the ET is essentially barrierless and the time evolution of the excited-state population along the reaction coordinate is not far from that associated with pure solvent relaxation. On the other hand, the ET in **BA** involves a small barrier, and, as a consequence, the time evolution of the fluorescence shows the decay of one band and the rise of the 'product' band, instead of a continuous shift as for **ADMA**. In this case, the survival probability,  $S_G(t)$ , can be directly determined from the time dependence of the LE fluorescence. The authors concluded that the determination of the intramolecular ET dynamics for any given highly coupled DA molecule requires first a careful estimation of the excited-state potential.

Despite the very good agreement between the experiment and the theoretical model used by Barbara and co-workers that involves mostly a solvation coordinate, additional experimental investigations of the excited-state dynamics of **ADMA** were subsequently reported. Staerk and co-workers compared the excited-state dynamics of **ADMA** and of pyrene-DMA (**PyDMA**, 20, Chart 5) in hexanol and octanol using transient electronic absorption and time-resolved fluorescence.<sup>248</sup> No emission that could be associated with the LE state could be observed with any of the molecules. This was interpreted as a  $LE \rightarrow CT$  transition faster than the  $\sim 7$  ps time resolution of their experiment. However, a continuous red shift of the emission band, attributed to the CT emission was observed with both **ADMA** and **PyDMA**. The  $\sim 50\%$  slower shift measured for **ADMA** compared to **PyDMA** and to the average solvation time was interpreted as an evidence of structural changes such as the population of a TICT state for **ADMA**, but not for **PyDMA**.

More recently, Martin and co-workers reported on a transient absorption study of **ADMA** in various solvents with a  $\sim 1$  ps time resolution.<sup>250</sup> Although the transient data did not

exhibit very strong spectral dynamics except for that associated with the shift of the stimulated emission band, the authors attributed the decay of a transient band with a maximum around 360 nm to the LE  $\rightarrow$  CT transition. In the most polar solvents, namely benzonitrile, ethanol, propanol and butanol, this LE band was found to have decay components longer than the average solvation time. The authors suggested that the LE  $\rightarrow$  CT transition is not barrierless as proposed by Barbara and co-workers<sup>246</sup> but is thermally activated with a small barrier. The authors proposed that this barrier is associated with the torsion of the anthryl-DMA bond and therefore the CT process is not entirely controlled by solvation but also involves the twist coordinate. However, the Barbara model for ADMA predicts that the long-time limit of the ET rate,  $k_{\text{ET}}(\infty)$  is equal to the inverse of the longer solvation time constant,<sup>246</sup> which, as shown in ref 22, can be substantially larger than the average solvation time. For example, the average solvation time of ethanol is 16 ps, whereas 50% of the solvent relaxation is associated with a 30 ps time constant. Therefore, LE  $\rightarrow$  CT time constants larger than the average solvation time, as reported above,<sup>248,250</sup> do not contradict the Barbara model and cannot be considered as an evidence of the involvement of intramolecular modes with large amplitude motion.

The role of solvation and high-frequency modes in the intramolecular dynamics of such a DA system was recently confirmed by a combined fluorescence up-conversion and transient electronic absorption study of perylene-DMA (PeDMA, 21a, Chart 5) and its cyano derivative (CPeDMA, 21b, Chart 5) in solvents ranging from tetrahydrofuran to acetonitrile, including a RTIL.<sup>249</sup> Whereas with PeDMA, the ET dynamics coincided well with the diffusive component of solvation, the ET in CPeDMA was substantially faster but remained slower by a factor  $\sim 2$  than inertial solvation (Figure 17). This difference was ascribed to the larger ET driving force

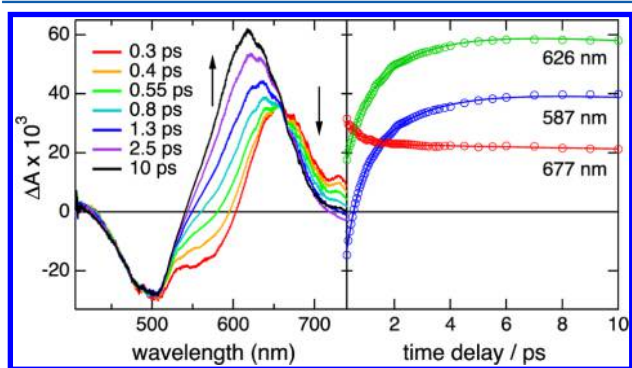
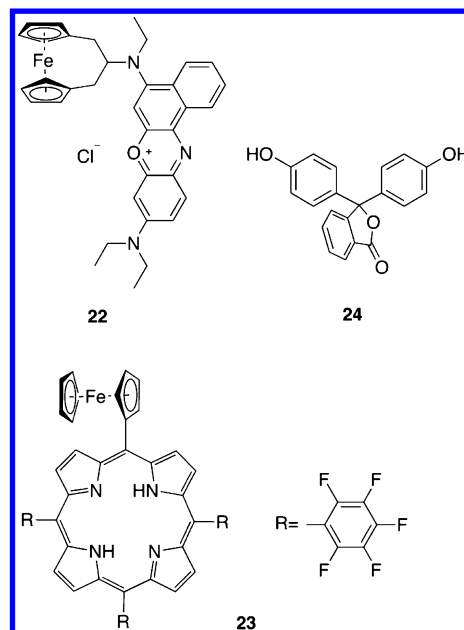


**Figure 17.** (left) Transient absorption spectra recorded at various time delays after 490 nm excitation of CPeDMA (21b) in dimethyl sulfoxide. The arrows point to the changes due the LE  $\rightarrow$  CT transition. (right) Time evolution at three representative wavelengths and best fits from a multiexponential global analysis. The LE  $\rightarrow$  CT transition is associated with 480 fs and 1.8 ps time constants. Reprinted from ref 249. Copyright 2008 American Chemical Society.

for CPeDMA and was qualitatively discussed in terms of the Sumi-Marcus model (section 2.1.4). For CPeDMA, inertial solvation almost suffices to make the activation barrier low enough for CT to be ultrafast. In this case, the high-frequency intramolecular modes play an important role. For PeDMA on the other hand, the entire solvation energy is needed to make the CT energetically feasible and thus ET cannot be faster than solvent relaxation.

Even faster intramolecular ET was reported. For example, Baigar et al. investigated a DA system consisting of Nile Blue covalently linked to a ferrocene donor (22, Chart 6) in ethanol

**Chart 6. Molecules Undergoing Sub-120 fs Intramolecular Electron Transfer upon Excitation**



using pump–probe spectroscopy with a 15 fs IRF and deduced an ET time constant of  $\leq 100$  fs, close to the inertial response of the solvent.<sup>251</sup> A similar ET time constant was observed by Kubo et al. with a free-base porphyrin linked to a ferrocene (23, Chart 6) in benzene and tetrahydrofuran.<sup>252</sup> Like Baigar et al., the authors observed a periodic oscillation of the pump–probe signal due to the excitation of a vibrational coherence. However, Baigar et al. concluded that, in their case, the oscillation was due to a wavepacket on the Nile Blue unit and did not play a significant role in the ET.<sup>251</sup> In the other case, Kubo et al. found that the Fourier-transform spectrum of the oscillation measured with the DA system contained bands that were not present with the porphyrin alone.<sup>252</sup> From the relative phase of the oscillations, the authors concluded that the wavepackets observed with the porphyrin alone were associated with ground-state vibrations and were generated upon impulsive stimulated Raman scattering (ISRS). However, other oscillations present only in the DA system were ascribed to the  $S_1$  state. As they remained visible until time delays of a few picoseconds, the authors suggested that they might still be present in the CT state and could point to coherent electron transfer.

More recently, Riedle and co-workers reported on the ET dynamics in phenolphthalein (24) which can be viewed as a  $D_2A$  system.<sup>253</sup> Upon local excitation of one of the subunits of 24 at 270 nm, ultrafast buildup of the donor cation with a rise time of 50 fs was observed in acetonitrile by transient absorption (Figure 18). The authors concluded that the ET in phenolphthalein is even faster than the inertial component of solvation and that the process is largely dominated by intramolecular modes. This was also supported by the observation of ultrafast ET in the structurally similar malachite green lactone in nonpolar solvents.<sup>253</sup>



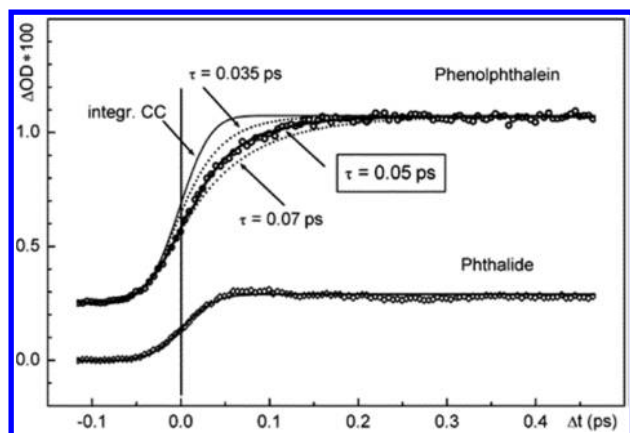


**Figure 18.** Time profiles of the transient absorption at 475 nm measured with phenolphthalein (**24**) and phthalide in acetonitrile. The transient absorption of **24** was ascribed to the phenol radical cation and that of phthalide to a local excited state. Simulated profiles assuming instantaneous rise (solid) or 35 and 70 fs rise times (dotted) are also shown. Reprinted from ref 253. Copyright 2003 American Chemical Society.

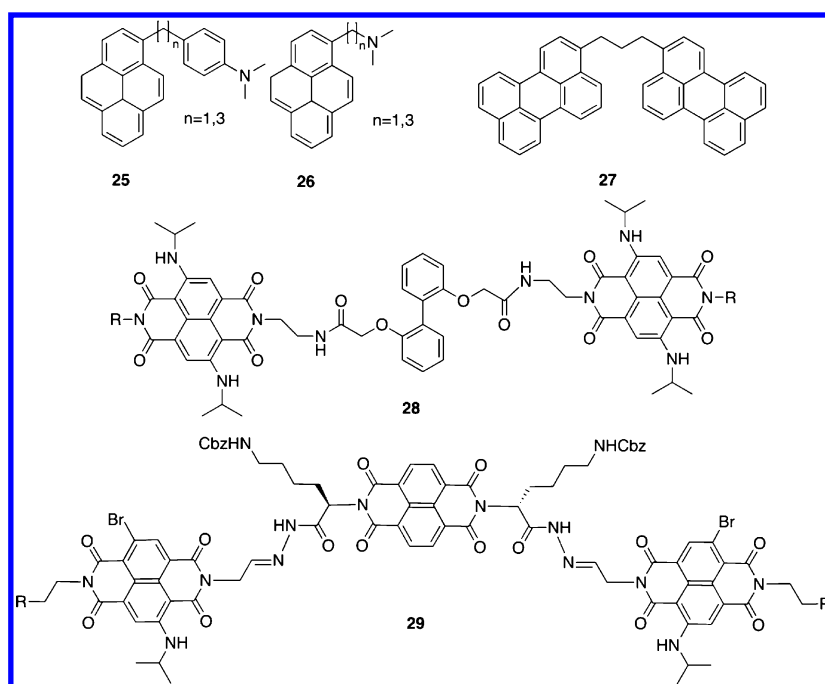
The above examples reveal that a general picture of the intramolecular ET dynamics in highly coupled DA systems is difficult to draw. Indeed each system behaves differently depending not only on the driving force, but also on the electronic coupling and on the structural flexibility. These parameters influence the shape of the excited-state potential along the reaction coordinate. In this respect, the approach proposed by Barbara and co-workers seems to be the most rigorous. They consider the reaction coordinate to be essentially a solvent coordinate. However, extensions of this model should be envisaged to account for ET in flexible molecules as well as for ET processes occurring on a similar or faster time scale than inertial solvation.

### 2.2.5. Charge Separation in Moderately to Weakly Coupled Systems.

Like ADMA, systems with moderate to weak electronic coupling contain well-defined donor and acceptor units. However, contrary to ADMA, these units are generally not directly linked by a single covalent bond but rather through a bridge that ensures a larger distance and hence a smaller coupling between the D and A moieties. Therefore, these systems will be hereafter abbreviated as D-B-A, where B stands for the bridging unit. A consequence of this smaller coupling is that, in general, the electronic absorption spectrum of such D-B-As does not exhibit a CT band. In fact, the absorption spectrum is essentially the composite of that of the individual D, B and A constituents. For the same reason, CT emission is usually not observed unless the bridge is long and flexible enough to allow folding and large through-space DA coupling. As a consequence, CT in these systems is almost complete and the ensuing state is usually called charge-separated state. For the majority of these D-B-As, the ET dynamics, which comprise the initial photoinduced CS and the ensuing CR, was rationalized using the semiclassical model for nonadiabatic ET or that for solvent-controlled ET. This is due to the moderate to weak electronic coupling that makes ET generally slower than relaxation phenomena. However, this is not always true and we will focus here on cases where the reaction occurs from a nonequilibrated state. There are numerous literature examples where ultrafast ET taking place on shorter time scales than that of diffusive solvent relaxation was observed, and for which nonequilibrium dynamics can be expected.<sup>254–258</sup> However, we will only discuss cases where nonequilibrium electron-transfer dynamics were specifically addressed.

**2.2.5.1. Influence of Structural Fluctuations on the Electron Transfer Dynamics.** Depending on its nature, the bridging in D-B-A systems can introduce substantial conformational flexibility that can lead to different mutual orientations and/or distances between the D and the A moieties. This can have a significant impact on the ET dynamics mostly because of

**Chart 7.** D-B-A Systems with Flexible Bridging Units



the dependence of the electronic coupling on the distance and the orientation. If this flexibility leads to a strong modulation of the coupling, the reaction might only be possible in a limited range of conformations. Therefore, depending on the equilibrium distribution of geometries, conformational changes may be required before the CS can become operative. This situation bears some analogy with the intermolecular ET processes, where the reactants have to diffuse, but here motion is much more restricted. In such cases, the observed decay of the excited state or the charge-separated state can follow complex nonexponential dynamics.

A strong entanglement between diffusion and CS was already reported by Mataga and co-workers with D-B-A systems consisting of a dimethylaniline or a dimethylamine donor covalently attached to an anthracene or a pyrene acceptor through an alkyl chain of varying length (25, 26, Chart 7).<sup>259,260</sup> The rise of the charge-separated state population was found to become faster with increasing solvent polarity but to slow down as viscosity was increased. This was ascribed to the occurrence of partially hindered rotation and translation of the A and D units associated with the alkyl chain dynamics that lead to favorable conformations for the CS. However, given the state of the transient absorption spectroscopy at that time, the data did not allow for detailed analysis of the CS dynamics to be performed.

Clear departure from monoexponential CS dynamics were reported in several more recent investigations of D-B-A system with flexible bridges, such as 27–29 (Chart 7).<sup>240,261–263</sup> In many cases, the decay of the excited-state population could be well reproduced with a biexponential function. A bimodal decay does not necessarily imply the existence of two conformers with distinct CS time constants but may be due to a distribution of conformations, and hence, of CS time constants. Kinetics resulting from a Gaussian distribution are indeed well-known to be properly reproduced with a biexponential function.<sup>264–266</sup>

However, if conformational fluctuations occur on the same time scale as the charge separation, the observed dynamics can become strongly nonexponential. Zhong and co-workers observed such a situation with the D-B-A 30 (Chart 7).<sup>267</sup> In water, this molecule was shown to exist in two different forms: 1) a stacked form, where the DA distance is the shortest and the CS is the fastest, with a  $\sim 700$  fs time constant, 2) a C-clamp form with a fluctuating DA distance and with CS occurring on a 100 ps time scale (Figure 19). In acetonitrile, only the C-clamp form was present. The fluorescence decay associated with the C-clamp population was best reproduced with a stretched exponential function with a stretch factor between 0.7 and 0.8 depending on the solvent.

The authors rationalized this fluorescence dynamics,  $I_{\text{fl}}(t)$ , in terms of a time-dependent CS rate coefficient,  $k_{\text{CS}}(t)$ :

$$I_{\text{fl}}(t) = I_{\text{fl}}(0) \exp\left[-k_{\text{fl}}t - \int_0^t k_{\text{CS}}(t') dt'\right] \quad (29)$$

where  $k_{\text{fl}}$  is the rate constant for the deactivation of the excited chromophore in the absence of charge separation. The time dependence of  $k_{\text{CS}}$  was associated with the temporal variation of the DA distance, itself assumed to be periodic with an angular frequency  $\omega$ :

$$k_{\text{CS}}(t) = k_{\text{CS,e}} \exp[-\beta \Delta d_{\text{DA}} \cos(\omega t)] \quad (30)$$

where  $k_{\text{CS,e}}$  is the CS rate constant at the equilibrium DA distance,  $\beta$  is the attenuation factor, and  $\Delta d_{\text{DA}}$  is the variation amplitude of the DA distance. The authors could reproduce the

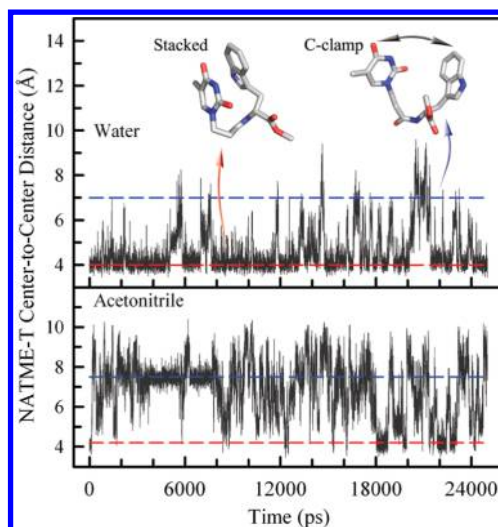


**Figure 19.** Fluctuations of the center-to-center distances between the indole ring and the thymine ring of 30 obtained from molecular dynamics simulations in water (top) and acetonitrile (bottom). The red and blue dashed lines correspond to the stacked and partially folded C-clamp forms, respectively. Reprinted from ref 267. Copyright 2012 American Chemical Society.

observed CS dynamics with this model assuming an oscillation period,  $T = 2\pi/\omega$ , between 20 and 50 ps, an attenuation factor  $\beta$  between 1 and  $1.4 \text{ Å}^{-1}$  and a  $\Delta d_{\text{DA}}$  value ranging from 0.7 to  $1.6 \text{ Å}$ , depending on the solvent. They showed that the stretched character of the fluorescence decay increased with  $\Delta d_{\text{DA}}$ .

Other studies focused on conformational changes that only affect the mutual orientation of D and A but leave the through-bond distance constant. Hochstrasser and co-workers investigated the relationship between the charge-separation dynamics and torsional angle between the aromatic planes of the D and the A moieties in the D-B-A system 31 (Chart 7), using polarized transient IR absorption spectroscopy.<sup>268</sup> The initial anisotropy values of the transient bleaches pointed to a mean interplanar torsional angle of about  $50^\circ$  in the ground state. On the other hand, from the time evolution of the anisotropy of the anion band, and considering that the charge recombination in this D-B-A is about 7 times faster than the separation, i.e.,  $k_{\text{CR}} = 22 \text{ ps}^{-1}$  and  $k_{\text{CS}} = 3.3 \text{ ps}^{-1}$ , the authors concluded that the CS occurred first in the D-B-A's with the smallest torsion angle ( $\sim 50^\circ$ ) and then in the D-B-A's with increasingly large angle.

A strong correlation between rotational diffusion and CS was observed by Duvanel et al. with the D-B-A system 32 (Chart 8).<sup>269</sup> In moderately to highly polar solvents, the fluorescence lifetime of the bodipy donor was found to vary between 18 to 50 ps vs 3.3 ns in toluene. This lifetime was independent of solvent polarity but correlated very well with solvent viscosity and with the experimentally measured reorientational time of the bodipy chromophore alone (Figure 20). This dependence was explained by a decrease of the through-space DA distance upon twisting motion of the bodipy around the single bond to the triptcene. Therefore, the measured dynamics reflected this motion rather than the charge separation itself.

**2.2.5.2. Electron Transfer Faster than Solvation or Independent of Solvent Polarity.** Ultrafast charge separation, either controlled by solvent relaxation or occurring on shorter time scales, was also observed with D-B-A or moderately coupled DA dyads. One of the earliest observations was

Chart 8. D-B-A Systems Undergoing Ultrafast Intramolecular Charge Separation upon Excitation

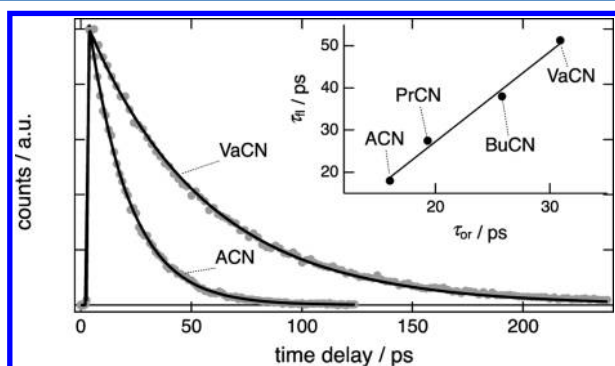
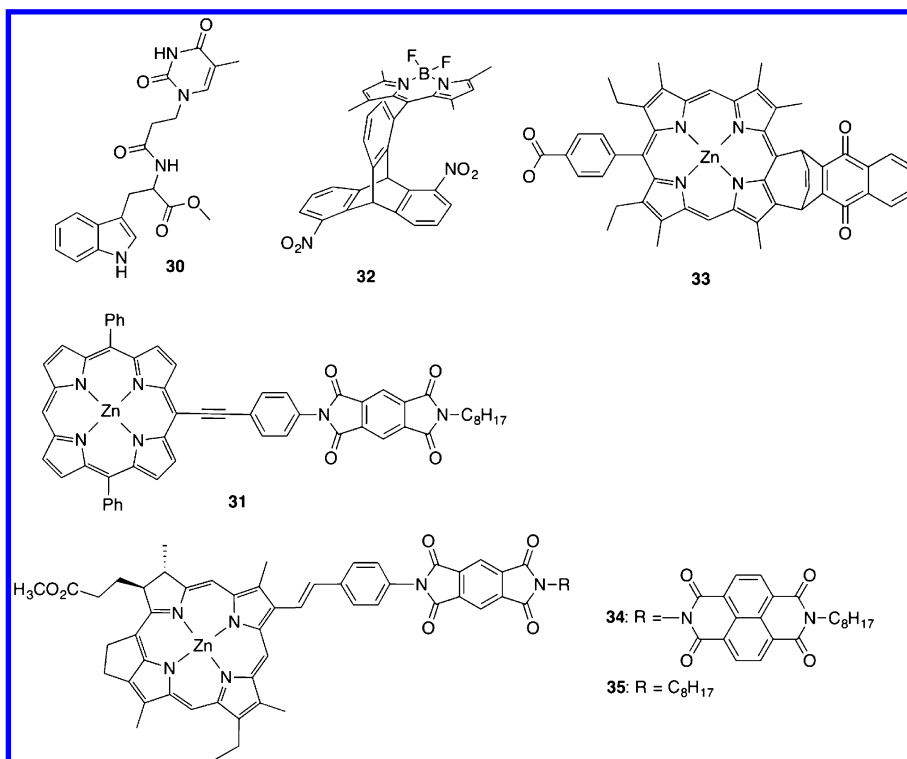


**Figure 20.** Time profile of the fluorescence intensity of 32 in acetonitrile and valeronitrile. Inset: correlation between the fluorescence lifetime of 32 and the reorientational time of the bodipy dye alone in solvents of increasing viscosity (ACN: acetonitrile; PrCN: propionitrile; BuCN: butyronitrile; VaCN: valeronitrile). Adapted from ref 269. Copyright 2007 American Chemical Society.

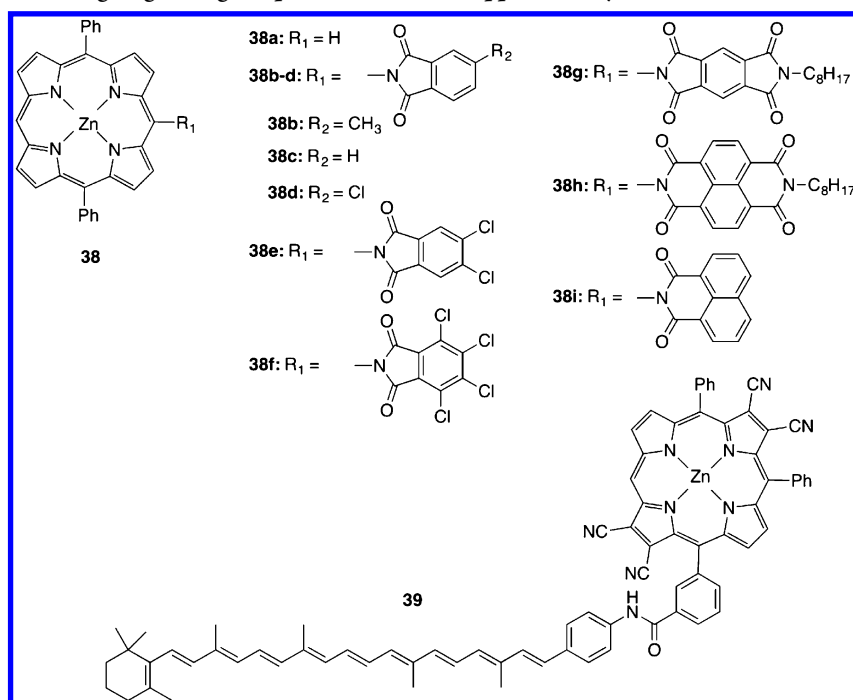
reported with a zinc porphyrin-quinone D-B-A system, where CS was found to occur with a 5.5 ps time constant in benzonitrile, very close to the 5.3 ps relaxation component of this solvent.<sup>270</sup> A few years later, MacPherson reported even faster CS in the D-B-A 33.<sup>271</sup> The rise time of the charge-separated state population was found to be essentially independent of the solvent polarity with time constants of 250, 200, and 330 fs in benzene, dichloromethane and benzonitrile, respectively. This is clearly faster than the diffusive relaxation components of dichloromethane and benzonitrile.<sup>22</sup> The absence of a solvent dependence was explained by the substantial CS driving force increasing from 0.23 to 0.8 eV with polarity. Therefore, solvation energy is not needed to make the CS energetically favorable. The authors suggested that CS in this dyad is mostly driven by intramolecular modes.

Ultrafast CS and weak solvent polarity dependence were also observed with the triad 34 and the dyad 35 (Chart 8).<sup>272</sup> In both cases, the CS driving force was already positive ( $-\Delta G_{cs} = 0.2$  eV) in toluene. In this solvent, CS in the triad was found to take place in less than 130 fs. The transient absorption band of the pyromellitimide acceptor anion was initially broadened on its red side and narrowed in a few picoseconds. This was explained by the population of the charge-separated state in a vibrational excited state and the subsequent cooling by intermolecular vibrational relaxation. This observation pointed to the predominant role of intramolecular modes in the CS dynamics of this triad. Interestingly, charge separation from the excited chromophore to the pyromellitimide was found to be slower in the dyad than in the triad. However, a 280 fs CS time constant was measured with the dyad in butyronitrile, i.e., much shorter than the diffusive relaxation time of 3.8 ps measured with this solvent.<sup>29</sup>

**2.2.5.3. Electron Transfer from an Upper Locally Excited State.** We now address intramolecular electron transfer processes occurring from an upper electronic excited state of the chromophoric unit. Although such processes do not necessarily follow nonequilibrium dynamics, they are worth discussing because they are exceptions of the well-known Kasha-Valilov rule that states that emission and photochemistry takes place from the lowest electronic excited states, i.e., the  $S_1$  and  $T_1$  states for closed-shell molecules. This rule is based on the ultrashort lifetime of upper excited states originating from the efficient internal conversion to nearby states of the same multiplicity and very fast vibrational relaxation. Thus, to take place from an upper excited state, ET has to be ultrafast and to occur on a similar time scale as internal conversion. Upper excited states were mostly exploited for ET reactions because of their higher energy, enabling ET reactions that are not operative from the  $S_1$  state or for exploring highly exergonic processes.



Chart 9. D-B-A Systems Undergoing Charge Separation from an Upper Locally Excited State



Zinc porphyrin (ZnP) is one of the few exceptions of Kasha's rule as it exhibits  $S_2 \rightarrow S_0$  emission (B/Soret band emission). However, contrary to the well-known azulene,<sup>273,274</sup> its  $S_2$  fluorescence lifetime is very short, and, in the case of zinc tetraphenylporphyrin, varies from 1 ps to about 2.5 ps depending on the solvent.<sup>275,276</sup> However, this lifetime can be sufficiently long for intramolecular CS to take place, as shown by Mataga and co-workers who investigated the  $S_2$  fluorescence dynamics of dyads consisting of a ZnP unit covalently attached to acceptors of varying strength (38b–h Chart 9).<sup>111,277,278</sup> The authors found that the  $S_2$  fluorescence dynamics of the ZnP unit accelerated substantially, but remained exponential, in the presence of the attached acceptor. Transient absorption measurements with 38g showed a buildup of the A<sup>•</sup> radical anion, pointing to the occurrence of CS from the  $S_2$  state.

The CS rate constants determined by comparing the  $S_2$  fluorescence decays with and without A was found to increase from 3.5 ps<sup>-1</sup> (38b) to 6 ps<sup>-1</sup> (38e) with increasing driving force up to  $-\Delta G_{CS} \sim 1$  eV in acetonitrile and then to decrease down to 1.5 ps<sup>-1</sup> (38h) by further increasing the driving force to 1.5 eV (Figure 21). This bell-shape dependence of the CS rate constant could be well reproduced with the semiclassical expression for nonadiabatic ET (eq 5). This result represents the first unambiguous observation of the Marcus inverted region for intramolecular photoinduced CS. Similar CS dynamics and driving-force dependence were observed in the viscous glycerol triacetate, despite its very slow average relaxation time.<sup>225</sup> To explain this, the authors invoked the inertial component of the solvation that is enough to make ultrafast CS operative. Very similar dynamics were observed in the quasi nonpolar toluene.<sup>277</sup> This unexpected result was explained by the crucial role of high-frequency intramolecular modes in ultrafast ET processes.

Charge separation from the  $S_2$  state of ZnP was also exploited by Hammarström and co-workers for the conception of an A<sub>1</sub>-D-A<sub>2</sub> optical switch, in which the CS direction could be chosen depending on whether the ZnP donor is excited to

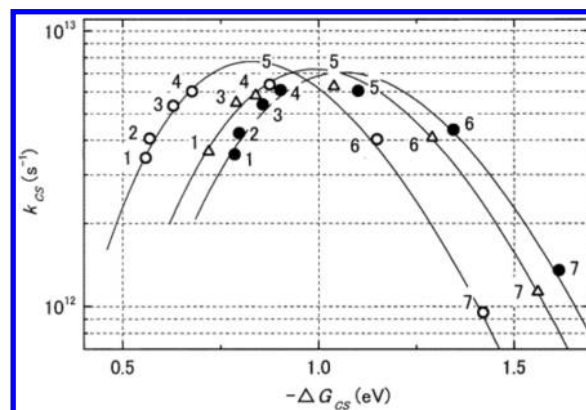


**Figure 21.** Driving-force dependence of CS in 38b–h upon local  $S_2$  excitation of the ZnP unit in tetrahydrofuran (empty circles), glycerol triacetate (empty triangles) and acetonitrile (filled circles) and best fit of eq 5 (1: 38b, 2: 38c; 3: 38d; 4: 38e; 5: 38f; 6: 38g; 7: 38h). Reprinted from ref 111. Copyright 2001 American Chemical Society.

the  $S_1$  (Q-band excitation) or to the  $S_2$  state (B band excitation).<sup>279</sup> To explore the feasibility of this idea, the authors investigated the excited-state dynamics of A<sub>1</sub>-D and D-A<sub>2</sub> (38i) dyads. In the first dyad, the CS state was below the local ZnP  $S_1$  state allowing CS upon  $S_1 \leftarrow S_0$  excitation. The charge-separated state of the second dyad (38i), D<sup>+</sup>-A<sub>2</sub><sup>-</sup>, was between the locally excited  $S_2$  and  $S_1$  state of ZnP in apolar and moderately polar solvents, and below the  $S_1$  state in more polar solvents (Figure 22). Ultrafast, <1 ps, population of the D<sup>+</sup>-A<sub>2</sub><sup>-</sup> state upon local  $S_2$  excitation could be observed upon monitoring the absorption of A<sub>2</sub><sup>-</sup> in tetrahydrofuran and more polar solvents. In tetrahydrofuran, the population of the charge-separated state was found to decay very rapidly to zero, whereas in the more polar solvents, it exhibited an initial decay on the sub-picosecond time scale followed by a  $\sim 10$  ps rise. The results in tetrahydrofuran were explained by ultrafast CR of the D<sup>+</sup>-A<sub>2</sub><sup>-</sup> state back to the lower-lying neutral  $S_1$  state,

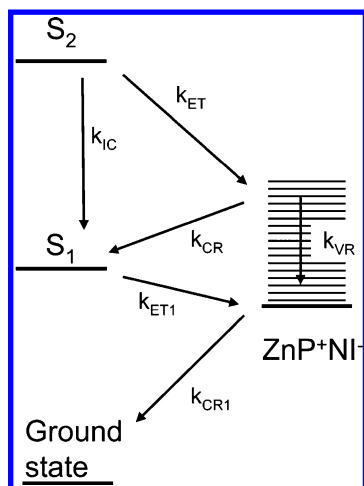


**Figure 22.** Energy-level scheme illustrating the charge-transfer processes in the dyad **38i** with hot charge recombination to the locally excited state of the Zn porphyrin unit. Reprinted from ref [279](#). Copyright 2010 American Chemical Society.

$D^*(S_1)-A_2$ . In the other solvents, the initial decay was attributed to CR from the vibrationally hot  $D^+-A_2^-$  state to  $D^*(S_1)-A_2$ , and the ensuing rise was explained by CS from the equilibrated  $D^*(S_1)-A_2$  state to  $D^+-A_2^-$  (Figure 22). The authors concluded that optical switching in an  $A_1-D-A_2$  should indeed be operative but would require optimization to inhibit CR to the local  $S_1$  state.

The intramolecular CS dynamics from the locally excited  $S_2$  state of ZnP-based dyads as well as the ensuing ET process were investigated theoretically by Ivanov and co-workers using the so-called stochastic point-transition model of electron transfer.<sup>280–284</sup> For this, the authors numerically solved the equations of motion of the diagonal elements of the density matrix. They considered three or four electronic states ( $S_2$ ,  $S_1$ , charge-separated and ground state) as well as vibrational levels of a single or of multiple high-frequency modes (Figure 23). These equations included the diffusion on the free energy surfaces along the solvent coordinate, the probability of ET from vibrational sublevels of the initial state to sublevels of the

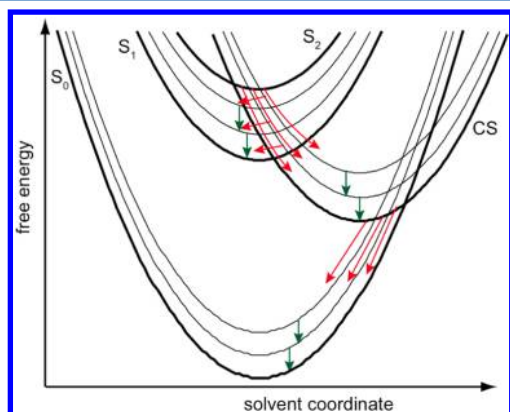


**Figure 23.** Cuts in the free energy surfaces of the ground, first, and second electronic excited states and charge-separated state along the solvent coordinate for a ZnP-based D-B-A system. The thin parabolas stand for vibrational excited states. The green and red arrows represent vibrational and solvent relaxation, respectively. ET can take place at each intersection of the parabolas. Adapted with permission from ref [284](#). Copyright 2015 Elsevier B.V.

final state, and the decay of the vibrational excited levels. Solvent relaxation was described as a sum of exponential functions to account for the inertial and diffusive components of solvation. The ET rate was calculated using the Zusman expression, and a vibrational relaxation time constant of 100 fs, corresponding to the fastest stage of the intramolecular vibrational redistribution of the high-frequency modes, was assumed. The authors could qualitatively reproduce the population dynamics of the ZnP-based dyads reported by the Mataga's and the Hammarström's groups.<sup>111,279</sup>

Apart from those mentioned above, unambiguous observations of CS from the local  $S_2$  state of ZnP are scarce. One of the reasons is that the  $S_2$  lifetime of ZnP tends to shorten upon attachment to a bridging or quenching unit. Such functionalization leads to a distortion of the molecule and a decrease of its symmetry that enhances internal conversion to the lower electronic excited state.<sup>285–287</sup> As a consequence, an acceleration of the  $S_2$  fluorescence dynamics upon attachment of a D or an A unit cannot simply be ascribed to CS unless the charge-separated state is clearly identified.

ZnP, like other metallo-porphyrins, has  $D_{4h}$  symmetry with degenerate  $S_1$  and  $S_2$  states, which can be populated from the ground state via the  $Q_x/Q_y$  and  $B_x/B_y$  transition dipole moments, respectively.<sup>288</sup> Using polarization anisotropy measurements with magnesium porphyrin (MgP), Hochstrasser and co-workers were able to show that the population transfer from one  $Q$  substate to the other takes place in 1.6 ps and is driven by solvent fluctuations.<sup>289</sup> Asymmetric substitution of these porphyrins lifts the degeneracy of the  $Q$  and  $B$  states. The Hochstrasser group investigated the effect of this loss of degeneracy on the CS dynamics of a MgP-benzoquinone dyad.<sup>290</sup> The  $Q_x$  state with its transition dipole moment oriented along the long molecular axis was found to experience a larger electronic coupling with the benzoquinone and to be at lower energy than the  $Q_y$  state. Upon excitation at 620 nm, mostly in the  $Q_y \leftarrow S_0$  band, ultrafast CS from the MgP to the quinone moiety in  $350 \pm 40$  fs was observed. The authors suggested that this time constant did not correspond to the CS step itself but rather to the  $Q_y \rightarrow Q_x$  transition, which acts as a rate limiting step.

Charge separation from an upper local excited state was also recently reported with a carotenoporphyrin dyad (**39**, Chart 9).<sup>291</sup> Here, optical excitation was performed to the local  $S_2$  state of the carotene unit. The charge-separated state was identified by the absorption band of the carotene radical cation around 1060 nm and the bleach of the porphyrin B band. From the multiexponential buildup of the charge-separated state population, the authors concluded that the CS occurs from the  $S_2$  state, from the vibrationally hot  $S_1$  state and from the thermalized  $S_1$  state of the carotene. Charge separation from the  $S_2$  state was estimated to take place in 600 fs, whereas CS from the equilibrated  $S_1$  state had a time constant 11 ps. Such ultrafast dynamics was ascribed to the substantial driving force that decreased from  $\sim 1.53$  to 0.74 eV upon relaxation from the  $S_2$  to the  $S_1$  states of the carotene.

Photoinduced ET processes from upper electronic excited states are still poorly documented and clearly deserve further attention. Recent investigations on conjugated polymers for organic photovoltaics have shown that the charge-transfer dynamics in these materials can be influenced by applying a second optical pulse in the visible region, a so-called push pulse, at a variable time delay after the initial pump pulse.<sup>292</sup> This approach is similar to that introduced by Wasielewski and co-

workers to realize an optical switch.<sup>293</sup> Using a D-A<sub>1</sub>-A<sub>2</sub> triad **40**, where A<sub>1</sub> is a stronger acceptor than A<sub>2</sub>, the authors demonstrated that two different charge-separated states could be populated, depending on whether single or double optical excitation was performed (Figure 24). The second excitation

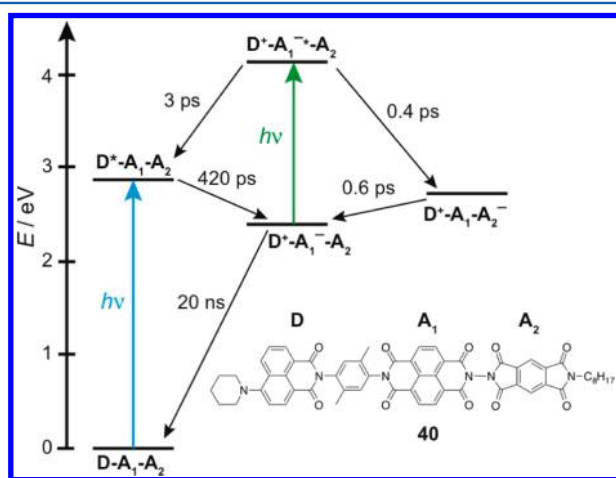


**Figure 24.** Energy-level diagram for the triad **40** with the various electron-transfer pathways and time constants. Adapted from ref 293. Copyright 1997 American Chemical Society.

lead to the population of a local excited state of the radical anion A<sub>1</sub><sup>−</sup> and was followed by CS to an upper charge-separated state. Apart from its potential practical applications, this pump–probe approach opens interesting perspective for a deeper understanding of the role of upper excited states.

#### 2.2.5.4. Electron Transfer from a Vibrationally Hot State.

In the examples discussed just above, CS from the vibrationally hot S<sub>1</sub> state was also invoked, in addition to CS from the S<sub>2</sub> state. Although the overall energy of the hot S<sub>1</sub> state just after internal conversion is essentially the same as that of the S<sub>2</sub> state, the ability of these two states to undergo ET is not the same. First, differences in the electronic coupling, *V*, can be expected as the electronic wave functions of these two states differ. Second, the partition of the energy among the electrons and the nuclei is not the same in both cases. According to the Golden-Rule formulation of the ET rate constant, eq 4, this should have a direct impact on the charge separation dynamics through the magnitude of the FCWD.

Evidence of intramolecular CS from a vibrationally hot electronic excited state, so-called hot CS, was reported by Zewail and co-workers with aminopurine covalently attached to one or two adenines, guanines, or 7-deaza guanines.<sup>294</sup> By comparing the decay of aminopurine fluorescence with the rise of the transient absorption of the charge-separated state, the authors proposed the existence of two ET pathways: (i) CS from the vibrationally hot S<sub>1</sub> state of aminopurine in less than ~200 fs and (ii) thermally activated CS from the equilibrated S<sub>1</sub> state with a ps time constant depending on the nature of the quencher, i.e., on the driving force.

Competition between hot and thermally activated CS was observed in a  $\pi$ -stacked ZnP-B-quinone D-B-A system (**41**, Chart 9).<sup>295</sup> In methyltetrahydrofuran, the rise of the ZnP cation absorption reflecting the population of the charge-separated state was found to be monoexponential between 320 and ~150 K with a time constant increasing from ~2 to 20 ps. At lower temperature, the rise was better reproduced by a biexponential function, with a ~20 ps component depending

on temperature and a subpicosecond and temperature-independent component. The relative amplitude of the fast component increased from about 0.1 to 0.4 upon lowering the temperature from 145 to 80 K. This behavior was rationalized using the energy level scheme shown in Figure 25. The slower

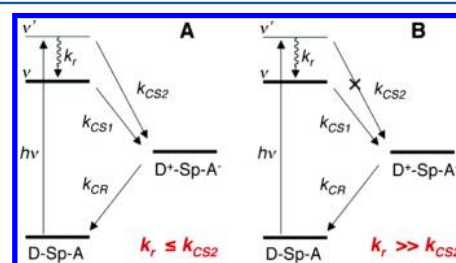


**Figure 25.** Energy-level scheme accounting for the temperature-dependence of the charge-separation dynamics in **41**. (A) At low temperature, hot charge separation (*k*<sub>CS2</sub>) is as fast as vibrational relaxation (*k*<sub>r</sub>) and is thus operative. (B) At high temperature, *k*<sub>r</sub> is larger than *k*<sub>CS2</sub> and only thermally activated charge separation (*k*<sub>CS1</sub>) is observed. Reprinted from ref 295. Copyright 2007 American Chemical Society.

and temperature-dependent rising component was ascribed to thermally activated CS from the S<sub>1</sub> state and the faster component was attributed to hot CS. As the latter was only observed below 145 K, this hypothesis implied that vibrational relaxation of the hot S<sub>1</sub> state decreased from (340 fs)<sup>−1</sup> to ~ (5 ps)<sup>−1</sup>, by going from 310 to 80 K. Therefore, at high temperature, vibrational relaxation is faster than the hot CS and only the thermally activated pathway is operative (Figure 25A). At lower temperature, the hot CS starts to compete with vibrational relaxation and becomes more effective as temperature decreases further (Figure 25B). On the other hand, the thermally activated CS was proposed to take place in three different regimes depending on temperature: nonadiabatic at high temperature, solvent-controlled at medium temperature and independent of solvent dynamics at lower temperature.

This temperature dependence of CS in **41** was subsequently investigated theoretically by Ivanov and co-workers using the stochastic point transition model discussed above.<sup>296</sup> The authors simulated the temporal evolution of the hot and the equilibrated S<sub>1</sub> states and that of the charge-separated state. The hot CS was found to be generally faster than the thermally activated one, mostly because of a lower barrier and a more favorable Franck–Condon factor. The temperature dependence of the slow CS component could also be reproduced. However, for this, the authors had to assume that at high temperature, CS takes place in the normal regime and its dynamics are solvent controlled, whereas at lower temperature, the process is in the inverted regime and is no longer affected by solvent dynamics.

Hot charge separation was also reported in an A-D<sub>4</sub> pentad, consisting of a naphthalene diimide with four ZnP substituents at the core positions (**42**, Chart 10).<sup>297</sup> The rise of the charge-separated state population was found to depend significantly on the excitation wavelength (Figure 26). Excitation at 600 nm to the S<sub>1</sub> state, centered mostly on the naphthalene diimide unit, was found to lead to a 4.6 ps exponential rise in polar solvents. Excitation at 550 nm to the local Q state of ZnP lead to the presence of a faster rising component of small amplitude, which however became dominant upon 400 nm to the B state of ZnP.



Chart 10. D-B-A Systems Undergoing Ultrafast Charge Separation upon Photoexcitation

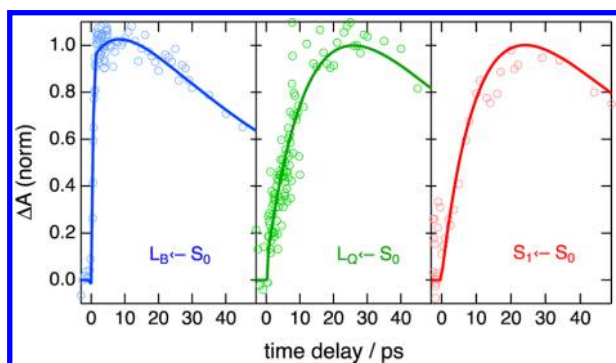
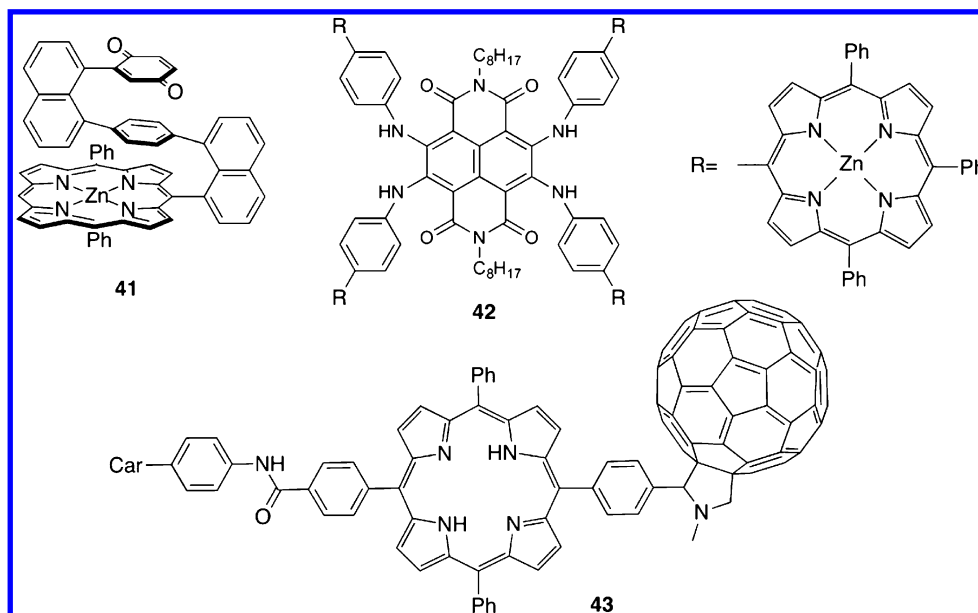


**Figure 26.** Time profiles of the transient absorption of the charge-separated state of **42** in benzonitrile upon local excitation of a porphyrin unit in the B band (blue) or Q-band (green) and upon excitation of the central naphthalene diimide core (red). Adapted from ref 297 with permission from the PCCP Owner Societies.

This  $\sim 500$  fs rising component was ascribed to hot CS from the **ZnP**  $S_1$  state rather than to CS from the local **ZnP**  $S_2$  state.

In the above examples, no indication of vibrational coherence in the CS process was observed, indicating that either the relevant vibrational modes were not coherently excited or the charge separation was not fast enough to compete with vibrational dephasing.

Evidence of vibrational coherence in CS was reported with an A-D<sub>1</sub>-D<sub>2</sub> triad, consisting of a free-base porphyrin (D<sub>1</sub>) substituted on one side by a fullerene (A) and on the other by a carotene (D<sub>2</sub>) (**43**, Chart 10).<sup>298</sup> Local excitation of the porphyrin with a 10 fs pulse centered at 550 nm resulted in an ultrafast population of the CS state with the electron on the fullerene and the hole on the porphyrin. The hole was found to subsequently hop to the carotene on a 100 ps time scale to populate a long-lived A<sup>-</sup>-D<sub>1</sub>-D<sub>2</sub><sup>+</sup> state. Due to the large spectral width of the pump pulse, the carotene was also excited. Because of this, the temporal evolution of transient absorption exhibited a strong periodic oscillation due to the coherent excitation of three vibrational modes of the carotene. However, after subtraction of the contribution due to direct carotene excitation

from the transient spectrum, the data revealed the presence of additional vibrational coherence with a  $\sim 30$  fs period which was assigned to carbon backbone vibrations across the porphyrin/fullerene region.

These observations of the effect of vibrational excitation on the dynamics of photoinduced CS in weakly to moderately coupled organic DA systems opens an interesting prospect for the control or at least the tuning of CS using selective vibrational excitation, as recently reported with platinum-based D- $\pi$ -A compounds.<sup>299</sup>

### 2.3. Intermolecular Electron Transfer

**2.3.1. Diffusional Effects.** The most general way to describe irreversible bimolecular electron transfer (as well as proton- or resonance energy-transfer) reactions may be to use a diffusion-reaction equation (DRE) approach. The following simple reaction scheme between an excited fluorophore, F\*, and a reaction partner, Q, may serve as starting point:



Here, the relevant quantity of interest is given by the distance- and time-dependent pair distribution function,  $n(r,t)$ , for the F\*/Q pair, the evolution of which can be described by the following diffusion reaction equation with appropriate boundary and initial conditions:<sup>300,301</sup>

$$\frac{\partial n(r,t)}{\partial t} = \underbrace{\hat{L}(r)n(r,t)}_{\text{diffusion}} - \underbrace{w(r)n(r,t)}_{\text{reaction}} \quad (32)$$

where  $\hat{L}(r)$  is the diffusion operator and  $w(r)$  is the reaction probability for the disappearance of the F\*/Q pair. Depending on the specific type of problem under investigation, this equation may now be subject to different forms of the diffusion operator and of the reaction probability. The diffusion operator may account for Coulomb attraction, in the case of charged reactants, interparticle potentials of mean force as a result of the solvent structure or allow for a distance-dependent diffusion coefficient as a result of the hydrodynamic effect. The reaction term, on the other hand, may account for a pure contact

reaction at distance  $\sigma$  with rate  $k$ , in the form of a delta function,  $w(r) = (k/4\pi\sigma^2)\delta(r - \sigma)$ , or for a distance dependent reaction probability of any suitable form. The experimentally observable quantities, like the time-dependent rate coefficient  $k(t)$ , or the excited-state survival probability,  $N(t)$ , can be obtained from the solution of the DRE via:

$$k(t) = 4\pi \int_{\sigma}^{\infty} w(r)n(r, t)r^2 dr \quad (33)$$

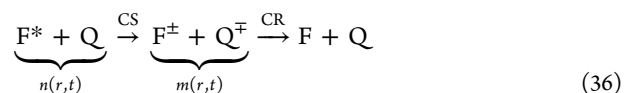
$$N(t) = N(0)\exp\left(-\frac{t}{\tau_0} - c \int_0^t k(t') dt'\right) \quad (34)$$

where the first term in the exponent of  $N(t)$  accounts for the intrinsic fluorophore decay with its fluorescence lifetime in the absence of quencher,  $\tau_0$ , and  $c$  is the bulk quencher concentration.

For certain simple reaction terms, analytical solutions to the partial differential equation and the ensuing time-dependent rate coefficient can be found, which made them popular for widespread use. Using a delta function reaction-term with an infinitely fast  $k$  gives rise to the famous “Smoluchowski” equation (cf. eq 35),<sup>302</sup> which, when modified to account for a still contact but now finite rate, is usually named “Smoluchowski Collins Kimball” model.<sup>303</sup> When the diffusion term contains a Coulomb potential to account for charged species, the “Debye” version of the model ensues.

$$k_{\text{smolu}}(t) = 4\pi DNR \left(1 + \frac{R}{\sqrt{\pi Dt}}\right) \quad (35)$$

Expanding the DRE approach to account for the irreversible recombination of the geminate radical ion pair, produced in (1), is straightforward.



Now the pair distribution function of interest is that of the charge-separated state,  $m(r, t)$ . The DRE resembles the one for the  $F^*/Q$  pair but is expanded with a source term, which depends on the dynamics of the  $F^*/Q$  pair.

$$\frac{\partial m(r, t)}{\partial t} = \underbrace{\hat{L}_{\text{CR}}(r)m(r, t)}_{\text{diffusion}} - \underbrace{w_{\text{CR}}(r)m(r, t)}_{\text{sink}} + \underbrace{w_{\text{CS}}(r)n(r, t)N(t)}_{\text{source}} \quad (37)$$

Now the experimental observable is the survival probability of the ion pair,  $P(t)$ , which can be calculated as follows:

$$P(t) = 4\pi c \int_{\sigma}^{\infty} m(r, t)r^2 dr \quad (38)$$

From this it is clear that, whereas for the CS process it is only necessary to solve eq 32, bimolecular CR is obviously more complicated, as it requires the solution of the coupled CS/CR problem, i.e., eqs 32 and 37.

The concentration dependence of  $N(t)$  is straightforward as a higher quencher concentration yields a faster  $F^*$  decay. The concentration dependence of the charge recombination step, on the other hand, is significantly more complex. Inspection of eq 38 reveals that, in a first approximation, the quencher concentration only affects the amplitude but not the time-

dependence of the observed ion signal. However, the more subtle effect of the influence of  $c$  on  $P(t)$  stems from the third term on the right-hand side in eq 37 and is introduced via the generation of ions and their ensuing spatial distribution, which strongly depends on quencher concentration, viscosity, driving force, etc.<sup>304,305</sup> The most striking difference between the initial CS and the ensuing CR step however can be found in their intrinsic nature. While bimolecular CS constitutes a bulk process, the subsequent CR process is considered to be a pair process.

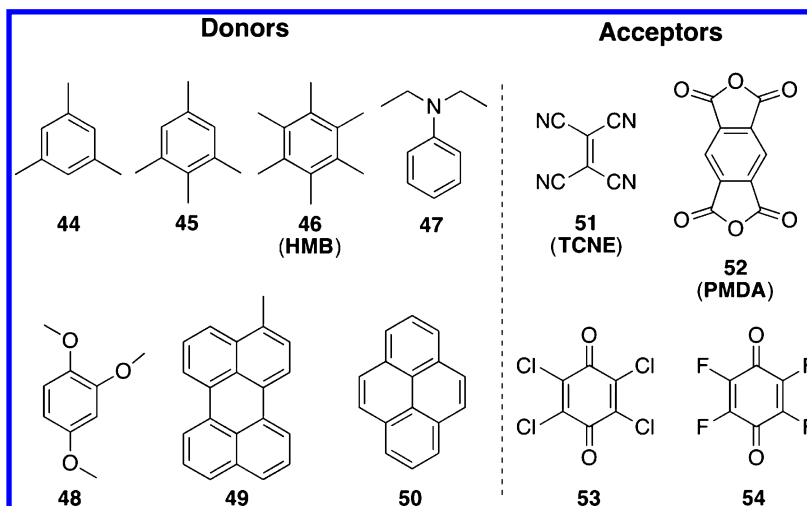
Comprehensive early reviews on diffusional effects in bimolecular reactions can be found in refs 306–308. A review exclusively focusing on the kinetics of fast fluorescence quenching processes can be found in ref 309. Burshtein wrote several comprehensive reviews on the DRE approach and its extensions and applications to diffusion influenced reactions, including irreversible and reversible charge separation, charge recombination and the effect of spin and external magnetic fields on the latter.<sup>301,310,311</sup>

**2.3.2. Charge-Transfer Dynamics of Excited Donor–Acceptor Complexes.** Solutions containing an electron donor and an electron acceptor are often characterized by an electronic absorption band that is not present in the spectra of the individual units. This band is due to a DA complex (DAC) and is associated with a transition involving substantial charge transfer from D to A.<sup>312</sup> Its transition energy correlates closely with the redox properties of the constituents. These species are sometimes called CT complexes, which is a misnomer, because these complexes are weakly polar in the ground state, as demonstrated by the weak solvatochromism of their absorption band. Whereas the structure of several DACs was determined in crystals,<sup>313,314</sup> that in solution is not really known, although a  $\pi$ -stack structure is generally assumed.<sup>315,316</sup> Several DACs, such as those containing substituted benzene donors, are characterized by two CT absorption bands.<sup>317–320</sup> This is due to the loss of degeneracy of the two HOMOs of benzene upon substitution.<sup>321</sup> Consequently, the two CT bands are associated with a one-electron transition from the HOMO and HOMO–1 of the donor to the LUMO of the acceptor. It was suggested that the two CT bands correspond to DACs with different mutual orientations of the constituents, favoring either the HOMO/LUMO or the HOMO–1/LUMO overlap.<sup>322</sup>

Most DACs are not fluorescent because of a very short excited-state lifetime and a small radiative rate constant associated with the CT emission. However, the fluorescence of the few emitting complexes was shown to be essentially identical to that of exciplexes generated upon diffusional fluorescence quenching.<sup>323</sup>

The first ultrafast spectroscopic investigations of DACs were mostly carried out by the Mataga group, using picosecond transient electronic absorption spectroscopy.<sup>324,325</sup> These authors found that upon excitation in the CT band of the complexes, the transient absorption spectra corresponded essentially to that of the radical ion pair  $D^+A^-$ . Some band narrowing was observed at early time delays and was ascribed to small structural relaxation. In most cases, these ion-pair populations were found to decay entirely to zero via charge recombination to the ground state. In the other few cases, the ion signal decayed only partially and remained constant within the time window of the experiment. The longer-lived residual was ascribed to free ions generated upon dissociation of the ion pair.

Chart 11. Typical Constituents of Donor–Acceptor Complexes



Mataga and co-workers performed the first investigation of the driving-force dependence of the CR dynamics of excited DACs in acetonitrile.<sup>326,327</sup> Compared to the CR dynamics of ion pairs generated upon diffusional ET quenching, which can be rationalized in terms of the semiclassical ET theory, eq 5, CR of excited DACs was found to be substantially faster and its rate constant exhibited an exponential driving-force dependence between  $0.5 \text{ eV} < -\Delta G_{\text{CR}} < 3 \text{ eV}$ . Measurements in other solvents pointed to a small influence of the polarity on the driving-force dependence. The authors suggested that the charge recombination in these complexes should rather be described with the expression developed for nonradiative transitions in the weak coupling limit.<sup>328,329</sup>

After these pioneering studies by Mataga's group, a substantial number of femtosecond studies on the excited-state dynamics of DACs were reported. Barbara and co-workers investigated arene/Br complexes and observed ultrafast ground-state recovery dynamics as well as an acceleration with increasing donor concentration.<sup>330,331</sup> No definitive explanation for this effect could be given, but the quenching of the excited complex by a donor and the ensuing formation of a DDA complex was tentatively ruled out. On the other hand, Jarzeba et al. found direct evidence of the formation of 1:1 and 2:1 complexes with the iodide/methylviologen systems.<sup>332</sup> In this case, CR of the 1:1 excited complex was found to be much faster than in the 2:1 complex, with time constants of 1 and 20 ps, respectively.

More recently, Mohammed et al. observed biphasic CR dynamics upon 800 nm excitation of the charge-transfer band of the methylperylene (49)/tetracyanoethylene (51, TCNE) complex (Chart 11).<sup>333</sup> About 90% of the excited-state population were found to decay with a 170 and 220 fs time constant in acetonitrile and dichloromethane, respectively, the remainder decaying on a  $\sim 10 \text{ ps}$  time scale.<sup>333</sup> Moreover, the early transient absorption spectra were dominated by a band similar to that of the methylperylene radical cation but broader and having a maximum at 555 nm instead of 540 nm (Figure 27). This band decayed almost entirely with the subpicosecond time constant to a residual band with a maximum at 540 nm. These dynamics were explained by the simultaneous excitation of DACs with different structures and coupling strengths: strongly coupled complexes with only partial CT character and undergoing ultrafast CR and less coupled complexes with

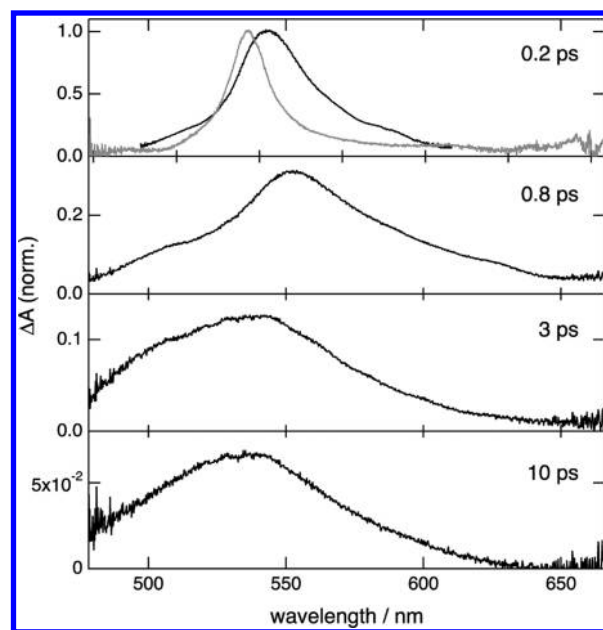


**Figure 27.** Transient absorption spectra recorded after 800 nm excitation of the methylperylene/TCNE complex in acetonitrile (black) and absorption spectrum of methylperylene radical cation (gray). Adapted from ref 333. Copyright 2008 American Chemical Society.

almost complete CT character and exhibiting a slower CR. The existence of a distribution of DA distances and its effect on the CR dynamics and, hence, of the free ion yield had previously been proposed by Braun and Sutin.<sup>334,335</sup>

In most of these ultrafast investigations, the CR dynamics were found to be consistent with the semiclassical ET theory (Section 2.1.2) for the inverted region.<sup>336,337</sup>

Wynne et al. studied the CR dynamics of the excited hexamethylbenzene (HMB, 46)/TCNE complex in a large variety of solvents and measured CR time constants ranging from 650 fs in acetonitrile to 2.75 ps in benzonitrile and 11.2 ps in carbon tetrachloride.<sup>338</sup> The authors tested different theoretical models to rationalize these findings. To limit the number of adjustable parameters, they used the frequencies of all the Franck–Condon active vibrational modes of this complex determined from its resonance Raman spectrum.



The electronic coupling, the solvent reorganization energy, as well as the driving force were obtained from the analysis of the CT absorption band. Using these parameters, they found that the semiclassical model overestimated the ET rate constants by a factor between 3 to 10 depending on the solvent. The best agreement was obtained with a variant of the hybrid model, eq 23, where all Franck–Condon active vibrational modes of the DAC were explicitly taken into account. With this approach, the amount of energy deposited in each vibrational mode could be determined. The results revealed that most of the energy is released into the high-frequency modes ( $>1000\text{ cm}^{-1}$ ).

Whereas all the above ultrafast investigations were performed with a single DAC, Nicolet et al. investigated the CR dynamics of a series of substituted benzene/pyromellitic dianhydride (52, PMDA) complexes in acetonitrile, acetone, valeronitrile, and ethyl acetate.<sup>339</sup> The driving force for the charge recombination could thus be varied between 1.4 and 2.4 eV. In all cases, the decay of the transient PMDA anion band could be well reproduced with an exponential function with a time constant ranging from 200 fs to 60 ps depending on the driving force and the solvent. In all solvents, the CR time constant was found to have a nearly exponential dependence on the driving force as previously observed by Mataga and co-workers.<sup>326,327</sup> As shown in Figure 28, this dependence as well as the effect of the solvent

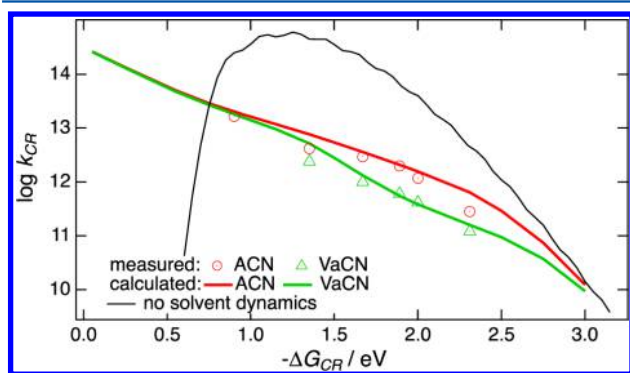


**Figure 28.** Driving-force dependence of the rate constant of charge recombination of excited benzenes/pyromellitic dianhydride complexes in acetonitrile (ACN) and valeronitrile (VaCN) and driving-force dependences calculated with the hybrid model, eq 23, and with the semiclassical model, eq 5. Adapted from ref 339. Copyright 2002 American Chemical Society.

could be well reproduced with the hybrid model, eq 23. The figure also shows the driving-force dependence predicted by the semiclassical model, eq 5, using the same parameters but without taking the finite solvent response into account. The predicted rate constants are substantially larger than the experimental ones, as also found by Wynne et al.<sup>338</sup> The hybrid model predicts intrinsically nonexponential dynamics with a slow initial decay and acceleration with time as relaxation along the slow coordinate  $X$  takes place. No clear evidence of a departure from exponential decay could be evidenced in this investigation. This was explained by a relatively small solvent reorganization energy and consequently a larger contribution of the high-frequency intramolecular modes.

An interesting feature of the hybrid model, which can be seen in Figure 28, is that, with the parameters used by Nicolet et al.,<sup>339</sup> the CR is predicted to be independent of the solvent and ultrafast in the driving-force range where the normal region is expected. This suppression of the normal region was explained

by the nonequilibrium nature of the CR: the ion-pair state is initially populated far from equilibrium and the crossing region between this state and the neutral ground state is reached upon relaxation (Figure 29). If the electronic coupling is large

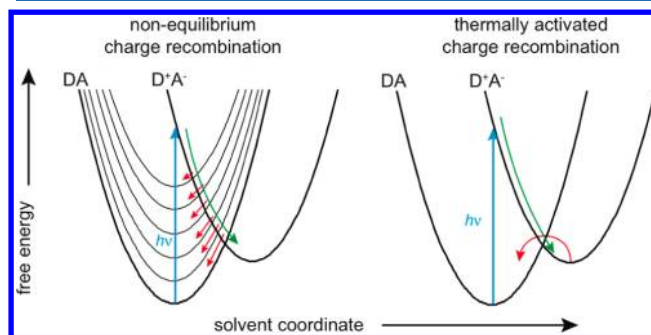


**Figure 29.** Free energy of the ground and excited states of a donor–acceptor complex along the solvent coordinate. The thin parabolas represent vibrational excited states, the green arrow the solvent relaxation, and the red arrows the charge-recombination pathways. (Left) charge recombination is faster than solvent relaxation and occurs out of equilibrium; (right) charge recombination is slower than solvent relaxation and is thermally activated.

enough, recombination takes place before the ion pair has equilibrated. On the other hand, if recombination does not occur during relaxation, the process is thermally activated and follows Marcus theory in the normal regime. Moreover, the independence of the solvent predicted in the low driving-force region was explained by the fact that inertial solvent relaxation, occurring on a sub-100 fs time scale in all solvents, is enough for the CR to become operative. However, if the CR driving force is larger, both inertial and diffusive relaxations are required and consequently an influence of the solvent on the recombination dynamics is observed.

The driving-force dependence of the CR of DACs, as well as the suppression of the normal region could be reproduced theoretically by Frantsuzov and Tachiya, who described CR as a nonradiative transition between two adiabatic states.<sup>340</sup> In this model, CR takes place from the equilibrated excited state and, thus, follows exponential dynamics. However, the upper adiabatic state is no longer a pure ion-pair state but rather a state with a partial CT character. This was in contradiction with the transient absorption results discussed above that revealed that the excited DACs are close to ion pairs.

A suppression of the normal regime due to the non-equilibrium nature of the CR was also predicted by theoretical investigations from Ivanov and co-workers.<sup>105,341</sup> The authors numerically solved the set of differential equations for the temporal evolution of the electronic ground- and excited-state populations as well as the population of the vibrationally hot ground state. These equations contained (i) a term accounting for the diffusion along a slow solvation and a fast intramolecular coordinate, (ii) the Zusman ET rate constant accounting for the transition from the excited state to a vibrational level of the ground state, and (iii) a term accounting for vibrational relaxation. The authors also proposed two different approaches to obtain an analytical expression for the description of such nonequilibrium dynamics.

These numerical simulations also showed that the non-exponential character of the decay of the excited-state population can be strongly attenuated by assuming a substantial

contribution from the high-frequency intramolecular modes to the total reorganization energy (Figure 30).

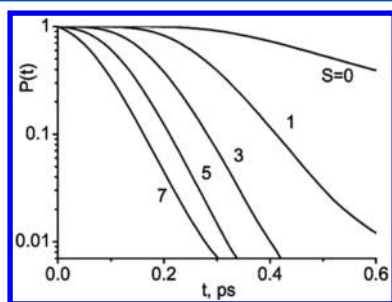


**Figure 30.** Simulations of the effect of the high-frequency intramolecular modes ( $S$  is the Huang–Rhys factor) on the time-dependence of the excited-state population of a donor–acceptor complex in acetonitrile ( $\Delta G = -0.5$  eV,  $\lambda_s = 1$  eV,  $V = 0.08$  eV,  $\omega = 0.1$  eV). Reprinted from ref 105. Copyright 2006 American Chemical Society.

The hybrid model was also shown to adequately account for the excited state dynamics of stilbene/viologen complexes.<sup>342</sup>

Because of its nonequilibrium nature, the CR dynamics of excited DACs depend on how far from equilibrium the excited CT state is initially prepared and should thus be influenced by the excitation wavelength (Figure 29). This idea was first explored theoretically by Ivanov and co-workers using a similar formalism as described above.<sup>343,344</sup> These authors showed that, unless very weakly exergonic ( $-\Delta G < 0.4$  eV), the CR slows down with decreasing excitation wavelength. This can be understood by considering that short wavelength excitation populates the excited state far from equilibrium and far from the crossing region between the excited and the ground state. Consequently, substantial relaxation is required before the crossing region is reached (Figure 31).

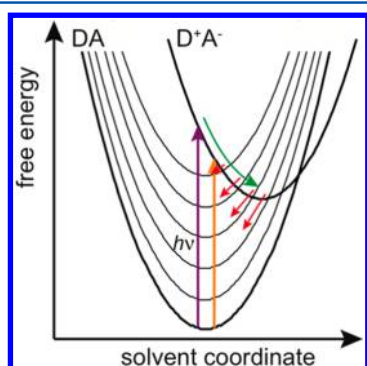


**Figure 31.** Free energy of the ground and excited states of a donor–acceptor complex along the solvent coordinate. The thin parabolas represent vibrational excited states, the green arrow the solvent relaxation, and the red arrows the charge-recombination pathways. Short-wavelength excitation (purple arrow) prepares the excited state further from equilibrium than long-wavelength excitation (orange arrow).

The excitation wavelength dependence of the excited-state dynamics of DACs was experimentally investigated by Nicolet et al. using substituted benzene/TCNE and substituted benzene/PMMA complexes in nitriles characterized by different relaxation times.<sup>345</sup> Three different types of excitation wavelength dependences were reported, one of them unrelated to

nonequilibrium dynamics. The latter was observed with DACs exhibiting two CT absorption bands such as diethylaniline (47)/PMMA. Charge recombination upon excitation in the high-energy CT band was found to be slower by a factor of  $\sim 1.5$  than upon low-energy CT excitation. This difference was explained in terms of a distribution of geometries, resulting in different overlaps of the HOMO and HOMO–1 of the donor with the LUMO of the acceptor.

Another excitation-wavelength dependence was observed with the isodurene (45)/TCNE complex in valeronitrile and octanenitrile but not in acetonitrile.<sup>345</sup> The decay of the TCNE<sup>•-</sup> band was found to be slower upon 480 nm than upon 620 nm excitation and to be nonexponential. These decays could be well reproduced using a compressed exponential function,  $f(t) \propto \exp[-(kt)^\beta]$  with  $\beta$  varying from 1.3 to 1.6 with decreasing excitation wavelength. A  $\beta > 1$  reflects the slow CR at early time as the excited state is populated far from the crossing region between the reactant and product states (Figure 30). This effect was not observed in acetonitrile, because the recombination is slower ( $\sim 1$  ps) than diffusive solvation.

A third type of excitation-wavelength dependence was measured with 1,2,4-trimethoxybenzene (48)/TCNE complex in acetonitrile only.<sup>345</sup> The decay of the TCNE<sup>•-</sup> signal upon long-wavelength excitation (620 nm) was found to be monoexponential with a  $< 100$  fs time constant. Upon shorter-wavelength excitation, the decay in acetonitrile was biphasic with a dominant  $< 100$  fs component and a minor  $> 100$  ps component. Only the fast decay component was measured in the other solvents, irrespective of the excitation wavelength. This effect was explained in terms of the free energy curves shown in Figure 29. The fast decay component of the excited-state population was attributed to hot CR, which is ultrafast because the excited-state population is not prepared far from the crossing region, independently of the excitation wavelength. In all cases, inertial solvent relaxation should almost suffice to reach this crossing region and to make the CR operative. The slow decay component was assigned to a fraction of the excited-state population that does not undergo the hot recombination and reaches equilibrium, from where the CR is thermally activated and, thus slower. The fact that the hot CR was only observed upon short-wavelength excitation was again explained in terms of a distribution of geometries as this complex exhibits two CT absorption bands. Finally, the absence of the slow component in valeronitrile and octanenitrile was accounted for by the longer time spent by the excited-state population in the reactive region due to the slower diffusional relaxation.

Several investigations of the excited-state dynamics of DACs with sub-100 fs time resolution revealed the presence of a temporal oscillation of the signal intensity due to vibrational coherence. The first observation was reported by Wynne et al. with the HMB/TCNE complex in apolar solvents.<sup>338</sup> An oscillation with a period of  $\sim 200$  fs corresponding to a frequency of  $165\text{ cm}^{-1}$  and a damping time of 1.2 ps was superimposed to the ground-state recovery dynamics measured using single wavelength pump–probe spectroscopy. This oscillation was assigned to a wavepacket generated upon impulsive stimulated Raman scattering (ISRS).

A similar oscillation in the ground-state recovery dynamics of a mesitylene (44)/Br complex in methanol was subsequently reported by Jarzeka et al.<sup>331</sup> The oscillation corresponded to a  $120\text{ cm}^{-1}$  vibration that was assigned to an intermolecular stretching mode of the complex in the ground state populated by ISRS.

A more detailed investigation on the origin of vibrational coherence in excited DACs was performed by Wynne et al. on the pyrene (50)/TCNE complex in several polar solvents.<sup>346,347</sup> Oscillations corresponding to a frequency of 170  $\text{cm}^{-1}$  were detected in both the ground-state bleach and in the stimulated emission signal recorded at 1215 nm. Whereas the latter could be undoubtedly assigned to a vibration of the complex in the excited state, the former could have two different origins: (i) coherence of a ground-state vibration produced by ISRS and (ii) coherent CR, i.e., modulation of the ground-state recovery due to the vibrational coherence in the excited state. Whereas ISRS induces a wavelength dependent phase, coherent CR leads to a stepwise decrease of the ground-state bleach. The latter should result in a stepwise increase of the ground-state recovery dynamics, as recombination occurs every time the wavepacket enters the region where the energy gap is close to zero (Figure 32B). As the measurements were

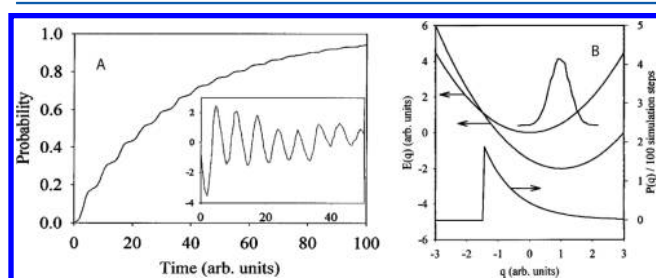


**Figure 32.** (A) Simulated time evolution of the ground-state population of a donor–acceptor complex with coherent charge recombination assuming the model illustrated in B. The inset shows the oscillatory component obtained as residuals of an exponential fit to the ground-state recovery. (B) Model used for simulating coherent charge recombination: the initial distribution on the excited-state potential is illustrated by the Gaussian distribution. The lower exponential curve represents the probability of the excited-state population to undergo charge recombination as it approaches the crossing region. Reprinted with permission from ref 346. Copyright 1996 American Institute of Physics.

performed without spectral filtering and as the phase of the oscillation was found to depend on the solvent, the authors suggested that the oscillation originated from coherent CR. The authors simulated the ground-state recovery dynamics assuming different dependences of the CR probability on the energy gap and found that, if the distance dependence is not too strong, the steps in the ground-state recovery cannot be well distinguished from an oscillation (Figure 32). Therefore, the authors ascribed the observed oscillation to coherent ET associated with an intermolecular vibration of the excited complex.

Vibrational coherence in the excited state of the HMB/TCNE complex was also observed by Rubtsov et al. using fluorescence up-conversion.<sup>348,349</sup> The fluorescence time profile was biphasic with a 105 fs component assigned to vibrational relaxation and a  $\sim 10$  ps component due to CR to the ground state. The superimposed oscillation, corresponding to a 160  $\text{cm}^{-1}$  vibration, similar to that observed by Wynne et al. in the ground-state recovery dynamics,<sup>338</sup> was tentatively assigned to an intermolecular mode of the excited complex. The authors stressed that large differences in intermolecular frequencies are expected between the ground and the excited states due to strong Coulombic interaction in the latter. Therefore, an

assignment of the oscillations on the fluorescence signal cannot be made on the basis of resonance Raman spectra.

To get a better insight into the nature of the coherently excited mode, Rubtsov et al. performed similar fluorescence up-conversion measurements with eight DACs, some with different donors but a common acceptor, namely TCNE and chloranil (53), and others with a common donor, hexamethylbenzene, but different acceptors, i.e., TCNE, chloranil and fluoranil (54).<sup>350</sup> Oscillations were observed in the fluorescence time profiles of all complexes (Figure 33). The oscillation

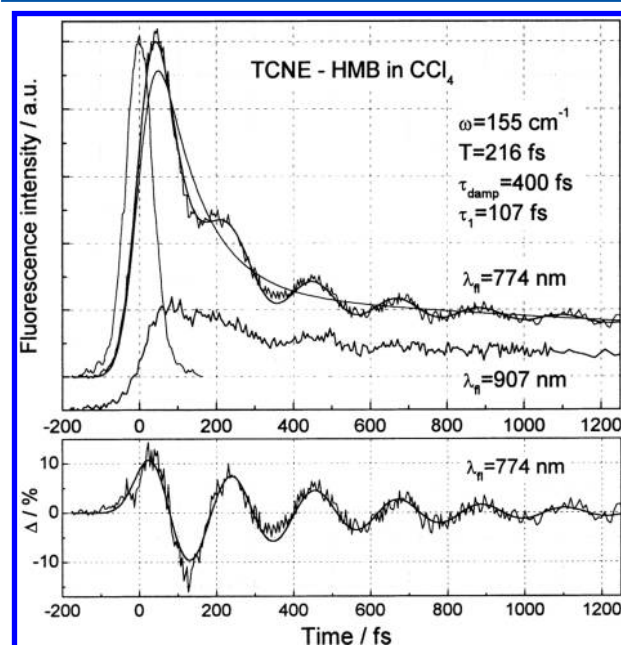


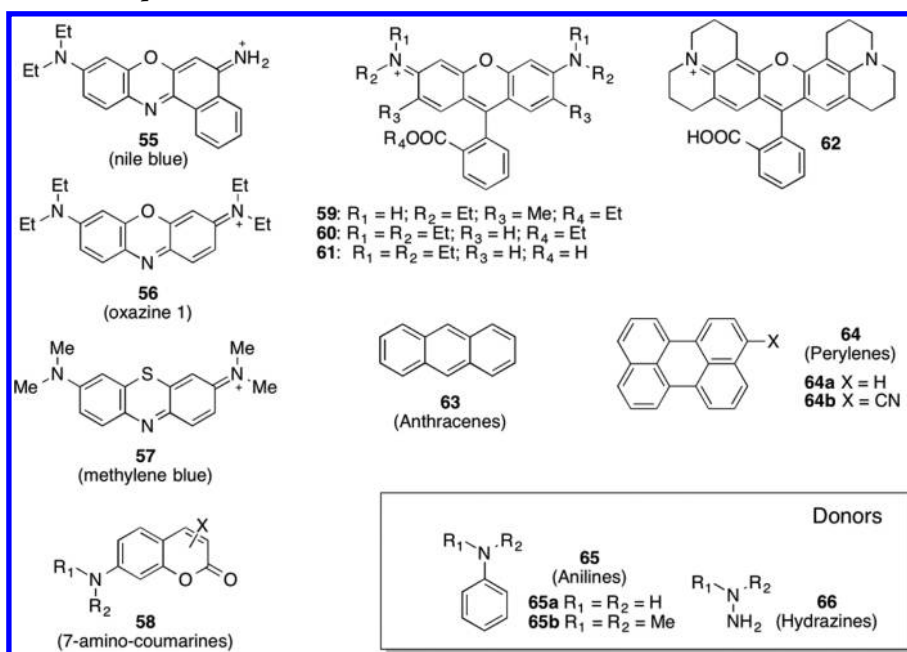
**Figure 33.** Fluorescence time profile measured with the HMB/TCNE complex at two wavelengths together with the instrument response function and (bottom) oscillatory component. Reprinted from ref 350. Copyright 1999 American Chemical Society.

frequency was found to only depend on the nature of the acceptor: around 155  $\text{cm}^{-1}$  for all D/TCNE complexes, 180  $\text{cm}^{-1}$  for D/chloranil and 212  $\text{cm}^{-1}$  for D/fluoranil complexes. From this, the authors concluded that the vibrational wavepacket originates from an intramolecular mode of the acceptor rather from an intermolecular mode as previously proposed. This was further supported by the good agreement between the oscillation and vibrational frequencies of the acceptor anions reported in literature. Several reasons for the absence of vibrational coherence from intermolecular modes were also proposed: (i) the frequency of these modes in the electronic ground state is small and thus several excited levels of these modes are populated at room temperature; thus, complexes with different distances are excited, leading to a randomization of the initial phase of the oscillation; (ii) the small binding energy of these complexes in the ground state leads to a distribution of geometries and thus of frequencies; and (iii) several intermolecular modes with similar frequencies can exist.

The authors also discussed the two mechanisms responsible for the presence of oscillations in the fluorescence time profiles: (i) the modulation of the transition energy due to the coherent wavepacket motion on the excited-state surface. This mechanism leads to a periodic shift of the emission band and consequently gives rise to a different phase of the modulation



Chart 12. Structures of the Acceptors and Donors Used in the Studies Presented Here



depending on whether the fluorescence is detected on the high or low energy side of the band; (ii) the modulation of the transition dipole moment due to vibronic coupling. In this case, the intensity of the whole emission band is modulated and no wavelength-dependent phase shift is observed. If both mechanisms are operative, their interference leads to an enhancement of the oscillation on the high-energy side of the spectrum (same phase of the oscillation) and to an attenuation of the oscillation on the low-energy side ( $\pi$  phase shift). As vibrational coherence was more visible when looking on the blue side of the emission band of the complexes, the authors concluded that both mechanisms were in operation.

Because of their ultrafast CR dynamics, these complexes are particularly well suited to investigate nonequilibrium effects. Despite the ultrafast spectroscopic investigations described above, there are still several aspects that need further scrutiny, such as the excitation wavelength dependence and the occurrence of coherent electron transfer.

**2.3.3. Bimolecular Charge Separation in Pure Donating Solvents.** Investigation of intramolecular electron transfer reactions allows deep insight into the dynamics of this process without the complication of the diffusion of the reactants, but the use of a covalently linked DA pair imposes several limits such as constrained spatial and orientational positions of the D and A units. The insights from electron transfer between freely diffusing reactants, on the other hand, are severely obscured by material diffusion processes, which may mask the intrinsic dynamics, especially if the latter are ultrafast.

One ingenious way to overcome this apparent dilemma consists in investigating charge-transfer reactions in pure electron-donating solvents, i.e., using the solvent itself as one of the reaction partners.<sup>351</sup> By doing so, the restrictions imposed on the mutual orientation and distance between the reactants are virtually lifted, while, at the same time, the effects of translational diffusion (at least for charge separation reactions) are minimized. Almost all examples in the literature in this respect, with exception of the initial works on this topic,<sup>351,352</sup> rely on aliphatic or aromatic amines as solvent and

fluorophores with relatively simple photophysics as electron acceptors (cf. Chart 12).

As shown below, this approach was revealed to be extremely powerful to investigate ultrafast, mostly faster-than-solvation charge-separation reactions.

The pioneering work was performed by Kemnitz, who monitored the fluorescence quenching of xanthene-based laser dyes in molten anthracene, phenanthrene and 1-chloronaphthalene and deduced rate constants as high as  $10^{12} \text{ s}^{-1}$ .<sup>351</sup> The driving-force dependence of these rate constants, which were obtained indirectly from relative fluorescence quantum yield measurements, could be adjusted with a Golden-Rule form of the ET rate constant, assuming an extremely low solvent reorganization energy of 50 meV. In a follow-up paper, Kemnitz and Yoshihara expanded the study to time-resolved fluorescence experiments of xanthene-based dyes in electron-donating, as well as electron-accepting solvents, such as *p*-benzoquinone, *m*-nitrobenzonitrile, or 1-chloronaphthalene, confirming the ultrafast character of these types of reactions.<sup>352</sup>

Later on, Kandori, Kemnitz, and Yoshihara confirmed that the ultrafast diffusionless fluorescence quenching of 55 in aniline (65a, AN) and *N,N*-dimethylaniline (65b, DMA) indeed arises from an ET reaction by directly monitoring the charge separation products using sub-picosecond visible transient absorption spectroscopy.<sup>353</sup> They found multi-exponential charge separation with components as short as 100 fs, followed by charge recombination to the electronic ground state within 2.7 and 4 ps for AN and DMA, respectively, thus having a full photocycle occurring within less than 10 ps. The ultrafast charge-separation step, which is significantly faster than solvation dynamics, was attributed to the small values of the (inner and solvent) reorganization energies. Yoshihara and co-workers also performed femtosecond fluorescence up-conversion experiments on a series of 7-aminocoumarin dyes dissolved in AN and DMA, observing nonexponential dynamics, with the fast processes being at least an order of magnitude faster than the relaxation of these solvents.<sup>354</sup> In

later works (vide infra) the authors went on to analyze these data using the 2D Sumi-Marcus model for ET (see section 2.1).

Nibbering and co-workers investigated the full photocycle between a coumarin (58) and three differently *N*-substituted anilines using fs Vis-pump/IR-probe spectroscopy.<sup>355</sup> The charge separation for all three reactant pairs was observed to proceed on two different time scales (500 fs and 7 ps) with hydrogen bonding not playing a crucial role in the dynamics. Charge recombination, on the other hand, took place on the 40–110 ps time scale.

Fleming and co-workers investigated the full photocycle of 59 in pure DMA and *N,N*-diethylaniline (47, DEA) using single color transient grating (TG) and three-pulse photon-echo peak-shift (3PEPS). While both techniques are four-wave mixing methods, TG and 3PEPS provide complementary information on population- and solvation-dynamics, respectively.<sup>356</sup> The TG and 3PEPS data were modeled using a three-level system using nonlinear response functions, accounting for reaction- as well as solvation-dynamics allowing the authors to treat the elementary ET reaction and the solvation process independently. It was found, that while the charge separation step occurred with 85 and 165 fs, for DMA and DEA, respectively, charge recombination was proposed to occur in 4 and 6 ps, and to be followed by vibrational cooling of the ground state in 20–50 ps. The assignment of the recombination was shown by Fayer and co-workers to be incorrect (vide infra).<sup>357</sup>

The full photocycles of the two xanthene-based dyes 59 and 62 in pure DEA were studied by Jiang et al.<sup>358,359</sup> using fs time-resolved multiplex transient grating and fs visible TA spectroscopies. The authors could disentangle the dynamics into three different regimes: (i) CS on the 200 to 500 fs time scale, (ii) IVR of the product state between 1 and 7 ps, and (iii) CR on the time scale of approximately 50 ps. None of the last three studies explicitly addressed the faster-than-solvation aspect of the charge separation reaction.

Tachiya and co-workers found indications for the pivotal role of intermolecular stretch vibrations in an ultrafast electron transfer reaction resulting in an exciplex.<sup>360</sup> They investigated the driving-force and emission-wavelength dependence of the fluorescence dynamics of various cyanoanthracenes (63) in pure AN and DMA using fluorescence up-conversion with a 240 fs IRF. It was found that the locally excited state fluorescence was quenched with a significantly faster-than-solvation time constant of approximately 200 fs for all 6 systems studied, covering a driving force range from 0.36 to 1.47 eV. This observed driving-force dependence was in striking contrast with the findings of Mataga and co-workers for charge recombination reactions in DA complexes (see section 2.3.2).<sup>361</sup> The experiments also showed the rise with the same 200 fs time constant of a weak and broad fluorescence band at significantly lower energies (see Figure 34), which the authors assigned to an exciplex. In summary, these observations were rationalized by invoking an adiabatic and barrierless exciplex formation along the coordinate of the intermolecular stretch vibration (cf. Figure 35).

**2.3.3.1. Coherent Vibrations.** The groups of Zinth,<sup>362–364</sup> Nagasawa,<sup>365,366</sup> and, recently, Scholes<sup>367</sup> invested significant experimental effort in elucidating the role coherent vibrations may play in electron transfer reactions. All of these investigations concentrate on the full photocycle of 56 in pure reactive DMA and inert 1-chloronaphthalene.

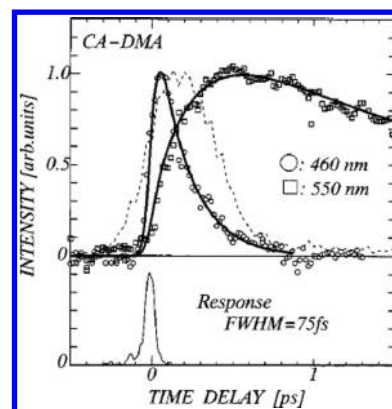


**Figure 34.** Fluorescence dynamics measured upon excitation of 9-cyanoanthracene in DMA at the wavelength of the locally excited state (460 nm) and of the exciplex state (550 nm). Reprinted with permission from ref 360. Copyright 2000 American Institute of Physics.

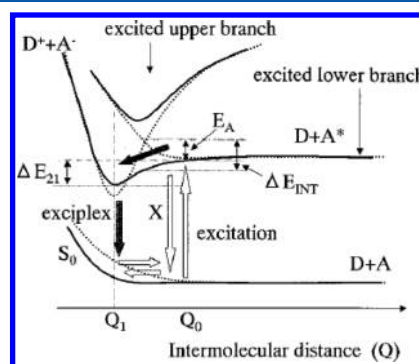


**Figure 35.** Tentative potential energy diagram for the ultrafast exciplex formation as a function of intermolecular distance,  $Q$ . Dashed lines denote diabatic electronic states, while solid lines indicate adiabatic potential curves. Reprinted with permission from ref 360. Copyright 2000 American Institute of Physics.

Zinth and co-workers used fs transient electronic absorption with a time-resolution better than 20 fs to monitor the ground-state bleach and the stimulated emission region of 56 (580–720 nm),<sup>362</sup> and later the charge-transfer products' absorption (440–500 nm).<sup>364</sup> This allowed them to split the dynamics of the photocycle into three main characteristic processes: (i) highly nonexponential ultrafast ET from DMA to 56 within 30–80 fs, (ii) recombination to the vibrationally hot ground state within 3.8 ps, and (iii) cooling of the latter on a 7 ps time scale. In addition, high-frequency vibrational wavepackets were observed not only in the ground-state bleach and excited-state absorption of 56<sup>362</sup> but also in the product dynamics, thus pointing to the importance of vibrational motions in the ET process.<sup>364</sup> Simulations using a microscopic quantum mechanical model consisting of three relevant electronic states, two strongly coupled vibrational modes and a dissipative environment allowed the observed charge separation dynamics to be semiquantitatively reproduced. Whereas the fast dynamics could be assigned to an adiabatic reaction, the subsequent slow-down of the reaction was assigned to relaxation and coupling to the thermal bath.<sup>363</sup>

Nagasawa and co-workers used a combination of degenerate four-wave-mixing in the range of 620 to 660 nm with a sub-15 fs time-resolution and broadband transient electronic absorption with a 30–45 fs time resolution.<sup>365,366</sup> In line with the

previous findings by Zinth and co-workers, the authors could quantify the slight difference of roughly  $6\text{ cm}^{-1}$  between the wavepacket frequency of **56** in the  $S_0$  ( $567\text{--}569\text{ cm}^{-1}$ ) and the  $S_1$  states ( $561\text{--}562\text{ cm}^{-1}$ ). The authors could also confirm that the dephasing time for the  $S_1$  vibrational coherence exceeded the ET time of  $60\text{--}80\text{ fs}$  by a factor of 2 to 3 (see Figure 36).

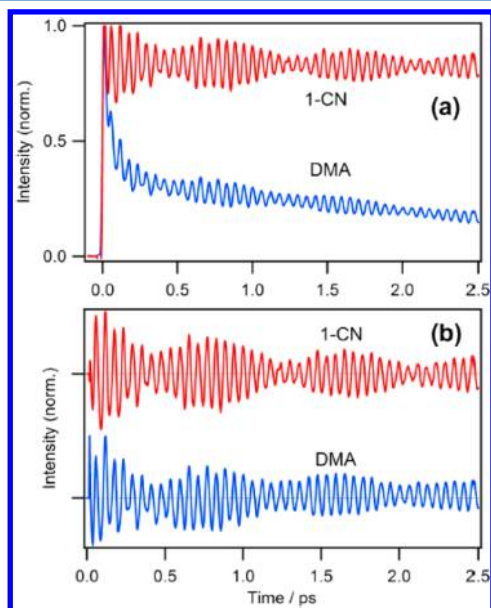


**Figure 36.** (a) Pump–probe signals measured upon 600 nm excitation of **56** in 1-chloronaphthalene (1CN) and DMA and (b) the normalized oscillatory parts. Reprinted with permission from ref 365. Copyright 2014 Elsevier.

However, the limited time-resolution in the spectral regions of the product ( $400\text{--}500\text{ nm}$ ) did not allow for the observation of coherent oscillations, as previously observed by Engleitner et al.<sup>364</sup>

The most recent contribution to this topic was reported by Scholes and co-workers, who used narrow- and broadband-pump transient electronic absorption, as well as 2D-electronic spectroscopy in the visible.<sup>367</sup> Here, on the one hand, the authors found the electron transfer to take place with a time constant of  $100\text{ fs}$ , while on the other hand, they could recover the  $S_0$  and  $S_1$  vibrational wavepackets and their respective frequencies, observed in previous investigations. However, based on their findings, they concluded that the observation of vibrational coherence surviving the electron transfer step was not to be interpreted as the outcome of a coherence transfer, i.e., a direct participation of this particular mode. Instead, the observed vibrational coherences were interpreted as being noninterfering “spectator” rather than electron transfer “promoter” modes.

**2.3.3.2. Electron Transfer in the Framework of the Sumi-Marcus Model.** The group of Yoshihara dedicated substantial effort to the systematic study of the effect of isotope substitution,<sup>368,369</sup> temperature,<sup>370</sup> driving force,<sup>368,369,371</sup> molecular size, and electronic structure<sup>372</sup> on the fluorescence quenching of phenoxazine- (**55**, **56**)<sup>370,373–376</sup> and 7-amino-coumarin-based (**58**)<sup>368,369,371,372,375</sup> fluorophores in pure anilines (**65**) or hydrazines (**66**). To this end, mostly single-wavelength fluorescence up-conversion with a time-resolution of  $60\text{--}80\text{ fs}$  was used to record the charge separation dynamics. In all these investigations, the two-dimensional Sumi-Marcus

model (cf. section 2.1) was applied to rationalizing the observed dynamics.

The observed fluorescence decays of phenoxazine-based laser dyes (**55** and **56**) in reacting solvents were hardly affected by solvation,<sup>373–375</sup> as these dyes exhibit very small Stokes shifts, or by excess energy, given that excited-state thermalization was shown to be ultrafast.<sup>375</sup> While the quenching of **55** and **56** in unsubstituted aniline was found to be multiphasic with the fastest component ranging from  $300$  to  $470\text{ fs}$ , respectively, that in DMA was originally found to be essentially monoexponential with time constants of  $280$  (**56**) and  $160\text{ fs}$  (**55**).<sup>374</sup> This made this initial CS step almost 50 times faster than the shortest diffusional component of solvent relaxation and more than 100 times faster than the mean relaxation times of these anilines, which had been determined to lie in the  $10\text{--}30\text{ ps}$  range.<sup>369</sup> In addition, the authors found that, whereas the dynamics of **56** in DMA were monoexponential and temperature independent, the long-time components of the multiphasic quenching dynamics in aniline exhibited a temperature dependence corresponding to an activation energy of  $1\text{ kcal/mol}$ .<sup>376</sup> Surprisingly, the authors found that the solvent relaxation times of aniline did not vary in the investigated temperature range ( $273$  to  $373\text{ K}$ ).<sup>370</sup> The Sumi-Marcus model could not only reproduce the mono- and multiexponential decays for the different systems, but was also able to account for the temperature dependence of the latter, when realistic sets of ET parameters were applied.<sup>370,373,376</sup> A few years later, the same group reinvestigated the **56**/DMA system using a fluorescence up-conversion setup with improved time resolution ( $70\text{ fs}$ ) and signal-to-noise ratio ( $S/N = 10^3$ ),<sup>377</sup> and found highly nonexponential fluorescence decays, ranging from sub- $100\text{ fs}$  to tens of ps, not only in AN but also in DMA. Additionally, they found that, contrary to their previous measurements,<sup>373</sup> the quenching of the **56**/DMA system depends on the fluorescence wavelength, the rate decreasing with increasing wavelength. Given that **56** exhibits almost no dynamic Stokes shift, the authors attributed both the nonexponentiality and the wavelength dependence to different configurations of **56** and DMA, each associated with different excited state energies, leading to different ET driving forces and rate constants (see Figure 37).

In a second series of studies,<sup>368,369,371,372,375</sup> Yoshihara and co-workers used fluorophores based on the 7-aminocoumarin core (**58**), which, contrary to the phenoxazine dyes, exhibit

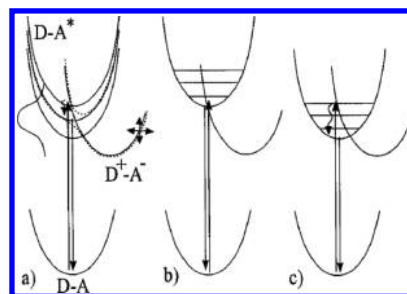


**Figure 37.** Tentative energy diagram explaining the wavelength dependent rate constants observed with the **56**/DMA system. (a) Vertically offset excited state surfaces denote the distribution of configurations. (b) Configuration with blue-shifted fluorescence and “fast” ET. (c) Configuration with red-shifted fluorescence and slow ET. Reprinted from ref 377. Copyright 1999 American Chemical Society.



significant dynamic Stokes shift, of the order of several 1000  $\text{cm}^{-1}$ . In this case, as electron transfer and solvation occur on similar time scales, the fluorescence dynamics were found to vary strongly with the emission wavelength.<sup>371</sup> While the ideal approach for studying these reactions would consist in analyzing the entire time-resolved emission spectra, the authors found that recording the fluorescence time profiles at a single properly chosen wavelength allowed complications due to solvent relaxation to be minimized.<sup>371</sup> Again, using the 2D Sumi-Marcus model with a nonequilibrium initial distribution of the excited fluorophore population ( $X(t=0) \neq 0$  for eq 20) the authors obtained excellent agreement with the experimental energy-gap dependence of the ET rate and could reproduce the observed turnover from quasi monoexponential decays at large driving forces to multiexponential decays at small driving force. This model also allowed the decrease of the observed Stokes shift with increased reaction rate to be explained, an effect that the authors denominated “chemical timing” of ET on the solvation process. While for fast systems the reaction proceeds via excited vibrational states before solvation is completed, the slower systems react with the solvent molecules already in the equilibrium configuration around the excited fluorophore.

The same group also systematically investigated the effect of H/D-isotope substitution on donors and acceptors as well as of the length of the alkyl substituents on the anilines.<sup>368,369</sup> The ET dynamics was found to be affected by the isotope exchange of the aniline hydrogens but not by the isotope exchange of the coumarins or of the aromatic and aliphatic hydrogens of the anilines.<sup>368</sup> In the former case, a slowing down of the ET rates by almost 20% was observed.<sup>368,369</sup> It was found to be more pronounced for the slower ET components and at low driving forces. In other words, ultrafast ET reactions were virtually unaffected by the H/D exchange on the quencher. In order to investigate the origin of these findings, the authors performed a thorough sensitivity analysis of all the relevant ET parameters in the framework of the Sumi-Marcus model, such as the reorganization energies, the driving force or the solvent relaxation times. The authors finally suggested that the small reduction of the driving force in deuterated solvents (by tens of meV), which is most likely being brought about by changes in the intermolecular hydrogen bonds, constituted the main origin of the observed isotope effect.<sup>368</sup>

In addition, the authors observed significant changes in the barrierless ET rates in anilines with differing numbers of alkyl *N*-substituents, which they attributed to changes in the electronic coupling element, *V*.<sup>369</sup> Varying the size of the alkyl substituents of *N*-monoalkylanilines did not lead to a significant effect on the dynamics, whereas a substantial slowing-down was observed with increasing the alkyl chain length of *N,N*-dialkylanilines.<sup>369</sup> In a similar series of experiments, Shirota et al. exchanged the anilines by aliphatic and aromatic hydrazines (**66**) as pure donating solvents and observed huge differences between these two types of donors, namely ET being almost 1 order of magnitude slower for the aliphatic hydrazine than for the two aromatic ones. The experimental findings were ascribed to electronic structural effects, with the coupling matrix element for aliphatic hydrazines being significantly smaller than for aromatic ones.<sup>372</sup>

**2.3.3.3. Population Distributions.** Beddard and co-workers investigated the full photocycle of **57** in AN and DMA at various temperatures using fs transient electronic absorption for the reaction dynamics, as well as optical Kerr effect and nuclear Overhauser effect measurements to obtain the solvent

relaxation times of the pure solvents.<sup>378</sup> Both charge separation and recombination were found to be ultrafast (sub-picosecond and sub-10 ps, respectively), almost temperature independent and significantly faster than the independently determined solvent dynamics. While the authors discarded the use of the Sumi-Marcus model, their attempts to describe the experimental observations using a Golden-Rule description failed. As a consequence, they proposed charge-separation from preformed “optimal” subensembles or electron transfer limited by nuclear tunneling.

Walker and co-workers probed the anisotropy of the product and reactant state of a 7-aminocoumarin derivative in pure DMA using fs transient electronic and vibrational absorption and concluded that ultrafast (4 ps) charge separation was preferentially occurring between reaction partners with their long axes oriented perpendicular.<sup>379</sup>

Very much in line with the series of experiments conducted by the Yoshihara group in the 1990s, Castner, Kennedy, and Cave thoroughly (re)investigated the fluorescence quenching dynamics of coumarins in pure electron donating solvents.<sup>380</sup> In particular, they studied (i) the quenching of six 7-amino-coumarin derivatives (**58**) in DMA, (ii) the quenching of one coumarin in eight electron-donating solvents, comprising substituted aromatic and aliphatic anilines as well as one phthalate, and (iii) the concentration dependent quenching of one coumarin by DMA in two nonreactive solvents using fs fluorescence up-conversion. These experiments were complemented with a combination of MD simulations, semiempirical quantum mechanical calculations, and application of the generalized Mulliken-Hush theory to evaluate the electronic coupling matrix element, *V*. The first two sets of experiments yielded results, which were mostly in line with the previous findings by Yoshihara and co-workers (vide supra). The fluorescence decays were observed to be nonexponential in almost all cases, and emission wavelength independent for fast and only moderately emission wavelength dependent for the slower reactions. Similar to ref 372, a significant slowing down, which could not be related to different driving forces but was attributed to changes in the electronic coupling, was observed for the aliphatic amines compared to the aromatic ones. In addition, and at odds with previous experiments, all fluorescence dynamics required an ultrafast (sub-200 fs) rising component, which the authors assigned to be consistent with the inertial part of the dynamic Stokes shift, thus constituting a prerequisite for the ultrafast electron transfer. The most striking insight, however, was obtained from the “dilution” experiments with nonreactive solvents. Upon exchanging only 2 of the approximately 15 nearest neighbors with an inert solvent led to a dramatic decrease of the observed ET rate by a factor of almost 3. From the MD simulation and quantum chemical calculations, the authors found that the electronic coupling, *V*, was not only dependent exponentially on interparticle distance, indicating that indeed only the first solvation shell is of importance, but that it was also strongly affected by the mutual orientation of the reactants (see Figure 38). This latter aspect led to dramatic temporal variations of *V*. From this, the authors concluded that, although many potential donors are available when working in pure donating solvents, only very few fulfill all the necessary requirements to undergo ultrafast ET, owing mostly to *V* being a highly dynamic and strongly fluctuating parameter.

The group of Vauthey opted for a different, structurally simpler class of fluorophores, namely perylene derivatives (**64**),

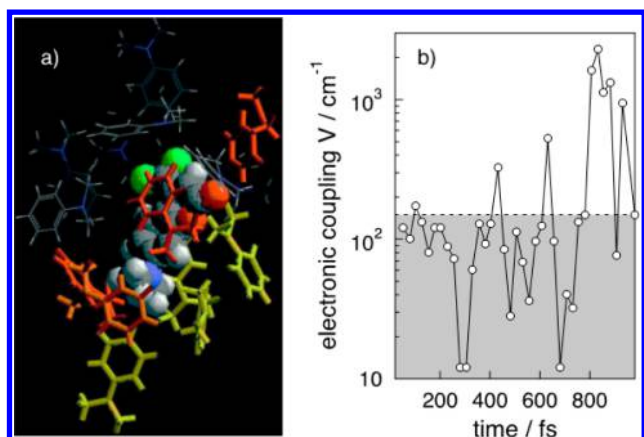


**Figure 38.** (a) Snapshot of the MD simulations of a coumarin and its nearest-neighbor DMA molecules at 40 ps. The coumarin is represented in colored spheres. The DMAs (sticks and cylinders) are color-coded according to the size of the electronic coupling element,  $V$  (gray:  $<50\text{ cm}^{-1}$ ; yellow:  $100\text{--}150\text{ cm}^{-1}$ ; red:  $>150\text{ cm}^{-1}$ ). (b)  $V$  as a function of time for a single coumarin-DMA pair. Adapted from reference 380. Copyright 2000 American Chemical Society.

for studying charge separation<sup>381,382</sup> and recombination<sup>382</sup> in pure donating solvents. To this end they performed fluorescence up-conversion measurements of a series of perylene derivatives in DMA,<sup>381</sup> and carried out, additionally to time-resolved fluorescence, femtosecond multiplex transient grating measurements of **64a** and **64b** in a series of amino substituted aniline derivatives.<sup>382</sup> In order to rationalize the pronounced nonexponentiality encountered with all fluorophores in pure DMA, the authors developed a phenomenological model accounting for three different subpopulations of fluorophore/quencher pairs within the first solvation layer:<sup>381</sup> (i) donors in an optimal position for electron transfer with  $k_{\text{et}}$ , (ii) donors that first have to rotate with  $k_{\text{rot}}$  and (iii) donors that need to undergo certain translational motion,  $k_{\text{trans}}$ , before ET. The total number of donor molecules in the first solvation shell, as well as  $k_{\text{rot}}$  and  $k_{\text{trans}}$  could be estimated independently, leaving as adjustable parameters only  $k_{\text{et}}$  and the probabilities for the donor to occupy any of the three “positions”. The so-obtained  $k_{\text{et}}$  values of approximately  $1\text{ ps}^{-1}$  were found to be significantly faster than solvation in DMA, which the authors rationalized using the Sumi-Marcus model. The average number of highly reactive sites, as also proposed by Castner et al., was found to be below one for apolar **64a**, but amounted to 3–4 for polar **64b**. This provided a clear-cut indication that dipole–dipole interactions and prealignment already in the ground state may play a crucial role for such types of reactions. Similar results were obtained in the second work, when comparing the dynamics of **64a** and **64b** in various anilines.<sup>382</sup> Again, similar intrinsic  $k_{\text{et}}$  were found for both fluorophores, but with a 3–4 times higher number of molecules in a proper geometry for the dipolar fluorophore. The observed solvent dependence could be ascribed to effects of the driving force and steric hindrance, especially in the case of bulky substituents on the aniline nitrogen. Observation of the charge separation products by monitoring either the exciplex by fluorescence or the excited state absorption using transient grating, clearly showed that the reaction products were formed in non-equilibrium, undergoing subsequent solvent relaxation. It was also observed that, once the charge separation had occurred, the pure donating solvent behaved just as any inert solvent,

with the reaction products essentially resembling the behavior of contact ion pairs. The charge recombination rates were found to show the typical behavior for systems in the Marcus inverted region, and showed different electronic couplings for the different anilines, which again could be traced back to steric hindrance on the amino nitrogen.

Pal and co-workers reinvestigated the quenching of a coumarin derivative (**58**) by three different amines<sup>380</sup> in the pure amines and upon dilution on isodielectric binary mixtures of cyclohexane and ethyl acetate.<sup>383</sup> Both the results and their interpretation were in agreement with the findings by Castner et al. and Vauthey and co-workers. The shortest lifetime contribution, which was assigned to the intrinsic electron transfer in perfectly oriented DA pairs, was found to be almost identical up to a critical amine dilution. The differences in the value of this critical dilution among aliphatic and aromatic amines were ascribed to differences in the electronic coupling element,  $V$ , due to differences in the localization of the HOMO of the amines.

Letrun and Vauthey brought additional insight into the above-mentioned interpretations by studying the effects of excitation wavelength and dielectric enrichment on the ET quenching of a set of **64a** and coumarin fluorophores with different permanent dipole moment by aromatic amines in apolar and polar solvents.<sup>384</sup> In apolar solvents only, a broadening of the absorption and emission spectra of the polar fluorophores, with a distinct excitation wavelength dependence was observed upon addition of slightly polar anilines. In addition, the strongly nonexponential fluorescence decays, as judged by the  $1/e$ -time, accelerated by up to a factor of 4–5 when exciting at the very “red-edge” of the absorption band compared to the “normal excitation” at the absorption maximum. The magnitude of this effect was found to increase with the polarity of the fluorophore. It is noteworthy, that upon “red-edge” and “normal” excitation, merely the relative amplitudes, but not the time constants changed, with the shortest lifetime around 1 ps being close to that observed by Yoshihara and co-workers in pure DMA.<sup>369</sup> The quencher concentration dependence of the red-edge over normal excitation rate,  $k_{\text{REE}}/k_{\text{NE}}$ , exhibited a clear maximum at approximately 0.5 M, with the effect disappearing at lower (0.01 M) and higher quencher concentrations (2–3 M) (see Figure 39). These observations clearly pointed toward dielectric enrichment, i.e., a preferential solvation of the polar fluorophore with the polar quencher in the otherwise apolar solvent environment, with subpopulations of increasing number of solvating quencher molecules absorbing more and more at lower energies. Using a distribution model of nearest neighbors, taking into account dielectric enrichment, provided a semi-quantitative explanation of the experimental findings.

**2.3.3.4. Diffusion Theories.** Fayer and co-workers tested the performances and limitations of the DRE approach for the combined problem of charge separation and recombination on the full photocycle of the **59** and **60** in DMA.<sup>357</sup> To this end the authors employed broadband fs transient electronic absorption covering a time window up to 12 ns with sub-100 fs resolution. The dynamics of the two main observables, i.e., the excited state and ion pair survival probability, were monitored experimentally by following the fluorophore stimulated emission signals and the excited state absorption of the neutral radical products. In doing so the authors obtained almost identical results for the two investigated systems. In brief, charge separation occurred nonexponentially on a time

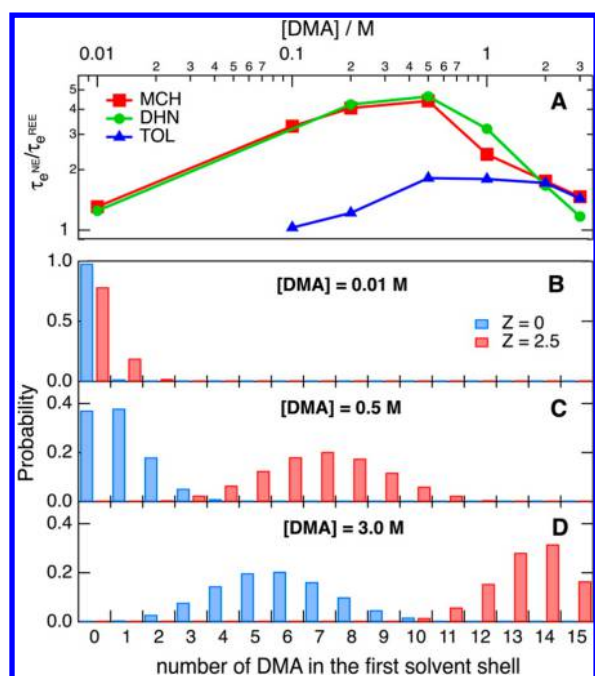


**Figure 39.** (A) Quencher concentration dependence of the effect of excitation wavelength (N: normal excitation; REE: red-edge excitation). (B–D) Probability to find  $n$  DMA molecules in the first solvent shell of the acceptor for different bulk concentrations with (red) and without (blue) accounting for preferential solvation. Reprinted from ref 384. Copyright 2014 American Chemical Society.

scale of 260 to 500 fs, with 59 being faster, followed by nonexponential charge recombination on the 22–25 ps time scale. In addition, both systems gave rise to constant charge separation signals at long times, indicating the formation of free ions with an efficiency of 2–3%. Given the significantly longer time-window of observation for the charge separation products, these findings complement the observations made for the 59/DEA system in refs 358 and 359 and are at odds with those found in ref 356. While Jiang et al. had missed the free ions, owing to the significantly shorter observation window of 130 ps (vs 12 ns), Xu et al. had assigned the 20 ps component to vibrational cooling in the electronic ground state. This misinterpretation may be attributed to the fact that only the ground-state recovery was monitored, while Fayer and co-workers using broadband detection found that the product decay matched the ground-state recovery.

Using the diffusion-reaction equation approach with a nonadiabatic Marcus expression for the charge separation process and an exponential recombination rate, Fayer and co-workers obtained qualitative agreement with the experimental findings, reproducing the time scales and essential features of the dynamics, like the nonexponentiality and the presence of free-ions. This is indeed quite remarkable, given the intrinsic limitations of the theoretical model, which is only suited for concentrations not higher than approximately 0.5 M and assumes an isotropic electronic coupling. The latter assumption has to be taken with caution, as in fact, the authors had, in line with the findings by Walker and co-workers,<sup>379</sup> observed a weak polarization anisotropy on the DMA cation signal, indicative of preferential mutual orientations of the reactants for charge separation.

Inspired by the results described in refs 381 and 382 and the success of the diffusion-reaction equation approach, Angulo et

al. revisited the charge separation reactions of perylene (64a) and 3-cyanoperylene (64b) in DMA.<sup>385</sup> Using fs fluorescence up-conversion, the authors studied the effect of dipole–dipole interactions and orientational diffusion on the concentration dependent quenching of dipolar 64b and dipolar 64a by weakly polar DMA in benzylacetate over a range of concentrations varying by 3 orders of magnitude, including pure DMA. At DMA concentrations up to 0.1 M, the ratio of the quenching rates for 64b and 64a was constant at around 2, most probably owing to the slightly larger ET driving force with 64b. Above this concentration, however, the quenching of 64b became increasingly faster than that of 64a up to a factor of almost 12 in pure DMA. In order to rationalize these findings, the authors proposed a DRE approach, which accounted for the preorientation of the 64b/DMA pair due to dipole–dipole interactions, rotational diffusion, as well as an orientation dependent reaction probability. Whereas the model was quite successful in accounting for the differences between 64b and 64a in pure DMA, it described relatively poorly the lower concentration data. The authors proposed various explanations and possible improvements of the theory: (i) the neglect of the hydrodynamic effect, i.e., the distance dependence of the translational and/or rotational diffusion coefficient,<sup>386</sup> (ii) the correct introduction of the quencher–quencher excluded volume effects in the diffusional operator,<sup>387</sup> and (iii) the neglect of possible fluctuations of the electronic coupling element,  $V$ .<sup>380</sup>

**2.3.4. Diffusion-Assisted Charge Separation.** Various groups investigated nonequilibrium effects in photoinduced bimolecular electron transfer using diffusional models. These effects originate from the competition between the intrinsic ET reaction and the material diffusion and result in a time-dependent rate coefficient, also called the “transient effect” (see Figure 40). Here we have sorted these studies into two parts:

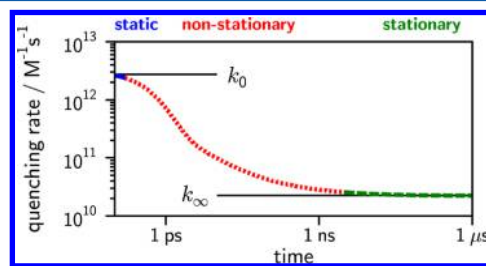


**Figure 40.** Time dependence of the quenching rate of a diffusion-assisted reaction. The reaction rate changes from the static or intrinsic rate,  $k_0$ , until reaching the stationary, i.e., diffusional, rate constant,  $k_\infty$ . Reprinted from ref 388, Copyright 2014 American Chemical Society.

First, we will address investigations of the applicability of diffusional theories and of their different variants to the quantitative description of ET reactions (vide supra). Second, we will discuss studies where this approach was systematically used to obtain insight into the underlying ET process.

**2.3.4.1. Testing the Diffusion Models.** The early attempts of applying DRE type models to quantitatively explain fluorescence quenching data (not necessarily electron transfer) had to overcome various limitations. Not only was the time-resolution of the employed set-ups usually not exceedingly large (at most in the sub-100 ps range), but most works limited themselves to models providing analytical solutions. Nonetheless, these early works applying the Smoluchowski<sup>389</sup> or Collins–Kimball approach<sup>390,391</sup> and, later on, approximate



analytical solutions for the Debye–Smoluchowski approach<sup>392–394</sup> clearly emphasized that an adequate treatment, based on a meaningful physical model, was mandatory for a proper description of the investigated processes.

It was however a seminal work by Fleming and co-workers that first provided a thorough comparison of the validity of DRE approaches, including those containing distance dependent reaction terms and requiring numerical solutions, to describe and recover the relevant parameters from a time-resolved experiment on bimolecular photoinduced electron transfer.<sup>395</sup> To this end, they analyzed the fluorescence quenching of **61** by ferrocyanide in water at various concentrations, using TCSPC and fluorescence up-conversion with time-resolution of 70 and 1–2 ps, respectively in combination with steady-state fluorescence experiments. The authors compared the following models: Smoluchowski, Collins–Kimball, Debye–Smoluchowski with radiation boundary condition, as well as two DRE, one with a uniform and one with an exponential distance dependence. The contact models clearly failed to reproduce the experiments at high concentration, which the authors ascribed to the neglect of static quenching in the intrinsic rate. The distance-dependent rate expressions, on the other hand, gave better, though still not fully consistent sets of parameters for all types of experiments. These apparent shortcomings of even the more sophisticated theories were ascribed to the limitations and simplifications inherent to the models. The authors suggested that the uncertainty about the exact form of the potential of mean force or the assumption of a completely angular independent intrinsic rate might be at the origin of these differences.

In another study, Fayer and co-workers measured the fluorescence quenching of **67** by **68** in liquid (diethylsebacate) and solid (sucrose octaacetate) solution using steady-state fluorescence and 70 ps TCSPC (Chart 13).<sup>396</sup> The authors

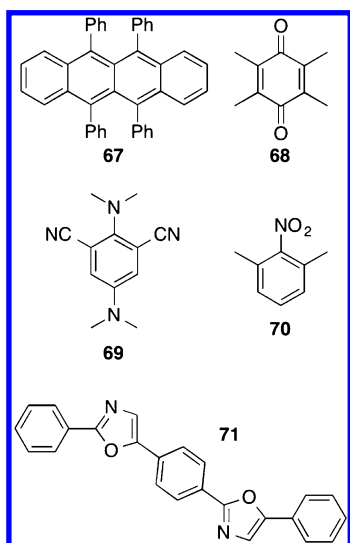
these parameters, within the very same DRE approach yielded a very good description of the fluorescence decays.

These initial results were complemented by a series of studies by the group of Lakowicz, who globally analyzed steady-state Stern–Volmer and time-resolved fluorescence modulation experiments.<sup>397–402</sup> It is noteworthy that, as emphasized by various groups,<sup>388,395,397,403,404</sup> a correct description of both types of experiments, which provide complementary information, is mandatory for concluding on the success of a given theoretical model. Similarly to Fleming and co-workers,<sup>395</sup> the Lakowicz group compared the Collins–Kimball model and the DRE approach with a uniform and an exponential distance dependent sink term, for the analysis of the fluorescence quenching of **71** by CBr<sub>4</sub> in propylene glycol.<sup>397</sup> In line with their subsequent findings with various fluorophore/quencher pairs,<sup>398–402</sup> the authors could clearly demonstrate the superiority of the DRE approach with an exponential sink term for describing ET reactions. The only observed case, where the Collins–Kimball model was found to be equally applicable, involved the heavy-atom induced intersystem crossing as fluorescence quenching mechanism.<sup>400</sup> Clearly, the series of papers by Lakowicz and co-workers significantly contributed to the acceptance of considering intermolecular ET reactions as distance dependent.

Shannon and Eads performed a comparative study, using the same models as in ref 395, of the fluorescence quenching of a 7-aminocoumarin by AN and DMA in methanol at different temperatures using steady-state and fluorescence up-conversion experiments. The intrinsically nonexponential fluorescence dynamics of the coumarin arising from relaxation processes required the authors to properly correct the dynamics measured in the presence of quencher, a strategy which was also applied later on by Vauthey and co-workers.<sup>388</sup> The authors could show that the two models with distance-dependent sink terms performed significantly better than the pure contact models. However, all models failed to reproduce the steady-state data with the time-resolved parameters, pointing toward fundamental omissions or simplifications in the model or to experimental problems.

The group of Fayer achieved a significant step in expanding the DRE-approach beyond the pure “solvent as a continuum”-description.<sup>386</sup> The theoretical inclusion of the hydrodynamic effect, i.e., the distance dependence of the mutual interparticle diffusion coefficient, and of the solvent structure via the two-particle radial distribution function, leading to a nonuniform quencher distribution around the fluorophore, was experimentally tested in ref 404. There, the authors performed time-resolved experiments (TCSPC with 70 ps) on the fluorescence quenching of **67** by **68** in three solvents of differing viscosity. The inclusion of the above-mentioned effects was complemented by the application of the complete distance-dependent Marcus expression for nonadiabatic ET as sink term in the DRE. By doing so, Fayer and co-workers could show that both of these newly included effects were crucial for a coherent description of the observed dynamics. A thorough analysis of the time profiles at various quencher concentrations allowed the authors to access the only two adjustable parameters in their model, the ET coupling matrix element,  $V$ , and its decay length,  $L$ . This is remarkable, as intramolecular electron transfer reactions do *per se* not allow for a separation of these two parameters. In a subsequent study with slightly improved time-resolution (35 ps),<sup>405</sup> the authors investigated the fluorescence ET quenching of **60** by DMA in several alcohols and alcohols

Chart 13. Structures of Selected Samples Used in Testing the Diffusion Models



based their data analysis on a DRE approach with an exponentially decaying distance-dependent sink-term, the parameters of which were obtained independently from the analysis of diffusionless experiments in solid solution. Simulations the fluorescence decays in liquid solution with

mixtures covering a viscosity range of almost 2 orders of magnitude (0.34 to 49.9 cP). By combining their time-resolved experiments with steady-state fluorescence data of a now more expanded set of data, they could impressively corroborate their previous findings. In providing all necessary model parameters from independent and alternative experiments or calculations, leaving only the ET coupling element and its decay length as adjustable parameters, they showed that only the most complete model (*vide supra*) was able to consistently reproduce the observed quenching dynamics. The unsurpassed degree of insight from such an elaborate analysis, even into the spatial solvent structure on the angstrom scale, was emphasized in noting that, for strongly hydrogen bonding solvents, the radial distribution function had to be adapted in order to account for a significantly larger “effective” solvent diameter. In doing so, the very same ET parameters as for the other solvents could be recovered.<sup>405</sup>

Almost at the same time as ref 404, Okada and co-workers analyzed the fluorescence quenching dynamics of a 7-aminocoumarin by DMA in anisole using fluorescence up-conversion in the framework of diffusional theories of different complexity.<sup>406</sup> In line with the aforementioned studies, the authors not only showed that the contact models (Smoluchowski and Collins–Kimball) were inadequate in reproducing the experimental observations, but also that the inclusion of solvent structure, via, e.g., a Lennard-Jones potential, into the diffusion reaction equation with a distance dependent sink-term was mandatory.

Burshtein and co-workers investigated the charge separation dynamics of the 64a/51 system in acetonitrile with a large driving force, placing it deeply in the Marcus inverted region.<sup>407</sup> To this end, the femtosecond fluorescence dynamics and the fluorescence quantum yields of 64a at multiple 51 concentrations were recorded. In order to consistently recover the excited-state dynamics of 64a at various 51 concentrations, the authors employed the DRE approach with two distance-dependent reaction terms, accounting for the reaction to the ion pair and to the ion pair with the 64a cation in its electronically excited state. In doing so, the authors could substantiate that the participation of excited ions could indeed constitute one of the plausible reasons for the absence of the Marcus inverted region in bimolecular photoinduced charge separation reactions.

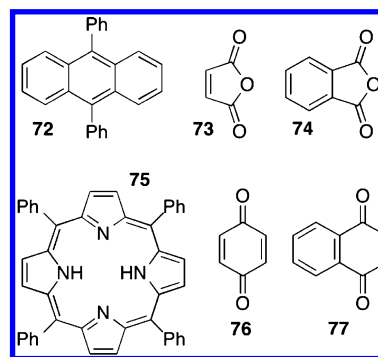
The most recent contributions to the systematic test of the DRE approach for bimolecular charge separation reactions can be found in refs 408 and 409. Here, a moderately exergonic bimolecular photoinduced charge separation reaction between two simple organic molecules (69/70) in the viscosity range of 2.2 to 62 cP was investigated using a combination of steady-state and time-resolved fluorescence spectroscopy with 200 ps<sup>408</sup> and later on 70 fs IRF.<sup>409</sup> Both studies confirmed the findings by Fayer and co-workers and emphasized that two conditions have to be fulfilled for a thorough understanding of these types of reactions: (i) a combined set of steady-state and high time-resolution emission experiments ensures that no fast components are missed and that the entire nonexponential dynamics can be monitored; (ii) only a DRE approach, which accounts for a distance-dependent ET probability, the hydrodynamic effect, as well as the solvent structure, is capable of reproducing the experimental data over a large range of viscosities, concentrations, and time-ranges with physically meaningful parameters.

### 2.3.4.2. Can Bimolecular Electron Transfer be Remote?

Although the contact models have been shown to have strong limitations, the application of their long-time asymptotic behavior can give useful insight.<sup>410</sup> The so-obtained effective quenching radius,  $R_Q$ , from, e.g., the Collins–Kimball model, allows for deciding whether the reaction takes place in contact or at remote distances. The interested reader is referred to ref 410 for a thorough discussion on the meaning of the effective quenching radius. Tachiya and co-workers, as well as Scully et al. used this to study the driving-force<sup>411,412</sup> or viscosity dependence<sup>413,414</sup> of  $R_Q$  for a variety of D/A pairs. From the analysis of the long-time fluorescence decays measured by TCSPC, and of the steady-state quenching, Tachiya and co-workers found a continuous increase of  $R_Q$  with increasing driving force for ET in polar acetonitrile as well as in medium polar tetrahydrofuran.<sup>411</sup> They could show that this trend was in good agreement with Marcus theory, when considering all distance dependent terms appropriately. More surprisingly, they also found a pronounced distance dependence of the ET in the nonpolar liquid paraffin for 5 D/A pairs covering a driving force range from 0.67 to 1.87 eV.<sup>412</sup> In lieu of a theoretical ET model for apolar media, they employed a simple exponentially decaying reaction probability as sink-term in the DRE.

Scully et al. could show that the fluorescence quenching of 72 by 73 in acetonitrile proceeded at distances larger than contact, and increasing with the solvent viscosity, the latter being adjusted by changing the pressure on the solvent (Chart 14).<sup>413</sup> This finding was again in full agreement with the

Chart 14. Structures of Selected Samples Used in Testing the Diffusion Models



predictions for the viscosity dependence of a diffusion-assisted reaction. In a later article, Scully et al. could also apply this methodology to the ET quenching of 75 by benzo- (76) and naphthoquinone (77) in alkanes of varying viscosity.<sup>414</sup> No variation of  $R_Q$  with viscosity was found for the reaction with low driving force (75/76), which was assumed to proceed via an exciplex and thus in close contact. The D/A pair with larger driving force, on the other hand, showed a clear increase with increasing viscosity, as expected for a distance-dependent reaction.

### 2.3.4.3. Accessing the Intrinsic Electron Transfer Rate, $k_0$

An interesting benefit of applying a DRE approach to bimolecular reactions is the access to detailed information on the reaction term, which is inaccessible if only the stationary data (i.e., long time limit) are analyzed. Several groups used this theoretical insight to investigate the driving-force dependence of intermolecular photoinduced ET reactions, as this type of

process constitutes one of the few, if not the only, example of electron transfer, that does not show the so-called Marcus inverted region, one of the reasons being that the intrinsic electron transfer rate is masked by diffusion.<sup>415,416</sup>

Mataga and his group were the first to become aware of this insightful approach and investigated the fluorescence decays, recorded with TCSPC, of a large series of D/A pairs in acetonitrile.<sup>417</sup> Using the simplified Collins–Kimball model rate, the authors found intrinsic ET rate constants,  $k_0$ , up to more than 1 order of magnitude larger than the diffusion limited rate,  $k_{\text{diff}}$ . With the driving-force range expanding up to 2.5 eV, no inverted region could be observed, despite the relatively large spread of the data. In a subsequent publication, Mataga and co-workers reinspected their previous TCSPC data and compared the DRE approach with a distance dependent Marcus-type sink term with the results of the Collins–Kimball model.<sup>418</sup> They found that their previous analysis was viable, as long as the intrinsic rate,  $k_0$ , did not largely exceed the diffusion rate,  $k_{\text{diff}}$ . The maximum deviation the authors observed between  $k_0$  and  $k_{\text{diff}}$  was slightly smaller than 2 orders of magnitude.

Angel and Peters used ps transient electronic absorption with the Collins–Kimball model to study the driving-force dependence of the ET between two derivatives of stilbene (**111**) and various cyanoethylenes (6 systems) in acetonitrile over a range of 2 eV.<sup>419</sup> The extracted rate constants were approximately 20 times larger than  $k_{\text{diff}}$  and did not show the Marcus inversion. Venkataraman and co-workers used TCSPC (with 280 ps resolution) to study the diffusive quenching of 8 Zn-porphyrins (**75**)/aromatic quencher pairs in a polar and an apolar solvent and applied the Collins–Kimball model to extract the intrinsic ET rates.<sup>420</sup> Quite like Angel and Peters, the authors found intrinsic rates up to 20 times larger than  $k_{\text{diff}}$  but without any sign of inversion. It is noteworthy that they observed a steady increase of the intrinsic rate up to almost 1.6 eV even in the quasi apolar toluene.

Murata et al. successfully determined the electronic coupling,  $V$ , and its decay length,  $L$ , from TCSPC experiments with approximately 60 ps time resolution for 5 D/A pairs in ethylene glycol.<sup>421</sup> For this, they used the DRE approach with the nonadiabatic Marcus expression, including all distance dependencies. The parameter spread when analyzing two different quencher concentrations was within 20%, with the spread between different pairs being significantly larger. The authors also noted that an improved time-resolution would allow for a better disentanglement of the otherwise partially correlated  $V$  and  $L$ . In fact, the more pronounced the transient effect, i.e., the higher the time-resolution and the viscosity, the larger the difference between  $k_0$  and  $k_{\text{diff}}$  and the easier the extraction of the relevant parameters.

Tachiya and co-workers investigated the bimolecular fluorescence quenching of various cyano-substituted anthracenes (**63**) by **DMA** in acetonitrile using fluorescence up-conversion with 240 fs IRF.<sup>422</sup> While the entire quenching dynamics in the 2–200 ps time-window and the 0.15–1.0 M concentration-range could be well reproduced using a DRE approach with a distance dependent reaction probability based on Marcus theory, it severely failed for shorter times. The observed ultrafast initial decay, whose amplitude was found to grow with increasing quencher concentration, could not be reproduced with the DRE approach, even when the solvent structure was taken into account, as suggested in ref 386. Tachiya and co-workers solved this problem by attributing the

ultrafast ET to a subpopulation of D/A pairs at short distances undergoing adiabatic electron transfer.<sup>360</sup> Inclusion of this fast channel into the DRE approach eventually allowed the recovery of a consistent description of the observed ultrafast dynamics.<sup>423</sup>

Recently, Vauthey and co-workers studied the driving-force dependence (0.63 to 2.37 eV) of 14 fluorophore/quencher pairs in acetonitrile.<sup>388</sup> For this, they combined fs fluorescence up-conversion, TCSPC and steady-state fluorescence experiments at various concentrations with a DRE approach similar to that in ref 386 accounting for solvent structure, hydrodynamic effect, and the full distance dependence of a multichannel electron transfer expression valid even at larger  $V$ . In order to extract the intrinsic ET rate,  $k_0$ , the observables from the DRE approach (steady-state quenching rate dependence on concentration, time-dependent quenching rate coefficient, diffusional rate) were fitted to all available experimental data sets for each reactant pair individually, using  $V$  and  $L$  as adjustable parameters (see Figure 41 for representative fits and the driving force dependence of  $k_0$ ).

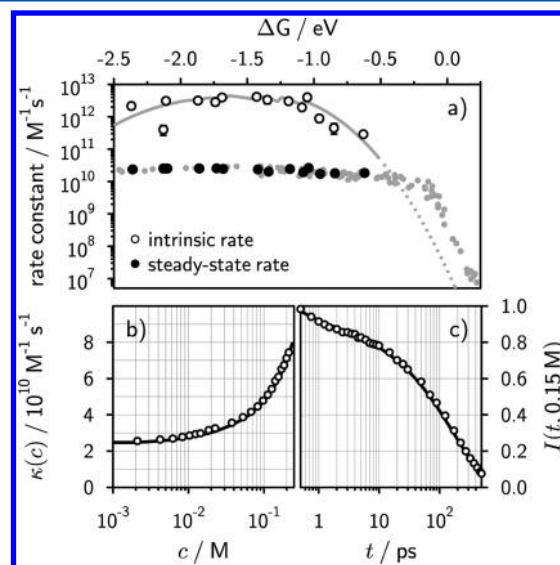


**Figure 41.** (a) Driving-force dependence of the intrinsic and the steady-state electron transfer rate of photoinduced bimolecular charge separation. (b) Concentration dependence of the steady-state (Stern–Volmer type) quenching coefficient. (c) Time dependence of the fluorescence intensity of a cyano-anthracene in the presence of **DMA**. Adapted from ref 388. Copyright 2014 American Chemical Society.

This combined theoretical and experimental effort on a large number of systems allowed the authors to obtain the driving-force dependence of  $k_0$ , similarly to the aforementioned studies. The obtained intrinsic ET rate constants were found to be up to 200 times larger than the diffusional rate and exhibited significantly less scatter than in the previous studies. This latter aspect was probably due to the use of a more comprehensive model and the fact that the experimental time-profiles were monitored over up to 4 orders of magnitude, in contrast with previous investigations using contact models and/or experiments with low time-resolution. The so-obtained driving-force dependence of  $k_0$  with a barely visible “Marcus inversion” at driving forces larger than 2 eV could be well rationalized using a single set of parameters within the employed combination of a state-of-the-art DRE model and a properly chosen expression for the ET probability.



The above examples demonstrate that a correct theoretical treatment of diffusion-influenced reactions may provide rich insight and otherwise inaccessible information on the underlying intrinsic reaction. Moreover, it is important to stress that a neglect of these nonequilibrium effects (that are inherent to diffusion-limited reactions) in the analysis of fluorescence quenching data can and most probably will lead to misleading if not outright wrong interpretations, especially when working in media of moderate to high viscosity, as shown in several recent studies.<sup>424–426</sup>

**2.3.5. Charge Recombination.** An important aspect of bimolecular photoinduced electron transfer reactions is the nature of the ensuing ion pair. From early experiments, based mostly on flash photolysis and picosecond transient absorption, two different types of radical ion pairs were proposed, with the type generated depending on the manner in which they were produced (see Figure 42). While charge separation between

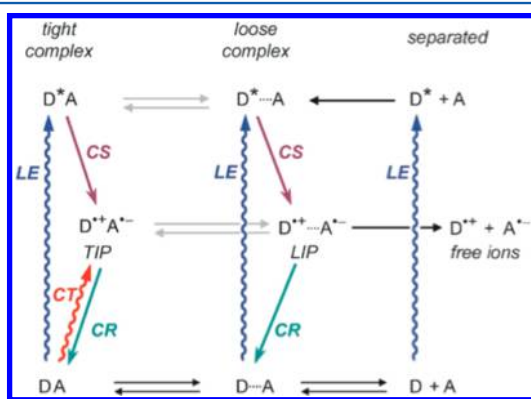


**Figure 42.** Scheme showing the different generation of TIPs and LIPs in liquid solution. Reprinted with permission from ref 427. Copyright 2008 Wiley.

freely diffusing reaction partners at relatively low concentrations was thought to lead to so-called “loose ion pairs” (LIPs),<sup>428–432</sup> the optical excitation of donor–acceptor (DA) complexes and of freely diffusing reactants at very high concentrations (~1 M) and/or in less polar solvents produced so-called “tight ion pairs” (TIPs).<sup>327,329,361,433</sup> Alternative names were used to assign these species, such as solvent-separated or solvent-shared ion pair (SSIP) and contact ion pair (CIP), instead of LIP and TIP, respectively. Independently of their exact denomination, the difference between these two types of ion pairs is mostly related to the electronic coupling, which is expected to be large for tight and small for loose ion pairs.<sup>434</sup> It is precisely this latter definition and, consequently, the different charge recombination dynamics that have led to the identification and assignment of TIPs and LIPs in the past. TIPs and LIPs can barely be differentiated from their electronic absorption spectra, at least in the visible region (cf. Figure 43).<sup>361</sup> As outlined in section 2.3.2, the driving-force dependence of the charge recombination of excited DA complexes (TIPs) departs from that predicted by Marcus theory, mostly at weak driving forces, where the normal region is either absent or hardly observed.<sup>327,329,361,433</sup> On the other hand, the driving-force dependence of the charge recombination of LIPs was shown to be in excellent agreement with the semiclassical Marcus ET theory.<sup>428–432</sup>

Recent experimental findings by Vauthey and co-workers,<sup>427,435</sup> however, put this probably slightly oversimplified

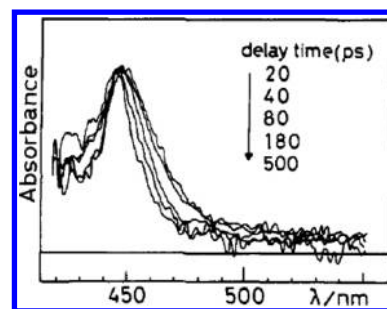


**Figure 43.** Transient absorption spectra measured at different time delays after charge-transfer excitation of the pyrene (50)/phthalic anhydride (74) complex, evidencing the transition from tightly bound ions to free ions at later times. Reprinted from ref 361. Copyright 1991 American Chemical Society.

picture into perspective. Investigating the charge recombination dynamics<sup>435</sup> and spectral characteristics<sup>427</sup> of the ion pairs produced upon ET quenching of 64a by 51 using single color,<sup>435</sup> as well as broadband transient electronic and vibrational absorption spectroscopy,<sup>427</sup> the authors observed clear and distinct spectral features in the IR for both tight and loose ion pairs.<sup>427</sup> This is at odds with the above-mentioned interpretation of TIPs and LIPs, as both types of pairs were generated upon locally exciting the fluorophore in a polar solvent and not via direct CT excitation of a DAC. In the first paper, only indirect evidence for this interpretation was found, as more than 90% of the ions disappeared within 10 ps and only a minor fraction of free ions was formed, in contradiction with the predictions from Marcus theory for the normal region.<sup>435</sup> In the second paper distinct IR bands could be unequivocally attributed to both species (cf. Figure 44) by comparison with experiments where TIPs were exclusively produced. This assignment allowed the identification of both species as primary

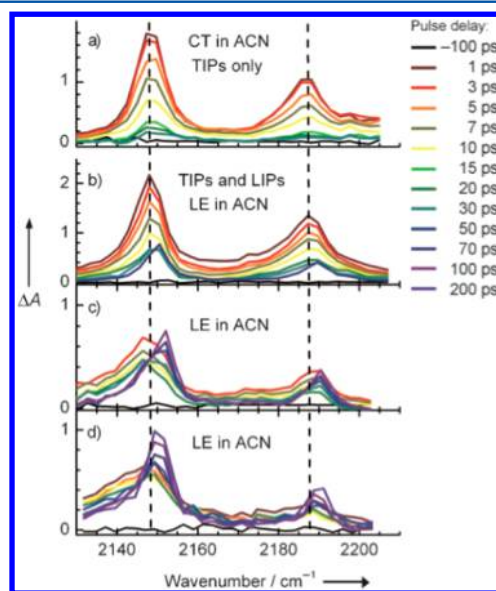


**Figure 44.** Time-resolved mid-IR absorption spectra in the CN stretching mode region of the radical anion of 51 in acetonitrile after local excitation of 49 in the presence of various concentrations of 51 (b–d; 0.9, 0.2, and 0.1 M) evidencing different spectral signatures for TIPs (positions indicated by dashed lines) and LIPs. (a) Spectra measured upon pure CT excitation. Reprinted with permission from ref 427. Copyright 2008 Wiley.

products upon local excitation of the fluorophore even in polar solvents.<sup>427</sup>

To circumvent the intricacies arising from diffusion in bimolecular reactions, Petersson and Hammarström investigated the charge separation dynamics in loose DA complexes consisting of a sulfonated Zn-porphyrin (derivative of **75**) and viologen derivatives.<sup>436,437</sup> The sulfonated Zn-porphyrin was excited locally to the vibrational ground state of its  $S_1$  state, into a vibrationally hot  $S_1$  state and into the  $S_2$  state. Using broadband fs transient electronic absorption, the authors could monitor and quantify all relevant reaction steps. From these spectra and from the analysis of the driving-force dependences of the charge separation and charge recombination rates in terms of Marcus theory, the authors deduced the reaction scheme depicted in Figure 45. While excitation into  $S_{1,v=0}$  and

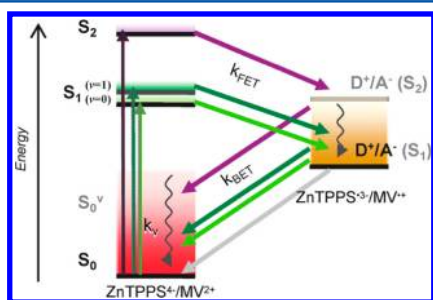


**Figure 45.** Energy-level diagram and tentative reaction pathways for the sulfonated Zn-porphyrin/ $MV^{2+}$  system upon excitation with different amounts of excess energy. Reprinted from ref 436. Copyright 2010 American Chemical Society.

$S_{1,v=1}$  resulted in photoinduced charge separation to the radical ions within 100 fs to 1 ps, depending on the driving force, excitation into the  $S_2$  state was inferred to result in the generation of the excited radical species. In refs 438 and 439 Vauthey and co-workers had demonstrated that this was indeed a feasible reaction pathway in porphyrins upon  $S_2$  excitation. The authors found that the amplitude of the hot ground state features correlated with the administered electronic excess energy. This indicated that both CS as well as CR were successfully competing with vibrational relaxation in the corresponding educt states. In particular, the excited radical ion pair, generated upon  $S_2$  excitation, quickly underwent IC to a vibrationally hot radical ion pair state. The ensuing CR to the electronic ground state, with rates from  $10^{11}$  to  $2 \times 10^{12} \text{ s}^{-1}$ , was also found to compete efficiently with IVR within the radical ion pair, thus carrying the vibrational excess energy from the initially locally excited state throughout the entire photocycle back to the electronic ground state.

The groups of Vauthey and Nibbering looked at the vibrational temperature of the ground state of various D/**51** pairs after an ultrafast CS and CR photocycle to obtain information on the possible formation of excited radical ions as primary CS product.<sup>440</sup> To this end, they employed fs time-resolved IR spectroscopy to monitor the CN-stretch region of **51**. Whenever electronically excited donor radical cations participated in the photocycle, very different residual vibrational temperatures were found for the donor and **51**, with the former being significantly hotter than the latter. On the other hand, when no excited ion was involved, both D and **51** reached an approximately similar final vibrational temperature.

**2.3.5.1. Diffusion Assisted CR.** As discussed above, CR in TIPs is ultrafast and, thus, occurs without significant diffusion

of the ions. The situation can be different with LIPs for which charge recombination could be coupled with substantial diffusion. Only a few studies have combined ultrafast time-resolved experiments, allowing the ion population to be followed in real-time, with theoretical models based on the DRE approach (see section 2.3.1).

In a series of investigations, the Fayer group combined several time-resolved techniques (fluorescence and visible pump–probe spectroscopy) with a DRE-based analysis on the full photocycle, i.e., excitation/CS/CR to the ground state, of various organic D/A pairs in solution.<sup>305,387,441</sup> The CS step and its DRE analysis were first reported in refs 396 and 404 whereas the whole photocycle was investigated in refs 305 and 387.

The photocycle of the **67/68** pair in diethylsebacate as liquid and sucrose octaacetate as solid solvent was first studied.<sup>387</sup> The experiments comprised steady-state and time-resolved emission spectroscopy with 70 ps time resolution as well as single color pump–probe spectroscopy with 100 ps resolution. This yielded the fluorescence quantum yield, the fluorescence dynamics of **67** as well as the pump–probe signal (reflecting mostly the ground-state recovery dynamics) as experimental observables. These were compared with their theoretical analogues from the use of a DRE approach with exponentially decaying distance dependent rates for CS and CR, a Coulomb interaction potential in the DRE for the ions, and accounting for fluorophore-quencher and quencher-quencher excluded volumes.<sup>442</sup> With the ET parameters obtained from the experiments in solid solution, where diffusion was absent, excellent agreement with the observed CS and CR dynamics in liquid solution was obtained. However, it is important to note that this was only possible when using the high-frequency dielectric constant in the Coulomb potential, as the low frequency value significantly underestimated the strength of the Coulombic interaction. The authors attributed this finding to the fact that at the short distance at which ET occurs, the molecularity of the solvent becomes important.

Fayer and co-workers extended the above study to two solvents of slightly elevated viscosity (approximately 6 and 18 cP).<sup>305</sup> Here, the authors used pump–probe spectroscopy to specifically monitor the ionic product band and applied a significantly modified and expanded theoretical model. As outlined above, the authors had shown in refs 386 and 404 how to include the solvent structure and the hydrodynamic effect and had convincingly demonstrated that these modifications to the theory were mandatory. In addition, the authors now also accounted for the fact that the recombination reaction proceeded at large driving force by using the semiclassical expression for the ET rate. The added information obtained from the pump–probe data also allowed for identifying the need to introduce a time-dependent dielectric constant, as a consequence of solvent relaxation.

In the most recent paper in this series, Fayer and co-workers significantly increased the observable time-window of their experiments by using broadband transient electronic absorption with a time-resolution of 100 fs to study the quenching of **59** by **DMA** in three organic solvents in the 0.3 to 1.3 cP viscosity range.<sup>441</sup> By properly selecting the observation wavelengths, they were able to access the transient concentration profiles of the excited state of the fluorophore and of the charge-separated state. In order to describe the experimental data, the DRE approach (with the appropriate distance-dependent reaction terms for ET, solvent structure and the hydrodynamic effect)

was used. Contrary to previous observations, the authors did not account for a time-dependent dielectric constant via the longitudinal relaxation of the solvent. Using the electronic coupling element,  $V$ , as the only and solvent independent fitting parameter, yielded excellent fits to the charge separation reaction in all solvents and at all concentrations studied (Figure 46). The recombination dynamics, on the other hand,

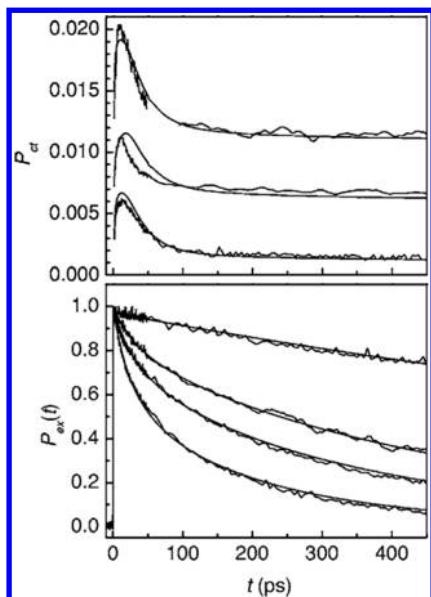


**Figure 46.** Fits and dynamics for charge separation (bottom panel) and charge recombination (top panel) of **59** by **DMA** in benzonitrile at 0.17, 0.27, and 0.48 M. The charge recombination data from low to high concentration are vertically offset by 0, 0.005, and 0.01, respectively. Adapted with permission from ref 441. Copyright 2006 American Institute of Physics.

especially at larger viscosities, were only moderately well reproduced, most probably due to the neglect of the solvent relaxation dynamics and thus of a time-dependent Coulomb potential. Nonetheless, the so-obtained ion dynamics were found to be approximately correct and reproduced the most prominent features.

Whereas the charge separation reactions investigated by the Fayer group exclusively occurred at relatively low driving force, Gladkikh et al. studied the recombination dynamics of the **64a**/**51** system, for which charge separation is highly exergonic and had been successfully described using a DRE approach with two active sink-terms.<sup>443</sup> The ion dynamics had been previously determined using single wavelength transient electronic absorption spectroscopy with a 100 fs time resolution, evidencing ultrafast charge recombination and vanishingly small free ion yields.<sup>435</sup> Building on the previously found double channel ionization the authors extended the theoretical description to incorporate hot recombination of the ion pair to the ground state by expanding the DRE with diffusion along the solvent reaction coordinate, in addition to diffusion along the spatial coordinate. In addition to the suggestion of Fayer and co-workers to include the hydrodynamic effect,<sup>404</sup> the spatial dispersion of the dielectric constant was also taken into account. However, whereas the charge separation dynamics could be very well simulated, the charge recombination dynamics could only be moderately well reproduced, the discrepancy being the largest at short (<20 ps) and long time (>1 ns). Nonetheless, the analysis allowed for a significant

insight into this rather complex reaction: the two ionization channels (to the ions in the ground state and excited states) were found to be responsible for two ion populations at different distances and thus with different ability to escape recombination. Most importantly, however, it was found that almost 90% of the ions underwent charge recombination when still vibrationally “hot”, i.e., before having relaxed to their ground state. This was identified as the main source of the relatively low free ion yields. The authors stressed that combining spatial diffusion and the dynamics along the solvent reaction coordinate is mandatory for a proper description of complex ultrafast processes.

While Gladkikh et al.<sup>443</sup> had successfully applied a modified version of the DRE approach to the accelerated charge recombination dynamics from nonequilibrated ion pair populations, Vauthey and co-workers studied recently the opposite case, namely the retardation of charge recombination due to solvent relaxation.<sup>444</sup> In this work, the charge recombination of ion pairs generated upon ET quenching of several aromatic hydrocarbons, including anthracene (**63**) and perylene (**64**) derivatives, by **DMA** was studied in three different solvents: (i) acetonitrile, a polar and fast relaxing solvent, (ii) benzyl acetate, a medium polar and slowly relaxing solvent and (iii) pure **DMA**, with similar polarity and dielectric relaxation times as benzyl acetate. The ion pair dynamics were monitored using fs transition electronic absorption and TCSPC for following the emission of the exciplex, while fs fluorescence up-conversion allowed the monitoring of the charge separation step. The experimental findings were as follows: (i) CR in pure **DMA** was almost 2 orders of magnitude slower than CS; (ii) CR in all three solvents exhibited the Marcus inverted region; (iii) CR was slowed down by solvent relaxation dynamics if the time scales of the two processes became comparable. While the first observation could be rationalized by the different nature of CS and CR, with the first being a bulk- and the latter being a pair-process, the authors had to use a modified DRE model to describe the solvent dynamic effect on the CR. To this end, a distance-dependent ET probability with a time-dependent driving force, which relaxed due to solvent relaxation,<sup>100</sup> was used as a reaction term in the DRE for the CR process. This model was found to give a significantly better description of the observed CR dynamics when compared to simpler ET models.

Summarizing, we would like to stress that the DRE approach, with its pronounced flexibility and generality and the ease of accessible numerical solutions, provides a useful framework for the understanding of all kinds of diffusion-assisted reactions. In particular it allows not only access to the intrinsic parameters of the underlying elementary processes (like ET) but also to the distance distribution of the reaction products. Especially the latter was shown to exhibit a pronounced effect on the fate of the ions and such important parameters as the free ion yield.

### 3. PROTON-TRANSFER REACTIONS

#### 3.1. Introduction

Similar to electron-transfer reactions, hydrogen atom or hydrogen cation transfer (hereafter both are referred to as proton transfer, PT) reactions are undoubtedly one of the most elementary and yet one of the most significant reactions in chemical and biological processes.<sup>445–448</sup> These reactions involve the transfer of a proton from a proton donor (AH) to a proton acceptor (B). Proton-transfer reactions can be divided into two main classes: intramolecular and intermo-



lecular PT. In intramolecular PT, the donor and acceptor moieties reside in the same molecule and are often directly hydrogen bonded to each other. In this case, the transfer does not necessarily result in the formation of charged species due to an electronic rearrangement and is sometimes considered as hydrogen atom transfer (several keto–enol tautomerizations, for example). In addition, the process does not require involvement of the solvent. In the intermolecular PT, the proton is transferred either to an external acceptor (bimolecular), such as an organic base, or to the solvent (pseudounimolecular) and in most cases results in the formation of ion pairs. Therefore, the process is usually strongly influenced by the solvent. We will structure the review based on this division into intra- and intermolecular PT, similarly to ET reactions.

Experimental observation of the initial processes in the proton-transfer reactions of ground-state species is complicated by the dynamic nature of the dissociation-association equilibrium. Discovery of excited-state acids enabled detailed time-resolved studies of the dissociation process. Excited-state acids (photoacids) are organic compounds that exhibit an increase in the acidity (decrease in  $pK_a$  value) upon excitation to a higher electronic state. The dissociation process of photoacids can thus be initiated by excitation with a laser pulse. Therefore, the reaction has a well-defined time zero and can be spectroscopically followed in time. Excited-state proton transfer (ESPT) serves as a model system for studying the microscopic reaction mechanism and has thus received great attention both from the theoretical and experimental viewpoints.

Several theoretical approaches for the PT reaction can be found in the literature. Descriptions of the free-energy relations were presented by Marcus,<sup>449–451</sup> Agmon and Levine,<sup>452–455</sup> and Arnaut and Formosinho,<sup>456,457</sup> for example. All these descriptions are based on the bond-energy bond-order (BEBO)<sup>458</sup> considerations to define the reaction coordinate for the free-energy surfaces. These models do not show the inverted region and the rate reaches its maximum value at very large driving force. Second, the reaction coordinate mainly originates from the bond rupture and bond formation. Both the models of Marcus, as well as that of Agmon and Levine are widely used for structure–reactivity correlations. According to the Marcus-BEBO model, the activation barrier can be determined according to<sup>449–451</sup>

$$\Delta G^\ddagger = \frac{\Delta G}{2} + \Delta G_0^\ddagger + \frac{\Delta G_0^\ddagger}{\ln(2)} \ln \left( \cosh \left[ \frac{\Delta G \ln(2)}{2\Delta G_0^\ddagger} \right] \right) \quad (39)$$

where  $\Delta G$  is the reaction free energy and  $\Delta G_0^\ddagger$  is the intrinsic barrier for a symmetric reaction ( $\Delta G = 0$ ). Agmon and Levine considered a mixing entropy term to account for the activation barrier. According to their model, the barrier is defined as<sup>452,455</sup>

$$\Delta G^\ddagger = \Delta G - \Delta G_0^\ddagger \ln(n^\ddagger)/\ln(2) \quad (40)$$

where  $n^\ddagger$  is the fractional bond order of the product in the transition state (TS).

$$n^\ddagger = \left[ 1 + \exp \left( -\frac{\Delta G \ln(2)}{\Delta G_0^\ddagger} \right) \right]^{-1} \quad (41)$$

When  $n^\ddagger$  is small, the TS is close to the reactant whereas at large value it is close to the product. The reaction free energy in both models is usually estimated from the excited-state acid dissociation constant ( $pK_a^*$ ) according to classical thermody-

namics and correlated to the rate with an Arrhenius-type equation.

Some of the most modern theories of the PT reaction are based on the seminal works of Hynes and co-workers.<sup>459–465</sup> They derived expressions for the reaction rate constants of intermolecular PT within a hydrogen-bonded contact pair in two separate regimes, adiabatic and nonadiabatic regime. The two regimes are characterized by a strong and a weak hydrogen bond, respectively. In both cases, the proton motion is fully quantum mechanical in character and the reaction coordinate is the solvent coordinate, contrary to the more traditional views. In the description of Hynes and co-workers, the rapidly vibrating proton follows the environment's slower rearrangement and the free energy of activation is largely determined by the solvent reorganization.

In the adiabatic regime, the proton motion does not involve tunneling but is still quantum mechanical. The zero-point energy of the proton lifts the energy above the proton barrier in the transition state and the PT proceeds without a classical barrier crossing. The quantum character of the proton is also manifested by delocalization of its wave function over the reactant and product wells in the transition state. In the case of a symmetric PT the adiabatic reaction rate constant is given by<sup>463</sup>

$$k_{PT} = \frac{\omega_s}{2\pi} \exp \left( -\frac{\Delta G_{AD}^\ddagger}{RT} \right) \quad (42)$$

where  $\omega_s$  is the solvent fluctuation frequency in the reactant well and  $\Delta G_{AD}^\ddagger$  is the activation free energy in the solvent coordinate. The activation free energy for an asymmetric reaction is related to the reaction free energy,  $\Delta G$ , by<sup>461</sup>

$$\Delta G_{AD}^\ddagger = \Delta G_0^\ddagger + \alpha_0 \Delta G + \frac{1}{2} \alpha'_0 \Delta G^2 \quad (43)$$

where  $\alpha_0$  is the Brønsted coefficient, the derivative of  $\Delta G^\ddagger$  with respect to  $\Delta G$ , and  $\alpha'_0$  is the derivative of  $\alpha_0$  with respect to  $\Delta G$ . Both  $\alpha_0$  and  $\alpha'_0$  are calculated for the symmetric reaction in a similar manner to  $\Delta G_0^\ddagger$ .

In the nonadiabatic regime, the two lowest vibrational levels of the proton are below the barrier in the transition state and the PT proceeds exclusively via a tunneling mechanism. In the simplest case, the nonadiabatic reaction rate constant for a symmetric PT is given by<sup>465</sup>

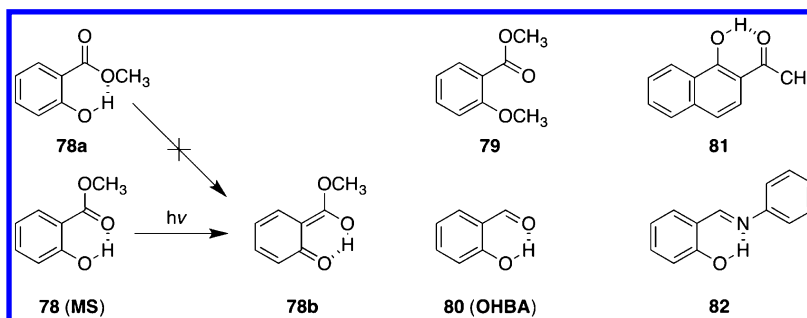
$$k_{PT} = \frac{C^2}{\hbar} \sqrt{\frac{\pi}{E_s RT}} \exp \left( -\frac{\Delta G^\ddagger}{RT} \right) \quad (44)$$

where  $C$  is the proton coupling constant representing the tunneling probability and  $E_s$  the solvent reorganization energy. The activation barrier is related to the reaction free energy by

$$\Delta G^\ddagger = \frac{(\Delta G + E_s)^2}{4E_s} \quad (45)$$

The above equations are derived for a fixed donor–acceptor distance where both the reactant and product states are in their vibrational ground state. In reality, the H-bond vibrations influence the DA distance therefore affecting the coupling. As the DA distance decreases, the coupling increases resulting in much faster rate. Second, higher vibrational states of the reactant and product may experience a different barrier for the tunneling process. To account for these effects,  $C$  would be replaced by the weighted quantum average over all the

Chart 15. Structures of Methyl Salicylate (MS) and Related Compounds



vibrational state-to-state transitions where the weight comes from the thermal occupation of the reactant vibrational level. All these effects have been thoroughly discussed in the literature.<sup>459,462,464,465</sup>

The first experimental observation of ESPT was realized by Weber in 1931, who reported on a pH dependent fluorescence spectrum of 1-naphthylamine-4-sulfonate, while the absorption spectrum stayed the same in that pH range.<sup>466</sup> However, it took almost 20 years before the first detailed description of the process. In 1950, Förster correctly attributed the dual emission of 2-naphthol in aqueous solution to the neutral and anionic species after ESPT to the solvent. The deprotonated conjugate base exhibited an unusually large Stokes shift while the methyl ether-derivative exhibited only a single emission band due to the absence of ESPT.<sup>467</sup> Soon after, Förster proposed a thermodynamic reaction scheme for the estimation of the excited-state acidities ( $pK_a^*$  values) of photoacids (see section 3.3).<sup>468</sup> The Förster cycle is still widely applied to characterize photoacids due to its robustness and simplicity.<sup>469</sup> A few years later, Weller formulated the photophysical reaction scheme for the ESPT process and related the steady-state emission properties to the rate constants of the occurring processes.<sup>470,471</sup> This enabled the calculation of the  $pK_a^*$  value from the ratio of the forward and backward PT rates. Eigen and co-workers further modified Weller's kinetic scheme postulating that an intermediate species, namely a contact ion pair, was the primary product of the initial short-range proton transfer followed by a diffusion-controlled step to produce the fully separated free ions.<sup>472</sup> The two-step Eigen-Weller model (Figure 53 in section 3.3) is still used as a basis in explaining the intermolecular ESPT reactions. The pioneering works of Förster, Weller, and Eigen paved the way for further experimental research on ESPT processes. In sections 3.2 and 3.3, we discuss the particularities of the intra- and intermolecular ESPT reactions, respectively, and show representative examples of different molecular classes exhibiting ultrafast ESPT.

### 3.2. Intramolecular Proton Transfer

Intramolecular ESPT (ESIPT) remains an active topic among researchers as demonstrated by periodic reviews on this subject.<sup>473–481</sup> Studies on such molecules can give valuable insights into the fundamental mechanism of the proton-transfer reaction but are also receiving increasing interest due to their potential in applications as luminescent materials and molecular probes, for example.<sup>482–484</sup> This owes to the extremely large Stokes shift of the ESIPT tautomer emission and the sensitivity of the tautomerization yield to the environment.

The range of reported molecules exhibiting ultrafast ESIPT is enormous and this review is by no means exhaustive. A

relatively recent review by Uzhinov and Khimich lists 122 ESIPT molecules and the authors conclude that in most systems, possessing a strong intramolecular hydrogen bond, the ESIPT is an ultrafast, barrierless, nonequilibrium process.<sup>481</sup> In the following discussion, we highlight a few typical and well-studied molecular classes exhibiting ultrafast, nonequilibrium ESIPT. The covered classes are based on salicylates, hydroxyflavones, and benzoazoles. These classes also represent the different reaction types, namely keto–enol type hydrogen transfer, proton transfer to an oxygen acceptor and proton transfer to a nitrogen acceptor, respectively. Several other classes undergoing single or double proton transfer, such as anthraquinones and bipyridyldiols for example, are not discussed here and readers are referred to the literature.<sup>485–512</sup>

#### 3.2.1. Methyl Salicylate and Related Compounds.

Methyl salicylate (**78**, **MS**, Chart 15) was the first reported compound in which ESIPT was observed.<sup>513</sup> Weller studied the absorption and emission spectra of this molecule and attributed the dual emission to an excited-state equilibrium between the initially excited neutral species and the zwitterionic tautomer resulting from the ESIPT reaction.<sup>514</sup> The absence of the red-shifted emission band in the methylated derivative, methyl 2-methoxybenzoate (**79**), supported this conclusion. Moreover, the excited-state potential was proposed to have two well-defined minima along the proton-transfer coordinate corresponding to the two tautomers.

However, Weller's ideas were questioned by later studies, which showed that the two emission bands had differing excitation spectra and that the ratio of the intensities of the two bands was strongly dependent on the solvent and the excitation wavelength, especially in protic solvents.<sup>515,516</sup> This led to the conclusion that the short wavelength emission band is mainly due to ground-state species that do not have a hydrogen bond between the phenolic hydrogen and the carbonyl group i.e. are either hydrogen bonded to the protic solvent or to the ester oxygen (**78a**).<sup>517,518</sup> Second, the lack of observed kinetics for the formation of the ESIPT product in the picosecond studies suggested that the process was extremely fast.<sup>519,520</sup> Smith and Kaufmann tried to resolve the ESIPT rate but they could only establish a lower limit of  $10^{11} \text{ s}^{-1}$  for the process. The observed kinetics were not influenced by lowering of the temperature down to 4 K or by deuteration within their time resolution.<sup>520</sup> All these observations were not consistent with the initial double-well model suggested by Weller. In addition, the zwitterionic tautomer was proposed to resemble a nonionic quinoid or keto form (**78b**) as originally suggested by Goodman and Brus.<sup>521</sup>

Herek et al. resolved the ESIPT dynamics of **MS** using femtosecond depletion spectroscopy. They monitored the rise of the tautomer fluorescence in the gas phase at room

temperature. The observed time constant for the ESIPT was found to be 60 fs without any deuterium isotope effect.<sup>522</sup> The authors proposed that the potential energy surface is highly asymmetric along the hydrogen-bond reaction coordinate and the initially prepared wavepacket evolves adiabatically toward a single minimum corresponding to the keto tautomer. In addition, they suggested that a reduction in the O–O distance by low-frequency vibrations could assist in the proton-transfer dynamics.<sup>480</sup>

More insights into the reaction mechanism and dynamics came from studies on related compounds, such as *o*-hydroxybenzaldehyde (**80**, OHBA). OHBA lacks the ester methoxy group and exists predominantly as a single internally hydrogen-bonded conformer in nonpolar solvents.<sup>523</sup> Stock et al. investigated the ESIPT of this compound in cyclohexane using two-color transient electronic absorption with 30 fs time resolution.<sup>524</sup> They observed a ca. 45 fs rise of the product emission, which they attributed to the ESIPT process. The rise could be modeled by a delayed step function rather than by an exponential rise. In addition, the rise was accompanied by coherent oscillations of the signal due to coherently excited vibrations in the product state (Figure 47). Three frequencies

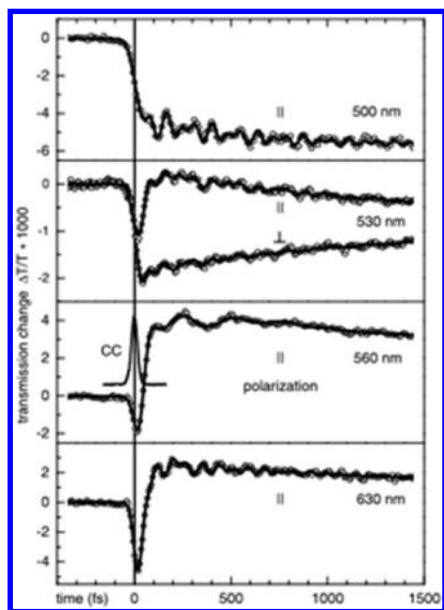


**Figure 47.** Transient absorption profiles measured at different monitoring wavelengths with OHBA (**80**) in cyclohexane (open circles) and best-fits of model functions (solid lines). The polarization of the probe is indicated in the figures. A typical cross-correlation measurement is overlaid with 560 nm signal. The oscillatory components are due to coherently excited vibrations in the product state. Reprinted with permission from ref 524. Copyright 2002 Elsevier.

of  $\sim 140\text{ cm}^{-1}$ ,  $\sim 280\text{ cm}^{-1}$ , and  $\sim 420\text{ cm}^{-1}$  were required to model the oscillatory contributions and attributed to an out-of-plane, and two in-plane skeletal deformations, respectively, based on DFT calculations. The two in-plane deformations strongly modulate the O–O distance. The fast initial ESIPT process was followed by vibrational relaxation and cooling of the solvent bath on a longer time scale. Based on their observation, the authors proposed that the ESIPT proceeds as a ballistic motion of the wavepacket along the skeletal coordinates associated with the reduction of the hydrogen

DA distance. In another study, Lochbrunner et al. observed no significant isotope effect for the deuterated analog of OHBA, demonstrating the absence of tunneling or reaction barrier in the process, in support of the ballistic mechanism.<sup>525</sup>

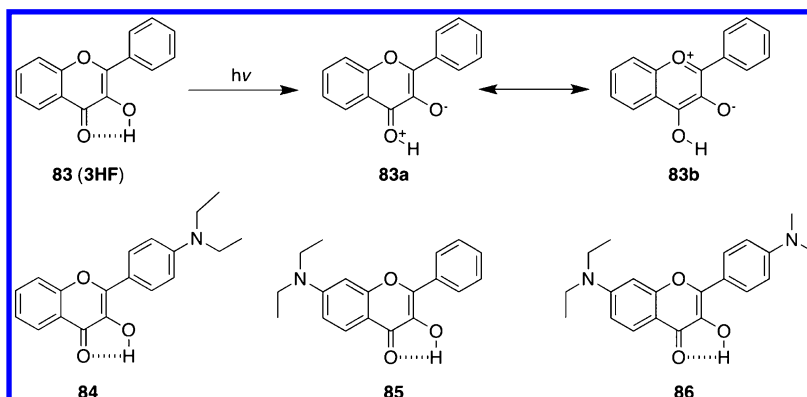
A similar ballistic ESIPT mechanism was proposed for a close analog, 1-hydroxy-2-acetonaphthone (**81**). It was originally investigated in the gas phase by Lahmani and co-workers<sup>480,526</sup> and subsequently in solutions and nanocavities by Douhal and co-workers.<sup>527–530</sup> The time resolution of these studies was, however, not sufficient to resolve the initial ESIPT process and the studies were focused on the subsequent internal twisting motion of the acetyl group and the nonradiative relaxation to the ground state. More recently, Lochbrunner et al. investigated the ESIPT in cyclohexane using resonance Raman spectroscopy and fs two-color and broadband transient electronic absorption, complemented with DFT calculations.<sup>531</sup> Similarly to OHBA, **81** has only a single stable ground-state structure possessing a strong intramolecular hydrogen bond in nonpolar solvents. The resonance Raman studies showed that excitation of **81** activates several low-frequency in-plane modes associated with deformations and bond-length changes in the naphthalene chromophore. These modes were also suggested to alter the intramolecular hydrogen-bond length. The fs two-color transient absorption data showed a rise of the tautomer emission with a delay of ca. 30 fs accompanied by coherent oscillations followed by slower relaxation in 150 fs ascribed to vibrational redistribution. The results were analyzed in a similar manner as in the case of OHBA. The oscillatory contributions with three main frequencies were attributed to coherently excited modes. The dominant contribution with a frequency of  $312\text{ cm}^{-1}$  was assigned to a skeletal in-plane vibration of the hydroxyl and acetyl groups based on the Raman measurements and DFT calculations. This mode leads to a bending of the donor and acceptor groups toward each other and significantly reduces the DA distance and was thus suggested to give the dominant contribution to the ESIPT process. Due to the fast time scale of the process, the authors suggested that the initial acceleration of the wavepacket is driven by the slope of the potential energy surface in the Franck–Condon region and points directly toward the tautomer minimum. The main findings were corroborated in a separate computational study by Ortiz-Sánchez et al.<sup>532</sup> They calculated one-dimensional potential energy surfaces for the ESIPT, which showed a negligible barrier. They subsequently performed quantum dynamics simulations of the ESIPT process using the calculated potential energy surfaces, which revealed a  $\sim 25\text{ fs}$  ESIPT time constant, in remarkably good agreement with the experimental study.

Examples of analogs using nitrogen as the proton acceptor have also been presented in the literature. The ESIPT dynamics of salicylidenaniline (**82**) and its derivatives were studied by several groups with ps time resolution<sup>533–535</sup> and later by Mitra et al.<sup>536</sup> with fs time resolution. Similarly to salicylaldehyde, the ultrafast initial proton transfer produces the vibrationally hot keto tautomer in few hundred fs followed by vibrational relaxation.

**3.2.2. Hydroxyflavones.** Another well-studied molecule undergoing ESIPT between a hydroxylic proton and a carbonyl oxygen is 3-hydroxyflavone (**83**, 3HF), an analog of the naturally abundant flavonol quercetin. Contrary to MS, the ESIPT in this case results in the formation of charged species due to the absence of a keto-type resonance structure. In an early report, Sengupta and Kasha already attributed the dual



Chart 16. Structures of 3-Hydroxyflavone (3HF) and Related Compounds



emission to the neutral form and to the zwitterionic tautomer, which is stabilized by the two resonant structures shown in Chart 16 (83a and 83b).<sup>537</sup> Strong normal fluorescence observed at low temperature in a hydrocarbon glass and isotope effect in methanol suggested a double-well potential energy surface with a significant activation barrier between the two forms. The increased normal emission in alcohols was proposed to originate from intermolecularly hydrogen-bonded species.

After this, 3HF was studied by several groups with varying time resolution.<sup>538–544</sup> Several reports focused on the solvent effects and reported a rise time of the ESIPT product emission of the order of tens of picoseconds.<sup>538–540</sup> McMorro and Kasha were, however, able to show that the spurious normal emission in nonpolar solvents was actually due to trace amounts of hydrogen-bonding impurities resulting in intermolecular hydrogen bonds.<sup>541</sup> They observed the pure tautomer emission in highly purified hydrocarbons even at cryogenic temperatures with a single-exponential rise<sup>545</sup> and proposed that the intrinsic ESIPT is an ultrafast and barrierless process. The biexponential kinetics observed in some other reports<sup>546,547</sup> were attributed to the internally and externally hydrogen-bonded species.

Later sub-picosecond studies focused on the time scale of the intrinsic ESIPT process.<sup>548–550</sup> Schwartz et al.<sup>548</sup> observed a  $240 \pm 50$  fs ESIPT time constant in a nonpolar environment followed by a slower  $\sim 10$  ps component using fs two-color transient absorption. The slower component was attributed to hydrogen-bonding impurities as suggested by the earlier studies. Surprisingly, the authors found an instrument-limited ESIPT time of  $<125$  fs in methanol. They proposed that the ESIPT rate in this case could be accelerated due to intermolecular modes of the cyclically hydrogen-bonded species. A more recent collaborative study by several groups found somewhat different time constants using transient electronic absorption.<sup>550</sup> They observed two transient bands in the visible region, in qualitative agreement with the previous measurements.<sup>549,551,552</sup> Both bands showed an ultrafast initial rise followed by a slower component attributed to the internally and externally hydrogen-bonded species, respectively. The two bands were proposed to originate from an equilibrium between the two resonance structures of the tautomer (83a and 83b). The authors assigned an instrument-limited time constant of  $\sim 35$  fs for the intrinsic ESIPT process in methylcyclohexane and acetonitrile, whereas a  $\sim 60$  fs rise was observed in ethanol. The deceleration of the ESIPT in ethanol was attributed to greater strength of solute–solvent interactions. The time scale

of the slow component due to the intermolecularly hydrogen-bonded species was close to the solvent relaxation time but was suggested to originate from desolvation or breakage of the intermolecular hydrogen bonds rather than from solvation-assisted ESIPT.

Studies on functionalized 3HF derivatives revealed interesting excited-state behavior.<sup>554–561</sup> Attachment of electron donating groups to the aromatic system strongly influences the electronic properties of the locally excited state resulting in charge-transfer character. This was shown to result in solvent-polarity dependent ESIPT and, in some cases, reversibility of the process.<sup>560</sup> Chou et al. presented several examples of such molecular systems and discussed the results in the context of proton-coupled electron transfer (PCET). The field was also recently reviewed.<sup>553,562,563</sup> In most examples, the normal form has a relatively different electric dipole moment in the excited state due to the CT character whereas the dipole moment of the excited proton-transfer tautomer is more similar to that of the ground state.<sup>559</sup> Therefore, ESIPT from the initially populated Franck–Condon state of the normal form is energetically more favorable and proceeds in competition with solvent relaxation (Figure 48). Solvent relaxation of the normal form (PE\* in Figure 48) changes the equilibrium polarization to unfavorable for the ESIPT. This results in a decrease of the rate due to a solvent-induced barrier. The overall ESIPT dynamics are therefore nonexponential. In highly polar solvents, the energy of the solvent equilibrated normal tautomer can be close to that of the proton-transfer tautomer resulting in equilibrium between the two states and significant emission from the normal form.<sup>560</sup>

Two exemplary cases of such systems are 4'-N,N-diethylamino-3-hydroxyflavone (84)<sup>560</sup> and 7-N,N-diethylamino-3-hydroxyflavone (85).<sup>561</sup> The CT character of the locally excited state of the normal form was evidenced by strong solvatochromism of its emission ( $ET_{eq}^*$  in Figure 49) whereas the proton-transfer tautomer emission (PCET<sub>eq</sub>\* in Figure 49) and the normal absorption showed negligible solvatochromism. Second, both compounds exhibited pronounced dual emission compared to the parent 3HF and the relative emission intensities of the two forms were strongly dependent on solvent polarity. Upon increasing polarity, the normal emission gained intensity, which could be attributed to two possible effects. First, the solvent-induced barrier for the ESIPT increases in the polar environment, and second, the ESIPT reaction can become reversible because the two states are closer in energy as seen from the peak positions of the emission bands in Figure 49. Equilibrium between the two states was observed

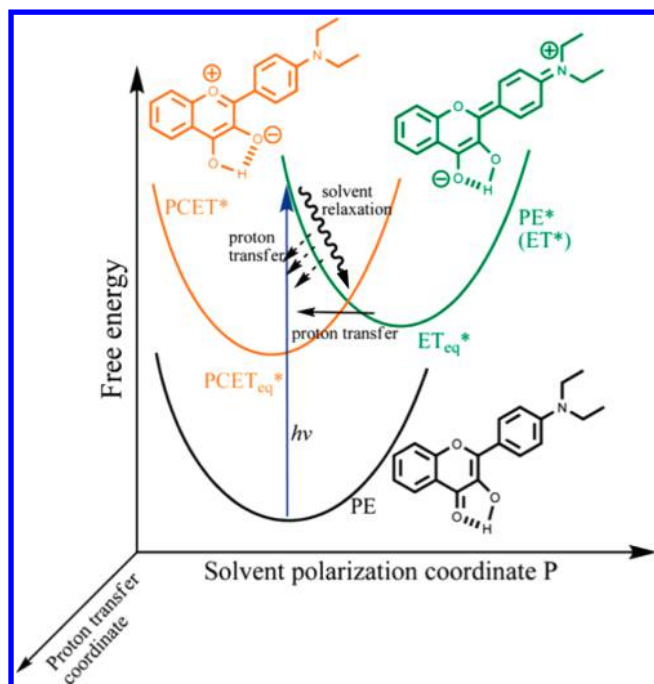


**Figure 48.** Potential energy surfaces and relaxation processes of different states of **84**. PE and PE\* (ET\*) correspond to the ground and excited states of the normal form and PCET\* to the proton-transfer tautomer. Reprinted from ref 553. Copyright 2010 American Chemical Society.

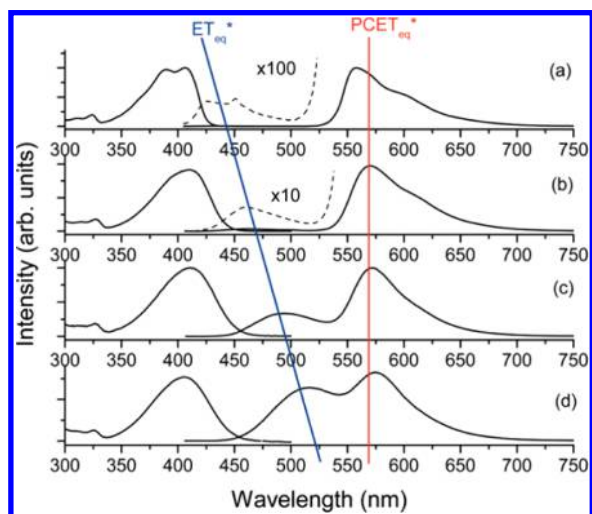


**Figure 49.** Absorption and emission spectra of **84** in (a) cyclohexane, (b) benzene, (c) dichloromethane, and (d) acetonitrile at room temperature. Reprinted from ref 553. Copyright 2010 American Chemical Society.

for **84**, whereas **85** exhibits irreversible ESIPT attributed to the much larger energy gap between the relaxed normal form and the proton-transfer tautomer. Interestingly, the solvent-polarity effects were completely switched off in 4'-N,N-dimethylamino-7-N,N-diethylamino-3-hydroxyflavone (**85**) due to dipole cancellation. This resulted in quantitative proton-transfer tautomer emission independent of the solvent polarity.<sup>559</sup>

Chou et al. investigated the ESIPT dynamics of **84** and **85** using fs fluorescence up-conversion and were the first to clearly identify an ultrafast component of the ESIPT process in polar solvents.<sup>560,561</sup> They observed multiexponential dynamics,

which were strongly dependent on the monitoring wavelength. Using spectral reconstruction, they were able to show that the emission spectrum consists of two separate bands already at short times (sub-picosecond) attributed to the normal and the tautomeric forms. At later time, the normal form exhibited a dynamic Stokes shift in competition with the ESIPT giving rise to the tautomer emission band. Population of the CT state was not observed as a separate step, contrary to the earlier report by Douhal and co-workers,<sup>558</sup> and was considered to take place through a direct optical transition. All the ultrafast dynamics were attributed to the solvent relaxation proceeding in competition with the ESIPT. The fast ESIPT component observed in all solvents was, nevertheless, significantly slower than that observed in the parent **3HF**. This was suggested to originate from an initial, non-negligible, solvent-induced barrier even in apolar cyclohexane. In addition to the ultrafast processes, both compounds showed a much slower polarity-dependent rate after the solvent relaxation. The solvent-dependent rate varied from a few ps in cyclohexane to a few tens to few hundreds of ps (for **84** and **85**, respectively) in acetonitrile. In polar solvents such as dichloromethane and acetonitrile, **84** exhibited a constant population decay over the whole wavelength range demonstrating the establishment of an equilibrium between the normal and the tautomeric forms after solvent relaxation. This also resulted in a much higher normal emission with increasing solvent polarity. The normal form of **85** did not show such a population decay and the emission intensity was relatively low in all solvents demonstrating an irreversible (unidirectional) reaction from the normal form to the proton-transfer tautomer. Additionally, the authors performed ab initio calculations to investigate the directions of the permanent electric dipole moments in the different states. The results clearly showed that the excited normal form had a significantly different dipole moment compared to those of the neutral ground state and the excited tautomer, thus explaining the observed behavior.<sup>559–561</sup>

Suda, Kimura and co-workers studied extensively the effect of excitation wavelength on the ESIPT dynamics of **84** in conventional solvents and in RTILs using fs Kerr-gated fluorescence.<sup>564–567</sup> They observed a clear decrease both in the rate and the yield of the tautomerization in RTILs (Figure 50b) and in the highly viscous glycerol triacetate upon increasing excitation wavelength. This effect was not observed in normal polar solvents such as acetonitrile and dimethyl sulfoxide. They suggested that excitation in the red edge populates a subensemble of species in a more polar microenvironment due to heterogeneities in the solvent. Therefore, the initially populated Franck–Condon state in the solvent coordinate and hence the solvent-induced barrier for the proton transfer depends on the excitation wavelength being higher for the longer wavelengths (Figure 50a). Due to slow solvation dynamics in RTILs and glycerol triacetate, the ESIPT occurs in competition with the solvent relaxation resulting in nonequilibrium dynamics. This was seen in the population dynamics obtained from spectral fittings of the time-resolved spectra with two log-normal functions. At least three rise components (instrument limited, few ps and few tens of ps) and a single decay component were required to simulate the population dynamics of the tautomer.<sup>565,567</sup> Despite the use of exponential functions to simulate the data, the authors noted that the behavior most likely represented a single continuous process with a time-dependent ESIPT rate due to the increasing reaction barrier upon solvent relaxation. RTILs

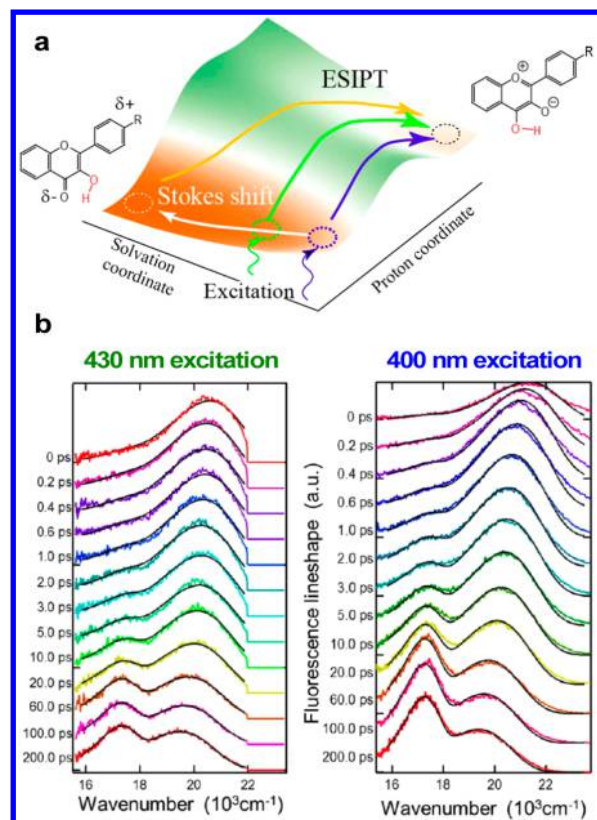


**Figure 50.** (a) Schematic illustration of the potential energy surface of **84** in the solvation and proton coordinates. The arrows indicate the reaction pathways at different excitation wavelengths. (b) Time-resolved emission spectra measured with **84** in 1-butyl-3-methyl-imidazolium hexafluorophosphate RTIL at different excitation wavelengths. The black solid lines represent the best fits with two log-normal functions. Adapted from ref <sup>567</sup>. Copyright 2013 American Chemical Society.

enable observation of the competitive processes on a much longer time scale due to the extremely slow solvent relaxation compared to conventional solvents.

**3.2.3. Benzoazoles.** Another type of ESIPT is observed in 2-(2'-hydroxyphenyl)benzothiazole (**87**, **HBT**) and related compounds. In this case, the ESIPT takes place from a hydroxyl donor to a nitrogen acceptor resulting in a neutral keto tautomer (**87a**). The ESIPT was already suggested by several early studies<sup>568–570</sup> but Elsaesser and Kaiser were the first to provide direct evidence for the keto–enol tautomerization using ps infrared spectroscopy. They observed the disappearance of the OH stretch mode and the appearance of two new IR absorption bands within 6 ps after excitation. These bands were attributed to NH and C=O stretching vibrations resulting from the tautomerization.<sup>571</sup> A few years later, Elsaesser et al. reported the first fs study on the ESIPT kinetics using transient electronic absorption spectroscopy. They observed a rise of the keto emission with time constants of ~160 and ~150 fs for the normal and the deuterated analog of **HBT**, respectively. The lack of an isotope effect suggested an essentially barrierless reaction. Second, based on the fast time scale of the process, the authors proposed that the ESIPT is assisted by large amplitude low-frequency vibrations.<sup>572,573</sup>

Riedle and co-workers investigated the tautomerization of **HBT** in cyclohexane with a much improved time resolution of ~30 fs using two-color transient electronic absorption. They

were able to resolve a rise time of ca. 30–60 fs for the keto emission depending on the probe wavelength.<sup>574,575</sup> Similar to **OHBA**, the rise was best modeled as a delayed step function convolved with the instrument response and was accompanied by coherently excited vibrational modes in the product state (Figure S1).<sup>576,577</sup> The two main oscillatory components with

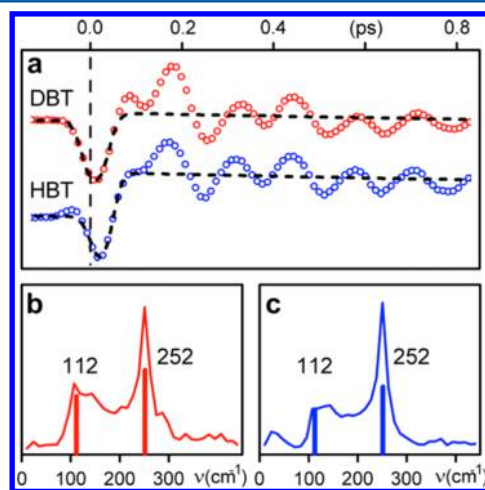


**Figure 51.** (a) Time profiles of the transmission change measured with **HBT** (blue) and its deuterated analog **DBT** (red) at the keto emission wavelength. The dashed lines represent the fits with an instant decrease followed by a delayed step increase. (b and c) Fourier-transform spectra of the oscillatory contributions of **DBT** (b) and **HBT** (c). Reprinted with permission from ref <sup>577</sup>. Copyright 2011 Elsevier.

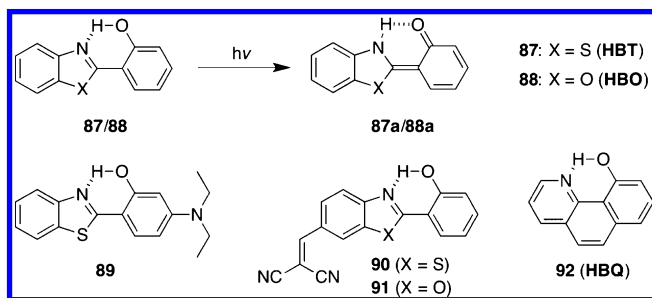
frequencies of ~110 and ~250 cm<sup>-1</sup> were attributed to in-plane bending and stretching vibrations of the entire molecular skeleton, respectively, in excellent agreement with ab initio calculations. These vibrations significantly modulate the O–N distance and can therefore promote the ballistic ESIPT process. The lowest frequency vibration of ~110 cm<sup>-1</sup> was identified as the coherently excited transition-promoting mode also supported by computational, resonance Raman and time-resolved IR studies.<sup>578–580</sup> Electronic excitation to the Franck–Condon state of the enol form initiates the nuclear motion along the O–N coordinate. Once the distance has contracted to a critical value, the electronic configuration changes extremely fast to adopt the keto-product configuration.<sup>581</sup> In this configuration, the ESIPT proceeds without a barrier and does not involve tunneling. The high-frequency proton follows the electronic changes adiabatically and forms the bond with the nitrogen acceptor. This was demonstrated by the observation of identical kinetics for the normal and deuterated forms of **HBT** (Figure S1).<sup>577</sup> Second, observation of identical oscillatory signals for the two analogs showed that the proton itself does not contribute to the wavepacket motion. After adopting the electronic configuration of the product state, the molecule is still far from the equilibrium geometry and starts to oscillate on the keto tautomer potential energy surface. This gives rise to other coherent wavepacket oscillations extending up to a few ps. The damping of the oscillations can be attributed to intramolecular vibrational redistribution and solvent-assisted vibrational relaxation processes.<sup>574,580</sup>

The closely related 2-(2'-hydroxyphenyl)benzoxazole (**88**, **HBO**) was shown to undergo a similar ESIPT from the hydroxyl group to the nitrogen. Ernsting and co-workers studied the dynamics of **HBO** in cyclohexane using fs transient



absorption and assigned a time constant of  $\sim 60$  fs for the ESIPT process.<sup>582</sup> In addition, they were able to observe a low-frequency vibronic progression of  $147\text{ cm}^{-1}$  in the fluorescence excitation spectrum in an argon matrix at 11 K, which they attributed to an in-plane vibration of the skeleton. Abou-Zied et al. studied the tautomerization in several solvents using fs two-color transient electronic absorption. The ESIPT kinetics were found to be solvent and isotope (H or D) independent with a time constant of  $\sim 170$  fs. The compound can, however, exist in multiple ground-state conformations of which only the internally hydrogen-bonded *syn*-enol (as in Chart 17) under-

**Chart 17. Structures of 2-(2'-Hydroxyphenyl)benzothiazole (HBT) and Related Compounds**



goes efficient ESIPT. The other conformations are either hydrogen-bonded to solvent or to the benzoxazole oxygen and their relative population is strongly solvent dependent. In nonpolar, noninteracting solvents, the compound is almost exclusively in the *syn*-enol conformation.<sup>583</sup> Later, Lochbrunner et al. observed a fast, step-like, rise of  $\sim 80$ – $90$  fs followed by coherent oscillations for **HBO** in cyclohexane using transient absorption with 30 fs time resolution.<sup>576</sup> Due to the similarity between the time scales and the coherent oscillations, the mechanism was suggested to resemble that of **HBT**.

In another study, Ernsting et al. investigated 2,5-bis(2'-benzoxazolyl)hydroquinone, a compound consisting of the same **HBO** subunit, in tetrahydrofuran using fs broadband transient electronic absorption with  $\sim 30$  fs time resolution. They were able to resolve all the involved species (normal, unrelaxed keto and relaxed keto forms) using spectral decomposition. In this compound, the ESIPT occurs in  $\sim 110$  fs driven by the coherent excitation of a skeletal bending vibration of  $118\text{ cm}^{-1}$  and the proton transfer occurs during the first half-cycle.<sup>584</sup> Recently, Wnuk and Kubicki et al. studied the ESIPT of the same compound in several solvents additionally using fs fluorescence up-conversion.<sup>585</sup> They concluded that the fast ESIPT is virtually solvent independent within their time resolution ( $\sim 100$  fs). Based on TCSPC measurements and computational results, they proposed that a solvent-dependent back reaction takes place resulting in an equilibrium between the two forms, which was seen as a constant population decay over the whole emission range. The calculated excited-state potential energy profile showed two minima of almost equal energies attributed to the normal and tautomeric forms. The two minima were separated by only a small energy barrier, supporting the equilibrium in the excited state.

Functionalization of the benzoxazoles with either electron-donating or electron-withdrawing groups can result in drastic changes in the proton-transfer properties.<sup>586–590</sup> Chou and co-workers demonstrated that the attachment of an electron-donating amine group on the phenol ring of **HBT** (**89**) results

in behavior similar to amine functionalized 3-hydroxyflavones. The initially excited state possesses CT character and a significantly different dipole moment from that of the ground state. The ESIPT occurs in competition with solvent relaxation resulting in an equilibrium between the normal and the tautomeric forms, both in nonpolar and polar aprotic solvents. The observed kinetics were solvent dependent and relatively complicated due to parallel solvation, as demonstrated by the fs fluorescence up-conversion and ps TCSPC studies.<sup>586</sup>

Recently, Douhal and co-workers reported on a similar behavior for a primary amine substituted benzoxazole where the substituent was on the benzoxazole moiety instead of the phenol ring. Using TCSPC and fs fluorescence up-conversion, they observed a relatively slow solvent-dependent ESIPT time constant from  $\sim 1.2$  ps in *n*-heptane to  $\sim 100$  ps in THF. All the ultrafast dynamics were attributed to the initial population of the charge-transfer state and subsequent solvent relaxation.<sup>588,589</sup> This is in contrast with the findings of Chou and co-workers who also considered the initial ultrafast ESIPT, which was observed as an initial rise of the keto emission on a sub-picosecond time scale before solvent relaxation.<sup>586</sup>

Contrary to the above-described behavior, malononitrile-functionalized compounds (**90** and **91**) have been shown to possess similar dipolar properties in the initially excited state and the ground state. The initially excited state undergoes concomitant proton and electron transfer with significant changes in the dipole moment followed by solvent relaxation (Figure 52). This was seen as virtually polarity-independent

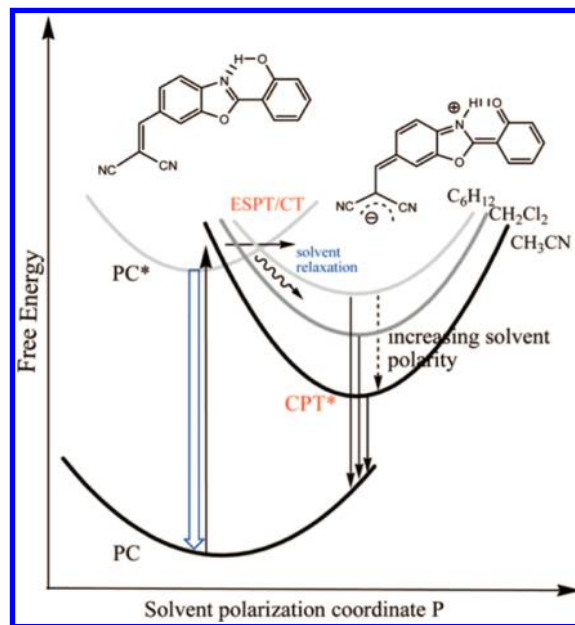


**Figure 52.** Potential energy surfaces and relaxation processes of the different states of **91**. PC and PC\* correspond to the ground and excited states of the normal form and CPT\* to the proton-transfer tautomer. Reprinted from ref 587. Copyright 2008 American Chemical Society.

absorption and emission spectra of the normal form, whereas the tautomer emission exhibited drastic bathochromic shifts upon increasing solvent polarity.<sup>587</sup> The behavior could be rationalized by the electron-donating properties of the azole nitrogen. The nitrogen is a poor electron donor in the enol form due to the delocalization of the lone pair electrons to the aromatic system. However, the nitrogen is converted into a

secondary amine upon proton transfer. The increased electron-donating character results in an adiabatic electron transfer to the malononitrile parallel to the proton transfer and increased dipole moment in the proton-transfer state. Chou and co-workers observed an increase in the ESIPT rate of the **HBO** derivative, **91**, upon increasing solvent polarity from 1.1 ps in cyclohexane to ~300 fs in acetonitrile in their fs fluorescence up-conversion measurements, whereas for the **HBT** derivative, **90**, the time constant was faster than the IRF (<150 fs) in all solvents. The acceleration of the ESIPT rate of **91** was attributed to the lowering of the solvent-induced barrier in more polar solvents.<sup>587</sup> The ESIPT rate of **90** was too fast in all solvents to observe this effect.

Kim et al. presented a similar example of functionalized **HBO** where the substituent is slightly less electron withdrawing (a single CN group) compared to the malononitrile compound.<sup>590</sup> In this case, the authors used fs fluorescence up-conversion with ~100 fs time resolution to measure the entire time-resolved spectra by scanning the mixing crystal angle and the monochromator simultaneously. In addition, they analyzed the obtained spectra globally with three log-normal functions to directly obtain the population dynamics. The three species were attributed to the enol, the neutral keto and the charge-transfer keto species. The observed ESIPT dynamics monitored from the decay of the enol population were governed by two time constants of 250 fs and 1.2 ps, independent of the solvent, which were attributed to two conformations due to the flexibility of the phenyl ring. Second, the authors suggested that the ICT process occurs subsequent to the ESIPT reaction with time constants of ~50 fs and 2.7 ps in diethyl ether. Therefore, only the charge-transfer keto species was subject to solvent relaxation and the enol and neutral keto emissions were treated as stationary in terms of peak position and bandwidth in the fitting model. The fit could adequately reproduce the experimental data but the authors had to use constraints in several parameters due to the instability of the analysis. This could suggest overfitting of the data and possibly two line-shape functions would have been adequate. The authors proposed that the ICT process is mainly controlled by the solvent relaxation due to the similarity of the time scales of these processes, whereas the ESIPT is controlled only by the intramolecular coordinates and is therefore solvent-polarity independent.<sup>590</sup>

Last, we turn to 10-hydroxybenzo[h]quinoline (**92**, **HBQ**), which can be considered as a rigid **HBT** with reduced conformational flexibility. Chou and co-workers were the first to demonstrate ESIPT in this compound.<sup>591</sup> They showed that the tautomer emission is free from solvent perturbations due to the strong intramolecular hydrogen bond making it an ideal candidate for detailed mechanistic studies. The unique tautomer emission was observed even in ethanol, contrary to several other ESIPT molecules.

The dynamics of the ESIPT reaction of **HBQ** were studied by many groups with ever improving time resolution. In an early study, Chou et al. were able to give an instrument-limited ESIPT time constant of ca. ≤160 fs in cyclohexane using fluorescence up-conversion and transient electronic absorption. They also suggested that the ESIPT populates a higher lying  $S_2$  state of the keto tautomer, which then undergoes internal conversion to  $S_1$  in ~330 fs and vibrational cooling in 8–10 ps to produce the relaxed keto form.<sup>592</sup> Takeuchi and Tahara studied the dynamics in the same solvent using broadband and two-color transient electronic absorption with 380 fs and ~30–

40 fs time resolutions, respectively.<sup>593</sup> The transient spectra were qualitatively quite different from those of Chou et al. but the observed kinetics after the ESIPT were in good agreement with the previous findings. The faster ~350 fs component was, however, attributed to an intramolecular vibrational energy distribution rather than internal conversion from  $S_2$ . This was also supported by the observation of long-lived coherent oscillations in the two-color experiment. The two-color experiment with better time resolution allowed the authors to resolve the initial rise of the keto emission with a  $25 \pm 15$  fs time constant. The signal was accompanied by coherent oscillations up to a few ps with frequencies of 242, 392, 550, and  $692\text{ cm}^{-1}$  determined from the Fourier transform of the oscillatory contribution. The lowest frequency mode was assigned to an in-plane skeletal vibration modulating the O–N distance in agreement with DFT calculations. Measurements with different excitation wavelengths and resonance Raman experiments suggested that the observed modes are coherently excited by the initial pump pulse. Much faster damping of the  $242\text{ cm}^{-1}$  oscillations (~500 fs) led to the conclusion that this mode is most strongly coupled with the reaction coordinate. Therefore, the ESIPT mechanism was suggested to resemble that of **HBT**.

Later studies revealed, however, distinct differences between the ESIPT mechanisms of **HBT** and **HBQ**. Schriever et al. compared the ESIPT dynamics of the two compounds in a combined experimental and computational study.<sup>594</sup> The experimental results were mostly in agreement with the previous observations providing no new insights. The classical dynamics simulation however suggested that **HBQ** experiences a much smaller variation in the O–N distance during the proton transfer, possibly due to the more rigid structure. This was interpreted as a partially proton-active mechanism where the movement of the proton itself plays a role in the process. **HBT** on the other hand showed a large decrease in the O–N distance prior to the ESIPT, exhibiting a fully proton-passive mechanism in agreement with the lack of an observed isotope effect. Recently, Joo and co-workers provided experimental evidence to support these conclusions.<sup>595,596</sup> They used fluorescence up-conversion with ~40 fs time resolution to monitor the decay of the enol form and the rise of the keto emission. The ESIPT time constants for the normal and deuterated forms of **HBQ** in methanol were 12 and 25 fs, respectively, whereas **HBT** showed a ca. 62 fs time constant without any isotope effect in cyclohexane.<sup>596</sup> The kinetic isotope effect of ~2 was proposed to originate from a fully active participation of the proton to the ESIPT process whereas in **HBT** the ESIPT is driven by the large amplitude skeletal vibrations without any involvement of the proton.

**3.2.4. Concluding Remarks.** In conclusion, ESIPT in internally hydrogen-bonded conformations is an ultrafast, barrierless nonequilibrium process. The ESIPT proceeds as ballistic motion and is assisted by skeletal vibrational modes without involvement of the solvent coordinates. The proton can have either a passive or an active role depending on the geometric constraints of the skeletal structure. In many cases, the interaction with the solvent results in a decrease in the ESIPT rate mostly due to the solvent perturbations to the intramolecular hydrogen-bond coordinates.

Attachment of electron-donating or electron-withdrawing groups on the ESIPT compounds drastically changes the behavior. The process becomes strongly solvent-polarity dependent due to the coupling of the charge-transfer and

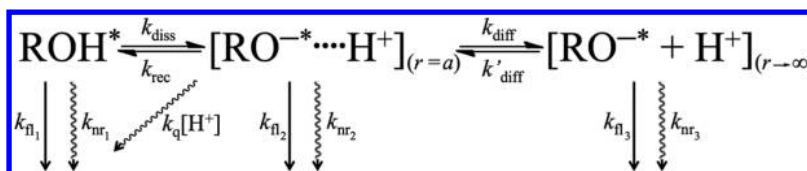


**Figure 53.** Photophysical scheme for the intermolecular ESPT process. Here,  $k_{\text{fl}}$  and  $k_{\text{nr}}$  are the radiative and nonradiative rate constants,  $k_{\text{q}}$  is the quenching constant by protons,  $k_{\text{diss}}$  and  $k_{\text{rec}}$  are the forward and backward PT rate constants producing the contact ion pair,  $k_{\text{diff}}$  and  $k'_{\text{diff}}$  are the forward and backward diffusional rate constants, and  $a$  is the contact radius.

proton-transfer processes. The ESIPT proceeds in competition with the solvent relaxation with significantly decelerated rate due to the solvent-induced barrier. This is manifested by nonexponential dynamics complicating the quantitative analysis. Strong theoretical background for proton-coupled electron-transfer reactions exists,<sup>597,598</sup> but a clear demonstration of connecting the nonexponential behavior to an appropriate model is missing.

### 3.3. Intermolecular Proton Transfer

Similar to intramolecular ESPT, intermolecular ESPT remains an active topic in science and has been periodically reviewed.<sup>599–606</sup> The two processes share some common features, such as that they are driven by a change in the electronic configuration upon optical excitation. Weller was the first to propose that in the case of hydroxyl-substituted aromatic compounds, the photoacidity originates from an intramolecular charge transfer (ICT) from the hydroxyl oxygen to the aromatic system.<sup>470</sup> Therefore, amplification of the ICT character of the locally excited state is expected to result in an enhancement of the acidity in the excited state. As will be shown later, this has been the main rationale toward the design of stronger photoacids.<sup>605</sup>

However, one can find significant differences between the two cases. Intermolecular ESPT requires the presence of an external proton acceptor, which in most cases is the solvent. Therefore, the reaction mechanism significantly differs from that of the ESIPT and has been proposed to involve an intermediate step. The widely accepted mechanism of intermolecular ESPT was originally proposed by Eigen and Weller (Scheme 1).<sup>472,599</sup> In this model, excitation of the protonated form of the acid (ROH) results in an initial short-range proton transfer to produce a contact ion pair. The contact ion pair can undergo subsequent diffusion-controlled separation into free ions. Both of the steps are usually considered to be reversible. Hence the separated proton can undergo geminate recombination without quenching of the fluorescence. The geminate recombination results in repopulation of the neutral excited state (ROH\*) at longer times with a nonexponential tail of its fluorescence decay, which was experimentally observed.<sup>607–610</sup>

The original kinetic model<sup>472</sup> based on the Eigen-Weller mechanism (Figure 53) used diffusional rate constants,  $k_{\text{diff}}$  and  $k'_{\text{diff}}$  obtained from the steady-state solution of the Debye-Smoluchowski equation (DSE).<sup>611,612</sup> Both the diffusion-controlled and the intrinsic dissociation ( $k_{\text{diss}}$ ) and recombination ( $k_{\text{rec}}$ ) rate constants were assumed to be time-independent. Therefore, the solution of the first-order rate equations based on Figure 53 resulted in purely (multi) exponential dynamics and was unable to explain the long-time nonexponential behavior.

Pines, Huppert and Agmon solved this discrepancy by describing the diffusional step using the numerical solution of

the DSE with back-reaction boundary conditions.<sup>613–619</sup> They considered the probability density functions of finding the geminate pair in the bound state,  $p^*(t)$ , or in the unbound state,  $p(r,t)$ , with separation  $r$ , where the separation is larger than the contact radius  $a$  ( $r \geq a$ ). The reactivity at the contact was accounted for using delta function “sink terms”,  $W_i = k_i \delta(r-a)/(4\pi a^2)$ . According to Figure 53, the spherically symmetric DSE can be written as<sup>617,619</sup>

$$\begin{aligned} \frac{\partial}{\partial t} p(r, t) = & r^{-2} \frac{\partial}{\partial r} D r^2 e^{-V(r)} \frac{\partial}{\partial r} e^{V(r)} p(r, t) \\ & - [W_{\text{rec}}(r) + W_{\text{q}}(r) + k_{\text{fl}_3}] p(r, t) \\ & + W_{\text{diss}}(r) p^*(t) \end{aligned} \quad (46)$$

which is coupled to a kinetic equation for the bound state:

$$\frac{\partial}{\partial t} p^*(t) = 4\pi \int W_{\text{rec}}(r) p(r, t) r^2 dr - (k_{\text{diss}} + k_{\text{fl}_1}) p^*(t) \quad (47)$$

In the above equations,  $D = D_{\text{H}^+} + D_{\text{RO}^-}$  is the mutual diffusion coefficient of the proton and the conjugate base,  $V(r) = -R_{\text{D}}/r$  is the Coulomb attraction potential, and  $R_{\text{D}}$  is the Debye radius.

$$R_{\text{D}} = \frac{|z_1 z_2| e^2}{k_{\text{B}} T \epsilon} \quad (48)$$

where  $z_1$  and  $z_2$  are the charges of the proton and the conjugate base and  $\epsilon$  is the dielectric constant of the medium. The experimentally accessible quantity, i.e., the “survival probability” of the unbound pair,  $S(t)$ , can be obtained by integration of the probability density function according to

$$S(t) = 4\pi \int_a^\infty p(r, t) r^2 dr \quad (49)$$

If the neutral and the anionic forms have equal lifetimes ( $k_{\text{fl}_1} = k_{\text{fl}_3}$ ), the total probability of finding the geminate pair in either the bound or unbound state is equal to the excited-state population as

$$p^*(t) + S(t) = \exp(-k_{\text{fl}_1} t) = \exp(-k_{\text{fl}_3} t) \quad (50)$$

The above equations cannot be solved analytically in the presence of the Coulomb attraction potential. Agmon and Krissinel developed, however, a specialized computer software to solve the equations numerically, which can then be compared with the experimental data.<sup>620</sup> In addition, Agmon and co-workers derived approximate solutions for several cases, where the long-time asymptotic behavior has an exact solution.<sup>617–619</sup> In the simplest case with equal lifetimes ( $k_{\text{fl}_1} = k_{\text{fl}_3}$ ) and in the absence of quenching ( $k_{\text{q}} = 0$ ), the probability of observing the initially prepared bound pair follows an asymptotic power law:

$$p^*(t) \sim \frac{K_{\text{eq}}}{(4\pi D t)^{3/2}} \exp(-k_{\text{fl}_1} t) \quad (51)$$



where  $K_{\text{eq}}$  is the association equilibrium constant defined as

$$K_{\text{eq}} = \frac{k_{\text{rec}} e^{-V(a)}}{k_{\text{diss}}} = \frac{k_{\text{rec}} \exp(R_D/a)}{k_{\text{diss}}} \quad (52)$$

The excited-state  $\text{p}K_{\text{a}}$  value can be calculated from the inverse of the association equilibrium constant according to

$$\text{p}K_{\text{a}}^* = -\log \frac{k_{\text{diss}} \exp(-R_D/a)}{k_{\text{rec}}} \quad (53)$$

In this special limit, the full behavior of the system can be obtained from a single kinetic trace of either the neutral or the anionic form. In other regimes, the behavior depends on the rate constants involved. For example, if the lifetime of the anion is longer than that of the neutral and the process involves quenching, the long-time asymptotes for the bound and the unbound pair follow  $\sim t^{-3/2} \exp(-k_{\text{q}3}t)$  and  $\sim t^{-1/2} \exp(-k_{\text{q}3}t)$ , respectively. The different regimes were experimentally observed and the results are in good agreement with the theory. Theoretical formulations and comparison with experiments are thoroughly discussed in the literature.<sup>606,616–619,621–623</sup>

Most ESPT compounds exhibit pronounced solvatochromic behavior. This is, of course, owed to the ICT character of the locally excited state inducing a large change in the dipole moment. The solvatochromism is not only dependent on the polarity but also on hydrogen-bond accepting and donating properties of the solvent.<sup>624–626</sup> In addition, ESPT usually results in the formation of charged species, amplifying the solvent effects in the conjugate base. A hydrogen bond donated by the solvent significantly stabilizes the ground-state anion, whereas a hydrogen bond accepted by the solvent stabilizes the excited neutral form. All factors make intermolecular ESPT a strongly solvent-controlled process, where not only the proton accepting and conducting properties but also the polarity of the solvent play a key role in the process.<sup>618,622,627–630</sup> Therefore, most studies were done in polar protic solvents such as water, methanol and ethanol.

The last major difference for the intermolecular ESPT is the characterization of the photoacidic compounds based on their  $\text{p}K_{\text{a}}^*$  values. In the case of the ESIPT, the  $\text{p}K_{\text{a}}^*$  does not appear to be the main factor determining the rate of the reaction, whereas in the case of intermolecular ESPT, the  $\text{p}K_{\text{a}}^*$  is directly related to the driving force of the reaction and can be calculated from a thermodynamic relation known as the Förster cycle. The Förster cycle is based on the assumption that there is a thermodynamic equilibrium both in the ground and excited states characterized by their equilibrium constants  $K_{\text{a}}$  and  $K_{\text{a}}^*$ , respectively. The second assumption of the Förster cycle is that the change in entropy is equal for both the ground- and excited-state reactions. Therefore, the change in  $\Delta G$  upon excitation can be expressed in the terms of  $\Delta H$ , which is related to the 0–0 transition energies according to the energy diagram in Figure 54.<sup>468,469</sup>

$$\Delta G^* - \Delta G = -RT \ln \frac{K_{\text{a}}^*}{K_{\text{a}}} = N_{\text{A}} h c (\tilde{\nu}_{00}^{\text{RO}^-} - \tilde{\nu}_{00}^{\text{ROH}}) \quad (54)$$

where  $\tilde{\nu}_{00}^{\text{RO}^-}$  and  $\tilde{\nu}_{00}^{\text{ROH}}$  are the 0–0 transitions of the anionic and neutral forms expressed in wavenumbers. This relation yields the familiar Förster equation:

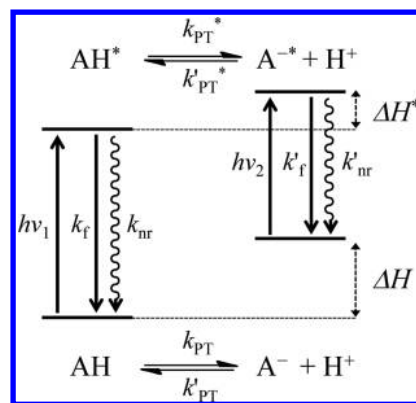


**Figure 54.** Förster-cycle energy diagram of the proton-transfer reaction. The excitation energies,  $h\nu_1$  and  $h\nu_2$ , correspond to the 0–0 energies of the neutral (ROH) and anionic (RO<sup>−</sup>) forms, respectively. The  $\Delta H$  values are the heats of formation. The relevant rate constants are also indicated:  $k_{\text{PT}}$  and  $k'_{\text{PT}}$  are the forward and backward rates of the proton transfer,  $k_{\text{f}}$  and  $k_{\text{nr}}$  the radiative and nonradiative rate constants. Asterisks indicate an electronically excited state.

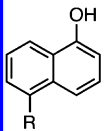
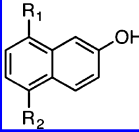
$$\text{p}K_{\text{a}}^* = \frac{0.625 K_{\text{cm}}}{T} (\tilde{\nu}_{00}^{\text{RO}^-} - \tilde{\nu}_{00}^{\text{ROH}}) + \text{p}K_{\text{a}} \quad (55)$$

This approach is still widely used to characterize photoacids due to its robustness and simplicity.<sup>469</sup> However, since  $\text{p}K_{\text{a}}^* = -\log(k_{\text{PT}}/k'_{\text{PT}})$  the value obtained from the Förster cycle should be considered as an approximation. A more appropriate way to estimate the  $\text{p}K_{\text{a}}^*$  is to determine the rate constants for the forward and backward process. This can be done by fluorescence titration as a function of pH as originally proposed by Weller<sup>470,471</sup> or more directly by analyzing the time-resolved data with an appropriate kinetic model, such as the DSE model.

Inherently, all intermolecular ESPT reactions can be considered as “non-equilibrium” reactions due to the diffusion-assisted separation and geminate recombination. We will however focus on the molecular classes which exhibit or at least approach ESPT time constants close to those of the vibrational or solvent relaxation processes. Since the  $\text{p}K_{\text{a}}^*$  is related to the ratio of the rate constants, lowering of the  $\text{p}K_{\text{a}}^*$  will accelerate the ESPT reaction. This limits our discussion to compounds exhibiting  $\text{p}K_{\text{a}}^*$  values close to or below 0. Some of the historical works are also reviewed showing the progress of the studies on ESPT reactions. The covered molecular classes, with increasing acidity, are naphthols, hydroxyquinolines, hydroxypyrenes, and cyanine-based photoacids.

**3.3.1. Naphthols.** Naphthols were one of the first studied compounds shown to exhibit ESPT to the solvent. The steady-state properties of 2-naphthol (**96**, **2N**) were investigated by Förster and Weller in the midtwentieth century (Chart 18).<sup>467,470,633</sup> The  $\text{p}K_{\text{a}}$  values of **2N** in the ground and first excited state were determined to be  $\text{p}K_{\text{a}} = 9.45$  and  $\text{p}K_{\text{a}}^* = 2.8$ , demonstrating only limited photoacidity in the excited state.<sup>632,633</sup> Weller estimated the  $\text{p}K_{\text{a}}$  values of 1-naphthol (**93**, **1N**) to be similar to those of **2N** using the fluorescence titration method.<sup>633</sup> However, later combined time-resolved (ns-TCSPC) and steady-state studies by Harris et al. showed that the emission of both the neutral and anionic forms of **1N** are strongly quenched by the aqueous protons, whereas the quenching rate is much lower for **2N**.<sup>634,635</sup> They refined Weller’s scheme to include the time-resolved data and

Chart 18. Structures of Naphthol-Derived Photoacids Together with the Ground- and Excited-State  $pK_a$  Values<sup>a,b</sup>

<b>1-naphthols<sup>a</sup></b>	
	<b>93 (1N):</b> R = H $pK_a = 9.4$ , $pK_a^* = -0.2$
	<b>94 (1N-5S):</b> R = $SO_3^-$ $pK_a = 8.4$ , $pK_a^* = -0.7$
	<b>95 (1N-5CN):</b> R = CN $pK_a = 8.1$ , $pK_a^* = -2.8$
<b>2-naphthols<sup>b</sup></b>	
	<b>96 (2N):</b> R <sub>1</sub> = H, R <sub>2</sub> = H $pK_a = 9.5$ , $pK_a^* = 2.8$
	<b>97 (2N-5CN):</b> R <sub>1</sub> = H, R <sub>2</sub> = CN $pK_a = 8.8$ , $pK_a^* = -1.2$
	<b>98 (2N-DCN):</b> R <sub>1</sub> = R <sub>2</sub> = CN $pK_a = 7.8$ , $pK_a^* = -4.5$

<sup>a</sup>From ref 631. <sup>b</sup>From ref 632.

established a new value of 0.5 for the excited-state  $pK_a$  of 1N whereas that of the 2N remained unchanged.

A few years later, Webb et al. reinvestigated the kinetics of 1N using a ps streak camera and steady-state spectroscopy.<sup>636,637</sup> The improved time resolution allowed them to directly observe a 35 ps decay of the neutral emission and a concurrent rise of the anion emission. They obtained a similar value of  $pK_a^* = 0.4$  but the rate constant for the deprotonation ( $k_{\text{diss}} = 2.5 \times 10^{10} \text{ s}^{-1}$ ) was found to be significantly higher than in the previous studies. The much higher rate constant was in strong contrast with that of 2N ( $k_{\text{diss}} = 7.5 \times 10^7 \text{ s}^{-1}$ ). Both the increased proton quenching and deprotonation rates in 1N were attributed to an inversion of the low-lying excited states. Similar to naphthalene, naphthols have two nearly degenerate low-lying states,  $^1L_a$  and  $^1L_b$ , with the corresponding transition dipole moments roughly aligned along the short axis (through atoms,  $^1L_a$ ) and the long axis (through bonds,  $^1L_b$ ). The  $^1L_a$  state possesses a much greater CT character with the charge density especially localized at the C5 and C8 atoms of the distal aromatic ring, whereas the  $^1L_b$  state has a much more diffusive nature. Therefore, the authors suggested that for 1N the emitting state is  $^1L_a$ , whereas for 2N it is  $^1L_b$ . Moreover, the strong proton quenching of 1N was suggested to originate from protonation of the aromatic ring at the C5 and C8 positions. This was supported by the observation of deuterium exchange upon irradiation of 1N under acidic conditions whereas 2N did not exhibit such a behavior.<sup>637</sup> These findings were also supported by later solvatochromism studies, which clearly demonstrated much stronger solvatochromic behavior for 1N. Moreover, Pines and co-workers suggested that the level inversion depends on the solvent polarity, with the  $^1L_a$  level becoming the dominant emitting state in polar solvents. The  $^1L_a$  state was also found to be further stabilized in hydrogen-bond donating solvents.<sup>624,638</sup>

The analyses of the kinetic studies by Harris, Webb and co-workers were based on the rate equations giving rise to exponential behavior. Pines and co-workers used the DSE model with coupled reversible and irreversible (quenching) back-reaction. They monitored the decays of the neutral and the anionic species using ps TCSPC and observed a nonexponential long-time behavior for the decays of both species.<sup>621,639</sup> When corrected for the finite excited-state lifetime of the anion, the long-time asymptotic behavior of the neutral and the anionic forms were shown to approach  $t^{-3/2}$  and  $t^{-1/2}$ , respectively. This demonstrated that both the

reversible adiabatic geminate recombination as well as the irreversible geminate recombination (quenching) are active in 1N and must be accounted for. The kinetics were quantitatively analyzed with the numerical solution to the coupled DSE equations, in full agreement with the theory.<sup>619</sup>

Both 1N and 2N do not deprotonate in alcohols or aprotic basic solvents limiting the studies to aqueous environment. Tolbert and Haubrich took advantage of the ICT rationale and postulated that an attachment of electron-withdrawing groups on the C5 and C8 positions, in particular, should stabilize the  $^1L_a$  state and result in an increased photoacidity. This turned out to be a very efficient approach to the design of stronger photoacids. They synthesized a series of cyano-substituted 1N and 2N derivatives, which exhibited greatly increased photoacidity and deprotonation even in alcohols, formamides and dimethyl sulfoxide (Figure 55).<sup>632,640</sup> The strongest photoacid,

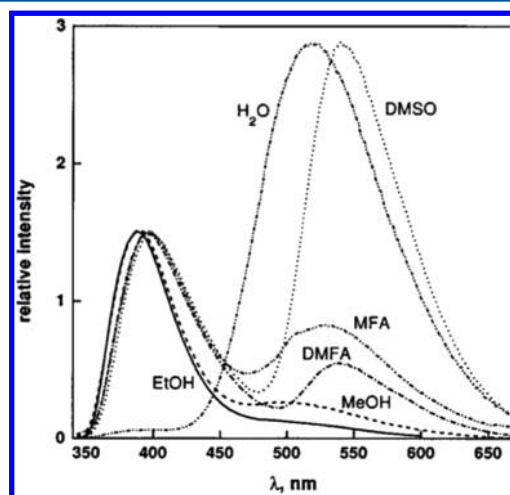


Figure 55. Steady-state emission spectra of 2N-5CN (97) in solvents where the ESPT takes place. The solvent abbreviations are DMSO = dimethyl sulfoxide, MFA = *N*-methylformamide, DMFA = dimethylformamide, MeOH = methanol, EtOH = ethanol, and H<sub>2</sub>O = water. Reprinted with permission from ref 618. Copyright 1999 American Chemical Society.

5,8-dicyano-2-naphthol (98, 2N-DCN) showed a then unsurpassed excited-state  $pK_a$  of  $-4.5$ . These compounds with enhanced photoacidity, negative  $pK_a^*$  values and the ability to deprotonate in organic solvents were named “super” photoacids.<sup>605</sup> The discovery of these compounds opened up new avenues for ESPT studies in nonaqueous environments.

Tolbert and Haubrich investigated the steady-state properties of the novel compounds in several organic solvents and solvent mixtures. Previous studies by Robinson and co-workers on unsubstituted naphthols and their sulfonated derivatives in aqueous alcohols explained the lack of ESPT in neat alcohols by the requirement of clusters of four water molecules as proton acceptors for the ESPT to occur.<sup>641–643</sup> Observed deprotonation of the novel cyano-compounds in alcohols and even in dimethyl sulfoxide demonstrated that other mechanisms must be active. The quenching of the fluorescence by water in aqueous tetrahydrofuran clearly correlated with the increased photoacidity, being strongest for the 2N-DCN with the lowest  $pK_a^*$  value. While 2N showed a fourth-order quenching dependence on the water concentration, it was reduced to second-order for 2N-5CN (97) and 2N-DCN (98). The

authors suggested that the molecularity of water in the ESPT reactions depends on the acidity of the proton donor.<sup>632,640</sup>

After this, the compounds were studied by many groups. Huppert, Tolbert, and co-workers investigated the ESPT rates of several monocyano 2N derivatives using ps TCSPC.<sup>644</sup> The rates were obtained with the use of the DSE model. The highest ESPT rate constants were observed for the 5CN ( $k_{\text{diss}} = 7 \times 10^{10} \text{ s}^{-1}$ ) and 8CN ( $k_{\text{diss}} = 2.7 \times 10^{10} \text{ s}^{-1}$ ) derivatives in agreement with the ICT rationale proposed for 1N. Second, the kinetic isotope effect was found to decrease upon increasing photoacidity. Therefore, the authors suggested that upon increasing photoacidity, the solvent reorganization becomes more important for the rate-determining step. Pines and co-workers reported on similar findings on the deprotonation of 1N-5CN (95) in water-methanol mixtures.<sup>645</sup> They analyzed the TCSPC traces using multiexponential functions. The ESPT time constant was found to decrease from  $\tau_{\text{PT}} = 8$  to 390 ps when going from pure water to pure methanol, accompanied by an increase in the kinetic isotope effect. Because of the similarity of the observed ESPT time constant and the Debye relaxation time of water over a large temperature range ( $-5$  to  $+40$  °C), the authors concluded that, in pure water, ESPT is mostly solvent controlled. Moreover, the authors suggested that the ESPT time in the solvent-controlled limit could vary between the longitudinal and the Debye relaxation time depending on the extent of the solvent rearrangement required to facilitate ESPT. In less polar methanol, ESPT becomes thermodynamically less favorable and is controlled by the intrinsic proton-transfer coordinate.

Carmeli et al. investigated the ESPT of the strongest photoacid, 2N-DCN, in methanol as a function of temperature using ps TCSPC.<sup>646</sup> They monitored the decay of the neutral form and analyzed the decays with the DSE model. At low temperature, the intrinsic ESPT rate was found to be similar to the dielectric relaxation time,  $\tau_{\text{D}}$ , whereas at high temperatures ( $>250$  K) the rate was significantly slower, eventually becoming almost temperature independent at  $T > 290$  K. The authors proposed that at low temperature, the ESPT is controlled by the dielectric relaxation, whereas at high temperature the proton-transfer reaction coordinate dominates. In follow-up studies, Huppert and co-workers extended the studies to other alcohols and 2N derivatives. The observations of these studies were broadly similar. The deprotonation rate constants were obtained from the DSE model, in a manner similar to the original study. The unusual temperature dependence was explained using the proton-transfer theory of Borgis and Hynes<sup>459</sup> based on the Landau-Zener curve crossing formulation<sup>647–649</sup> and was attributed to a continuous transition from the nonadiabatic regime (high temperature) to the solvent-controlled adiabatic regime (low temperature).<sup>650,651</sup> The two regimes were bridged using a rate expression similar to that derived by Rips and Jortner<sup>94</sup> for electron transfer.

$$k_{\text{PT}}(T) = \frac{k_{\text{PT}}^{\text{NA}}(T)k_{\text{PT}}^{\text{AD}}(T)}{k_{\text{PT}}^{\text{NA}}(T) + k_{\text{PT}}^{\text{AD}}(T)} \quad (56)$$

where NA and AD refer to the nonadiabatic and adiabatic rate constants.

Solntsev et al. investigated the solvent effects on the steady-state and time-resolved properties of 2N-5CN in a series of papers.<sup>618,622,625</sup> As expected from the increased photoacidity, 2N-5CN exhibited much stronger solvatochromic shifts

compared to the parent 2N. However, the solvatochromism was found to be significantly dependent on the specific interactions. The emission frequency of 2N-5CN did not correlate with the solvent polarity parameter,  $\pi^*$ , whereas the methoxy-derivative, unable to donate a hydrogen bond or undergo ESPT, did show such a correlation. The frequency difference of the two was, however, found to correlate well with the hydrogen-bond accepting parameter of the solvent,  $\beta$ , suggesting that the hydrogen bond is significantly strengthened in the excited state. Contrary to this behavior, increasing the hydrogen-bond donating ability of the solvent,  $\alpha$ , resulted in a blue shift of the spectra. This behavior was attributed to a cleavage of the hydrogen bond donated from the solvent in the excited state. Both correlations were attributed to the ICT character of the excited state. Upon excitation, the electron density from the hydroxyl oxygen is transferred to the distal aromatic ring. This weakens the hydrogen bond donated by the solvent and strengthens the bond accepted by the solvent.<sup>618,625</sup>

The ESPT rates were analyzed from the ps TCSPC decays with the use of the DSE model. The intrinsic deprotonation was found to be fastest in neat water and significantly slower in all other studied solvents, contrary to what would be expected from the proton solvation energies. Therefore, the authors suggested that the  $\text{p}K_{\text{a}}^*$  (and hence the rate) is determined by a subtle interplay between the different solvent properties. In addition to the solvent polarity, the solvent basicity is of key importance in solvating the proton, whereas the solvent acidity stabilizes the anion. Water appears to be the best polar solvent to stabilize both the proton and the anion.

Recently, Nibbering, Pines, and co-workers studied a series of 5-substituted 1N derivatives using steady-state, fs transient vibrational absorption and ps TCSPC spectroscopies.<sup>631</sup> They determined the  $\text{p}K_{\text{a}}^*$  values using the Förster cycle method and found a good correlation between the Hammett's  $\sigma_{\text{p}}$  value and the  $\text{p}K_{\text{a}}$  both in the ground and excited states (Figure S6). The

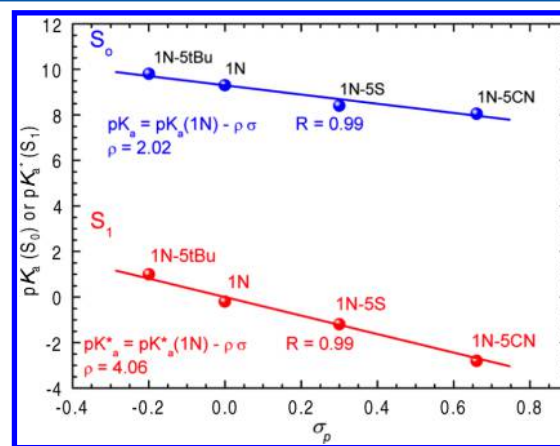


**Figure S6.** Ground- and excited-state  $\text{p}K_{\text{a}}$  values of 5-substituted 1N derivatives as a function of Hammett's  $\sigma$  values. The slopes and R parameters are indicated in the figure. Adapted from ref 631. Copyright 2013 American Chemical Society.

slope of the Hammett correlation was twice as large for the excited state compared to the ground state. This demonstrated that the electronic distribution in the excited state is more strongly influenced by the substitution. Second, they determined the deprotonation rates either using time-resolved IR spectroscopy or TCSPC. In the IR measurements, they followed two marker bands attributed to the acid and conjugate



base forms, respectively. The rate constant was obtained from a monoexponential fit to the kinetic traces. No reversibility or diffusion was considered. A similar approach was used for the TCSPC measurements although only the decay of the neutral emission was considered. The fastest ESPT time constant of 5.9 ps was observed for 3,6-disulfonyl-1-naphthol, close to that of 1N-5CN (8 ps) investigated earlier by Pines and co-workers.<sup>645</sup> The authors found a free-energy correlation between the  $pK_a^*$  values and the deprotonation rate constants using both the model derived by Marcus for the outer-sphere electron transfer, eq 3, and the subsequently modified version based on the semiempirical BEBO model, eq 39.<sup>449,450</sup> The correlation could be even extended to include the results of related compounds (Figure 57). The obtained rate constant for the activationless

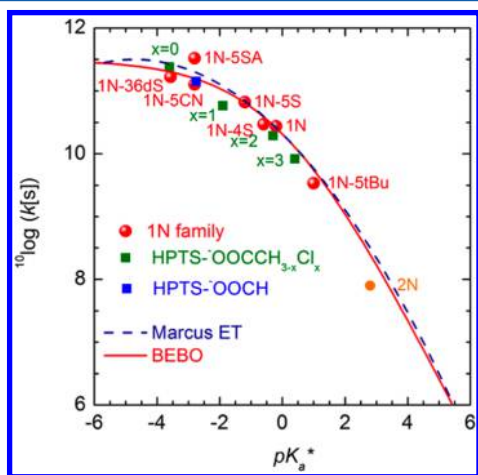


**Figure 57.** Free-energy correlation of the  $pK_a^*$  values and the ESPT rate constants found for 1N derivatives, 2N and HPTS with carboxylate bases. The dashed line represents the correlation with the Marcus-ET model, eq 3, and the solid line that with the Marcus-BEBO model, eq 39. The parameters for the fits are  $\log(k_0) = 11.5$  for the activationless PT and  $\Delta G_0^\ddagger = 6.7$  kJ/mol for the intrinsic barrier. Adapted from ref 631. Copyright 2013 American Chemical Society.

proton transfer and the intrinsic barrier were  $k_0 = 3 \times 10^{11} \text{ s}^{-1}$  and  $\Delta G_0^\ddagger = 6.7$  kJ/mol, respectively. Both models gave an equally good correlation, only differing in the region of the strongest photoacids, where Marcus-ET theory predicts the inverted region whereas the BEBO model approaches the maximum value. Thus, even stronger photoacids would be required to reach the high driving force region where the models start to deviate.

**3.3.2. Hydroxypyrenes.** Studies on hydroxypyrenes, such as 8-hydroxypyrene-1,3,6-trisulfonic acid (**99**, HPTS) were instrumental in mechanistic investigations of the intermolecular ESPT reactions. HPTS is especially well suited for these studies due to its relatively strong excited-state acidity ( $pK_a^* = 0.4$ ),<sup>652</sup> high quantum yield, good solubility, photostability and ready availability. In addition, the recombination kinetics both in the ground and excited state are accelerated due to the quadruple negative charge of the deprotonated species. The steady-state properties of HPTS were investigated by Förster and Weller in their pioneering studies.<sup>468,633</sup> Later, Förster and Völker studied the ground-state recombination kinetics with ns flash photolysis in the seminal paper published soon after Förster's death. The recombination rate constant was found to be  $k = 1.9 \times 10^{11} \text{ M}^{-1} \text{ s}^{-1}$ , the fastest bimolecular rate reported at the time.<sup>653</sup> Subsequently, HPTS was used in several pH-jump experiments,

which focused both on the dissociation and recombination kinetics.<sup>652,654–657</sup> Observation of the geminate recombination in HPTS was reported by Pines and Huppert and eventually led to the formulation of the DSE model in collaboration with Agmon.<sup>607,608</sup> HPTS was particularly suited for this as the radiative rates for both the neutral and the anionic forms are nearly identical and the compound does not exhibit significant quenching by protons, thus simplifying the analysis.<sup>610,613</sup>

The first fs studies were instrumental in elucidating the initial steps of the dissociation process. Whereas the early studies placed the ESPT time constant in the range of  $\sim 100$  ps, Tran-Thi and co-workers showed that the ESPT to water proceeds in three successive steps with time constants of 0.3 ps, 2.2 and 87 ps.<sup>660</sup> They used fs fluorescence up-conversion to monitor the emission of both the neutral and the anionic forms. The two fastest time constants were accompanied by a red shift of the neutral emission band. They attributed the fastest component to solvent relaxation, as it was also observed for the anion upon direct excitation under alkaline conditions. The second time constant was attributed to the formation of the special hydrogen-bonded network with the surrounding water facilitating the ESPT. The last step was assigned to the dissociation into free ions with a time constant of 87 ps. In the follow-up studies, in collaboration with Hynes, Tran-Thi and co-workers further investigated the nature of the intermediate steps using solvatochromic studies, fs fluorescence up-conversion and transient absorption.<sup>661–663</sup> They studied HPTS and other pyrene derivatives in organic solvents and aqueous solutions. The observed dynamics both with the fs up-conversion and transient absorption in water were in agreement with the previous study. The intermediate time constant was instead attributed to a transition from the initially excited  $^1L_b$  state to the more polar  $^1L_a$  state. This was supported by the increased solvatochromic behavior of the emission ( $^1L_a$ ) compared to the absorption ( $^1L_b$ ) and the lack of mirror image symmetry in all studied solvents. The level inversion was suggested to originate from the solvent relaxation of the  $^1L_a$  state with increased ICT character.

Nibbering and co-workers investigated the possibility of the level inversion using fs mid-IR spectroscopy. They monitored the IR-active bands of HPTS and its methoxy-derivative, MPTS (**101**), in water and deuterated water, dimethyl sulfoxide, and methanol.<sup>664</sup> The O–H stretching mode ( $\sim 3400 \text{ cm}^{-1}$ ) of HPTS in dimethyl sulfoxide was found to broaden and upshift with time constants of 300 fs and 4 ps, which were attributed to the solvation dynamics. Similar solvation dynamics were reported by Pines et al. on a closely related photoacid, 8-hydroxypyrene-1,3,6-tris(dimethylsulfonamide) (**102**, HPTA), in organic solvents using transient electronic absorption.<sup>658</sup> The O–H stretch region in water was masked by the absorption of the solvent but the authors observed a broad red-shifted transient band which was attributed to a more strongly hydrogen-bonded O–H stretch in water. This transient decayed with time constants of  $\sim 300$  fs, 3 ps, 90 and 200 ps. The two fastest time constants were again attributed to the solvent dynamics, the 90 ps time constant to the ESPT and the longest one to rotational diffusion. The assignment was done based on the lack of spectral evolution of the transient bands between  $1400\text{--}1600 \text{ cm}^{-1}$  during the first 20 ps. The authors concluded that no change in the electronic level or protonation state occurs between 150 fs (IRF) and 20 ps. Based on the solvent-dependent vibrational signature and steady-state absorption spectra, the authors suggested that the  $^1L_a$  and  $^1L_b$

states were heavily mixed, with the extent of mixing being largest in water. This mixed state is reached directly upon optical excitation without any level crossing.

Huppert and co-workers proposed another explanation for the intermediate step. They investigated the ESPT dynamics in aqueous solutions using ps TCSPC and fs transient electronic absorption.<sup>666</sup> They noticed that the rise of the anion emission monitored by the TCSPC contained an instrument-limited component with an amplitude of 22% followed by a slower component with a time constant of ca. 100 ps. The transient absorption signal exhibited three time constants of  $\sim 0.8$ , 3, and 100 ps, similar to the previous measurements. The fastest time constant was attributed to solvation but the interpretation of the intermediate time constant was different from that of Tran-Thi and co-workers. They proposed an extended model consisting of two reversible reactive steps followed by the diffusion-controlled separation into free ions. The intermediate time constant of  $\sim 3$  ps was attributed to the first reactive step producing contact ion pairs. The equilibrium constant of this step was suggested to be relatively small ( $K_{\text{eq}} = 0.5$ ) and therefore only  $\sim 30\%$  of the anionic species is formed with this time constant. The initial step was followed by the slower  $\sim 100$  ps step to produce solvent-separated ion pairs, which further dissociated by a diffusion-controlled process into free ions. The short-time behavior could be adequately fitted with rate equations derived for the reversible two-step process. The diffusion-assisted separation and recombination had to be considered for the long-time TCSPC decays, which was achieved with a modified version of the DSE model including the additional reactive step. In a follow-up study, the model was tested against the effect of excess protons.<sup>667</sup> There, the experiments were repeated in the presence of varying concentrations of strong acid. The amplitudes of both the long and the intermediate components were found to decrease upon increasing the acid concentration. The results were analyzed with the previously suggested model including the excess acid concentration. The results appeared to be in good agreement with the model, supporting its validity.

Fayer and co-workers made several contributions to elucidate the nature of the electronic states of HPTS and its derivatives.<sup>668–671</sup> In the first of them, they used steady-state fluorescence anisotropy and magnetic circular dichroism to investigate the ordering of the  $^1L_a$  and  $^1L_b$  states. They convincingly demonstrated that, in the protonated form of HPTS, the states are heavily mixed, in agreement with the findings of Nibbering. The transition dipole moments of the two states are nearly parallel, contrary to the parent pyrene, and the  $^1L_b$  state has significant oscillator strength due to intensity borrowing from the  $^1L_a$  state. However, based on the comparison with other substituted pyrenes, the  $^1L_a$  state was shown to be the lowest singlet excited state of HPTS in all studied solvents. The energy gap between the states is significantly increased upon deprotonation and the intensity of the  $^1L_b$  state decreases as a result of the diminished mixing with the  $^1L_a$  state. Second, the authors demonstrated that the solvent dependence of the emission spectra could be properly reproduced with a Brownian oscillator model, in which the coupling of the electronic state to the solvent via hydrogen-bonding interactions is the main cause for the broadening and loss of the vibronic progressions.<sup>668</sup>

In the follow-up studies, Fayer and co-workers investigated the ESPT dynamics in water and organic solvents using fs transient electronic absorption.<sup>669</sup> First, they characterized the

dynamic Stokes shifts of HPTS in solvents where the ESPT does not occur. They modeled the time-dependent pump–probe spectra as a linear combination of the short-time spectrum with its derivative with respect to frequency to account for the dynamic shift. Next, they measured the transient spectra in water and heavy water where the ESPT does occur. The results were analyzed assuming two species, the neutral and the anion, and the dynamic Stokes shift of the neutral species, which was explicitly taken into account using the derivative method. Their model had only two adjustable parameters, one for the Stokes shift and another for the relative populations of the neutral and anionic forms. The simulated results were in excellent agreement with experimental data over the whole wavelength region (Figure 58). In addition, the

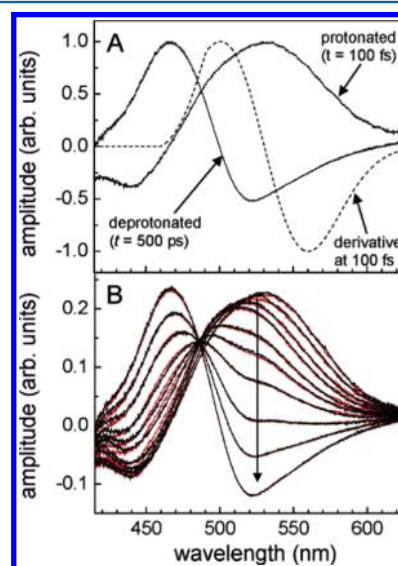
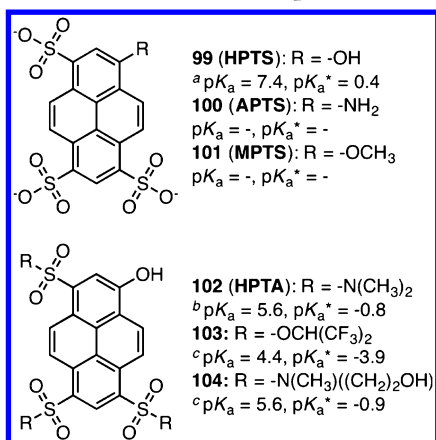


**Figure 58.** (A) Three spectral components used to model the transient absorption spectra measured with HPTS in D<sub>2</sub>O. (B) The measured (black) and simulated (red) transient spectra at 100 and 600 fs and 2, 9, 50, 90, 180, 300, and 500 ps. The arrow in B indicates the direction of time. Adapted from ref 669. Copyright 2007 American Chemical Society.

obtained time constants were in good agreement with the previous results. The Stokes shift occurred in  $\sim 950$  fs and the ESPT showed biexponential kinetics with time constants of 2.5 and 88 ps. The authors also analyzed the ESPT dynamics with a kinetic model based on rate equations and the results were found to be in good agreement with those of Huppert and co-workers. However, the amplitude of the fast time component was roughly two times smaller, which was attributed to an improper description of the dynamic Stokes shift in the previous study.

Subsequently, Fayer and co-workers studied the solvation and deprotonation dynamics of three pyrene derivatives, HPTS, HPTA, and APTS (100, Chart 19) in several organic solvents.<sup>670,671</sup> HPTA is a much stronger photoacid than HPTS and can also deprotonate in dimethyl sulfoxide. APTS, on the other hand, is a strong photoacid in its protonated state, producing a neutral  $-\text{NH}_2$  group upon ESPT. These three pyrene derivatives enabled more detailed studies on the initial steps of the ESPT process in organic solvents. In DMSO, HPTA was found to first undergo a transition to another electronic state before the delayed onset of the anion emission at longer wavelength. The transient spectrum of this state was

Chart 19. Structures of Pyrene-Derived Photoacids together with the Ground- and Excited-State  $pK_a$  Values<sup>a,b,c</sup>



<sup>a</sup>From ref 652. <sup>b</sup>From ref 658. <sup>c</sup>From ref 659.

identical to that of the anion. A similar transition was observed for APTS, which cannot undergo ESPT, in hydrogen-bond donating solvents such as formamide. The time constant of the transition (5.4 ps) was equal to the solvation time of HPTS measured in the same solvent. Contrary to this behavior, HPTA complexed with triethylamine in benzene showed a direct deprotonation without any intermediates. Similar behavior was observed for the protonated APTS in aqueous solution.

The overall behavior was attributed to a slow (few ps to 10 ps) charge redistribution preceding the ESPT step. Surprisingly, for HPTS and HPTA, this CT state was observed only in solvents which facilitate the ESPT, whereas the methoxy-derivative, MPTS, did not show the CT state at all. This was attributed to specific solvent interactions required for the charge redistribution step. Some support for this interpretation was gained from the behavior of APTS, which showed the CT state only in hydrogen-bond donating solvents. It was also suggested that the charge redistribution in APTS occurs after deprotonation and cannot be observed in water due to the relatively slow ESPT. The process was suggested to be ultrafast (<150 fs) in the HPTA-triethylamine complex due to the pre-established strong hydrogen bond in the ground state. Based on these new results, the authors attributed the previously observed biexponential decay of HPTS in water to the initial charge redistribution followed by the ESPT, contrary to their previous report<sup>669</sup> and that of Huppert and co-workers.<sup>666</sup> The interpretation remains somewhat ambiguous, particularly in organic solvents. However, recent reports strongly suggested that the contact ion pair is the direct product of the initial proton transfer step both in water and organic solvents.<sup>672–675</sup>

Recently, Jung and co-workers demonstrated that the photoacidity of the HPTS derivatives can be greatly enhanced by increasing the electron-withdrawing strength of the aromatic substituents.<sup>659</sup> They synthesized a series of novel photoacids by replacing the sulfonic acid groups by more electron-withdrawing sulfonamide or sulfonic ester groups. All compounds showed negative  $pK_a^*$  values (−3.9 for the most acidic compound) and substantial deprotonation yields in dimethyl sulfoxide placing them in the category of “super” photoacids. These compounds retained the high quantum yield, relatively long lifetime and photostability of the parent HPTS, making them ideal candidates for ESPT studies. Jung et al. subsequently investigated the solvatochromism of the com-

pounds in comparison with the methoxy-derivatives using different solvatochromic scales.<sup>626</sup> They found a strong correlation between the photoacidity and the polarity of the excited state. The permanent dipole moments of both the hydroxy- and the methoxy-compounds were found to increase significantly upon excitation (~14 D). This clearly demonstrates that the charge redistribution in these enhanced acids takes place even in the absence of ESPT contrary to findings of Fayer and co-workers. The solvent basicity was found to be less significant to the solvatochromism contrary to some of the previous studies.<sup>618</sup>

In collaboration with Huppert and Pines, Jung et al. characterized the ESPT dynamics of two of the novel photoacids, **103** and **104**, with  $pK_a^* = -3.9$  and  $-0.9$  respectively, in water, methanol and ethanol.<sup>676</sup> The fluorescence decays were measured using ps TCSPC and fs fluorescence up-conversion (340 fs IRF) and analyzed using either the DSE model (long-time behavior) or a multi-exponential function. The stronger photoacid, **103**, showed a much smaller decrease in the ESPT rate constants,  $k_{PT}$ , upon decreasing the solvent polarity compared to **104**, in line with previous findings. The rate constants in water, methanol, and ethanol were  $3 \times 10^{11} \text{ s}^{-1}$ ,  $8 \times 10^9 \text{ s}^{-1}$ , and  $5 \times 10^9 \text{ s}^{-1}$  for **103** and  $7 \times 10^{10} \text{ s}^{-1}$ ,  $4 \times 10^8 \text{ s}^{-1}$ , and  $2 \times 10^8 \text{ s}^{-1}$  for **104**, respectively. The authors correlated the rates of these, as well as the rates of previously studied photoacids, with the  $pK_a^*$  values using both the Marcus-ET model, eq 3, and the Marcus-BEBO model, eq 39, in all three solvents (Figure 59). The  $pK_a^*$  values

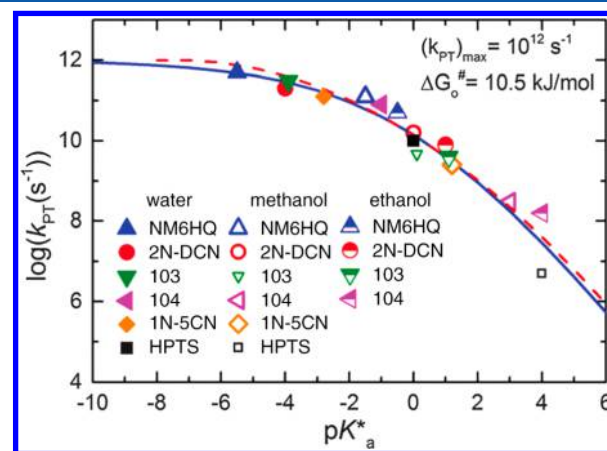


**Figure 59.** Free-energy correlation found for the pyrene-derived photoacids **103** and **104**, and others in water (full symbols), methanol (open symbols) and ethanol (half open symbols). The  $pK_a^*$  values in methanol and ethanol have been shifted by 4 and 5  $pK_a$  units, respectively. The dashed line was calculated from the Marcus–ET model, eq 3, and the solid line from the Marcus–BEBO model, eq 39. Adapted with permission from ref 676. Copyright 2014 PCCP Owner Societies.

in methanol and ethanol had to be shifted by 4 and 5  $pK_a$  units, respectively, to obtain a good correlation. The obtained parameters for the activationless ESPT and the intrinsic barrier were  $k_0 = 10^{12} \text{ s}^{-1}$  and  $\Delta G_0^\ddagger = 10.5 \text{ kJ/mol}$ , respectively. Both values are slightly higher than those obtained by Nibbering and Pines for 1N derivatives.<sup>631</sup> Based on the correlation found, the authors suggested that the inhibition of the ESPT rate in alcohols as compared to water mainly originates from the solvent effect on the dissociation constant and hence on the driving force of the reaction. The prefactor was suggested to be



largely independent of the protic solvent and to represent the relatively slow solvent rearrangement required to facilitate the proton transfer to the solvent.

The above-mentioned cases focused on proton transfer to solvent representing a pseudounimolecular reaction. Another interesting aspect of proton transfer is the truly bimolecular ESPT that occurs in the presence of bases such as acetates. Pines, Fleming and co-workers demonstrated that the intrinsic ESPT rate to acetates is directly accessible at high base concentrations (8 M). They measured the ESPT rate constant of several naphthol- and hydroxypyrene-derived photoacids in the presence of acetate and formate bases using ps TCSPC. The observed intrinsic rate for the **HPTS**-acetate pair was  $k_{\text{PT}} = 7 \times 10^{10} \text{ s}^{-1}$ . Moreover, they correlated the observed rates with the  $\text{p}K_{\text{a}}^*$  values using the free-energy relation derived by Agmon and Levine, eqs 40 and 41.<sup>452,454,455</sup> The total free-energy change was calculated from the  $\text{p}K_{\text{a}}$  values of both the acid and the base according to  $\Delta G = \ln(10)(\text{p}K_{\text{acid}} - \text{p}K_{\text{base}})$  RT. The correlation was found to be very good even after including results from previous studies. The activationless rate and intrinsic barrier obtained from a correlation over 11  $\Delta \text{p}K_{\text{a}}$  units were  $k_0 = 2 \times 10^{11} \text{ s}^{-1}$  and  $\Delta G_0^\ddagger = 10.5 \text{ kJ/mol}$ , respectively, in good agreement with other studies.

Huppert and co-workers reinvestigated the bimolecular ESPT in the **HPTS**-acetate pair at lower base concentrations (0.5–4 M) using a combination of ps TCSPC and fs two-color transient absorption.<sup>677</sup> They analyzed the results with an approximate analytical solution of the DSE equation in a Coulomb potential originally derived by Szabo.<sup>308</sup> However, they had to include two exponential functions into the analysis of the transient absorption traces with time constants of  $\sim 0.7 \text{ ps}$  and  $\sim 1\text{--}3 \text{ ps}$ , which were attributed to the solvation dynamics and hydrogen-bond rearrangements based on the original report by Tran-Thi and co-workers. All measurements were adequately fitted with the model yielding an intrinsic ESPT rate constant of  $k_{\text{PT}} = 1.6 \times 10^{11} \text{ s}^{-1}$ , more than two times larger than the value obtained by Pines and co-workers. This can be attributed to the improved time resolution and different analysis method of the present study.

More recently, Pines, Nibbering, and co-workers reported on several investigations of bimolecular ESPT between **HPTS** and acetate (0.5–4 M) in  $\text{D}_2\text{O}$  using fs transient IR absorption.<sup>665,678–681</sup> They monitored specific marker bands in the mid-IR region ( $1400\text{--}1800 \text{ cm}^{-1}$ ) attributed to the photoacid and conjugate base forms of **HPTS** and to the acetic acid. This enabled direct monitoring of both the departure of the proton from the photoacid and arrival to the base (acetate). They observed that the rise of the acetic acid signal occurred on multiple time scales. Part of the rise was found to be instrument limited ( $<150 \text{ fs}$ ) with an increasing amplitude at higher base concentrations followed by slower components. Second, the rise of the anionic form of **HPTS** at lower base concentrations appeared faster than the rise of the acetic acid signal.

The instrument-limited rise was attributed to an ultrafast ESPT in preformed “tight” complexes between **HPTS** and the acetate bases, whereas the slower component was suggested to originate from the diffusive reaction. The disagreement between the rise times of the anionic form of **HPTS** and acetic acid was explained by an initial dissociation of uncomplexed **HPTS** to water followed by proton scavenging by the acetate. The kinetics were analyzed with the approximate solution derived by Szabo<sup>308</sup> based on the DSE model (referred to as Smoluchowski–Collins–Kimball, SCK,<sup>303</sup> model by the

authors) similarly to Huppert and co-workers. The authors found that an additional static reaction rate of  $(6 \text{ ps})^{-1}$  was required to adequately model the data. This additional component was attributed to the reaction in a “loose” complex where the 6 ps time constant represents the solvent reorientation required to facilitate the ESPT.<sup>678,679</sup>

In the follow-up investigations, the same authors extended the studies to include weaker chloroacetate bases ( $^-\text{OOC}-\text{CH}_{(3-x)}\text{Cl}_x$ ,  $x = 1\text{--}3$ ) and a broader detection window up to  $\sim 1900 \text{ cm}^{-1}$ .<sup>665,680,681</sup> The weaker bases were found to significantly slow down the processes and increase the concentration of the “loose” complexes. With these improvements, the authors were able to observe the hydrated deuterium at  $\sim 1850 \text{ cm}^{-1}$  prior to the appearance of the protonated acetate (Figure 60). Based on the spectral properties of the IR

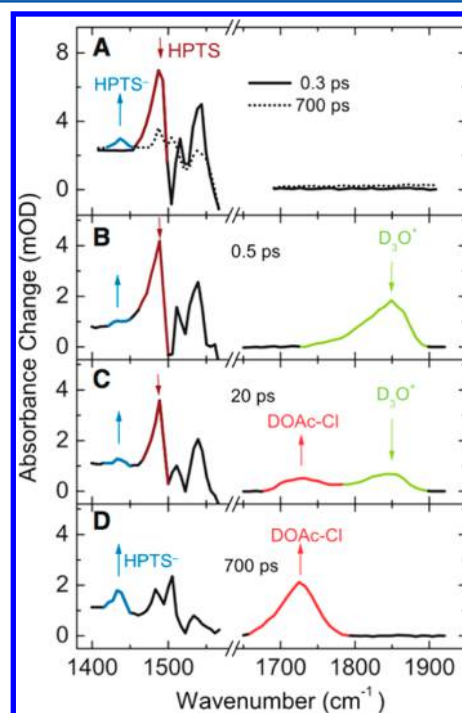


**Figure 60.** Transient IR spectra showing the response of the marker modes of the neutral (brown,  $1486 \text{ cm}^{-1}$ ) and the anionic (blue,  $1435 \text{ cm}^{-1}$ ) forms of **HPTS**, and the DOAc-Cl (red,  $1725 \text{ cm}^{-1}$ ) and  $\text{D}_3\text{O}^+$  (green,  $1850 \text{ cm}^{-1}$ ) after optical excitation in  $\text{D}_2\text{O}$ . (A) no added base, (B to D) 1 M DOAc-Cl. Reprinted with permission from ref 665. Copyright 2005 The American Association for the Advancement of Science.

absorption signal of the hydrated deuterium,  $\text{D}_3\text{O}^+$ , it was suggested to resemble the eigen-cation<sup>472</sup> with three additional hydrogen-bonding partners. Detailed kinetic analysis of the dynamic behavior allowed the authors to identify multiple reactive pathways with varying numbers of water molecules between the acid and the base. The main reaction pathway for moderate to strong bases was identified as the “loose” complex where there is only a single water molecule between the reaction partners, whereas the weaker bases exhibited an increasing amount of long-range PT. Second, the reaction mechanism was suggested to be sequential, Grotthuss-type,<sup>682,683</sup> proton hopping where the proton is first transferred to the water followed by an uptake by the base.<sup>680,681</sup>

Siwick, Bakker, and co-workers extended the investigations of Pines and Nibbering and provided an alternative view into the

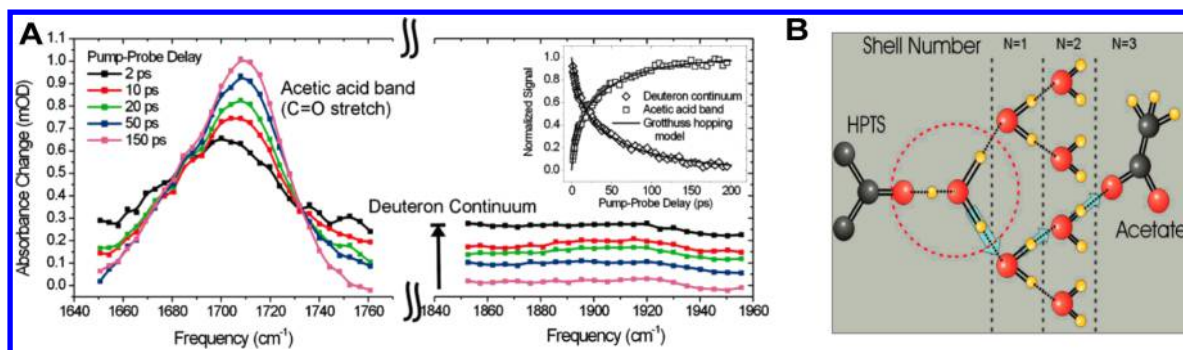


**Figure 61.** (A) Transient IR absorption spectra measured with HPTS in the presence of acetate showing the marker signal corresponding to the acetic acid ( $\sim 1710\text{ cm}^{-1}$ ) and the deuteron continuum. (B) Grotthuss hopping model in aqueous environment. The scheme shows the different solvation shells and the proton relay pathway as indicated by the blue arrows. Adapted from ref 684. Copyright 2007 American Chemical Society.

mechanistic picture of bimolecular ESPT.<sup>684–689</sup> They used the same method to monitor the transient IR marker bands of HPTS and acetates in water and heavy water. The observations were largely the same but they observed a broad continuum signal over the whole detection window, contrary to the studies by Nibbering et al. The continuum signal appeared within the temporal resolution of the experiment ( $\sim 200\text{ fs}$ ) and partially decayed with the concomitant appearance of the HPTS anion and the acetic acid signals in neat water (Figure 61A). This was explained by an initially prepared state in which the proton is loosely bound to the hydroxyl oxygen, giving rise to the strong continuum signal. The full deprotonation was suggested to decrease the absorption coefficient of the solvated proton resulting in the partial decay of the signal upon full dissociation. Second, the authors did not observe any delay between the rise of the HPTS anion signal and the acetic acid signal in the presence of the acetate ( $0.5\text{--}4\text{ M}$ ). The major difference with respect to the previous studies was, however, the model used to analyze the obtained results.

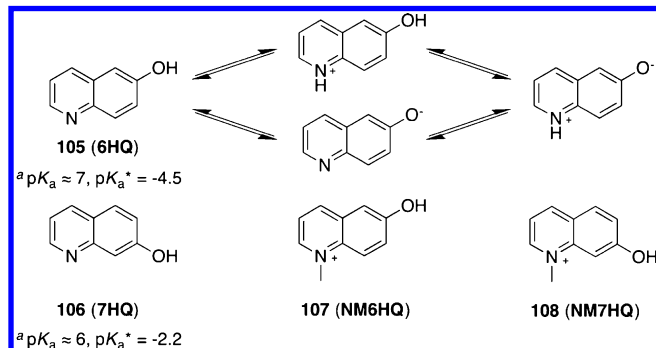
Bakker and co-workers derived a completely new model based on the Grotthuss-like hopping mechanism (Figure 61B).<sup>684,685</sup> They considered an initial distribution of solvent-separated complexes between the acid and the base differing in the number of the water molecules separating the pair. This statistical distribution depended only on the concentrations of the acid and the base. The reactivity was not limited to the maximum number of water molecules separating the pair but the rate was assumed to decrease exponentially with the number of water molecules as  $k = nk_0\Delta^{N-1}$ , where  $k_0$  is the intrinsic PT rate constant across a single water molecule,  $n$  is the number of bases in the  $N$ th solvation shell,  $N$  is the number of water molecules separating the pair, and  $\Delta$  is the factor by which the PT rate decreases with each additional water molecule separating the pair. The decrease in the rate represents the time that the system has to wait until the right hydrogen-bond configuration between the reactive pair is established. When the optimal configuration is established, the reaction was assumed to be ultrafast. The diffusion of the acetate bases was taken into account by allowing them to hop between the solvation shells at a rate given by the diffusional constant. Based on the above considerations, the authors simulated the survival probability of the protonated HPTS, which was compared with the experimental data. The model was found to be in excellent agreement with the experimental results both at short and long times. The obtained intrinsic PT rate constants for water and heavy water were  $(1.2\text{ ps})^{-1}$  and  $(1.8\text{ ps})^{-1}$ , respectively, reproducing the kinetic isotope effect of

the proton hopping rate in water. A constant value of  $\Delta = 0.2$  was found for both solvents demonstrating the rapid decrease (factor of 5) in the rate upon increasing separation. The value was suggested to originate from the structure and hydrogen-bond connectivity, specific to a certain solvent, water and heavy water being identical in this sense. At the relatively high base concentrations used in the experiments ( $0.5\text{--}4\text{ M}$ ), the diffusional effects were shown to play only a minor role in the dynamics. The nonexponentiality was proposed to mainly originate from the distribution of the separation distance and hence the distribution of the rates. The main advantage of this approach was that the dynamics were analyzed within the same model, whereas the previous approaches combined static components with the diffusional models.

In subsequent publications, Bakker and co-workers also considered two parallel pathways, namely the direct pathway described above and an initial deprotonation to water followed by proton scavenging by the base,<sup>686,689</sup> salt effects<sup>687</sup> and diffusional approaches based on an extended Smoluchowski model.<sup>688</sup>

**3.3.3. Hydroxyquinolines.** Hydroxyquinolines can be considered as substituted naphthol-analogs where the imine nitrogen acts as a strong electron-withdrawing group on the aromatic system. This results in strong enhancement of the photoacidity due to the increased ICT character of the locally excited state. The electron density is highly localized on the quinoline nitrogen in the excited state, which results in much more versatile behavior compared to naphthols. In addition to photoacidity, the hydroxyquinolines exhibit strong photo-basicity of the quinoline nitrogen due to the electronic redistribution upon excitation. These two effects are strongly coupled to each other in a cooperative manner. Deprotonation of the hydroxyl group increases the basicity of the nitrogen, whereas protonation of the nitrogen increases the acidity of the hydroxyl group. Due to this effect,  $N$ -protonated (cationic) 6-hydroxyquinoline (**105**, **6HQ**) is able to deprotonate even in  $10\text{ M}$  perchloric acid solution, whereas the oxygen-deprotonated (anionic) form shows proton uptake even in  $12\text{ M}$  NaOH solution!<sup>691</sup> The zwitterionic tautomer is strongly stabilized by an ICT process resulting in a quinoid-like resonance structure possessing a relatively small permanent dipole moment, as demonstrated by its negative solvatochromism. The bifunctional nature of the compound results in additional complexity of the prototropic behavior both in the ground and excited states. First of all, the compound can exist in four different prototropic forms (Chart 20). The dominant species under acidic, neutral, and basic conditions are the

Chart 20. Structures of Hydroxyquinoline-Derived Photoacids together with the Ground- and Excited-State  $pK_a$  Values<sup>a,b</sup>



<sup>a</sup>From ref 690. <sup>b</sup>The  $pK_a$  values refer to the N-protonated forms. The values for the N-methyl compounds are expected to be similar to those of the N-protonated forms; however, varying values appear in the literature depending on the method of determination.

protonated (cation), neutral, and deprotonated (anion) forms, respectively. Second, the tautomerization can proceed in multiple different ways, i.e., deprotonation followed by proton uptake, proton uptake followed by deprotonation, or a concerted mechanism. These forms and pathways were investigated by several groups.<sup>690–705</sup>

Jang and co-workers studied the tautomerization mechanism of 6HQ in aqueous solutions using ps TCSPC (70 ps IRF).<sup>701</sup> Based on the analysis of the fluorescence decays, they proposed that the initial step in the cycle is the protonation of the imine in 15 ps followed by a deprotonation of the enol group in 40 ps. Moreover, they claimed that the ICT proceeds as a distinct process with a time constant of 11 ps after the deprotonation under neutral pH. The time constant was deduced from the difference between the decay of the zwitterionic fluorescence and the rise of the quinoid-like tautomer fluorescence. In a subsequent study, Jang and co-workers extended the investigations to intermediate pH values, kinetic isotope, and temperature effects. In addition, the decays were measured with better time resolution (~25 ps).<sup>706</sup> The interpretation of the data was completely different from the initial study. The observed enol deprotonation at pH 3 was significantly faster (~10 ps) than the proton uptake at pH 7 (46 ps) and hence the deprotonation was suggested to be the initial step under neutral conditions. Second, the ICT step was not considered at all. The authors considered multiple reactive species,  $H_2O$ ,  $H_3O^+$ , and  $OH^-$ , for the different reactive steps and determined the fractions of each pathway as a function of pH.

Poizat et al. revisited the photophysics of 6HQ in aqueous solutions to provide a comprehensive picture of the excited-state prototropic behavior.<sup>707</sup> They monitored the transient spectra of 6HQ and its methoxy-derivative, 6MQ, in neutral, acidic, and alkaline aqueous solutions using fs broadband transient electronic absorption. The improved time resolution allowed them to resolve a deprotonation time constant of ~2.2 ps in acidic solution, more than 1 order of magnitude faster than the observed imine protonation in 1 M KOH solution (~30 ps). This was one of the fastest ESPT times ever observed. By comparing the transient spectra of 6HQ and 6MQ under different conditions, the authors were able to assign the spectral changes at neutral pH to different reactive steps. The initial step was shown to be the deprotonation of the

enol hydrogen with  $\tau \approx 2$  ps followed by protonation of the imine nitrogen with a time constant of  $\tau = 38$  ps. Based on the similar time scale of the deprotonation under neutral and acidic (imine already protonated) conditions, the rate was suggested to depend on the solvent dynamics rather than on the properties of the solute, as the protonation of the imine was expected to significantly increase the acidity of the enol group. Second, the authors suggested that the formation of the quinoid-like tautomer is unidirectional rather than an equilibrium reaction due to the strong resonance stabilization. This renders the definition of  $pK_a^*$  meaningless in the case of 6HQ. The same was suggested for 7HQ.<sup>702</sup>

The tautomerization mechanism of 7HQ received considerable attention in water, alcohols, and organic solvents in the presence of hydrogen-bonding additives.<sup>708–721</sup> The mechanism slightly differs from that of 6HQ due to the closer proximity of the acid–base groups. This enables the formation of a hydrogen-bond wire between the groups facilitating the tautomerization via a Grotthuss-type proton relay mechanism. The proton relay in organic solvents can be facilitated by water,<sup>714</sup> alcohol<sup>713,716</sup> and acetic acid<sup>710</sup> wires. Acetic acid was also shown to enable the tautomerization of 6HQ in organic solvents, but a higher stoichiometry (1:1 for 7HQ and 1:2 for 6HQ) is required due to the longer distance of the acid–base groups.<sup>722,723</sup>

Jang and co-workers demonstrated that 7HQ forms stable cyclic 1:2 complexes with both water and alcohols in nonpolar organic solvents<sup>713–715,719</sup> and investigated the phototautomerization using a ps streak camera. The decay of the neutral species showed a fast decay component (~38 ps in the presence of  $H_2O$ ) with a concurrent rise of the tautomer emission, which was directly attributed to the tautomerization step. Additionally, the neutral emission exhibited a slower decay component, which was explained by noncyclic or 1:1 complexes unable to undergo tautomerization. The tautomerization rate was strongly dependent on the hydrogen-bond donating ability ( $\alpha$  parameter) of the alcohol used. Therefore, the authors suggested that the process is mainly controlled by the initial protonation of the imine followed by very rapid deprotonation without a stable intermediate.<sup>713,716</sup> On the other hand, the deprotonation of the enol group was suggested as the initial step in the presence of water in diethyl ether. A recent computational study, however, showed that the transition state is product-like and therefore the mechanism can be considered to be concerted.<sup>717</sup> In the presence of both water and alcohols, the tautomerization exhibited a relatively large kinetic isotope effect (KIE = 15 in methanol). The determined activation energies were small and independent of the isotope. Second, the tautomerization was completely inhibited below the freezing point of the solvents. Therefore, the authors proposed that the tautomerization proceeds via tunneling, which is assisted by the solvent fluctuations.

The tautomerization mechanism of 7HQ in protic bulk solvents is somewhat more complex. The mechanism was suggested to be a stepwise process but controversial reports about the initial step appear in the literature.<sup>708,712</sup> Second, different prototropic forms (mostly the neutral and the tautomer) and conformers (cis–trans) are present in the ground state, which can give rise to different reaction pathways upon excitation.<sup>720</sup> Kwon and Mohammed approached this problem using two methyl-functionalized 7HQ derivatives (6Me-7HQ and 8Me-7HQ).<sup>721</sup> The steric hindrance forces the –OH group into a cis (6Me-7HQ) or a trans (8Me-7HQ)



configuration. Moreover, the formation of the water wire is prevented in **8Me-7HQ**. The authors investigated the fluorescence decays using fs fluorescence up-conversion at different pH values. The neutral form of **8Me-7HQ** showed a biexponential decay with time constants of 3.2 and 91 ps whereas the tautomer showed a rise time of 109 ps. Based on the measurements at different pH values, the initial step was attributed to a reversible deprotonation of the enol group followed by an irreversible protonation of the imine group resulting in the formation of the tautomer. The authors analyzed the results according to this kinetic scheme to obtain the rate constants for the different processes. **6Me-7HQ** showed much richer dynamics. The main decay component of the neutral and the rise component of the tautomer were observed with a  $\sim 20$  ps time constant. In addition, both the decay and the rise showed minor components with similar lifetimes to **8Me-7HQ**. Therefore, the authors suggested that both deprotonation to water and tautomerization via the water wire are active in this molecule. The 20 ps component was thus attributed to the direct tautomerization in the cyclic complex. However, the authors proposed that the initial step with a 20 ps time constant is the deprotonation of the enol group to the water wire followed by an extremely rapid protonation of the imine nitrogen by the hydrated proton without the buildup of a stable intermediate. The two pathways are illustrated in Figure 62. The slower ESPT rate in the cyclic complex compared to the deprotonation to the solvent was suggested to originate from the stability of the water wire and the decreased acidity and basicity of the functional groups due to partial charge delocalization in the complex.

As already suggested by Bardez and co-workers,<sup>691,702,703</sup> protonation of the imine nitrogen strongly increases the acidity

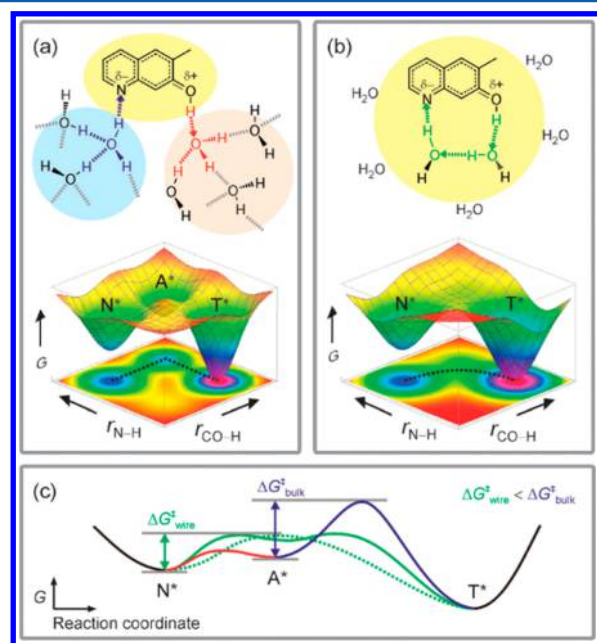


**Figure 62.** Two possible pathways for the solvent mediated tautomerization of **6Me-7HQ** in aqueous solution together with illustrative potential energy surfaces. (a) Stepwise mechanism. (b) Concerted mechanism. (c) Potential energy diagrams along the reaction pathways. Because the concerted mechanism does not produce a stable intermediate, the maximum is better represented as a transition state (dotted line). Reprinted with permission from ref 721. Copyright 2012 PCCP Owner Societies.

of the enol hydrogen in hydroxyquinolines. Therefore, methylation of the imine nitrogen is expected to result in even stronger photoacids. Second, this simplifies the prototropic behavior significantly. This was demonstrated by Kim and Topp who investigated two *N*-methyl-derivatives, **NM6HQ** and **NM7HQ**, using fs fluorescence up-conversion.<sup>724</sup> The observed ESPT times for **NM6HQ** and **NM7HQ** in slightly acidic solution were  $2.0 \pm 0.1$  ps and  $4.5 \pm 0.2$  ps, respectively. The time constant of **NM6HQ** was in excellent agreement with the ESPT time constant of **6HQ** in acidic solution (2.2 ps) reported by Poizat et al. Second, the authors characterized the spectral evolution in basic solution. The observed dynamic Stokes shift exhibited two time constants of 0.22 and 1.04 ps. The authors suggested that the shorter time constant could be due to a rapid ICT process converting the zwitterionic form into the quinoid-like structure and the second due to the subsequent solvent relaxation. However, based on the intensities of the spectra, the transition dipole moment did not change during the solvation process suggesting the presence of only a single electronic state.

Both the solvation and the ESPT dynamics of **NM6HQ** were subsequently investigated by Mosquera, Ernstring, Kovalenko, and co-workers using broadband transient electronic absorption with sub-100 fs time resolution.<sup>629,725</sup> They convincingly demonstrated that the stationary and time-dependent solvatochromic behaviors of the **NM6HQ** anion simply originate from a dielectric relaxation and do not involve a change in the electronic state. The obtained spectral response function was in excellent agreement with those of other solvent probes (coumarins 343 and 153) and could also be reproduced from the dielectric spectrum of the solvent. Second, the authors undertook detailed investigations of the ESPT process of protonated **6HQ** and **NM6HQ** in water, alcohols and acetonitrile in the presence of water. The ESPT dynamics were obtained after spectral decomposition of the broadband transient absorption spectra. The different spectral components were ground-state bleach (blue in Figure 63), excited-state

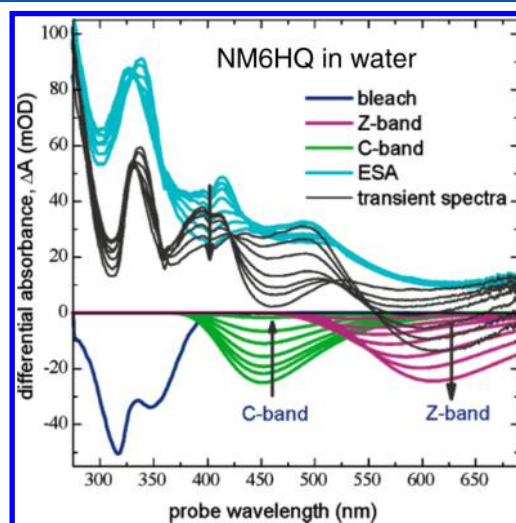


**Figure 63.** Spectral decomposition of the transient spectra (black) measured with **NM6HQ** in neutral water. The different contributions from the bleach (dark blue), excited-state absorption (light blue), and stimulated emission consisting the initial cation emission (C-band, green) and tautomer (Z-band, magenta) are shown. Reprinted from ref 629. Copyright 2007 American Chemical Society.

absorption (cyan in Figure 63), cation emission (green in Figure 63), and tautomer emission (magenta in Figure 63). The ESPT could be monitored from the decay of the initial cation emission and the concomitant rise of the tautomer emission obtained from the band integrals of the transient spectra. Second, the solvent relaxation could be monitored from the dynamic Stokes shift of the emission bands. **6HQ** and **NM6HQ** cations showed indistinguishable ESPT kinetics as already suggested by earlier studies<sup>707,724</sup> and hence the authors considered only the kinetics of protonated **6HQ**. The decay of the cation emission and the rise of the tautomer emission could be approximately reproduced with a three-exponential function with time constants of  $\sim 70$  fs, 420 fs, and 2 ps. Previous reports had only recognized the longest time constant for the ESPT process. Moreover, the deprotonation kinetics closely followed the solvent relaxation function in all solvents. Comparison between the solvent relaxation functions,  $C(t)$ , and the ESPT dynamics,  $S(t)$ , in several solvents are shown in Figure 64. The

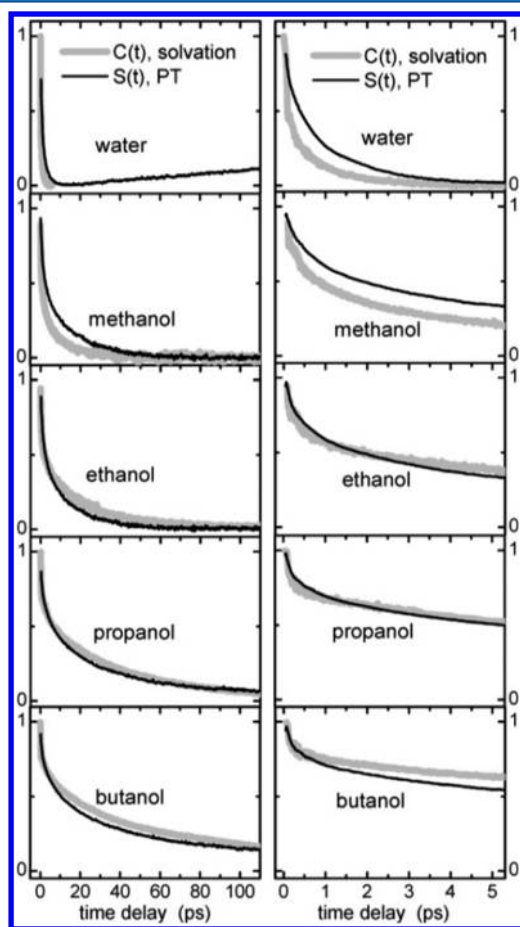


**Figure 64.** Comparison between the PT dynamics,  $S(t)$  (black), and the solvent relaxation function,  $C(t)$  (gray), of **6HQ** cation in protic solvents.  $C(t)$  was measured with **NM6HQ** in water, methanol, and ethanol and with coumarin 153 in propanol and butanol. The left and the right panels show the comparison in long and short time scales, respectively. Reprinted from ref 629. Copyright 2007 American Chemical Society.

close resemblance of the proton-transfer dynamics with the solvent relaxation function strongly indicated that the ESPT is solvent-controlled,  $C(t)$  being the true reaction coordinate, as suggested by the theoretical formulations of Hynes and co-workers.<sup>463</sup> Slightly slower ESPT dynamics (factor of ca. 2)

compared to the solvent relaxation, however, suggested a small but nonzero barrier. Second, the faster ESPT at longer time scale in ethanol, propanol and butanol suggested that the short-time solvent reorganization may be sufficient to complete the ESPT in these slower relaxing solvents.<sup>629</sup>

Next, the authors focused on the ESPT in acetonitrile–water mixtures. Surprisingly, a small contribution from the tautomer was observed even in neat acetonitrile, which was attributed to the residual water present in spectroscopic-grade solvents. Based on the DFT-calculated binding energy and the amount of residual water present in the solvent, virtually all photoacid molecules were suggested to be bound to at least one water molecule already in the ground state. Upon increasing the concentration of water, the relative contribution of the tautomer emission increased on two different time scales. The fast initial kinetics were independent of water concentration, whereas the long-time kinetics became faster at higher water concentration. The latter was ascribed to a diffusional process, whereas the former represented the fast solvent-controlled ESPT in the preformed complex. Based on the diffusional rate constants derived from multiexponential analysis of the data, the authors suggested that diffusion of only one bulk water molecule to the **6HQ**: $\text{H}_2\text{O}$  complex is sufficient to facilitate the ESPT process.<sup>629</sup> Similar observations were recently reported also for alcohol additives in neat acetonitrile.<sup>726</sup>

Solntsev and co-workers also investigated the ESPT and, in particular, the long-time decay behavior of **NM6HQ** in various protic solvents.<sup>727,728</sup> The authors claimed that the long-time fluorescence decay in alcohols is nonsingle exponential, and attributed this to the reversibility of the process, contrary to previous reports.<sup>629,691,707</sup> However, solvent relaxation or other processes were not considered as the origin of the nonsingle exponential behavior. Moreover, initial attempts to analyze the time-resolved data with the use of the DSE model were unsuccessful. This was attributed to the complications arising from the highly anisotropic charge distribution in the excited state and the presence of the counterion. The authors performed extensive Brownian dynamics simulations in butanol to investigate these effects in detail. They were able to show that the presence of the counterion results in nonstationary interaction potentials and decreased diffusion coefficients for both the counterion and the proton due to the mutual Coulomb interaction. After adapting the mutual diffusion coefficient and the time-dependent effective potential based on the output of the Brownian dynamics simulations, the problem could be solved numerically with the DSE model producing nearly identical results. The results were also in good agreement with the experimental data especially at long times. The ultrafast decay and rise components were not fully reproduced by the simulations, which most likely originates from the multiexponential nature of the solvent-controlled ESPT process. The simulations assumed a single rate constant for the contact reaction.<sup>728</sup> Based on the obtained results, the authors estimated the excited-state  $\text{p}K_a$  to be  $-7$ ! This is in strong contrast with the value of  $-4$  estimated by Kovalenko and co-workers based on the Förster cycle.<sup>629</sup> Nevertheless, at that time, **NM6HQ** appeared to be the strongest photoacid reported to date.

In a follow-up study, Solntsev and co-workers investigated the effects of solvent and temperature on the ESPT process in alcohols using mostly ps TCSPC. They measured the fluorescence decays as a function of temperature in ethanol,

propanol, and butanol. The forward and backward rate constants were obtained from fits using the DSE model with the adapted diffusion coefficient and effective potential used in the previous study. Contrary to the previously observed non-Arrhenius behavior of the naphthol-based “super” photoacids, **NM6HQ** showed nearly linear Arrhenius plots with a relatively constant activation energy. The determined activation energies were significantly smaller than those of the previously studied **2N-DCN**, which was attributed to a much higher excited-state acidity of **NM6HQ**. The ESPT was concluded to be solvent-controlled based on fs fluorescence up-conversion measurements. The ESPT time constants obtained from average lifetimes of the multiexponential analysis were shown to be close to the Debye relaxation times of the solvent.<sup>727</sup> However, comparison of a single ESPT time constant with the Debye relaxation time of the solvent is questionable as demonstrated by the study of Kovalenko et al.<sup>629</sup>

In a recent publication, Solntsev and co-workers presented a more detailed discussion about the nonexponential nature of the deprotonation process of **NM6HQ** in butanol. They showed that both the decay of the cation and rise of the tautomer emission could be approximated by a three-exponential function or by three rate distributions with relatively narrow widths. These rates or distributions were each suggested to have a different origin. The fastest component, faster than the Debye relaxation of the solvent, was proposed to originate from an increased acidity of the solvent molecule in the electrostatic field of the counterion. The second component, close to the Debye relaxation time, was ascribed to proton abstraction by a normal solvent molecule and slowest component was suggested to involve some diffusive motion prior the proton transfer. However, Kovalenko and co-workers already demonstrated that the ESPT dynamics closely follow the solvent relaxation function, which is well known to exhibit nonexponential behavior.<sup>22,629</sup> Hence, it seems more plausible that the ESPT is a nearly barrierless, solvent-controlled process and therefore follows the non-exponential solvent relaxation.

Mosquera, Pérez Lustres and co-workers proposed an alternative explanation for the multiexponential decay of **NM6HQ** in alcohols.<sup>675</sup> They measured the solvatochromic behavior and fluorescence decays in several alcohols using steady-state and time-resolved methods. They reconstructed the time-resolved fluorescence spectra from the ps TCSPC fluorescence decays. The concentrations of the **NM6HQ** cation and the tautomer were subsequently obtained from the band integrals of the time-resolved spectra using two log-normal functions. The decay of the cation showed biexponential behavior with a concurrent rise of the tautomer emission, which then decayed with a single exponential. The authors showed that the biexponentiality could not originate from the solvation dynamics because the solvent relaxation showed a single exponential behavior on the ps time scale under consideration. Hence the behavior was attributed to reversibility of the initial dissociation step according to the Eigen–Weller model.<sup>472,599</sup> The initial step, mostly completed within the time resolution of the ps experiment, was ascribed to the reversible short-range proton transfer producing the contact ion pairs. This is followed by the diffusion-controlled separation into the free ions. The latter process could, in principle, be also reversible but the purely single exponential decay of the tautomer emission and low concentrations of protons suggested an irreversible reaction contrary to the reports of Solntsev and co-

workers. The nonexponential behavior observed in the earlier reports could originate from the solvent relaxation, the biphasic decay of the cation emission and the partial overlap of the cation and tautomer emission bands. This was circumvented in the present study with the use of band integrals rather than single wavelength decay traces.

The kinetics were analyzed according to rate equations derived from the Eigen–Weller model (Figure 53) assuming an irreversible second step and similar spectral properties for the contact ion pair and the free ions. The ultrafast initial deprotonation, not temporally resolved here, was accounted for using nonzero initial concentrations of the ion pairs. A global fit with the kinetic model was in very good agreement with the data (Figure 65). The authors were able to obtain all

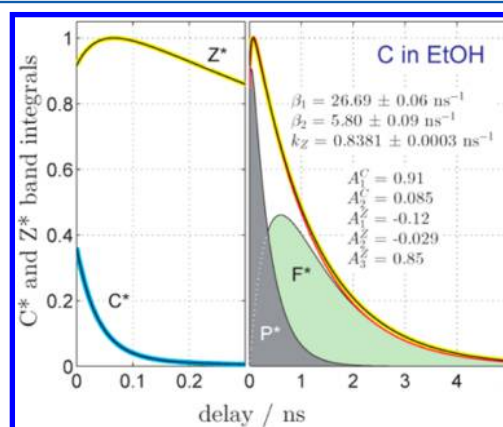


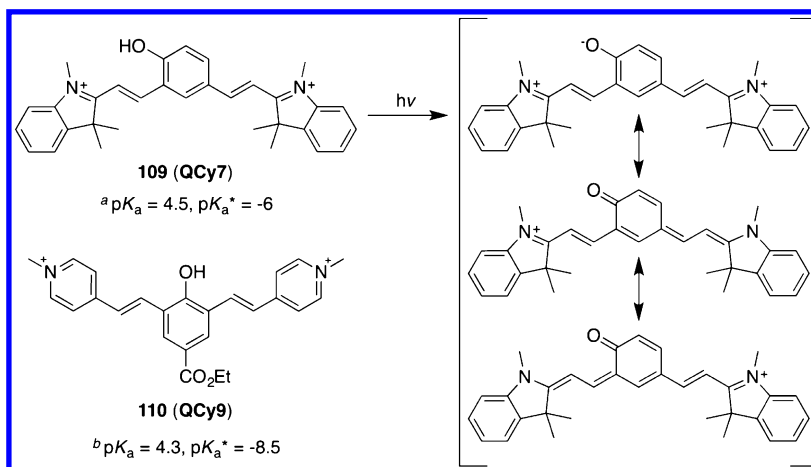
**Figure 65.** (left) Early temporal evolution of the cation ( $C^*$ , cyan) and the tautomer ( $Z^*$ , yellow) band integrals from the ps measurements of **NM6HQ** in ethanol, and best biexponential ( $C^*$ ) and triexponential ( $Z^*$ ) fits. The decay constants and associated amplitudes are indicated in the legend. (right) Full temporal evolution of the tautomer, decomposed into the individual contributions from the contact ion pairs ( $P^*$ , gray) and the free ions ( $F^*$ , light green). The red solid line represents the global fit with the amplitudes constrained to the analytical forms derived from the kinetic model (see text). Reprinted from ref 675. Copyright 2013 American Chemical Society.

the individual rate constants and concentrations of the involved species with the use of the kinetic model. Interestingly, the results showed that a significant amount of the tautomer emission originates from the contact ion pairs, which dissociate on a 500 ps to ns time scale. The initial ps deprotonation time was comparable to the slowest solvent relaxation time, observed separately, demonstrating a solvent-controlled reaction. Second, the rate constant responsible for the separation of the contact ion pair was inversely dependent on the viscosity of the solvent demonstrating the diffusion-control of this step.<sup>675</sup>

Consequently, the results were largely in agreement with the previous study by Kovalenko and co-workers but extended the observations to the long-time scale processes. The two studies emphasize the importance of solvation both intrinsically to the process as well as from the analysis point of view. Solvation should be explicitly considered to gain access to the real unobscured population dynamics. Monitoring of the band integrals seems to be a straightforward way to directly access the population dynamics without complications from solvation.

**3.3.4. Cyanine Photoacids.** Recently, Huppert and co-workers reported on investigations of a novel class of “super” photoacids based on quinone-cyanine dyes.<sup>674,729–735</sup> These



Chart 21. Structures of Quinone-Cyanine Based Photoacids together with the Ground- and Excited-State  $pK_a$  Values<sup>a,b</sup>

<sup>a</sup>From ref 729. <sup>b</sup>From ref 730.

compounds are the strongest photoacids reported to date and exhibit ESPT time constants in the sub-picosecond regime, approaching the rates of the fastest intramolecular proton-transfer reactions. The  $pK_a^*$  values of the two more thoroughly studied compounds, QCy7 (109) and QCy9 (110), were estimated with the Förster cycle method to be -6 and -8.5, respectively. The extremely high excited-state acidity is partly explained by the relatively low  $pK_a$  already in the ground state ( $\sim 4$ –5). Second, the deprotonated form is strongly stabilized by resonance structures due to the charge migration to the positively charged nitrogen groups (Chart 21).

In the initial studies, Huppert and co-workers investigated QCy7 and two of its sulfonated derivatives in aqueous solutions using fs fluorescence up-conversion.<sup>729,731</sup> The decay of the ROH\* form showed nonexponential behavior, which was analyzed using a sum of stretched exponential ( $\exp[-(t/\tau)^\beta]$ ) functions. No justification for the use of the stretched exponential function was, however, proposed. All compounds exhibited an ultrafast  $\sim 100$ –200 fs component, which was attributed to solvent relaxation. The intermediate decay component with the largest amplitude slightly varied between the different compounds (430 to 640 fs) with a  $\beta$  parameter of  $\sim 0.83$ . The RO<sup>-\*</sup> form showed a rise with a similar time constant as the main decay component of the ROH\* form. Hence it was attributed to the ESPT process. These rates are 3–4 times higher than the ESPT rate measured for NM6HQ, ca. (2 ps)<sup>-1</sup>. The long-time component was suggested to originate from the reversibility of the process. For QCy7, the long-time asymptote approached  $\sim t^{-3/2}$  whereas the two negatively charged sulfonated derivatives exhibited much slower decay with  $t^{-0.8}$  to  $t^{-0.9}$ . The long-time behavior was ascribed to the geminate recombination. In the sulfonated compounds, the recombination is strongly accelerated due to a higher attractive potential of the negatively charged photoacids. The DSE model could, however not be applied due to the highly nonspherical shape of the photoacids and the geminate recombination was only qualitatively discussed.

In subsequent studies, Huppert and co-workers investigated an even stronger photoacid, QCy9 (110), in water and heavy water using fs fluorescence up-conversion (340 fs IRF).<sup>730</sup> The compound shows an unprecedented  $pK_a^*$  of -8.5 as estimated with the Förster cycle method. Similarly to QCy7, the fluorescence decay of the ROH\* form was analyzed with a

sum of three exponential functions in water and with a sum of two exponential and two stretched exponential functions in heavy water. In both solvents, the fastest component (with a  $\sim 100$  fs and  $\sim 200$  fs lifetime in water and heavy water respectively) was also the decay component with the largest amplitude ( $>80\%$ ). The amplitude did not vary significantly over the emission band of the ROH\* form. The rise of RO<sup>-\*</sup> showed a similar major component with equal time constant and was thus attributed to the ESPT process,  $k_{PT} = 10^{13} \text{ s}^{-1}$  and  $0.5 \times 10^{13} \text{ s}^{-1}$  in H<sub>2</sub>O and D<sub>2</sub>O. These are the fastest intermolecular ESPT rates reported to date. No solvation was, however, taken into account, contrary to the previous report on QCy7. This could somewhat decrease the accuracy of the determined time constants. Nevertheless, QCy9 clearly undergoes ESPT with a much higher rate than QCy7. The intermediate components with time constants of  $\sim 500$  fs and  $\sim 900$  fs in H<sub>2</sub>O and D<sub>2</sub>O were suggested to originate from the contact ion pairs according to the Eigen–Weller model, whereas the slower decay components were ascribed to the geminate recombination.

The intermediate time scale process was further investigated using low-temperature steady-state and ps TCSPC spectroscopy as well as fs fluorescence up-conversion and broadband transient electronic absorption.<sup>674,735</sup> The steady-state emission spectra of both QCy7 and QCy9 showed an abrupt change in the shape at low temperature ( $T \leq 150 \text{ K}$ ) both in H<sub>2</sub>O and D<sub>2</sub>O. The long-wavelength emission band attributed to the deprotonated form, RO<sup>-\*</sup>, blue-shifted by about 1000 cm<sup>-1</sup>. At these low temperatures, the proton hopping time in ice is significantly longer. A similar effect on the steady-state emission spectra was observed at high concentrations of strong mineral acids and in neat trichloroacetic acid. The intensity of the long-wavelength RO<sup>-\*</sup> emission band was significantly reduced and a new band appeared at shorter wavelength. The kinetics of the emission bands of QCy9 in neat trichloroacetic acid was investigated using fs fluorescence up-conversion. The decay of the neutral form showed biphasic dynamics with a fast ( $\sim 15$  ps) and a slow ( $\sim 200$  ps) component. The intermediate band showed a fast rise followed by a  $\sim 300$  ps decay. The long-wavelength band, attributed to the free ion pairs, showed slow rise with a large amplitude, followed by an exponential decay on a much longer time scale. All these observations pointed to an

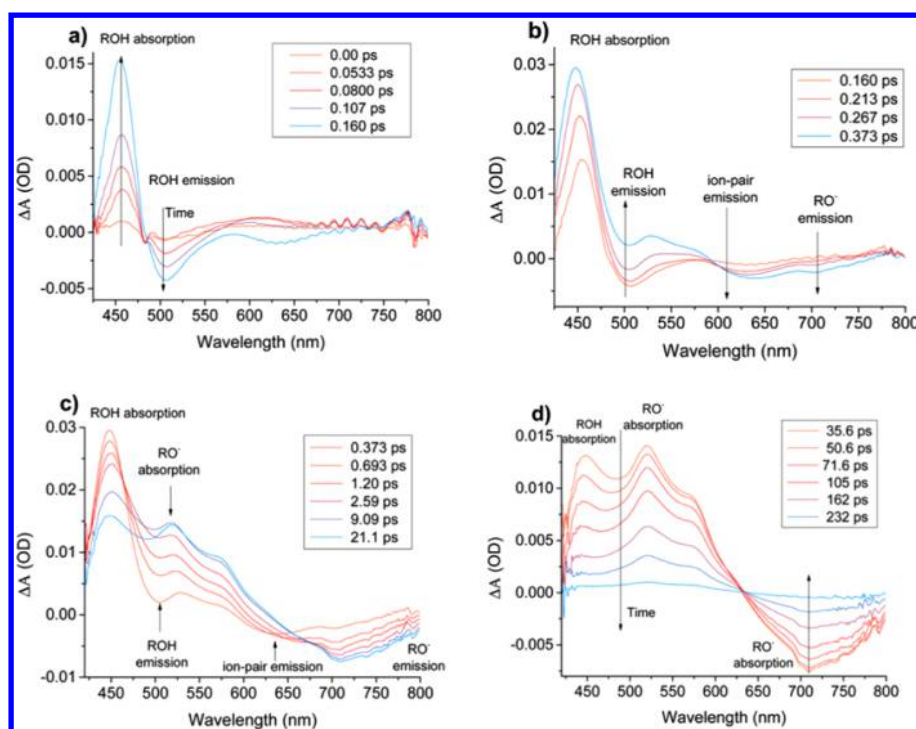


**Figure 66.** Transient absorption spectra measured in 6 M HCl aq. upon excitation of the neutral form of **QCy9** at different time scales: (a) 0 to 0.16 ps, (b) 0.16 to 0.37 ps, (c) 0.37–21 ps, and (d) 36–232 ps. Reprinted from ref 674. Copyright 2014 American Chemical Society.

intermediate species emitting at shorter wavelength compared to the free, fully solvated anion.

The behavior was further investigated using fs broadband transient absorption. The transient spectra in slightly acidic aqueous solution showed the fast formation of anionic species emitting both at the intermediate and long wavelength regions consistent with the ultrafast ESPT time constant observed in the previous experiments. In time, the intermediate emission decreased in intensity with a concurrent increase of the long-wavelength emission. A global analysis of the data yielded time constants of  $\sim 130$  fs and  $\sim 230$  fs for the formation and  $\sim 1.15$  ps  $\sim 1.6$  ps for the decay of the intermediate species in  $\text{H}_2\text{O}$  and  $\text{D}_2\text{O}$ , respectively. The kinetic isotope effect of the decay of the intermediate species was thus about 1.4, similar to that of proton diffusion in water. In the presence of strong acids in high concentrations, the time scales of the processes were significantly longer and the amplitude of the intermediate species was much higher. In 6 M HCl solution (Figure 66), the initially observed species was the excited neutral form due to a ca. three times slower deprotonation compared to neutral water. The neutral form showed an induced absorption at  $\sim 460$  nm and emission at around 505 nm. During the first ps, the emission of the neutral form decreased and a new band at  $\sim 630$  nm, attributed to the intermediate species, appeared. The intermediate emission band decayed on a much longer time scale with a concomitant rise of the long-wavelength emission band at around 710 nm. Based on all the observations, the intermediate species was attributed to the contact ion pair formed after a short-range proton transfer. The concentration of the contact ion pair was demonstrated to strongly depend on the concentration of the bulk protons and the temperature. At low temperature, the proton diffusion or hopping time significantly decreases slowing down the separation into free ions. A high acid concentration, on the other hand, increases the recombination processes shifting the equilibrium toward

the neutral and the contact ion pair. Second, at high acid concentration the amount of water available to accept the protons significantly decreases. Variation in the experimental conditions allowed the authors to identify the intermediate contact ion pair both spectrally and kinetically.<sup>674</sup>

Huppert and co-workers also investigated the ESPT process of the two compounds in methanol and ethanol using ps TCSPC and fs fluorescence up-conversion.<sup>732</sup> They found that the ESPT rate of the weaker acid, **QCy7**, decreases in alcohols being  $k_{\text{PT}} = 1.2 \times 10^{12} \text{ s}^{-1}$ ,  $0.8 \times 10^{12} \text{ s}^{-1}$ , and  $0.7 \times 10^{12} \text{ s}^{-1}$  in water, methanol, and ethanol, respectively, as deduced from the multiexponential analysis of the decay of the neutral form. Surprisingly, **QCy9** did not show such a behavior and the fastest decay component, ascribed to the ESPT process, was  $k_{\text{PT}} = 10^{13} \text{ s}^{-1}$  in all three solvents.

The origin of the ultrafast ESPT was discussed in the framework of the Marcus-BEBO model.<sup>449,450</sup> According to this model, the activation barrier decreases upon increasing driving force and the transition state shifts closer to the reactant configuration. In the extreme case of an activationless process, the reaction occurs at the reactant potential energy minimum without the need of solvent reorganization. The ESPT is then determined by the intermolecular coordinates of the donor-acceptor pair and, in this case, was suggested to be driven by the intermolecular vibration of  $\sim 200 \text{ cm}^{-1}$  modulating the DA distance. Intermolecular hydrogen-bond stretching vibrations of  $\sim 170 \text{ cm}^{-1}$  were observed for water using Raman spectroscopy.<sup>736</sup> The reaction would then occur during the first half of the vibrational period of  $\sim 200$  fs. This mechanism closely resembles that of the intramolecular ESPT where the reaction mainly depends on the vibrational modes modulating the DA distance. Hence the observed  $k_{\text{PT}} = 10^{13} \text{ s}^{-1}$  for the intermolecular ESPT seems to be an upper limit in protic solvents. This limit is reached by the strongest photoacid **QCy9**.<sup>734</sup>

**3.3.5. Concluding Remarks.** The behavior of different photoacids strongly depends on the driving force of the reaction. Weaker photoacids with  $pK_a^* > 0$  are not capable of undergoing ESPT in nonaqueous environments and the deprotonation, even in water, is relatively slow and competes with the excited-state decay. Stronger photoacids with  $pK_a^* \approx -2$  in the regime of “super” photoacids are able to deprotonate in other protic solvents and in some organic solvents such as dimethyl sulfoxide or formamide. In most cases, the reaction still proceeds after solvent relaxation as a normal over-the-barrier process. Several free-energy relations were successfully applied to correlate the ESPT rates of these compounds with the  $pK_a^*$  values. Upon increasing driving force, the process becomes mostly solvent controlled. A good example is **NM6HQ** with a  $pK_a^* = -6$ . The ESPT kinetics follow the solvent relaxation function and show nonexponential behavior. Care must be taken in the analysis of this class of compounds as the solvation and ESPT dynamics occur on the same time scale. With the last class of photoacids with  $pK_a^* < -6$ , the ESPT becomes faster than the solvent relaxation and appears to be controlled by intermolecular vibrations rather than the solvent relaxation. This was recently demonstrated. In this case, the ESPT mechanism resembles that of the intramolecular ESPT and proceeds in sub-100 fs time regime.

The nonequilibrium behavior of the PT reactions is usually approximated using either rate equations or diffusional models representing the two extreme cases, short and long time behavior. The initial steps in the dissociation cycle of the strongest photoacids are clearly solvent-controlled and involve the intermediate contact ion pair whereas the dissociation and recombination are purely diffusive processes. Some examples of combining the diffusive models with static exponential components exist but a unified theory accounting for the full behavior within a single model remains missing.

## 4. PHOTOCHROMIC REACTIONS

### 4.1. Photoisomerization

Isomerization upon photoexcitation was thoroughly studied over the past decades. Among small organic prototype systems, stilbene (111), stiff stilbene (112), and azobenzene (113) are the most prominent ones in the literature. Cyanine dyes were also extensively used to investigate barrier-activated and barrierless processes and to test experimental results against existing theories. This section reviews studies of photoinduced cis–trans isomerization with these model systems, which do not involve chemical bond breaking or formation, contrary to those discussed in section 4.4. A large number of studies were devoted to the photoisomerization of biologically relevant systems, like the green fluorescent protein or retinal proteins.<sup>737–740</sup> The latter were even a major driving force in the development of ultrafast laser spectroscopy.<sup>741–745</sup> However, the course of the reaction in these chromophores is in general largely influenced by the complex embedding protein environment, which is beyond the scope of this review.

Figure 67 shows the possible mechanisms for the trans-to-cis isomerization of azobenzene, which, among the systems discussed here, has the largest number of hypothetically accessible reaction pathways. These are (i) the torsion around the central double bond, (ii) the inversion on one of the two nitrogen atoms, and (iii) the concerted twist of the three central bonds.<sup>746</sup> Corresponding mechanisms can be expected to be at the base of most cis–trans isomerizations.<sup>747</sup>

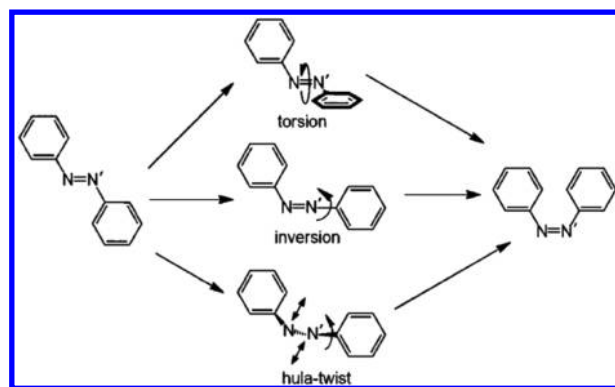


**Figure 67.** Possible isomerization mechanisms in azobenzene. Reprinted from ref 746. Copyright 2014 American Chemical Society.

In stilbenes and azobenzenes, torsion and inversion involve a large amplitude motion of at least one phenyl ring, whereas the concerted twist (often called hula twist) leaves the phenyl rings almost in place. Therefore, the former two mechanisms can be expected to exhibit a dependence on solvent viscosity while the latter should remain rather unaffected by changes of viscosity. An inversion at a carbon atom in stilbene, in analogy to the inversion on one of the nitrogen atoms in azobenzene, is not possible as the motion is hindered by the ethylene hydrogen atoms.<sup>748</sup>

For molecules undergoing ultrafast isomerization even under strong steric constraints, as in azobenzene and retinals, a mechanism involving large amplitude motion can be ruled out as the main reaction pathway. Among other mechanisms, the concerted twist motion was first proposed by Liu and Asato to account for the observed ultrafast dynamics of retinals in the strong constraints of a protein binding pocket.<sup>747</sup>

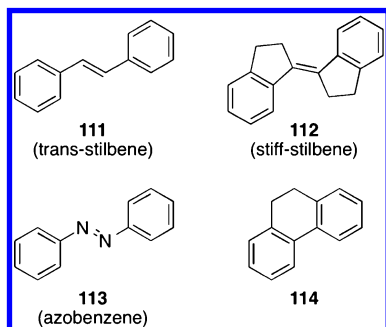
Until the 90s, isomerization was generally discussed in a one-dimensional two-state picture with an avoided curve crossing and a dark or “phantom” state from which isomerization occurs upon a non-radiative transition across the gap of the avoided curve crossing. The understanding of isomerization taking place on a multi-dimensional potential surface led to more elaborate pictures invoking conical intersections as the means for ultrafast internal conversion between different electronic states.<sup>749–755</sup> The complexity of the excited-state potential surface gives rise to various barrier-activated and barrierless relaxation processes. Multiple pathways on a single potential surface are at the origin of multiphasic relaxation kinetics.<sup>746,756–760</sup>

**4.1.1. Stilbene.** Stilbene has become one of the experimentally most studied model systems of photoisomerization, because, in this small and simple molecule, the reaction coordinate can easily be separated from other internal coordinates.<sup>748,757</sup> Early time-resolved works have been reviewed by Waldeck.<sup>761</sup> The steady-state properties of stilbenes were extensively reviewed by Görner and Kuhn.<sup>762</sup> In short, both trans and cis isomers exhibit a strong absorption band located between 260 and 350 nm due to a  $\pi\pi^*$  transition. The trans isomer is the energetically more stable one. The cis isomer can be obtained by photoisomerization of the trans isomer upon irradiation in the UV spectral region. The cis isomer in the ground state is metastable at room temperature and undergoes isomerization back to the trans isomer via a thermally activated process. Upon photoexcitation of the cis isomer, a dihydrophenanthrene (114, **DHP**)-like reaction product is formed (Chart 22).<sup>748</sup> The appearance of this



photoproduct can be used as indicator whether a reaction path involves the *cis* configuration on the  $S_1$  manifold.

Chart 22. Structures of the Stilbenes and Azobenzene



1,1'-Biindanylidene, also called stiff stilbene (**112**), was widely used for comparison because the rotation around the central double bond is the only possible isomerization mechanism, while otherwise it is structurally very similar to parent stilbene. The isomers of stiff stilbene exhibit very similar absorption and emission spectra compared to the parent stilbene,<sup>748</sup> slightly red-shifted and with a more pronounced vibrational structure.

Experiments in the late 1960s and early 1970s by Saltiel and co-workers revealed that the fluorescence quantum yield of the  $S_1$  state of the trans isomer strongly depends on temperature and solvent viscosity.<sup>763–765</sup> Comparing isomerization yields of perhydro- and perdeuterostilbene in direct and sensitized excitation led to the conclusion that the two reaction pathways share a common point on the  $S_1$  electronic state where the branching takes place. An isomerization pathway via the triplet manifold, as had been proposed earlier, could be excluded. A geometry, where the planes of the two phenyl rings are perpendicular to each other, often called a phantom state because it is not observable, was assigned to this point.

The first theoretical concepts useful for describing said phantom state were proposed by Orlandi and Siebrand where the authors described the stilbene molecule as two interacting benzyl radicals.<sup>766</sup> The resulting potential energy diagram is depicted in Figure 68. Therein, the  $S_2$  state is situated closely above the  $S_1$  state in the trans configuration. In the twisted geometry it is to be found below the  $S_1$  state and forms an avoided curve crossing with the ground state. This model was

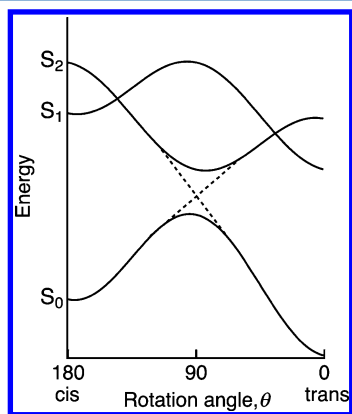


Figure 68. Proposed schematic potential diagram of stilbene as a function of the rotation angle about the central bond.

in accordance with the experimental data available in the early 1970s.

With progress in experimental time resolution, the lifetime of the excited state of *cis*-stilbene in the gas phase could be determined by Greene and Farrow to be 320 fs.<sup>767</sup> In the liquid phase, the first time-resolved measurements by Hochstrasser and co-workers<sup>768,769</sup> revealed a lifetime of the phantom state in *trans*-stiff stilbene of 10 ps. The same research group also studied the influence of the solvent on the isomerization yields and rates,<sup>770</sup> and analyzed the results in the framework of barrier crossing models by Kramers and by Grote and Hynes.<sup>771–773</sup> The observed isomerization rate constant can be expressed as a friction-dependent correction to the rate given by transition state theory. The latter tends to overestimate reaction rates because it does not take into account solvent friction effects.<sup>80</sup> In both models, the original one by Kramers and the modified one by Grote and Hynes, the isomerization rate constant,  $k_{iso}$ , can be expressed as

$$k_{iso} = F(\eta) \exp\left(-\frac{E_b}{k_B T}\right) \quad (57)$$

where  $E_b$  is the height of the barrier and  $F(\eta)$  is a friction dependent frequency factor. The Kramers model applied to stilbene isomerization takes its starting point at the Langevin equation with the dihedral angle between the two phenyl groups as coordinate. Assuming that the solvent fluctuations are much faster than isomerization, the random force reduces to a delta function and the friction is described by a constant, which accounts for the net effect of the solute–solvent interaction. In the limit of high friction, the Kramers model predicts that, at a given barrier height, the rate drops with the inverse of the friction,  $k_{iso} \propto 1/\eta$ , also called Smoluchowski approximation. In the low viscosity limit, the frequency factor becomes friction-independent.<sup>770</sup> The experiments by Hochstrasser and co-workers showed good agreement of the stiff stilbene isomerization rates with the Kramers model in the Smoluchowski limit. With *trans*-stilbene, however, the match was poor and the frequency-dependent model, introduced by Grote, Hynes and van der Zwan,<sup>771–773</sup> had to be applied to properly reproduce the experimental observations. This model uses a generalized Langevin equation, which describes the viscosity contribution by using a memory kernel containing the solvent-averaged time correlation function of the random force. The model takes into account that the dynamics at the barrier may take place on a similar or at even shorter time scales than the fluctuating solute–solvent interaction. Later, the Hochstrasser group realized that, when using values for the friction constant obtained from rotational anisotropy instead of applying Stokes–Einstein–Debye friction, Kramers theory in the Markovian limit can also reproduce the observed rates.<sup>769</sup>

The Fleming group performed a series of experiments on *trans*- and *cis*-stilbene and on diphenylbutadiene from isolated molecule conditions up to 3000 atm pressure in the solution phase.<sup>774</sup> According to Kramers theory, the rate constants should first increase with increasing viscosity in the low friction limit and subsequently decrease with increasing viscosity in the high friction limit. The experimental observations were in qualitative agreement with these predictions. Picosecond time-resolved anisotropy measurements on absorption and fluorescence were used to obtain the rotational diffusion times of *trans*-stilbene.<sup>775</sup> The authors re-examined their own data and those measured by Hochstrasser and co-workers,<sup>769</sup> using the

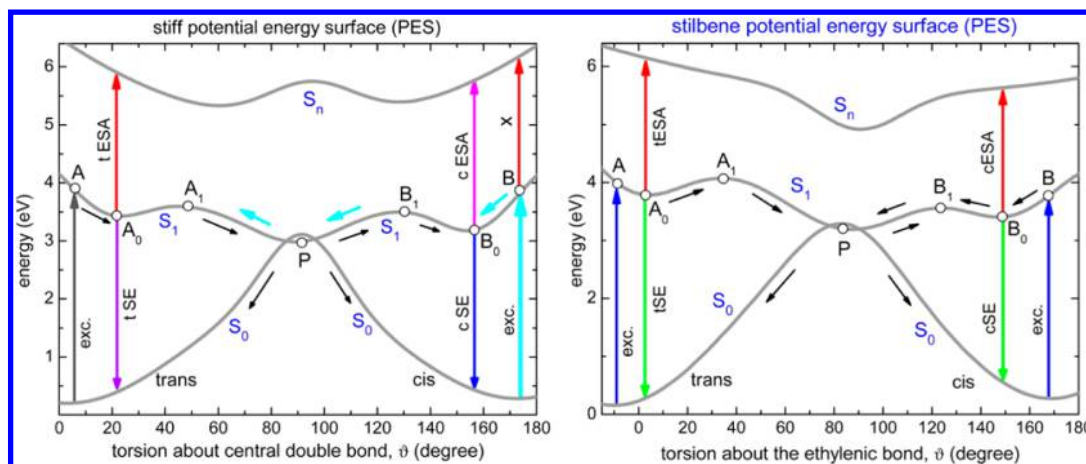


**Figure 69.** Schematic potential energy surfaces of stiff stilbene (left) and parent stilbene (right) in hexane (see text for details). Adopted from ref 748. Copyright 2014 American Chemical Society.

obtained values for the rotational friction. The experimentally determined frequency factor plotted against the shear viscosity and the angular momentum correlation function were perfectly reproduced by a Kramers fit. However, the Grote–Hynes model could reproduce the data equally well. The same group also studied the isomerization dynamics of *cis*-stilbene in a variety of solvents,<sup>776</sup> and over a wide range of temperatures.<sup>777</sup> Isoviscosity plots in small alcohols were found to be nonlinear, whereas the lifetimes in *n*-alcohols and in *n*-alkanes correlated well with each other when plotted against the chain length. It was inferred that macroscopic viscosity is a poor measure for the friction felt by the molecules during isomerization.

It is important to note here that all the works on Kramers and related theories presented so far discuss isomerization reactions in a one-dimensional picture. Newer concepts involving CIs (to be discussed later) show that the potential energy surfaces may strongly depend on solvent properties and local electric fields, especially in regions where multiple electronic states are degenerate or nearly degenerate. In these conditions and under the presence of larger coping the Born–Oppenheimer approximation is no longer necessarily valid. The shape and especially the curvature of the potential at the barrier enter into the expressions of the Kramers and Grote–Hynes models. One can thus expect that the local shape of the potential energy surface around CIs may strongly influence the dynamics of trajectories passing through such a region. Furthermore, the calculated rates strongly depend on the model chosen for the microscopic friction. However, the findings obtained in the publications summarized so far still provide valid information. Revisiting these systems with the improved experimental and computational techniques available now, as was already undertaken in the case of stilbene, azobenzene and a model cyanine dye (see below), would probably be worthwhile.

Tahara and co-workers reported on vibrational wavepacket dynamics observed on the  $S_1$  electronic state of both *trans* and *cis* isomers,<sup>778,779</sup> which were in agreement with the resonance Raman experiments of Iwata and Hamaguchi.<sup>57</sup> The observed dephasing of the wavepacket motion was faster than the  $S_1$  population decay. Therefore, they attributed it to a mode which is not directly involved in the isomerization. In contrast, vibrational wavepacket dynamics observed in other experimental and theoretical works are often assigned to the reactive modes, e.g., ref 780.

Fuss and co-workers determined the lifetime of the perpendicular minimum of photoexcited *cis*-stilbene in the gas phase.<sup>781,782</sup> From the analysis of the observed wavepacket dynamics as a function of probe conditions, a detailed picture of the reaction pathway on the excited-state potential energy surface was drawn. Within that framework, two conical intersections need to be passed to reach the ground state.

Recent transient electronic absorption measurements with greatly improved photometric resolution and FSRS experiments by the Ernsting group on stiff stilbene,<sup>748</sup> and stilbene<sup>757</sup> give an even more detailed spectroscopic picture of the reaction dynamics. The early emission spectrum of the excited *trans* isomer of stiff stilbene was found to resemble the steady-state emission in glycerol where the rotational motion is so hindered by viscosity that the main contribution to the steady-state emission spectrum was found to be due to nontwisted molecules. This emission, with a 0.3 ps decay time, was therefore attributed to the emission from the Franck–Condon configuration. The corresponding excited-state absorption (ESA) from the *trans* configuration (tESA) diminished and red-shifted with a time constant of 0.4 ps, whereas the ESA of the *cis* configuration (cESA) appeared on the same time scale. On the other hand, the bleach of the *trans* configuration remained unchanged until 1 ps, pointing to the formation of the *cis* configuration in the  $S_1$  state. The tESA decayed in 5 ps, while the cESA decayed somewhat more slowly, and the bleach mostly recovered within 5 ps. Isomerization and vibrational cooling were complete after 100 ps. An additional band of a DHP-like product was also observed. This product is known to be a side product of the *cis*-to-*trans* isomerization, indicative of a nonzero population of the  $S_1$  state in the *cis* configuration.

When exciting the *cis* configuration, the authors observed that the emission spectrum at 0.5 ps was equal to the stationary spectrum, while the cESA resembled that found in the parent stilbene. It was therefore assumed that the pathways resemble each other in both systems. The decay of these signals was found to be strongly solvent dependent. Vibrational wavepackets were also observed in the cESA signal. A separate band assignable to the perpendicular configuration was not observed (as opposed to azobenzene, see next section). The observed transients were consistent with an intermediate *trans* population on the  $S_1$  surface. However, contrary to the *trans*–*cis* pathway, a unique assignment was not possible.





accordance with the results of Lednev et al.<sup>794</sup> Vibrational wavepacket dynamics were observed during the departure from the Franck–Condon region. With the trans isomer, the photoproduct appeared with time constants of 0.32 and 2.1 ps. The data were interpreted as indication of inversion as the isomerization mechanism. Similar time constants were obtained using fluorescence from the trans and cis isomer.<sup>797</sup> The longer time constant in the range of 10 ps was attributed to vibrational cooling of the reaction product in the ground state. Time-resolved infrared absorption measurements revealed the same time scale for vibrational cooling of the photoproduct.<sup>800,801</sup> This interpretation differs from earlier publications and from recent work by the Ernsting group discussed later on.<sup>746</sup> The interpretation of vibrational cooling was supported by Tahara and co-workers,<sup>802,803</sup> and by Braun and co-workers.<sup>798</sup> The latter studied both isomers upon  $\pi\pi^*$  excitation by transient electronic absorption. The results were discussed in terms of the scheme depicted in Figure 70, which is itself a similar picture as drawn by Moore and co-workers.<sup>794</sup> After optical population of the  $S_2$  state, fast motion along the rotational coordinate with a time constant of 130 fs leads to the  $S_1$  potential energy surface, which is reached with high excess energy. As can be seen from the slope of the  $S_1$  surface, the further isomerization reaction then proceeds via the inversion coordinate to the cis ground state. Here, branching takes place, where a large number of molecules make a direct movement to the CI (420 fs, isomerization quantum yield  $\phi_1$ ) and a smaller number of molecules follow a diffusive path (2.9 ps, isomerization quantum yield  $\phi_2$ , indicated by the loop). The potential energy landscape also shows the possibility of branching at the transition point between the  $S_2$  and  $S_1$  potential energy surface with a further isomerization along the rotational coordinate. The question mark indicates that the spectroscopic data do not support this particular path. Within this interpretation, rotation is only needed to reach the (single) avoided curve crossing point to the  $S_0$  manifold situated on the inversion coordinate.

Tahara and co-workers performed time-resolved Raman studies on the trans isomer.<sup>802</sup> Several transient Raman bands assigned to the  $S_1$  state and appearing immediately after photoexcitation indicated a prompt internal conversion from the  $S_2$  state. Vibrational cooling of the ground state could again be determined to occur within 16 ps by monitoring anti-Stokes bands of the  $S_0$  state. The NN stretching frequency in the  $S_1$  state was found to be very close to the corresponding one in the ground state, indicating that the double bond character is retained in the excited state and during isomerization. As a consequence, the torsion mechanism was excluded and inversion was proposed as the reaction pathway. The authors further concluded that isomerization does not occur on the  $S_2$  state or during the  $S_2$  to  $S_1$  internal conversion. Time-resolved fluorescence experiments from the same group supported these findings.<sup>803</sup> Fluorescence from the  $S_2$  state was found to have a lifetime comparable to the 230 fs IRF. The yield of  $S_2$  to  $S_1$  relaxation was determined from a comparison of  $S_2$  and  $S_1$  fluorescence quantum yields and was found to be close to unity. Therefore, the authors again excluded isomerization via rotation in the  $S_2$  state. Furthermore, they concluded that upon  $S_2$  excitation, all population relaxes first to the same region of the  $S_1$  potential energy surface as upon  $S_1$  excitation, before reaching the CI to the ground state.

Temps and co-workers studied the fluorescence from a rotation-restricted azobenzene compared to unsubstituted

azobenzene.<sup>804</sup> The kinetics of an azobenzene capped by a crown ether and a chemically similar open form were almost indistinguishable from one another. Therefore, a common isomerization mechanism was invoked, specifically inversion since rotation was blocked in the capped form. But a so-called *hula twist* reaction was mentioned to be possible as well.

Diau and co-workers studied the fluorescence anisotropy of *trans*-azobenzene and obtained results that contrasted with previous works.<sup>805</sup> They observed anisotropy decays indicating out-of-plane CNNC-torsional motion, whereas under hindrance in viscous ethylene glycol the measured anisotropy decay was consistent with an in-plane only movement. The conclusion was that torsion would be the main mechanism in low viscous solvents, whereas in high viscous environments, inversion should be the dominant one.

The common view of inversion as the main isomerization mechanism outlined here was recently reviewed by Bandara and Burdette.<sup>786</sup> Some new light, however, was shed on the isomerization mechanism of *trans*- and *cis*-azobenzene through recent work by Ernsting and co-workers.<sup>746</sup> Broadband transient electronic absorption, fluorescence and Raman spectroscopies were used and transient absorption was extended to the UV to observe the complete evolution of the  $\pi\pi^*$  band. The finding, discussed below, are summarized in Figure 71.

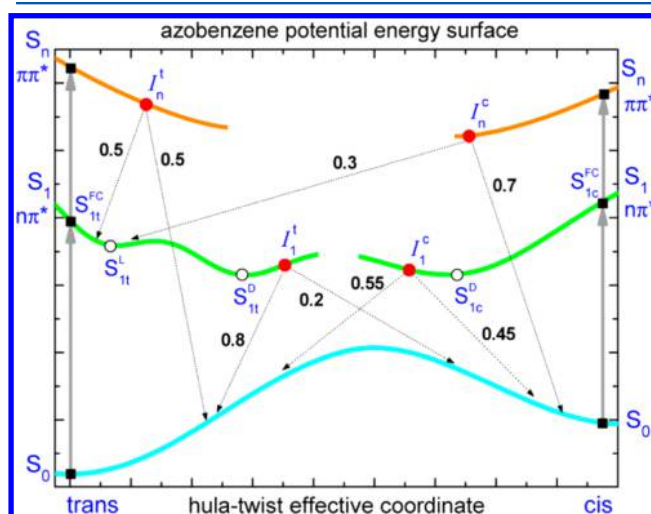


**Figure 71.** Azobenzene potential energy surface and relaxation/isomerization pathways consistent with experiment and calculations. Independence of the dynamics on solvent viscosity suggests the hula-twist isomerization coordinate. Closed squares mark wavepacket positions upon vertical  $n\pi^*$  ( $S_1$ ) or  $\pi\pi^*$  ( $S_2$ ) excitation, while open and closed circles denote stationary points and conical intersections ( $I$ ), respectively. Relaxation/isomerization via the intersections is indicated by dashed arrows marked with yields in *n*-hexane. Reprinted from ref 746. Copyright 2014 American Chemical Society.

When exciting the  $n\pi^*$  transition of the trans isomer, the tESA signal was found to decay in 0.3–0.4 ps and 2.5–3.5 ps. The bleach increased between 0.2 and 1 ps, due to the overlay of a decaying tESA contribution, and recovered within 16 ps. Upon  $n\pi^*$  excitation of the cis isomer, an early, strongly nonexponential evolution was found within the first ~0.1 ps and exponential fits were only possible after 0.3 ps. The ground-state products appeared at 0.3 ps, grew in 1.1 ps and cooled at times >4 ps. Again, a bleach recovery within 16 ps was found. Upon  $\pi\pi^*$  excitation, both isomers exhibited spectral

dynamics with isosbestic points on a 80 fs–0.2 ps time scale, which was attributed to  $S_n \rightarrow S_1$  internal conversion. The recovery of the bleach band observed in the trans-to-cis direction had an additional time constant of 1.2 ps reflecting an additional pathway. The evolution of the kinetics after 4 ps was attributed to the  $S_1 \rightarrow S_0$  internal conversion because cooling was inconsistent with the evolution of the cis spectra. After subtracting transient bleach and product spectra, the pure ESA signal showed an additional contribution at 300 nm rising with a time constant of 1 ps, while the original ESA bands decayed on the same time scale. This ESA was attributed to an intermediate “dark” state decaying in 16 ps through the  $S_1 - S_0$  conical intersection.

The interpretation in ref 746 differs substantially from previous publications by the Zinth group,<sup>795–797,806</sup> and by Tahara and co-workers,<sup>802,803</sup> who assigned the time constant of 16 ps to vibrational cooling. However, the new information obtained in the UV spectral region gave a clear indication that cooling makes only a minor contribute to the signal on that time scale. This was further confirmed by time-resolved fluorescence measurements pointing to a 12 ps contribution and supportive of a long-lived species.

By comparing absolute intensities, Ernsting and co-workers concluded that 50% of the  $S_2$  population upon  $\pi\pi^*$  excitation does not reach the  $S_1$  state at the same region as under  $n\pi^*$  excitation. This differs from the conclusions by Tahara and co-workers that all of the  $S_2$  population passes through the same  $S_1$  region as under  $n\pi^*$  excitation. However, Ernsting and co-workers pointed out that the latter conclusions critically depend on the absolute values of parameters like lifetimes, which differ by up to 30% in reports from different groups.

The short-time kinetics of the trans isomer were found to be solvent independent, whereas the long-time kinetics depended on solvent polarity/proticity but not on viscosity. From the comparison with the values obtained for stilbene it was concluded that the isomerization mechanism must be different. The various reaction pathways are depicted in Figure 71 and were described as follows. Both trans-to-cis and cis-to-trans conformations isomerize upon photoexcitation to the  $n\pi^*$  ( $S_1$ ) state through CIs to the ground-state manifold. Contrary to stilbene there is not a single branching point in azobenzene, but two independent CIs leading to different yields when starting from the cis or trans conformation, respectively. Similar to stilbene, in the cis-to-trans isomerization the CI is reached in a barrierless relaxation whereas in the trans-to-cis isomerization a thermally activated barrier of 8 kJ/mol has to be overcome. When photoexciting in the  $\pi\pi^*$  band, the dynamics become even more complex. Both cis and trans isomers enter a CI on a barrierless pathway from the Franck–Condon active region. Each of these CI provides two pathways, leading (a) to the  $S_1$  state in the trans conformation and (b) to the ground-state, but through a region on the  $S_1$  state which is not reached by  $n\pi^*$  excitation. Under steric constraints the latter pathway is shut down, leading to a full population transfer to the  $S_1$  state and relaxation to the ground state along the same pathway as under  $S_1$  excitation. Quasi-stationary intermediates were found in the transient spectra for which there were no indications on the inversion pathway in the available quantum chemical calculations. The inversion as an isomerization mechanism was therefore ruled out. Instead, the hula twist was proposed as the most probable mechanism being consistent with the experimental findings. The independence of the isomerization

dynamics on viscosity further supported the hula twist motion being the most probable isomerization mechanism.

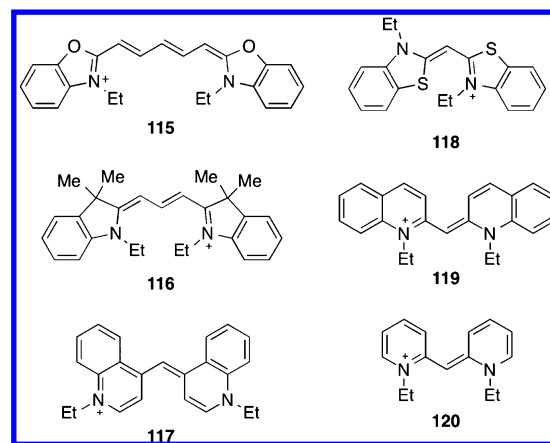
Numerous quantum chemical calculations were performed on the  $S_0$  and  $S_1$  potential energy surfaces of azobenzene and on possible reaction pathways.<sup>788,789,807–815</sup> Many of these studies considered torsional motion as the reaction coordinate,<sup>807–812</sup> though the hula-twist motion seem to be the most probable one,<sup>747,788,789,813–815</sup> with regard to the experimental findings.<sup>746</sup>

Unraveling the mechanism of the ultrafast isomerization dynamics of the retinal chromophore of the rhodopsins was an important driving force in the development of ultrafast lasers.<sup>816–819</sup> Being beyond the scope of this review, which is not focused on biological systems, it is still worth noting that this was also the first system for which a “pedal-like” isomerization under strong steric constraints, the hula-twist motion, was proposed.<sup>747,820</sup> As mentioned before, the very same mechanism was also recently proposed as the most likely one to be found in azobenzene.<sup>746</sup> On the other hand, none of the molecular systems in liquids investigated over the past few decades seem to exhibit such a highly efficient one-way reaction pathway as retinal. Even when a direct road without barriers leads straight to the CI, which guides the reaction to the product state, it still seems to be necessary to appropriately dress the shape of the excited state potential surface by means of a specially tailored environment as to obtain straightforward channelling, as it is achieved by the binding pocket of retinal in the protein environment.

**4.1.3. Cyanine Dyes.** Since the 1980s, cyanine dyes have received considerable attention by the time-resolved spectroscopy community. The work on cyanine dyes until 1999 was reviewed by Behera and co-workers.<sup>821</sup> Time-resolved studies in that period used cyanine dyes mainly to investigate thermally activated and barrierless photochemical reactions and to test corresponding theories by Kramers, by Grote and Hynes,<sup>771,772</sup> and by Bagchi, Fleming, and Oxtoby.<sup>822</sup>

Within this framework, Velsko, Waldeck, and Fleming showed that the rate constants of the ground- and excited-state isomerization of **115** correlate with solvent viscosity in linear alcohols (chart 23).<sup>823</sup> However, one-dimensional Kramers theory was not able to reproduce the experimental data when describing the friction by the overall rotation time or by solvent viscosity. A frequency-dependence of the friction, as suggested by Grote and Hynes,<sup>771,772</sup> had to be introduced to

**Chart 23.** Structures of the Cyanine Dyes Discussed in This Section



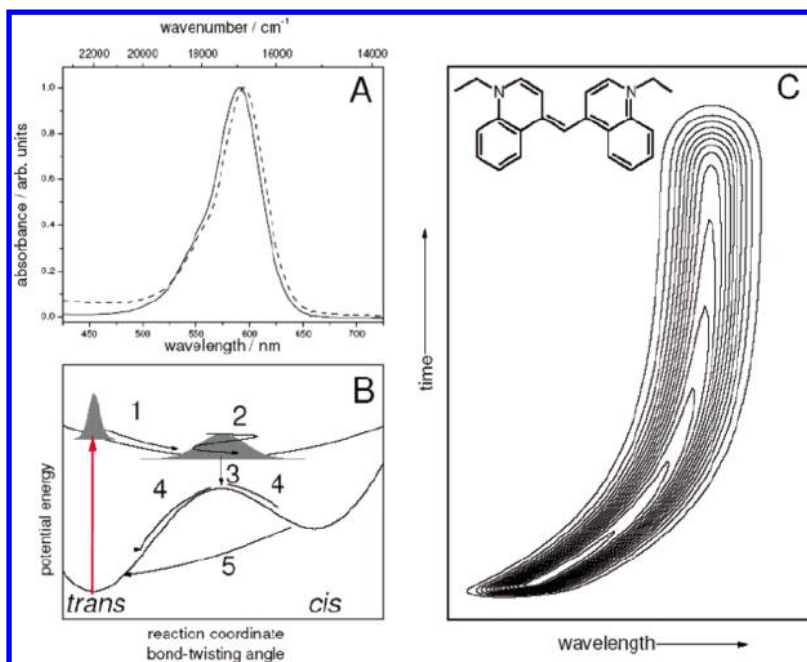


**Figure 72.** (A) Steady-state absorption spectrum of **117** in methanol. (B) Schematic one-dimensional model accounting for the photoinduced processes. (C) Schematic contour plot illustrating the temporal evolution of the emission as the system evolved on the excited-state potential. Reprinted from ref [835](#). Copyright 2007 American Chemical Society.

improve the fits. The authors concluded that more experimental data would be needed to understand the reasons for the breakdown of Kramers theory and to clarify the interplay between the frequency dependence of friction on one side and the barrier height and sharpness on the other side.

The solvent effect on the barrier crossing during photoisomerization of various cyanine dyes was studied by Sundström and co-workers,<sup>824</sup> measuring the ground-state recovery. The authors found a power law dependence of the relaxation rate on the solvent viscosity

$$k_{\text{iso}} \propto \eta^{-\alpha} \quad (58)$$

where  $\eta$  is the solvent viscosity and the parameter  $\alpha$  is used to characterize the viscosity dependence of the nonradiative relaxation rate. A good match with experimental data was found for various cyanine dyes in different solvents. Based on this viscosity dependence, the isomerization mechanism was interpreted as torsional motion of the quinolyl groups about the C–C bond in the polymethine chain. The Sundström group also investigated the solvent-dependent barrier height of the excited-state photoisomerization of **116** in *n*-alcohols and found substantial changes between different solvents.<sup>825</sup> Deviations from Kramers theory were discussed in terms of potential barrier shifts. Sundström and co-workers also compared the photoisomerization dynamics of **117** and *trans*-stilbene in *n*-alcohols as model systems for barrierless photochemical reactions.<sup>826</sup> For the latter two, an Arrhenius-type temperature dependence was found, also supported by fluorescence up-conversion measurements.<sup>827</sup> The cyanine dye on the other hand exhibited a more complex behavior, which did not fit into the framework of an Arrhenius-type temperature dependence.

Vauthey reported on the isomerization dynamics of a thiacyanin dye in the  $S_0$  and  $S_1$  electronic states in different classes of solvents and at different temperatures using transient grating spectroscopy.<sup>828</sup> None of the obtained data sets could be reproduced using Kramers theory, even when

using modified values for the friction, because the experimentally obtained isomerization rates were larger than predicted by the hydrodynamic Kramers model. Using a frequency-dependent friction as proposed by Bagchi and Oxtoby,<sup>829</sup> agreement with the Grote–Hynes model<sup>771</sup> was found.

Xu and Fleming reported on the isomerization dynamics of **117** studied by three-pulse photon-echo, transient grating and transient absorption techniques.<sup>830</sup> A multimode Brownian oscillator model based on the various Feynman diagrams associated with the different experimental techniques was used to rationalize the obtained kinetics. The transient grating signal probing the  $S_1 \leftarrow S_0$  transition showed a fast component of about 100 fs and a slower one of a few picoseconds. In the transient absorption experiment, a monoexponential ground-state recovery was observed and attributed to a bond twisting in the excited state because the rate was found to depend strongly on solvent viscosity and temperature. Furthermore, the isomerization yield was found to depend on the excess energy of the photoexcitation. The slow relaxation process of a few picoseconds on the excited-state potential energy surface was identified as the overall rate-determining process. The authors concluded that, though the three employed experimental techniques had been shown to yield the same results when monitoring solvation dynamics, they resulted in very different and apparently contradictory wavelength dependencies in the case of the isomerization dynamics studied. Despite the simplicity of the molecular system, the dynamics turned out to be sufficiently complex such that using only a single technique could have easily led to misinterpretations. As a matter of fact, the development of broadband techniques, which enable access to reliable photometric information, was only at its starting point at the time of this study. With the improvement of spectroscopic tools and computational power and methods, the research after the year 2000 could gradually shift toward a detailed monitoring and modeling of the



photoinduced population on the excited-state potential energy surface, away from pictures involving one-dimensional and sequential pathways.

Robb, Olivucci, and co-workers reported on CASSCF studies on polymethine cyanines where they found a sequential deactivation pathway. This involved first a barrierless skeletal stretch coupled with a twisting motion, followed by a decay to a TICT state which finally decayed to the photoproduct via an adjacent CI.<sup>831</sup> The findings could account for the bimodal fluorescence decays observed by Sundström and co-workers.<sup>827</sup> The realization that ultrafast internal conversion, which is often mediated by a CI, requires at least two molecular coordinates to occur, was a major development in this field.

Gerber and co-workers reported on the isomerization reaction of **118** investigated by single-wavelength and broadband transient absorption.<sup>832,833</sup> Supported on a semiquantitative level by quantum chemical calculations, a CI was invoked to account for the observed  $S_1$  to  $S_0$  internal conversion. Part of the population relaxed back within 10 ps to the initially photoexcited trans isomer, whereas the remainder deactivated to the cis isomer, which was proposed in two different configurations, labeled d-cis and cis. Both d-cis and cis underwent a sequential and thermally activated back-reaction, with d-cis decaying to cis within 600 ps and cis decaying back to the trans form in 45 ps. Biphasic kinetics as well as the computational results suggested that two competing pathways were operative on the  $S_1$  potential surface. The authors suggested that potentially two separate CIs could connect the  $S_1$  and  $S_0$  surfaces, leading to the two different cis isomer conformations. In coherent control experiments,<sup>834</sup> the isomerization yield was found to depend on the phase- and amplitude-shape of the excitation pulse.

A series of papers on time-resolved studies of cyanine dyes were published by Dietzke et al. Figure 72B schematically shows the reaction scheme deduced from the transient absorption experiments presented in refs 835 and 836. Optimization of the absolute yield of the photoisomerization of **119** could be achieved by coherent control,<sup>835,836</sup> while the relative yield did not depend on laser parameters. It seemed that the shape of the excitation pulse could be optimized such that the interplay between population transfer from the  $S_0$  to the  $S_1$  state and the onset of the moving wavepacket on the  $S_1$  potential energy surface led to a more efficient population of the  $S_1$  state. Inhibiting a higher order Rabi-like pump-dump step during excitation was proposed to be the main mechanism. Three-pulse photon-echo and transient grating experiments showed that the internal conversion rates did not follow a conventional shear viscosity dependence.<sup>837</sup> The authors suggested that the local solvent friction would have to be taken into account. The dynamics observed in transient absorption measurements on pseudocyanine were discussed in a one-dimensional picture with the torsion angle as reaction coordinate.<sup>837,838</sup> Spectral dynamics were attributed to the motion of a wavepacket created by photoexcitation on the excited-state potential well toward the sink region. The dynamics were discussed with a sequential model of three distinct processes: (i) spectral broadening of the initially created population distribution, (ii) directed and barrierless excited-state torsional motion, and (iii) Brownian torsional motion coupled to the transition back to the ground-state. A pump-shaped dump sequence was used to identify the observed nuclear motions.

Nuclear wavepacket motion in the photoisomerization of **117** in ethylene glycol was reported by Tahara and co-workers using a pump-dump-probe spectroscopy.<sup>839</sup> In this technique, the excited-state population was dumped back to the ground state through stimulated emission. The efficiency of the dumping step was then monitored by means of a third ultrashort pulse. Three time scales were found in the transients, 100 fs, 7 ps, and 17 ps. The first was ascribed to the escape of the  $S_1$  population from the initial Franck–Condon region. The second, identical to the lifetime of the  $S_1$  excited-state absorption deduced from transient absorption experiments, was ascribed to the passage through the  $S_1/S_0$  CI. The slowest time scale was attributed to vibrational cooling, though other potential contributions could not be excluded. Short rise times in the dumping efficiency were observed to depend on the wavelength of the dumping pulse. The authors interpreted this finding as the signature of a wavepacket motion on the  $S_1$  potential energy surface. The evolution of the wavepacket on the simplified upper potential surface is shown in Figure 73.

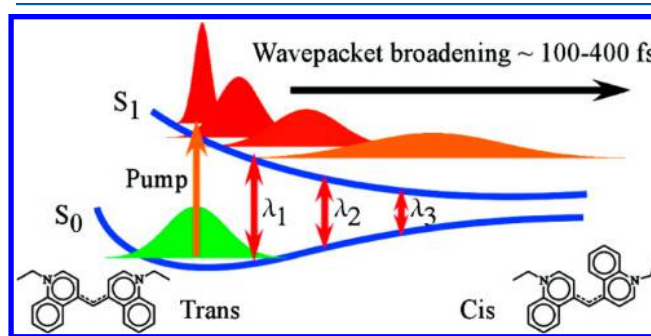


**Figure 73.** Schematic illustration of the wavepacket motion on the  $S_1$  potential during trans-cis photoisomerization of **117** deduced from pump-dump-probe experiments. Reprinted from ref 839. Copyright 2011 American Chemical Society.

Opposing slopes of the  $S_0$  and  $S_1$  surfaces when leaving the Franck–Condon region, rising on  $S_0$  and decreasing on  $S_1$  specifically, were invoked to account for the observed slowdown of the dumping efficiency when dumping further in the near-infrared. Since the potential difference decreases along the reaction coordinate when moving away from the Franck–Condon region, the Franck–Condon window for dumping shifts to the red during the evolution of the wavepacket toward the bottom of the excited-state potential well. Accordingly, as the wavepacket is probed more in the red part of the spectrum, the signal measured after the dump pulse appears later. The authors proposed that, similar to gas phase experiments, the obtained information could be used in combination with MD simulations to obtain information on the shape of the excited-state potential surface.

Solvent tuning of a CI in a merocyanine derivative was reported by Haas and co-workers.<sup>841</sup> The prediction of a lifetime shortening as a function of solvent polarity<sup>842</sup> was verified. In toluene, a lifetime of the excited state of 0.3–0.4 ps was found, whereas in the substantially more polar acetonitrile the lifetime increased to 0.9–1 ps. The effect was attributed to the dependence of the  $S_1 - S_0$  gap on the environment.

Ernsting, Santoro, and co-workers<sup>840</sup> studied the barrierless photoisomerization of the “simplest cyanine” **120** using three broadband techniques: transient electronic absorption, time-resolved fluorescence and time-resolved Raman spectroscopy.

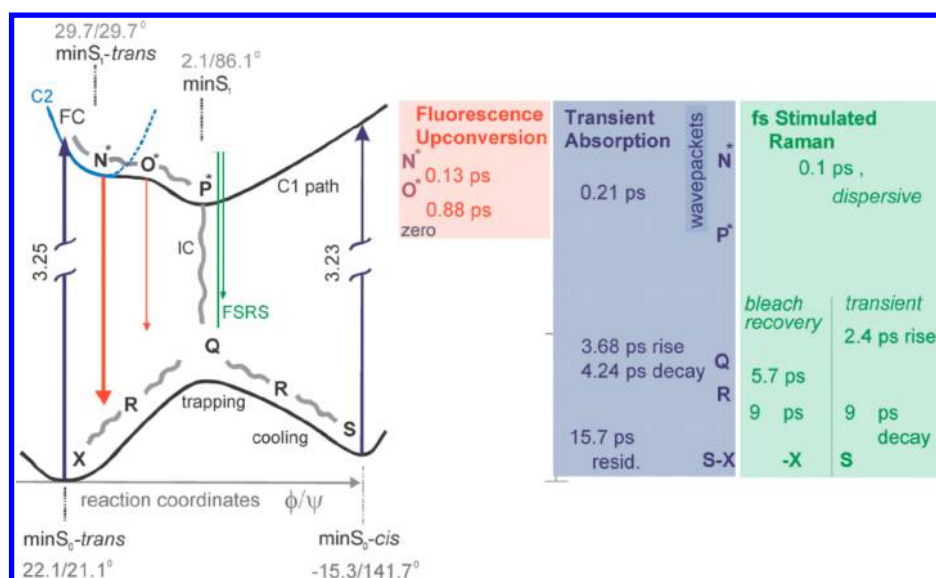


**Figure 74.** Summary of quantum-chemical calculations (left) and observations (right) on **120**. The reaction coordinate along the minimum energy pathway is to be found in the plane spanned by the two dihedral angles  $\phi$  and  $\psi$ . Reprinted with permission from ref 840. Copyright 2012 PCCP Owner Societies.

Promptly rising stimulated emission was found to decay during the first 320 fs after photoexcitation, while red shifting and broadening at the same time. Meanwhile, the ground-state bleach remained unchanged. Within 1.5 ps, the stimulated emission disappeared and the bleach started to recover on the same time scale. These observations were attributed to internal conversion to the hot ground state. The corresponding spectral signature grew to a maximum at 5 ps. Time-resolved fluorescence revealed bimodal kinetics together with a red shift. The authors attributed these dynamics to an initial emitting state decaying within 130 fs to an intermediate weakly emitting state with a lifetime of 880 fs. To obtain an isolated Raman spectrum of the excited state, the amplitude of the observed electronic ground-state bleach was used for subtracting a scaled ground-state Raman spectrum from the experimental raw data. The optimal residual was found by minimization. The initial transient Raman spectrum was found to decay within 90 fs, close to the time resolution of the experiment. The subsequent signature grew in within 5 ps and changed gradually to the “final” transient Raman spectrum at 29 ps. Using quantum-chemical calculations, the authors determined the minimum energy structures of the  $S_0$  and  $S_1$  potential energy surfaces, as well as the minimum energy path from the Franck–Condon region to the global  $S_1$  minimum. Furthermore, vibrational resonance Raman spectra were calculated for the three different isomers. A series of seven empirical states named N, O, P, Q, R, S and X (Figure 74) with virtual species-associated spectra were then used to analyze the experimental observations in a global multiexponential fashion and to map the experimental transients to regions of the minimum energy path. Figure 74 shows the reaction pathway as proposed in ref 840. The authors concluded that, even with the simplest cyanine and a large amount of high-quality spectroscopic data from three different experimental methods, it was not possible to derive a picture of the barrierless photoisomerization based on experimental observations only.

It seems worthwhile to note that though the potential energy diagram in Figure 74 differs only in the details of the shapes of the potential wells from those presented in the earlier works

there is an important change in the underlying picture. Earlier schemes commonly depict potential energy curves on a one-dimensional reaction coordinate whereas Figure 74 illustrates a reaction pathway following the minimum of a potential energy surface of higher dimensions. Of course, the former schemes are also understood to be part of the full multidimensional configuration space. However, in the early era of ultrafast spectroscopy it had not been yet established that a one-dimensional picture misses the possibility of a conical intersection being involved and disregards therefore an important, if not the most important, class of reaction and relaxation pathways involved in ultrafast isomerization reactions.

**4.1.4. Concluding Remarks.** Three decades of intensive research on ultrafast isomerization dynamics revealed that even in very small molecular systems with only a single possible reaction coordinate, like in stiff stilbene, reactions show quite complex dynamics. In only slightly more complex molecular systems the dynamics can be considerably richer, including violation of the Kasha–Vavilov rule. Influences of the fluctuating solvent environment may lead to branching into several different and competing pathways as observed in stiff and parent stilbene. The complexity of the multidimensional excited-state potential energy surfaces adds further challenges to experimental and computational studies. We are probably still at the starting point of a more detailed understanding of ultrafast isomerization, which is only likely to be achieved through identifying common patterns in systematic libraries of high quality experimental and computational data yet to be collected. The example of retinal on the other hand shows that such reactions can be channelled with very high efficiency into a single direction when a direct pathway without barriers leads straight into the CI. This is noted to be particularly efficient when the chromophore is contained within a specially tailored environment which removes all the bumps and potholes to be found on common photochemical roads.

## 4.2. Conical Intersections

Figure 75 illustrates the progress in understanding ultrafast internal conversion processes in photochemical reactions over

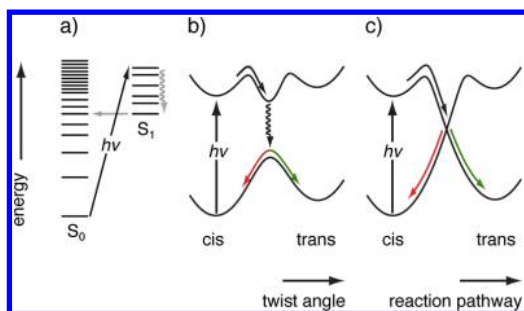


**Figure 75.** Illustration of evolution of the representation of an internal conversion (red arrow in b and c) or of a photochemical process, e.g., cis–trans isomerization (green arrow): (a) Fermi golden rule picture, (b) avoided crossing picture, and (c) current conical-intersection picture.

the past decades from a Fermi golden rule picture to CIs. Basic aspects of the theory of nonadiabatic transitions were recently reviewed by Malhado, Bearpark, and Hynes,<sup>843</sup> and by Takatsuka and co-workers.<sup>844</sup> Here, a short historical overview of the models is given as they were invoked to rationalize experimental findings in the domain of ultrafast spectroscopy. Early models of nonradiative transitions were founded on Fermi's golden rule in the context of energy level diagrams on the basis of the Born–Oppenheimer approximation.<sup>845–847</sup> These pictures are essentially zero-dimensional, in the sense that the nuclear coordinates are integrated out when determining the coupling matrix elements.<sup>848</sup> The simplest picture, which displays both the decay of the  $S_1$  state population and the population of the  $S_0$  state, is a one-dimensional two-state model with an avoided curve crossing. The first time-resolved experiments on photoisomerization were mostly interpreted with such a picture in mind. However, the predicted rates turned out to not be in agreement with experimental observations once femtosecond time resolution was achieved.<sup>741,767,777,849–851</sup> In addition, the more detailed the information the emerging experimental methods were able to provide, the more difficult it became to account for the observations with pictures based on concepts which are essentially one-dimensional.

Since then, a picture emerged which takes into account CIs, i.e., regions of the configuration space where multiple electronic states are degenerate.<sup>752,852,853</sup> When the coupling between the adiabatic states becomes large in such regions, as a consequence, the Born–Oppenheimer approximation breaks down. Emerging computational methods showed that CIs are present in many chemical systems. It is now well accepted that

CIs play a central role in photochemistry,<sup>749–755</sup> because they often provide efficient pathways for rapid nonadiabatic transitions between electronic states.

Dynamics through CIs must involve at least two dimensions because, in a single dimension, an avoided crossing would be found instead of a CI. Hence, one-dimensional schemes or schemes based on a single reaction coordinate are no longer appropriate when the observed rates are beyond predictions of the energy-gap law. Two different types of CIs can be distinguished,<sup>755,848,854–858</sup> so-called peaked and sloped CIs (Figure 76). The former exhibit a funnel-like shape and provide very fast pathways, whereas the latter resemble a potential well with a barrier to be overcome before crossing to the lower electronic manifold may occur. Sloped versus peaked CIs in *trans*- and *cis*-stilbene, respectively, could for example account for the barrier crossing observed in the *trans*-to-*cis* isomerization in stilbene and stiff stilbene, and barrierless dynamics in the *cis*-to-*trans* reaction. Both of these examples were discussed in section 4.1.

Isomerization through CIs was reviewed a decade ago by Levine and Martinez.<sup>848</sup> Using ethylene as example, they showed that an adequate description needs at least two dimensions and three electronic states. The picture shown in Figure 75c gives a brief schematic between CIs and isomerization.

It has been pointed out that the shape of the potential energy surface in the vicinity of CIs seems to be very sensitive to the electric field around the molecule.<sup>755,848,859</sup> Apparently, such a mechanism is used by nature to optimize the yield of the retinal isomerization by steering the reaction with very high speed into a single channel. Hynes and co-workers discussed peaked versus sloped CIs in the context of the influence of the solvent on the photoisomerization of the protonated Schiff base.<sup>755,857</sup> Yarkony,<sup>754</sup> Takatsuka and co-workers,<sup>844</sup> and Malhado et al.<sup>843</sup> reviewed the increasing recent efforts toward the understanding of nonadiabatic photochemical processes beyond the Born–Oppenheimer approximation.

#### 4.3. Nonreactive Processes

In pure photophysical cycles, where the final “product” state is identical to the initial “reactant” state, ultrafast nonradiative deactivation processes were observed in several classes of substances. The understanding of internal conversion has been pioneered by Englman and Jortner,<sup>90</sup> who formulated the energy gap law for relaxation between electronic states or involving the rearrangement of an electronic state in the essentially zero-dimensional framework of Fermi's golden rule. From the refined understanding of internal conversion through

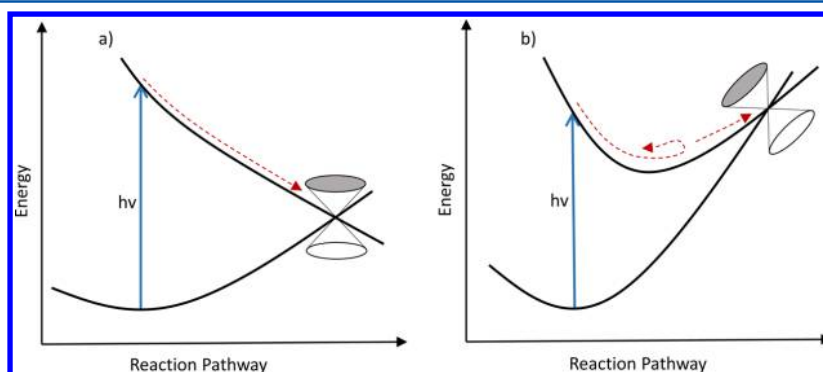


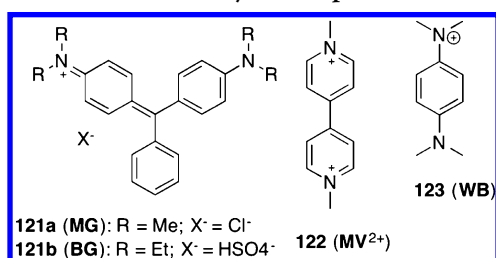
**Figure 76.** Schematic representation of peaked (a) and sloped (b) conical intersections.



CI as outlined in the previous section, it is clear that electronic relaxation processes with rates beyond those predicted by the energy gap law need to involve at least two intramolecular coordinates, like the combination of a stretch and a twist. A relaxation along a single coordinate would lead to avoided curve crossings and essentially point back to the energy gap law.

Many molecular systems have been investigated during the past decade, which exhibit nonradiative deactivation rates beyond the energy gap law.<sup>860–865</sup> Among them, open-shell ions are known for the ultrafast nonradiative decay of their excited states. Here, we concentrate on the excited-state dynamics of these radical ions and limit ourselves to a single example of a neutral molecule, namely malachite green (121a, MG; Chart 24). In most of these cases, the ultrafast

**Chart 24. Structure of Some of the Molecules Undergoing Ultrafast Nonradiative Decay after Optical Excitation**



nonradiative decay was proposed to involve substantial nuclear motion, similar to the isomerization reactions discussed in section 4.1. However, contrary to these processes, the passage through the CI is not followed by further nuclear motion toward a product, but continues with nuclear motion back to the initial ground-state geometry (Figure 75c).

In the group of substituted triphenyl methane dyes, a well-known example of ultrafast nonradiative deactivation is MG. The first time-resolved experiments by Ippen et al. revealed a ground-state recovery of MG of 2.1 ps in methanol.<sup>866</sup> The time constant of this process was found to depend on solvent viscosity. After this report, several investigations of the excited-state dynamics of MG, focusing on its viscosity and/or concentration dependence, were published.<sup>867–872</sup> Based on these results and on QC calculations,<sup>873</sup> it now generally accepted that the excited-state decay of MG and close derivatives involves large amplitude motion of the phenyl substituents around the bond to the central methane carbon toward a CI with the ground state. Once in the ground state, the molecule undergoes back-twist to the equilibrium ground-state geometry. This viscosity dependence of the excited-state lifetime of MG was subsequently used to probe friction at various interfaces.<sup>872,874–876</sup>

Open-shell radicals are generally nonfluorescent because of a very short-lived  $D_1$  state. Gummy et al. investigated the ground-state recovery dynamics of the perylene radical cation,  $\text{Pe}^+$ , as well as the radical anions of perylene and anthraquinone.<sup>877</sup> They found that, whereas the excited-state lifetime of  $\text{Pe}^+$  in a boric acid glass amounted to  $35 \pm 3$  ps, the  $D_1$  lifetime of all three radical ions in liquid was shorter than 15 ps, the IRF of the experiment. Later on, Brodard et al. found a 100 ps lifetime for  $\text{Pe}^+$  in low-temperature rigid matrices.<sup>878</sup> On the other hand, Zhao et al. found <200 fs excited-state lifetime for biphenyl and naphthalene radical cations in boric acid glass and confirmed the longer decay time of  $\text{Pe}^+$ .<sup>879</sup> In a subsequent series of three papers, Bearpark, Robb, and co-workers reported

on quantum-chemistry calculations of the excited-state dynamics of naphthalene,<sup>880</sup> pyrene,<sup>881</sup> and perylene radical cations.<sup>882</sup> For the former two cations, they found the presence of two sloped  $D_2/D_1$  and  $D_1/D_0$  CIs associated with in-plane distortion that could easily be accessed to upon  $D_{n>2} \leftarrow D_0$  excitation.<sup>880,881</sup> For  $\text{Pe}^+$ , no such planar  $D_1/D_0$  CI could be identified,<sup>882</sup> explaining the longer excited-state lifetime of this cation, compared to those of naphthalene and pyrene.

Hammarström and co-workers studied the femtosecond dynamics of the methyl viologen radical cation (122) using transient electronic absorption.<sup>883</sup> A rapid deactivation within 0.7 ps was found as well as an intermediate with a 1 ps lifetime. A signal decaying on a 16 ps time scale was attributed to a contribution from the hot ground state. The authors explained these dynamics using a model with a branching from lowest vibrational level of the  $D_1$  state toward the two intermediate states, one of them being identified as the vibrationally hot ground state. The spectrum of the first intermediate could not be assigned due to its broad and unstructured nature, though it was obvious that it belongs to the ground-state manifold since it is populated upon leaving the lowest level of the  $D_1$  state. In comparison with signatures of hot ground-state populations to be found elsewhere,<sup>440</sup> the isolated signature of a ground-state vibration in a transient electronic absorption spectrum found here seems to be rather unique.

The ultrafast internal conversion of two fullerenes ( $\text{C}_{60}$ ), specifically mono- and dianions, in solution was studied by Meech and co-workers.<sup>884</sup> The ground-state recovery kinetics showed a 3.5 ps exponential decay of the bleach signal to a long-lived plateau in the monoanion and a dominant 400 fs recovery in the dianion. By comparison with gas-phase experiments, it was concluded that mainly intramolecular processes are responsible for this ultrafast internal conversion. The plateau was attributed to a long-lived bottleneck state, the latter due to its population on a few picosecond time scale. Low-lying vibronic states of the Jahn–Teller ground-state manifold were proposed or a photoinduced process in the excited state like an electron detachment as possible candidate for the ultrafast nonradiative decay.

The excited-state dynamics of Wurster's blue (123, WB) were studied by Grilj et al. using combination of fluorescence up-conversion, transient electronic absorption and quantum-chemical calculations.<sup>65</sup> The emission yield upon  $D_1 \leftarrow D_0$  excitation was found to strongly depend on temperature. The  $D_1 \rightarrow D_0$  fluorescence quantum yield increased from <10<sup>−5</sup> (the detection limit) at room temperature to 0.02 at 82 K. Over the same temperature range, the fluorescence lifetime changed from 210 fs to 650 ps. Transient electronic absorption measurements showed that the ultrafast decay of the  $D_1$  state lead directly to the vibrationally hot  $D_0$  state. Interestingly, these dynamics were found to be essentially independent of the solvent. These results could be rationalized with the help of quantum-chemical calculations that identified a  $D_1/D_0$  CI, separated from the Franck–Condon active region by a shallow barrier, associated with the torsion a dimethylamino group (Figure 77). This investigation was later extended to Wurster's salts with other N substitutions.<sup>885</sup> All the cations in this study were found to have a ~ 200 fs excited-state lifetime at room temperature and to light up below 120 K, with the exception of one with bulky isopropyl nitrogen substituents, which did not exhibit any detectable fluorescence even at 12 K. The authors suggested that, whereas the twist motion of an amino group could explain the ultrafast decay of the Wurster's salts with

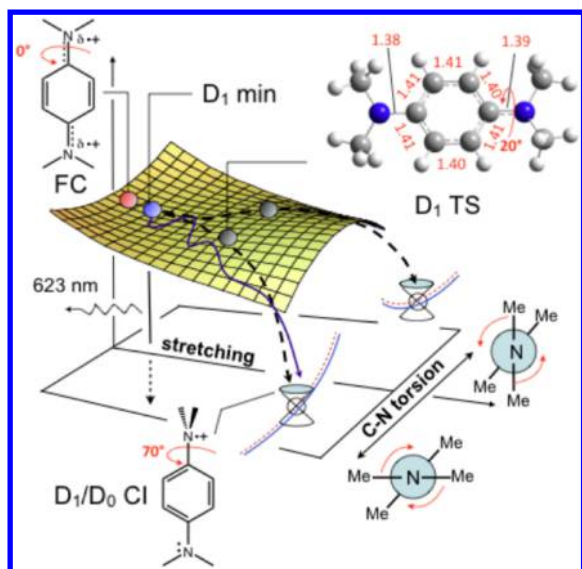


**Figure 77.**  $D_1$  potential energy surface of **WB** in methanol along the two coordinates responsible for the ultrafast nonradiative decay. The two paths from  $D_1$  toward  $D_1/D_0$  CIs are represented with dashed lines. Reprinted with permission from ref 65. Copyright 2011 Wiley-VCH Verlag GmbH & Co.

small substituents, another CI involving other coordinates, like pyramidalization, should be responsible for the nonradiative decay of the Wurster's cation containing bulky substituents.

Ultrafast internal conversion via CIs can generally be anticipated to occur with flexible molecules, especially those for which the excited-state equilibrium geometry differs largely from that of the ground state. The prevalence of CIs for the radical ions of rigid molecules such as naphthalene or perylene may be surprising at first glance. However, these molecules become much more “floppy” upon ionization and subsequent  $\pi\pi^*$  excitation. This, together with their generally high density of electronic excited states and their relatively small  $D_1$ - $D_0$  gap, explains why their photophysics are apparently dominated by CIs.

#### 4.4. Photochromic Systems Undergoing Bond-Rupture

Photochromic systems undergoing bond-breaking/making (Figure 78), either via electrocyclic reactions (diarylethenes, fulgides) or simple bond rearrangement (spiro-compounds/chromenes), are currently receiving a lot of attention as molecular and biomolecular switches for numerous applications ranging from photocontrolled switching of enzyme activity, optical data storage to the modulation of energy and electron transfer processes.

On the other hand, from a fundamental point of view, they constitute excellent prototypic systems for studying the impact of the nature of the relevant electronic states and the chemical structure (or the dynamics) of the molecular environment on the ensuing ultrafast dynamics. This then also enables a study of their influence on parameters as diverse as photostability or product quantum yields. In particular, many of the studied systems have at least one CIs. The topology around these, which determines the fate of the excited state species, shows distinct temperature and solvent dependent dynamics and may even exhibit pronounced excitation wavelength effects. In many cases the excited state lifetimes are so short that hot ground-state features and vibrational cooling dynamics, as well as

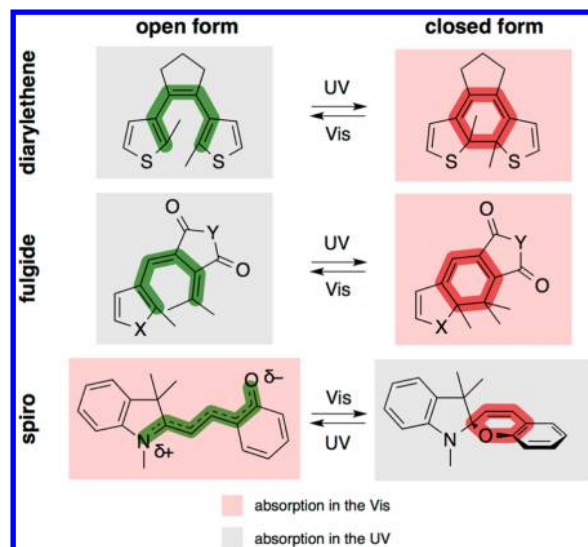


**Figure 78.** Open and closed-ring forms of the three classes of substance discussed.

subsequent product isomerization reactions in the ground state, are commonly observed.

Here we will discuss the ultrafast dynamics of the most prominent photochromic species but restrict ourselves to studies performed after the review by Tamai and Miyasaka.<sup>886</sup> One of the most simple imaginable systems that undergoes a ring opening/closing reaction is 1,3-cyclohexadiene/1,3,5-hexatriene. However, its dynamics were recently exhaustively reviewed by Weber and Das<sup>887</sup> as well as Arruda and Sension.<sup>888</sup>

**4.4.1. Diarylethenes.** Diarylethenes (DAEs) can be viewed as stilbene derivatives, with the phenyl rings of stilbene replaced by five- (or higher) membered heterocyclic rings, such as thiophene, furan or benzothiophene rings, which possess low aromatic stabilization energy. While their exceptional properties and versatile use as technologically relevant photochromic molecules have been extensively reviewed by Irie and co-workers,<sup>889,890</sup> their thermal stability, the spectral differences between their open- and closed-ring isomers, as well as the large number of coloration/decoloration cycles they can undergo have made them ideal candidates for mechanistic investigations using ultrafast optical spectroscopy.

The photochromism of DAEs is based on the pericyclic ring-opening and ring-closure reaction between the central 1,3,5-hexatriene and 1,3-cyclohexadiene moieties<sup>891</sup> according to the Woodward–Hoffmann rules<sup>892</sup> (Figure 79). It allows for a vast variation of color changes by structural modification of the heterocyclic rings.<sup>890</sup>

The ultrafast excited-state dynamics of DAEs were studied extensively in the liquid phase,<sup>893–924</sup> as well as in the solid phase to a lesser extent,<sup>895,925–929</sup> and were extensively reviewed in the recent literature.<sup>886,888,890</sup>

Despite the various possible chemical modifications, both on the central double bond bearing cyclopentene and on the heteroaromatic rings, there are common features to all of the diarylethene molecules studied so far by ultrafast techniques, which are tentatively summarized in the potential energy diagram shown in Figure 80 and the absorption spectra in Figure 79: (i) The closed-ring isomer (C) has a pronounced absorption band in the visible region, which is well separated from the absorption spectra of the open-ring isomers (O),

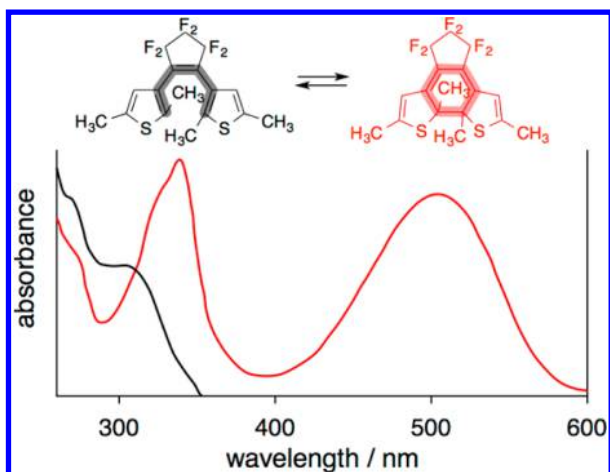


**Figure 79.** Chemical structures of the open- (black) and closed-ring isomers of **125b** and corresponding absorption spectra. Adapted from ref 890. Copyright 2014 American Chemical Society.

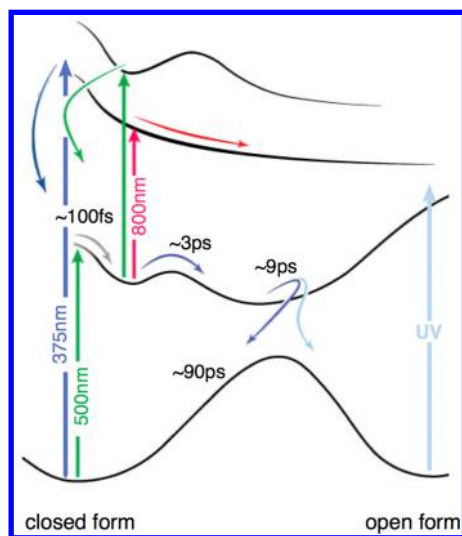


**Figure 80.** Tentative potential energy scheme for the ring opening/closing reaction of DAEs. The pump–pump–probe pathways and the corresponding tentative excited state potentials are also given. The times are indicative for **124b** and taken from ref. <sup>917</sup> Adapted from ref 920. Copyright 2014 American Chemical Society.

which absorb at higher energies. (ii) The open-ring form exists as parallel (P-form) and antiparallel (AP-form) conformers, with only the AP-form being able to undergo the ring-closing reaction (see e.g. scheme 16 in ref 889 for the geometry of the two forms). (iii) The ring-closure reaction proceeds in an activationless manner whereas (iv) the ring-opening process is an activated process. Chart 25 gives an overview of the open-form structures of the relevant samples discussed in this subchapter.

**4.4.1.1. Thiophene-Substituted DAEs (124–125).** **4.4.1.1.1. Cyclization.** In a series of papers, Ern et al. investigated the cyclization (and reversion, vide infra) dynamics of **125c**,<sup>898</sup> a dianthryl derivative<sup>899</sup> (**ant-125a**) and a dibenzoyl-phenyl-ethynyl (**bpe-125a**) derivative<sup>902</sup> of **125a** using fs transient electronic absorption. For all three samples a mixture of reactive AP and unreactive P-form open conformers was excited. After excitation both types of conformers underwent fast electronic-conformational relaxation within approximately 1 ps. Subsequently the unreactive conformer showed

fluorescence with a lifetime distribution of 100 to 400 ps.<sup>899</sup> The reactive AP-form conformer, on the other hand, relaxed to a precursor state, the lifetime of which was strongly dependent on the energy of the  $S_1$  state of the open isomer. This lifetime increased from 2 to 6 and to 10 ps for  $S_1$  energies decreasing from 4.1 to 3.5 and to 3.2 eV for **125c**, **bpe-125a**, and **ant-125a**, respectively. Calculations based on the collective electronic oscillator approach<sup>930,931</sup> pointed toward a rather flat energy surface along the reaction coordinate (the carbon–carbon distance between the methyl-group-bearing carbon atoms of the two thienyl groups) up to a distance of approximately 3 Å. The slope of the energy surface at closer distances, i.e., the region of the conical intersection between  $S_1$  and  $S_0$ , becomes steeper the larger the excitation energy of the molecule. Thus, the cyclization reaction was found to be essentially downhill and barrierless.<sup>902</sup>

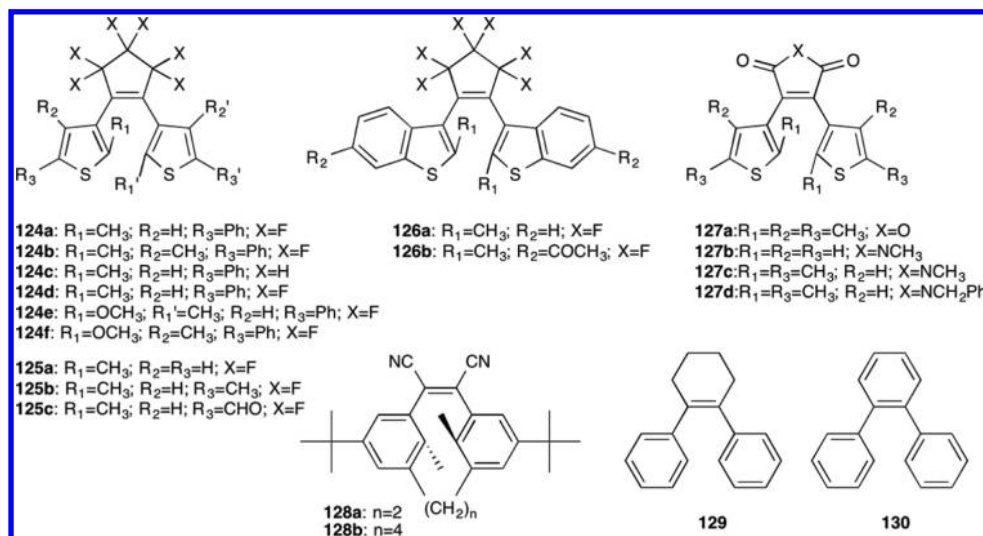
In support with a barrierless process, Bertarelli and co-workers observed an ultrafast cyclization of a polymer of **125a** in chloroform on a sub-200 fs time scale using broadband transient electronic absorption.<sup>901</sup>

Okabe et al. used picosecond time-resolved Stokes Raman spectroscopy with a time resolution of 4 ps to study the cyclization of **125b** in 1-butanol and ethylene glycol.<sup>907</sup> The cyclization, which was monitored by following the time evolution of two Raman bands at 1551 and 1592  $\text{cm}^{-1}$  (ascribed to the closed form in the electronic ground state), was found to occur in 4 ps and to be followed by vibrational cooling with a 10 ps time constant. The viscosity independence of the cyclization pointed to a barrierless or only slightly activated reaction. Time-resolved fluorescence experiments yielded a distribution of sub-ns to ns lifetimes, which were attributed to the emission of the unreactive parallel open-form conformer.

Hania et al. investigated the ring-closing reaction of **124a** and **124c** in cyclohexane at room-temperature using polarization selective broadband transient electronic absorption with a 90–110 fs time resolution.<sup>903,910</sup> For both molecules, which only differed in the substituents of the central double-bond bearing five-membered ring, the ring closing dynamics could be subdivided into three steps, namely preswitching, ring-closing and postswitching dynamics. In the preswitching step, the Franck–Condon excited state rapidly mixes with nearby dark states, leading to excited state relaxation to a partially ring-closed state on the 50 (**124a**) to 70 fs (**124c**) time scale. In the ring-closing step, population transfer to the hot ground state of the closed form takes place on the 0.9 (**124a**) to 4 ps (**124c**) time scale. Finally, in the postswitching step, the hot ground state relaxes to thermal equilibrium during the first 100 ps, thus completing the switching process. The open conformers which were unable to undergo cyclization experienced preswitching dynamics, which were then followed by population relaxation to the ground state of the open form. Comparing the two compounds Hania et al. concluded that, while the fluorinated switch **124a** was better, i.e., faster and more efficient than the nonfluorinated switch **124c**, the latter provided a much clearer experimental picture of the involved mechanisms.

Almost ten years later, Elles, Scopigno, and co-workers investigated the cyclization dynamics of **124b** using fs broadband transient electronic absorption and fs stimulated resonance Raman in cyclohexane at room temperature.<sup>919</sup> The higher structural selectivity offered by transient vibrational over transient electronic spectroscopy allowed them to gain further insight into the structural evolution after UV excitation. By



Chart 25. Most Prominent DAE Structures Investigated by Ultrafast Spectroscopy<sup>a</sup>

<sup>a</sup>If the primed and unprimed substituents are identical only the unprimed one is explicitly given.

tuning the Raman pump wavelength to the corresponding resonances, the authors could selectively monitor the resonance enhanced Raman signal of the nonreactive open form and of the closed product form. The electronic spectra, on the one hand, allowed the assignment of a complete electrocyclization within a few hundred fs, very much in line with the findings by Hania et al.,<sup>910</sup> while the nonreactive open-ring conformer underwent intersystem crossing with a 23 ps time constant. The temporal evolution of the high frequency C=C stretch mode of the central ethylenic bond (at 1503 cm<sup>-1</sup>), on the other hand, which is very sensitive to the degree of conjugation along the backbone of the molecule and thus to cyclization, did not reach the equilibrium ground state of the closed-ring product for several tens of ps. The two complementary techniques thus allow disentangling the sub-picosecond electronic dynamics from the accompanying much slower structural rearrangement, which extended up to 100 ps.

**4.4.1.1.2. Cycloreversion.** In parallel to the above-mentioned cyclization, Ern et al. also studied the cycloreversion reaction of **125c**, **ant-125a**, and **bpe-125a**.<sup>897,899,902</sup> The combination of the collective electronic oscillator approach, semiempirical calculations and femtosecond transient electronic absorption allowed for a clear picture of the cycloreversion reaction. Immediately after excitation, the systems underwent structural relaxation in 0.3–1 ps, evolving along the potential energy surface toward a minimum, itself separated from the CI responsible for the cyclization/cycloreversion process by an energy barrier. The decay of the excited-state population in this potential energy minimum occurs via efficient radiationless deactivation in approximately 10 ps and rather inefficient cycloreversion with time constants of 325 ps for **125c** and ca. 100 ps for **ant-125a**. For **bpe-125a** variations in the cycloreversion yield by a factor of 6 were found, depending on the different closed-ring isomers of the benzoyl-phenyl-ethynyl substituents.

Okabe et al. used picosecond time-resolved anti-Stokes Raman spectroscopy with a 4 ps time resolution to study the cycloreversion reaction of 1,2-bis(3,4-dimethyl-5-phenyl-2-thienyl)perfluorocyclopentene in acetonitrile.<sup>907</sup> The vibrationally excited S<sub>0</sub> state of the open-form was populated within the time-resolution of the experiment and decayed within 16 ps. In

addition, the authors concluded that the excess energy generated by the cycloreversion reaction was mainly localized on the C=C stretching mode of the cyclopentene moiety (at 1599 cm<sup>-1</sup>) rendering it the main promoting mode of the reaction.

Mathies and co-workers investigated the cycloreversion of **124b** in cyclohexane using 2D FSRs.<sup>922</sup> By monitoring the time evolution of 21 excited-state Raman modes, the following steps could be resolved: (i) nuclear relaxation out of the Franck–Condon region within 0.5 ps, (ii) passage through the transition state region with a 3 ps time constant, and (iii) evolution of the system toward the CI between S<sub>1</sub> and S<sub>0</sub> with ca. 6 ps time constant. Moreover, careful examination of the oscillations of the excited-state Raman peak frequencies and amplitudes and analysis of the correlations between different vibrational mode properties allowed the authors to sort the modes into reactive and unreactive ones. They could demonstrate that, whereas the 191 cm<sup>-1</sup> methyl wag plays an important role in the initial stages of the cycloreversion, the strong anharmonic coupling between this mode and the 467 cm<sup>-1</sup> C–C bend, as well as the 1333 cm<sup>-1</sup> C–C stretch is critically involved in the crossing of the transition state region. Similarly, the authors could also identify the unreactive modes responsible for the low overall quantum yield of the cycloreversion reaction.

Several groups found that the yield of the cycloreversion of diarylethenes is significantly enhanced upon multiphoton excitation, making it an interesting reaction from the technological (multiphoton gating)<sup>890</sup> as well as the mechanistic points of view.<sup>900,909,917,920,932</sup>

Irie, Miyasaka, and co-workers used 100 fs and 15 ps pulses in the visible to investigate the effect of multiphoton excitation on the cycloreversion reaction of **124a**<sup>900,909,932</sup> and **124d-f**<sup>933</sup> in *n*-hexane as a function of the laser excitation intensity, wavelength and pulse duration. For the fs-experiments, the conversion yields were as low as under continuous illumination (1–2%) and independent of the excitation intensity. However, the ps-experiments resulted in yields of up to 40–70%, strongly dependent on the excitation intensity (Figure 81a).<sup>900</sup> Both, femto- and picosecond experiments gave a ground-state recovery time of 0.7–10 ps.<sup>909,933</sup> The authors were able to

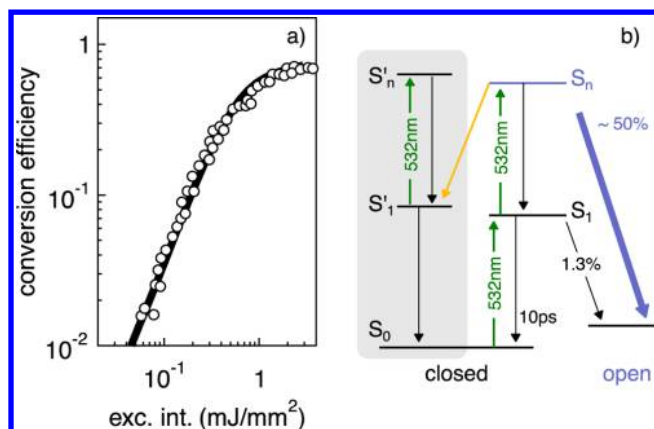


**Figure 81.** (a) Excitation-intensity dependence of the ring-opening efficiency of **124d** in *n*-hexane using 15 ps, 532 nm laser pulses. The solid line is calculated using the reaction scheme in (b). Adapted from ref 909. Copyright 2004 American Chemical Society.

rationalize all their results using a reaction scheme (Figure 81b) in which the leading photons of the ps pulse promoted the molecule to the lowest electronically excited state, from where it is re-excited from the trailing photons to a higher electronic state with a more favorable cycloreversion yield. The absence of an enhancement with fs pulses substantiated the sequential nature of the two-photon process. Additional one-photon absorption experiments using a ns pulse at 266 nm, where effective multiphoton processes are negligible, recovered the results of the steady-state and femtosecond experiments, providing further evidence that it is the nature of the excited electronic state that is of crucial importance rather than the energy of the incident light.<sup>909</sup> One-photon pumping in the UV did however significantly enhance the cycloreversion for a left-right asymmetric derivative of **124a** (1-(2-methyl-3-benzothieryl)-2-(2,4-dimethyl-5-phenyl-3-thienyl)-perfluorocyclopentene). This led the authors to conclude that the selectivity of the cycloreversion reaction can be attributed to the population of a specific electronically excited state, which is optically forbidden for **124a** and more allowed for its asymmetric derivative.<sup>932</sup>

Ward et al. gained significant insight into the excited-state topology of **124b** using fs electronic pump-probe and one- and two-color<sup>920</sup> pump-repump-probe spectroscopy. They found that the initially excited molecule first had to cross an activation barrier on a time scale of ca. 3 ps before the secondary pump (at 500 nm) could indeed enhance the reaction yield (with an optimal time-delay of 5 ps), while re-excitation before crossing the S<sub>1</sub> barrier had no impact on the cycloreversion yield. These observations imply a large change of the topology of the higher excited state as the molecule moves along the reaction path (Figure 80).<sup>917</sup> The decrease of the optimal time-delay between pump and repump pulses for cycloreversion enhancement from 5 ps down to 100 fs upon using a repump pulse at 800 nm instead of 500 nm suggested a strong sensitivity of the higher excited state(s) to the initial motion away from the Franck-Condon region of the S<sub>1</sub> state.<sup>920</sup>

**4.4.1.2. Benzothiophene-Substituted DAEs (126).** **4.4.1.2.1. Cyclization.** Shim et al. investigated the cyclization of **126a–b** in chloroform using steady-state as well as fs and ps time-resolved fluorescence spectroscopy in combination with quantum chemical calculations.<sup>911</sup> Both samples showed

biphasic fluorescence decays with 1 and 100 ps lifetimes. As the unreactive P conformer was assumed to not significantly contribute to the time-resolved emission spectra, given its low radiative rate constant, the biphasic emission decay was interpreted as originating from at least two different conformations of the reactive AP-form conformer. While one subpopulation undergoes fast direct cyclization, probably through a CI, the other subpopulation undergoes activated cyclization driven by solvation-controlled conformational reorganization. The cyclization for **126a** occurred mostly via the “slow conformation”, while the fast channel played a more pivotal role in the cyclization dynamics of **126b**.

Irie, Miyasaka, and co-workers dedicated a series of three papers to the viscosity,<sup>915</sup> temperature<sup>916</sup> and solvent polarity dependence<sup>923</sup> of the photochromism of **126a**. To this end, they employed transient electronic absorption spectroscopy with approximately 80–100 fs time resolution in combination with reaction quantum yield measurements. Excitation of the mixture of reactive and unreactive conformers resulted in biphasic dynamics with lifetimes in the 0.4–1.5 ps and 130–200 ps ranges. The short component, attributed to the ultrafast cyclization of the reactive conformer, was found to be completely independent of solvent viscosity over more than 1 order of magnitude<sup>915</sup> and almost independent, i.e., without a clear observable correlation, of solvent polarity.<sup>923</sup> In addition, the cyclization reaction yield was found to be independent of temperature over a range of almost 100 K.<sup>916</sup> Contrary to the interpretation by Shim et al. the second, ca. 150 ps long, component was attributed to the dynamics of the AP conformer undergoing intersystem crossing to the triplet state without any cyclization.<sup>915</sup> These experimental findings led the authors to conclude that the fate of the reactive AP conformer, such as the cyclization or deactivation back to the open-ring isomer was entirely determined by the CI, which can be reached without a barrier.

**4.4.1.2.2. Cycloreversion.** Shim et al. also studied the cycloreversion reaction of **126a** in *n*-hexane using femtosecond time-resolved fluorescence and transient absorption measurements.<sup>908</sup> Both types of experiments showed a biphasic decay of the photoexcited closed-form conformer with 4 and 22 ps, as well as oscillations of the signal intensity due to a vibrational wavepacket at 66 cm<sup>−1</sup>. The short component could not be unequivocally ascribed to any process, and the 22 ps component was suggested to reflect the time scale of the wavepacket dynamics along the S<sub>1</sub> potential energy surface. From the insensitivity of the emission decay on the pump wavelength together with the observed wavepacket motion, the authors concluded that the energy barrier for the cycloreversion was reasonably high and that the ring-opening reaction proceeded essentially via nonadiabatic curve crossing of the initially prepared state and the open-form ground state.

In analogy to the studies on the multiphoton gated cycloreversion of the structurally similar **124a**,<sup>900,909,932</sup> Miyasaka et al. performed fs and ps experiments on the cycloreversion of **126a**.<sup>906</sup> In agreement with the findings for **124a**, they observed an enhancement of the cycloreversion of more than a factor of 50 upon ps excitation when compared to fs or steady-state experiments. This was qualitatively rationalized with an analogous reaction scheme as for **124a**.

In addition to the cyclization of **126a**, Irie, Miyasaka and co-workers also studied the temperature<sup>916</sup> and solvent polarity dependence<sup>923</sup> of the cycloreversion of **126a**. In clear contrast to the cyclization, which was almost independent of both

parameters, the cycloreversion showed clear temperature and solvent polarity dependence. Upon increasing temperature, the cycloreversion yield increased at the same time as the excited closed-ring lifetime decreased. From a classical kinetic analysis of their combined reaction yield and time-resolved results, the authors concluded that the potential energy surface of the  $S_1$  state could be viewed as adiabatic with both reactions (cyclization and cycloreversion) proceeding through a common CI. The pronounced temperature dependence of the cycloreversion yield was attributed to the competition of the different temperature dependencies of the reaction over the activation barrier leading to the CI,  $k_{CI}$ , with a nonradiative deactivation process recovering the closed-ring conformer,  $k_n$  (see Figure 82).<sup>916</sup> On the other hand, the cycloreversion yield

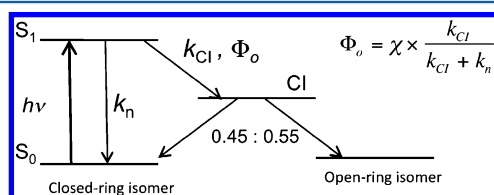


**Figure 82.** Reaction scheme for the cycloreversion of **126a**. Reprinted from ref 916. Copyright 2012 American Chemical Society.

decreased with an increase in solvent polarity. By applying the same kinetic scheme as before, the authors concluded that both  $k_{CI}$  and  $k_n$  increased with increasing solvent polarity, the latter being more effective than the former. In addition, the excited state transient absorption time-profile of the excited closed-ring form exhibited strong oscillations corresponding to a  $62\text{ cm}^{-1}$  vibrational wavepacket in both polar and apolar solvents, with the former exhibiting an additional large shift to higher energies within a few 100 fs. This was interpreted as simultaneous structural rearrangement and solvent relaxation from the Franck–Condon to the equilibrium state.<sup>923</sup>

#### 4.4.1.3. Maleic Anhydride Containing DAEs (**127**).

Miyasaka, Irie and co-workers employed ps transient electronic absorption and time-resolved emission spectroscopy to investigate the effect of solvent viscosity on the cyclization and cycloreversion reaction of **127a** in a series of long chain aliphatic solvents.<sup>904</sup> Immediately after excitation of the open-ring form, the reactive AP form could either directly undergo fast and viscosity independent cyclization within the 15 ps time-resolution of the setup, or it could relax into a CT type state. Cyclization occurred from this relaxed and fluorescing state on the time scale of several 100 ps with a moderate viscosity dependence. For the cycloreversion reaction on the other hand, which proceeded on the time scale of a few ps, only a very weak viscosity dependence of the yield was found. The authors concluded from this that the process is controlled by the fast inertial solvent motion in the first solvation shell, rather than by the slower diffusive friction.

Zinth and co-workers applied actinometry and fs transient electronic absorption to investigate the cyclization reaction of a series of bis(thiophen-3-yl)maleimides, **127b–d**, in acetonitrile.<sup>912</sup> Almost no cyclization was observed for the sterically unhindered **127b** and the entire excited-state population was found to mostly decay via internal conversion on the ns time scale. Like most other DAEs, two open-form conformers coexist in the ground state for the sterically stronger interacting samples **127c** and **d**, with only the AP-form capable of undergoing cyclization in 16 ps. The unreactive P-form decayed

to the ground state of the open form on the ns time scale. The comparison of **127b** with **c** and **d** pointed to the steric interactions, present in **c** and **d**, as a necessary requirement for sampling a large conformational space in the excited state and thus enabling ring closure.

**4.4.1.4. Other DAEs.** Aloïse et al. investigated the effect of solvent polarity, excitation wavelength and chemical structure on the photocyclization of two bridged metacyclophan-1-enes using fs transient electronic absorption spectroscopy and quantum-chemistry calculations.<sup>914</sup> Excitation of **128a** into its  $S_1$  state yielded the hot ring-closed ground state product almost quantitatively within 120 fs. Higher excitation energies, on the other hand, resulted in the population of the hot  $S_1$  state, whose dynamics were found to occur along two distinct pathways toward ring-closure. One was identical to that found upon lower excitation energy, and the second was found to depend on solvent polarity and to be slower by more than 1 order of magnitude. While the first reaction pathway was ascribed to a nonadiabatic transition to the  $S_1$  state of the closed form and subsequent internal conversion, the second pathway was suggested to take place adiabatically through a conical intersection with some CT character and, hence, the solvent polarity dependence. For **128b**, with a significantly enlarged distance between the two reactive carbons, only the less efficient adiabatic pathway, with 10–20 ps dynamics, was found.

Buckup et al. reported on the cycloreversion reaction of a series of diarylethene-based photoswitchable deoxyuridine nucleosides bearing different substituents on the thiophene moiety.<sup>921</sup> Employing sub-20 fs pulses for pumping the closed photoswitch at 500 nm, the authors observed multiphasic excited-state deactivation in less than 500 fs, which, in line with findings for the structurally similar **124b**,<sup>920</sup> were interpreted as passing over a shallow barrier before reaching the open-isomer conical intersection. The observed coherent oscillations with a frequency of  $140\text{ cm}^{-1}$ , which appeared on the excited-state absorption dynamics were assigned to ring deformation vibrations and were considered as indication for a ballistic motion on the excited-state surface. Moreover, the product branching and yields were governed by subtle topological details at the  $S_1/S_0$  CI.

Bragg and co-workers investigated the photocyclization of *o*-terphenyl<sup>918,934</sup> (**130**) in various solvents and of 1,2-diphenylcyclohexene<sup>934</sup> (**129**) in tetrahydrofuran using fs transient electronic absorption. From the comparison of the ultrafast dynamics of **130**, with significant structural constraint on the central C=C bond bridging the phenyl rings, with that of the unconstrained **129**, the authors found that cyclization of **130** was significantly slower than that of **129** which occurred in less than 1 ps. They thus evidenced the importance of the twisting motion around this central C=C bond for cyclization.<sup>934</sup> A more systematic investigation on the solvent dependence of the cyclization dynamics of **130** revealed (see Figure 83), that the fast structural relaxation dynamics in the excited-state, with time constants of 1.6 and 4.2 ps in hexane and dioxane, was followed by vibrational relaxation of the ground state of the ring-closed product on the tens of ps time scale and thermal cycloreversion within tens of ns. Surprisingly the authors found a better correlation of the excited-state relaxation dynamics with the solvent density than with viscosity. This slowdown with increasing solvent density suggested that solute–solvent collisions play the most prominent role in the



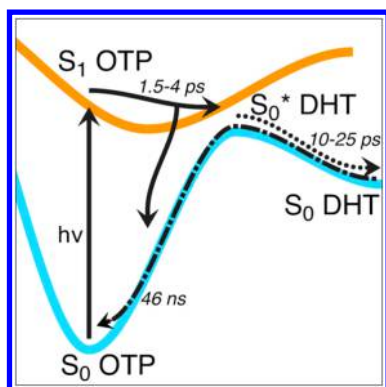


**Figure 83.** Proposed qualitative picture of the relaxation pathways of 130 upon UV excitation. Reprinted from ref 918. Copyright 2012 American Chemical Society.

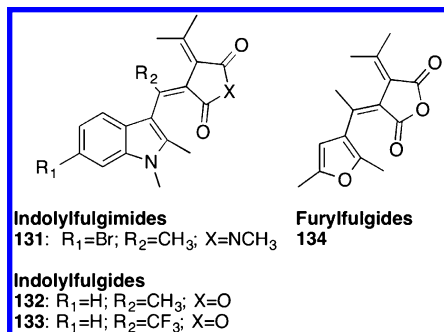
deactivation of the wavepacket initially launched on the excited-state potential energy surface.<sup>918</sup>

**4.4.2. Fulgides/Fulgimides.** Fulgides and fulgimides constitute another important class of photochromic molecules, whose photochromism is again based on the pericyclic cyclization and cycloreversion between the central 1,3,5-hexatriene and the 1,3-cyclohexadiene. These thermally stable and irreversible photochromic compounds show good photostability over many illumination cycles.<sup>935</sup> This made them serve as paradigm molecules for optical switching and data storage applications.<sup>936,937</sup> In addition, they found relatively widespread use in such diverse areas as switches of enzymatic activity<sup>938,939</sup> or as photoinduced modulators of electron and electronic energy transfer.<sup>940</sup>

In analogy to the DAEs, we focus on works after the review by Tamai and Miyasaka.<sup>886</sup> In addition, we do not address the ultrafast dynamics of furylfulgides, as this topic was well covered by a recent review by Renth et al.<sup>941</sup>

Again, it is useful to point out the similarities of all studied systems (see Chart 26 for the structures): (i) the photochromic

**Chart 26. Most Prominent Fulgide/Fulgimide Compounds Investigated by Ultrafast Spectroscopy**



system consists of two colorless open forms and one colored photocycled form (C-form). Only one of the open forms (usually referred to as E-form) can undergo ring-closing, while the other (called the Z-form) can merely isomerize to the E-form upon photoexcitation (Figure 84). (ii) The ring-closure proceeds in a usually ultrafast manner and is essentially activationless.<sup>942–950</sup> (iii) Cycloreversion<sup>932,942–944,946,951–957</sup> is an activated process, which shows a strong solvent polarity,<sup>943,947,954</sup> temperature,<sup>947,953,954,958</sup> and excitation wavelength dependence.<sup>932,954,955</sup>

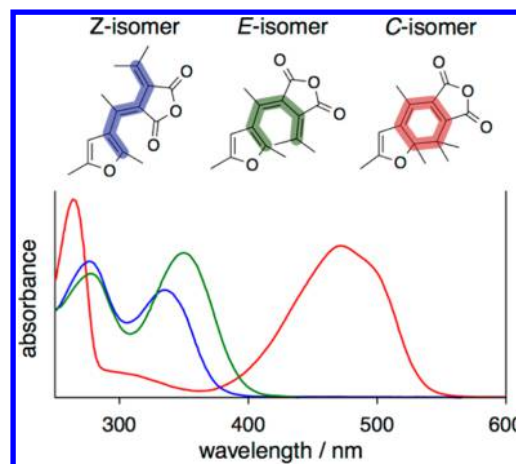


**Figure 84.** Structures and absorption spectra of the three isomers of 134 in *n*-hexane. Adapted with permission from ref 959. Copyright 1996 Elsevier B.V.

**4.4.2.1. Indolylfulgimides.** The groups of Braun and Gilch thoroughly investigated the cycloreversion<sup>942–944,951,952,954</sup> and cyclization<sup>942–944</sup> reactions of 131 using a combination of fs UV/vis<sup>942,944,951,954</sup> and mid-IR<sup>943,944,951,952</sup> transient absorption as well as Kerr-gated broadband fluorescence<sup>942</sup> spectroscopy. Transient absorption experiments yielded common biphasic dynamics for the cycloreversion,<sup>951</sup> with the faster component attributed to the actual cycloreversion of 131 and the slower component assigned to the vibrational cooling of the ground state of the E conformer (Figure 85). DFT calculations allowed for an unequivocal assignment of the observed IR modes in the 1300–1800  $\text{cm}^{-1}$  range to normal modes of educts and products.<sup>952</sup>

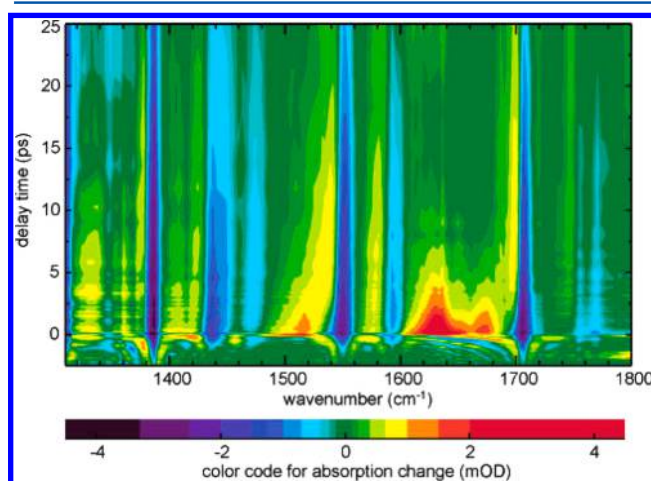


**Figure 85.** Transient IR spectra measured after photoexcitation of the C-form of 131. Short time dynamics are attributed to the cycloreversion reaction, while the longer dynamics are identified as vibrational cooling of the ground state species. Reprinted from ref 952. Copyright 2006 American Chemical Society.

In subsequent works<sup>943,954</sup> similar transient absorption measurements revealed the possible involvement of a solvent-polarity dependent activation energy in the ring-opening, with the reaction being faster by a factor of 1.5–2 in apolar than in polar solvents.<sup>943,954</sup> The ring-closure, on the other hand, was found to proceed on the sub-picosecond time scale without any

appreciable activation barrier, to be followed by ground-state vibrational cooling on the tens of ps time scale.<sup>943</sup>

Important insight into the topology of the excited-state potential energy surface for the full photocycle, comprising ring opening and closing, was gained from the combined transient electronic absorption and Kerr-gated broadband fluorescence experiments by the Gilch group on **131** in acetonitrile.<sup>942</sup> Both cyclization and cycloreversion were found to exhibit ultrafast biphasic dynamics, in 55 and 400 fs for cyclization and in 90 fs and 2.4 ps for cycloreversion. The transient absorption experiments revealed additional slower dynamics in the 10 ps range, attributable to vibrational cooling of the hot ground-state species. Based on the strong differences in the emission spectra of the open and closed forms, the authors proposed a two-dimensional model with separate reaction paths for the two reactions (Figure 86). Within less than 100 fs after the

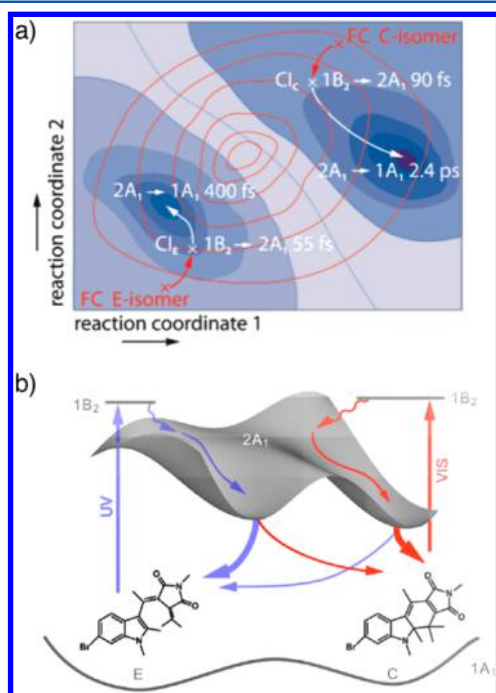


**Figure 86.** Tentative 2-dimensional excited state potential energy surface scheme for the complete photocycle of **131**. (a) the reactive zone with the two CIs. Reprinted with permission from ref 942. Copyright 2007 American Chemical Society. (b) Sketched view of the entire surface including the tentative ground state potential. Reprinted with permission from ref 944. Copyright 2008 Elsevier.

excitation to the 1B<sub>2</sub> state, the C or E-isomers undergo internal conversion to the 2A<sub>1</sub> state via two distinct conical intersections, thus accessing different minima, which mark the branching points for the photoreaction and/or further internal conversion to the 1A<sub>1</sub> ground state.<sup>942</sup> This interpretation was fully supported by a subsequent study by Braun and co-workers who additionally used transient vibrational absorption spectroscopy.<sup>944</sup>

The group of Braun and co-workers undertook a comparative investigation on the effect of thermal and optical excess energy on the cycloreversion of **131** (and **132**, with an analogous result) using fs transient electronic absorption and quantum efficiency measurements in toluene and acetonitrile.<sup>954</sup> From the quantum yield measurements, the authors found that both temperature as well as optical excess energy significantly

enhanced the ring-opening, thus violating the Kasha-Vavilov rule. However, a thorough analysis of the Arrhenius plots, performed vs thermal and optical energy, clearly revealed that the optical excess energy only contributed by 13–20% to the enhancement of the cycloreversion. The authors could rationalize this finding by arguing that vibrational relaxation in the excited state, required to significantly populate the low frequency modes associated with the reaction, was too slow to compete with the ring-opening reaction itself and/or the intermolecular energy redistribution.

Recently, Slavov et al. reported on the full photocycle of a water-soluble derivative of **131**, bearing carboxylic acid groups on the imide-N and R<sub>2</sub> using fs transient electronic absorption and broadband fluorescence spectroscopy.<sup>948</sup> The observed photocycle dynamics in organic solvents closely matched the previous findings for **131**.<sup>942,944</sup> In water, however, the cycloreversion was found to be almost twice as fast as in polar solvents and even slightly faster than in apolar solvents, illustrating the pivotal influence of excited-state proton transfer on the relaxation dynamics of this type of fulgimides. On the other hand, the cyclization reaction was ultrafast (0.4 ps) and independent of the solvent.

**4.4.2.2. Indolylfulgides.** Using a combination of fs mid-IR experiments between 1200 and 1900 cm<sup>-1</sup>, CASSCF and TDDFT calculations, Nenov et al. could provide a thorough and comprehensive description of the full photocycle of all three conformers of **133** in tetrachloroethylene.<sup>946</sup> In line with the results from Zinth and co-workers,<sup>955</sup> who had investigated **133** in cyclohexane using fs transient electronic absorption, the authors found biphasic behavior for the cycloreversion upon excitation into the S<sub>1</sub> state. The 2.2–3 ps lifetime was attributed to the excited-state decay of the C-form, while the 10–20 ps components were ascribed to vibrational cooling of the hot C and E-form in the electronic ground state. Previously, Braun and co-workers had shown that the cycloreversion of **133** constituted an activated process with a significant activation energy.<sup>958</sup> The cyclization reaction, on the other hand, showed ultrafast excited-state deactivation dynamics in the 0.3–0.45 ps range,<sup>945,946</sup> independent of the excitation wavelength and solvent polarity.<sup>945</sup> These fast dynamics were again followed by vibrational cooling of the hot electronic ground state within 10–20 ps.<sup>945,946</sup> Based on these experiments and high level quantum-chemical calculations, Nenov et al. established a schematic reaction scheme (Figure 87), comprising three conical intersections and including the unreactive Z-conformer. Contrary to the groups of Gilch and Braun for **131** (vide supra), the authors invoked a common conical intersection (CI<sub>C/E</sub>), through which cyclization and cycloreversion proceeded with high yield. While the unreactive Z-conformer deactivates via internal conversion to either the Z or E ground state (via CI<sub>Z/E</sub>), the population of the closed-form C-isomer bifurcates and deactivates either through the “unreactive” CI<sub>C</sub> or the “reactive” CI<sub>C/E</sub>. On the other hand, two-thirds of the population of the cyclizable open-form E-conformer evolves ballistically toward the “reactive” CI<sub>C/E</sub> while the remaining population undergoes deactivation/isomerization via CI<sub>Z/E</sub>.

Zinth and co-workers studied the efficiency and dynamics of the cycloreversion of **133** in cyclohexane upon excitation into different excited electronic states using fs transient electronic absorption spectroscopy.<sup>955</sup> Excitation into the S<sub>1</sub> state resulted in a reaction quantum yield for cycloreversion of only 7%. However, excitation into a surprisingly long-lived (0.5 ps) higher electronically excited state, S<sub>N</sub>, at 340 nm, resulted in an

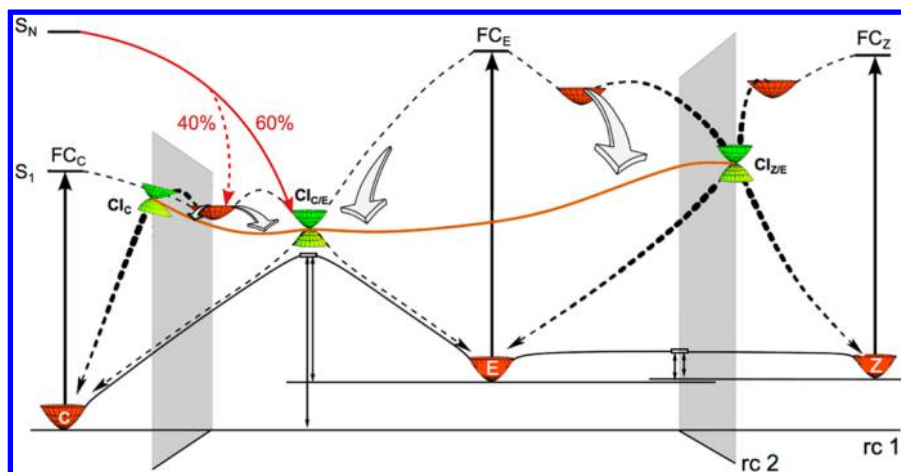


**Figure 87.** Schematic reaction scheme of **133** including the relaxation channels of the excited state and the effect of excitation wavelength on the cycloreversion. Adapted from ref [946](#). Copyright 2012 American Chemical Society.

almost 4–5 times higher quantum yield in violation of the Kasha-Vavilov rule. Similar findings had previously been reported for a variety of DAEs cycloreversion reactions (vide supra). These observations could be rationalized within the reaction scheme outlined above (Figure 87). The “unreactive” CI ( $CI_C$ ) exclusively afforded the closed-ring conformer, while the reactive one ( $CI_{C/E}$ ) led to a branching between (a) reaction to the ring-open E conformer and (b) unreactive decay to the closed-ring conformer. Excitation into the  $S_N$  state thus led to 60% of the population bypassing the  $S_1$  surface and directly deactivating via the “reactive”  $CI_{C/E}$  and only 40% experiencing the same dynamics as if excited into the  $S_1$  state.

Braun and co-workers studied the effect of temperature and optical pre-excitation on the reaction yield of the cycloreversion of **133** using fs visible pump–probe and pump–pump–probe spectroscopy in dioxane.<sup>[958](#)</sup> The temperature-dependent pump–probe measurements yielded decreasing cycloreversion times and increasing quantum efficiencies with increasing temperature, confirming the activated nature of the ring-opening. In particular, as shown in Figure 87, two activated processes with different pre-exponential factors and activation energies leading to the two conical intersections for internal conversion (via  $CI_C$ ) and reactive ring opening (via  $CI_{C/E}$ ) could be identified. Even more interestingly, the authors showed that a nonequilibrium ground state of the C-form, produced upon pre-exciting the open E-form at 400 nm and subsequent cyclization, could significantly accelerate the ring-opening dynamics, triggered by pumping at 630 nm. Such preexcitation resulted in an increase of the quantum yield of ring-opening by a factor of almost 3. Apparently, the vibrational modes that are excited as a result of the ring-closing process also play a pivotal role in the subsequent ring-opening reaction, rendering the cycloreversion of **133** a highly mode-specific photochemical reaction.

In a series of two papers, Brust et al. reported on the cycloreversion of **132** in acetonitrile.<sup>[953,954](#)</sup> In agreement with their own findings on the structurally almost identical **133**, the authors observed a biphasic and temperature dependent cycloreversion reaction. Again, the short 0.7 ps component was ascribed to solvation dynamics, while the slower 12 ps process was assigned to the excited-state decay of the C-form and the related product formation.<sup>[953](#)</sup> In addition, experiments comparing the effect of thermal and optical excess energy on

the ring-opening agreed with the results obtained for the indolylfulgimide **131** (vide supra).<sup>[954](#)</sup>

The most recent contribution to the understanding of the full photocycle of **132** can be attributed to Slavov et al.<sup>[947](#)</sup> Temperature and solvent dependent quantum efficiency measurements confirmed previous findings that the cyclization reaction proceeds in a barrierless manner, while the cycloreversion is thermally activated with a solvent polarity dependent barrier. Moreover, the strong periodic oscillation observed in the transient absorption data was assigned, based on quantum-chemistry calculations, to the out-of-plane motion of the indolyl and the succinic rings. This mode was shown to be one of the main contributors to the reactive coordinates of the cycloreversion.

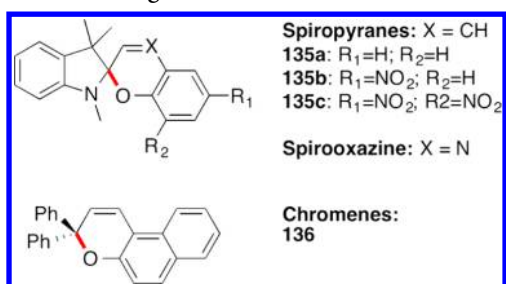
**4.4.2.3. Furylfulgides.** The cyclization,<sup>[949,950](#)</sup> cycloreversion,<sup>[932,956,957](#)</sup> and isomerization<sup>[960](#)</sup> of **134** and related derivatives were extensively studied by the groups of Miyasaka, who focused on multiphoton effects on the ring-opening, as well as by Temps and Renth, who concentrated on structural effects. These efforts were thoroughly reviewed very recently by Renth et al.<sup>[941](#)</sup>

**4.4.3. Spiro-Compounds and Chromenes.** Photochromic systems based on spiro-compounds and chromenes were intensively studied<sup>[961](#)</sup> owing to their versatility in multiple applications<sup>[962](#)</sup> as diverse as organic optoelectronics<sup>[963,964](#)</sup> to switches in biological systems.<sup>[965](#)</sup>

The photochromism of these two classes is based on the photoinduced heterolytic carbon–oxygen bond cleavage (in the pyran or oxazine unit) in the ring-closed form, giving rise to the formation of zwitterionic merocyanines (spiropyrans) or quinoidal open-form conformers (spirooxazines, chromenes). Here, in contrast to the two previous classes of photochromic compounds, the open-form is strongly colored due to the enhanced  $\pi$ -delocalization, whereas the ring-closed form is generally colorless as conjugation of the  $\pi$  electron system is significantly reduced either by the orthogonal position of the two heterocycles (spiro-compounds) or by the broken conjugation on the fully substituted carbon located on the pyran ring (chromenes). Another important difference compared with DAEs or fulgides is the number of isomers. Here, the open form can exist in 8 different isomeric forms, arising from the cis/trans configuration of the three double bonds. Chart 27 gives an overview of the closed-form structures of the relevant samples discussed in this subchapter.



Chart 27. Spiro and Chromene-Based Structures, with the Bond Broken during the Reaction in Red



In a series of four papers, Fidler and co-workers reported on the dynamics of the ring-opening reaction of **135a**<sup>966</sup> and **135b**<sup>967–969</sup> in various solvents. In contrast to previous results,<sup>970</sup> where sub-picosecond formation of the merocyanine (MC) form was deduced from transient electronic absorption, transient IR spectra **135a** at wavenumbers characteristic for the MC form pointed to much slower product formation.<sup>966</sup> Internal conversion of the spiro-form was found to occur on the sub-picosecond time scale and to be the most important (90%) deactivation pathway of the excited state. The other minor pathways lead to the population of an intermediate of “unknown nature”, which subsequently produced MC in 28 ps. In the first investigation of the ring-opening dynamics of **135b** the yield of product formation was found to depend on the excitation wavelength and to be monoexponential in the polar acetonitrile (7–10 ps) and biexponential (5–30 and 100 ps) in the apolar tetrachloroethene. The excitation-wavelength dependence was attributed to the cooling of hot product states, whereas the bimodal dynamics in the apolar solvent were assigned to the production of an additional MC isomer.<sup>967</sup> Using fs transient vibrational absorption spectroscopy, the authors observed an energy gap dependence for the efficient S<sub>1</sub> → S<sub>0</sub> internal conversion process of **135b**, which was weaker than expected from the well-established energy gap law and could be satisfactorily attributed to large conformational changes between the S<sub>0</sub> and S<sub>1</sub> states.<sup>969</sup> In the follow-up paper on **135b**, the authors expanded their arsenal of experimental techniques with fs transient vibrational absorption and time-resolved emission spectroscopy.<sup>968</sup> The combination of the three complementary techniques allowed the essential reaction steps to be pinned down (Figure 88). The initially populated spiro S<sub>1</sub> state undergoes ultrafast (<0.2 ps) branching into the hot spiro S<sub>0</sub> state, intersystem crossing to the spiro T<sub>1</sub> state and ring-opening into the MC T<sub>2</sub> state. The hot spiro ground state cools within 47 ps, while the spiro triplet state decays via oxygen quenching. On the other hand, the T<sub>2</sub> state of MC undergoes internal conversion within 0.5 ps and subsequent vibrational cooling (17 ps) to the relaxed T<sub>1</sub> state, which is itself converted into an additional MC isomer on the 350 ps time scale.

Brixner and co-workers studied the full photocycle of **135c**,<sup>971</sup> as well as its cyclization from different open-form isomers<sup>972</sup> using fs transient electronic and vibrational absorption spectroscopy. In addition, the authors used three-color pump–repump–probe experiments for demonstrating how entire opening (closure)/closure (opening) cycles could be achieved within 40 ps (6 ps) via ultrafast bidirectional switching.<sup>971</sup>

In agreement with previous indirect evidence for a photoinduced ring-closing reaction of **135c**,<sup>973</sup> Buback et al.

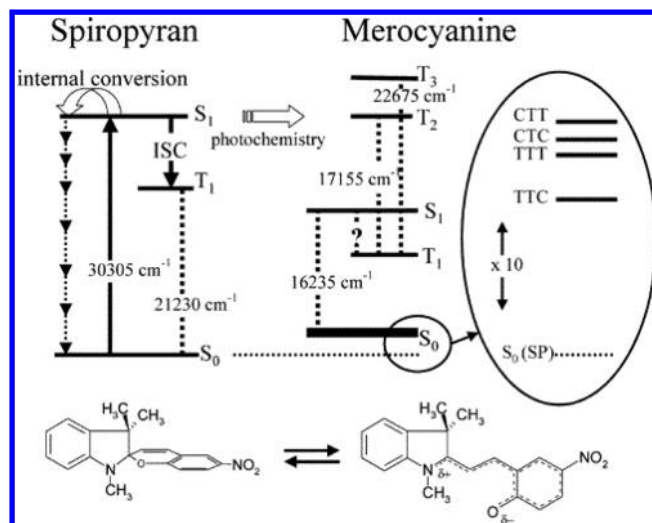


Figure 88. Tentative reaction scheme for the ring-opening reaction of spiropyran **135b**. Reprinted from ref 968. Copyright 2005 American Chemical Society.

could only observe a biphasic decay of the bleach of the opening form when using transient electronic absorption. However, using transient vibrational absorption, the authors could clearly monitor unambiguous spectral evidence of the formation of the spiro-form on the sub-100 ps time scale. The longer time constant of 830 ps was only observed in the visible region and could be assigned to the ring closure of a second MC isomer. Contrary to **135b**, the authors could rule out the possible involvement of triplet states in the cyclization of **135c**. The cycloreversion of **135c**, on the other hand, occurred on the sub-picosecond time scale, yielding a vibrationally hot *cis* MC form, which subsequently decayed within 34 ps to a distribution of ring-open isomers. The formation of the thermodynamically most stable isomers eventually took place on a significantly longer time scale.

In a subsequent work, the same group undertook a thorough investigation on the competition between the ring-closing and isomerization reactions of a mixture of the *trans/trans/cis* and all-*trans* isomers of **135c**.<sup>972</sup> From fs transient electronic absorption measurements at 6 different excitation wavelengths and global analysis of the resulting data at times where vibrational cooling was over, the authors could show that isomerization occurred exclusively during vibrational relaxation on the excited state surface, and not via a CI. Once the cooling had ceased, isomerization was no longer possible and the two excited isomer populations underwent internal conversion back to the ground state or ring-closure along separate pathways. The ring-closure yields were found to occur with 30–40% quantum efficiencies whereas the isomerization efficiency in both directions was less than 2%.

Wachtveitl and co-workers investigated the full photocycle of a water-soluble spiropyran derivative using transient electronic and vibrational absorption spectroscopy (Figure 89).<sup>974</sup> They found that the ring-opening reaction from the short-lived spiro S<sub>1</sub> state (1.6 ps) proceeded through branching at a CI with an efficiency of only 3.3%. They also observed that the ring closure reaction occurs with an efficiency of less than 20% from a vibrationally hot MC ground state, itself populated within 3.2 ps via internal conversion.

Favaro and co-workers observed ultrafast ring-opening dynamics in <200 fs with several spiropyrans and oxazines,<sup>975</sup>

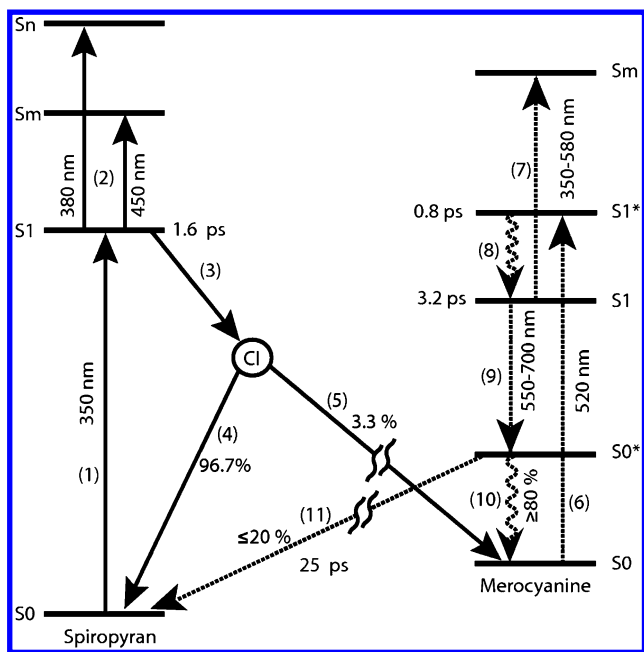


**Figure 89.** Reaction pathways for ring-closure and reversion of a water-soluble spiropyran in a simplified potential energy scheme. The ring-opening proceeds through the conical intersection (CI), whereas the ring-closure takes place from the hot ground state of the merocyanine. Reprinted from ref 974. Copyright 2012 American Chemical Society.

whereas Kumar et al. measured ultrafast internal conversion (300 fs) in the open-form of a spiropheanthrooxazine using a sub-40 fs transient electronic absorption, thus not allowing significant ring-closure to take place.<sup>976</sup>

Cordes and co-workers,<sup>977</sup> could draw a conclusive picture of the ultrafast photochemical ring-opening reaction of 136, which had been previously studied by several groups using transient electronic absorption spectroscopy.<sup>978–981</sup> In addition to previous studies, which had relied on visible TA, Cordes and co-workers additionally used broadband fluorescence spectroscopy and could elaborate a reaction scheme (Figure 90), consistent with all the experimental data, that differed from

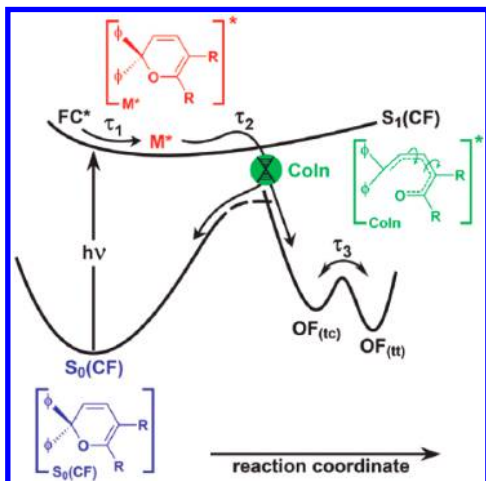


**Figure 90.** Tentative reaction scheme for the ring-opening reaction of the closed form (CF) of 136 upon UV excitation. Reprinted with permission from ref 977. Copyright 2013 The Royal Society of Chemistry.

those proposed previously.<sup>977</sup> In brief, the Franck–Condon excited state undergoes vibrational relaxation, bond-alternation or solvent relaxation within 200 fs to the energy minimum  $M^*$  on the  $S_1$  surface. Transition along the flat excited state surface over an almost insignificant activation barrier to the ground state via a CI occurs within 1–1.5 ps. This transition was clearly evidenced by the disappearance of the fluorescence and the rise of spectral features of the product. Most of the excited-state population undergoes ring-opening at the CI, with the remainder decaying to the ring-closed electronic ground state. However, during its cooling, the ring-open form can convert to the other open form.

**4.4.4. Concluding Remarks.** In summary, we can conclude that the dynamics of these types of photochromic systems are rich and diverse and depend critically on the topology of the excited-state potential energy surface(s). Many of the systems show strong excitation wavelength or even intensity dependence. Pinning down of the precise evolution of the systems along the excited state PES, the possible importance of coherent effects involved (e.g., in ring-opening reactions), or merely the determination and rationalization minute structural changes may exert on product yields, renders each of the investigated systems a new challenge, require the combination of multiple experimental techniques, and make drawing general conclusions a difficult task.

## 5. FINAL REMARKS

Thanks to the developments in ultrafast spectroscopic techniques, computational methods, and theoretical models, our understanding of the ultrafast photochemical reactions in liquids has increased tremendously. The present pictures of all the reactions discussed depart substantially from those proposed a few decades ago. The level of precision offered by the spectroscopic and the computational techniques is such that it is becoming possible, in some cases at least, to draw a very detailed picture of the course of a photochemical process. However, the more precise the picture, the more one realizes that each molecular system is unique and that drawing a general scheme for a given reaction is not always feasible. Indeed, the course of the reaction depends critically on the shapes of the multidimensional potential energy surfaces of the ground and excited states along the reactive coordinates. If, on the one hand, the reaction involves mostly solvent modes and leads to minor changes in the intramolecular nuclear coordinates, as it is the case for many charge-transfer processes, the free energy of the relevant states along the reaction coordinate is parabolic within the linear response approximation. This simplicity allows for developing relatively simple theoretical models, such as the Marcus model. These models can be used to make semi-quantitative predictions on the rate constant of the reaction for a given system, provided that a few parameters, which can be determined or estimated independently, are known. Such models can be relatively simply extended to include non-equilibrium effects and to account for the time-dependent reaction rate coefficients. On the other hand, if the reaction involves mostly intramolecular coordinates and substantial structural changes (as it is the case for cis–trans isomerizations), the potential-energy surfaces along the reaction coordinate are no longer parabolic and the elaboration of a general model, valid for a wide range of compounds, is no longer feasible. In these cases, knowledge of the potential-energy surfaces is needed to rationalize experimental data and to allow predictions on how variation of a given experimental

parameter, such as temperature, solvent, or excitation wavelength, may affect the dynamics. Probably the best approach to draw a consistent picture for this type of processes is to combine several spectroscopic techniques as well as quantum-chemical calculations.

Although nonequilibrium effects are ubiquitous in the above-discussed reactions, they have not yet been systematically investigated. They are often neglected and the measured population changes are analyzed assuming exponential dynamics, and quantified using classical kinetics. Although this approach gives “simple” numbers that are sometimes useful, it does not account properly for the reaction dynamics and can lead to erroneous conclusions. Moreover, it misses the opportunities offered by nonequilibrium effects for the development of photochemistry beyond the Kasha–Vavilov rule. Clearly further work in this direction is needed.

## AUTHOR INFORMATION

### Corresponding Author

\*E-mail: [Eric.Vauthey@unige.ch](mailto:Eric.Vauthey@unige.ch).

### ORCID

Eric Vauthey: 0000-0002-9580-9683

### Notes

The authors declare no competing financial interest.

### Biographies

Tatu Kumpulainen studied chemistry at the Tampere University of Technology where he obtained his diploma in 2010, working in the group of Helge Lemmetyinen. In 2015 he completed his Ph.D. in the group of Fred Brouwer at the University of Amsterdam, focusing on excited-state proton-transfer reactions. Since then he has been a postdoc in the group of Eric Vauthey at the University of Geneva. His research interests include proton- and electron-transfer processes in liquid phase.

Bernhard Lang studied physics at the University of Freiburg im Breisgau, where he obtained his diploma in 1994. In 1998 he received his Ph.D. from the University of Würzburg. After two postdocs at the University of Lausanne and the University of Geneva he became senior research associate in the group of Prof. Eric Vauthey at the University of Geneva. Over the past years his research activity has been on using ultrafast spectroscopy in the liquid phase to study solvation dynamics and electron transfer reactions, as well as achieving absolute photometrics in electronic transient absorption spectroscopy in the femtosecond to microsecond time domain.

Arnulf Rosspeintner studied chemistry at the Graz University of Technology and the University of Sevilla and obtained his diploma in 2003. After his Ph.D. (2008) in the group of Günter Grampp at the Graz University of Technology studying diffusion-influenced reactions, he pursued a postdoc in the group of Georg Gescheidt (2008–2010), working on the time-resolved EPR spectroscopy of photoinitiators. Since then he has been postdoc (2010–2013) and maître assistant (since 2013) in the group of Eric Vauthey at the University of Geneva. His research interests include intra- and intermolecular electron transfer reactions, magnetic field effects, and two-photon absorption spectroscopy.

Eric Vauthey obtained his chemistry diploma (1986) and Ph.D. (1989) from the University of Fribourg. After postdoctoral research at Imperial College London and ETH Zurich, he started independent research in Fribourg in 1992. He has been a Professor at the University of Geneva since 2001. His main research interest is the dynamics of

molecular photoinduced processes in the condensed phase and at interfaces: <http://www.unige.ch/sciences/chifi/Vauthey/index.php>.

## ACKNOWLEDGMENTS

We wish to warmly thank Prof. Anatoly Ivanov (Volgograd State University) for enlightening discussions on the electron transfer theories, as well as Mr. Joseph Beckwith for a careful proof-reading of the manuscript and for his invaluable advices for a proper usage of written English. We are grateful to the University of Geneva and the Swiss National Science Foundation (project no. 200020-165890) for their continuous financial support.

## ABBREVIATIONS AND ACRONYMS

2D-EV = two-dimension electronic-vibrational (spectroscopy)  
A = (electron) acceptor  
AH = acid  
B = base  
BEBO = bond-energy bond-order  
CI = conical intersection  
CR = charge recombination  
CS = charge separation  
CT = charge transfer  
D = (electron) donor  
DAC = donor–acceptor complex  
DAE = diarylethene  
D-B-A = donor-bridge-acceptor  
DFT = density functional theory  
DRE = diffusion-reaction equation  
DSE = Debye–Smoluchowski equation  
ESIPT = excited-state intramolecular proton transfer  
ESPT = excited-state proton transfer  
ET = electron transfer  
FSRS = femtosecond stimulated Raman spectroscopy  
FWCD = Franck–Condon weighted density of state  
HOMO = Highest occupied molecular orbital  
ICT = intramolecular charge transfer  
IRF = instrument response function  
ISRS = impulsive stimulated Raman scattering  
IVR = intramolecular vibrational redistribution  
LE = locally excited  
LIP = loose ion pair  
LUMO = lowest unoccupied molecular orbital  
MD = molecular dynamics  
P(AP)-form = parallel (antiparallel) form  
PCET = proton-coupled electron transfer  
PICT = planar intramolecular charge transfer (state)  
PT = proton transfer  
RICT = rehybridized intramolecular charge transfer (state)  
RTIL = room-temperature ionic liquid  
TCSPC = time-correlated single photon counting  
TD-DFT = time-dependent density functional theory  
TICT = twisted intramolecular charge transfer (state)  
TIP = tight ion pair  
TS = transition state  
WICT = wagged intramolecular charge transfer (state)

## REFERENCES

- (1) Polanyi, J. C.; Zewail, A. H. Direct Observation of the Transition State. *Acc. Chem. Res.* **1995**, *28*, 119–132.



- (2) Czerlinski, G. H.; Eigen, M. A Temperature-Jump Method for the Examination of Chemical Relaxation. *Z. Elektrochem. Angew. Phys. Chem.* **1959**, *63*, 652–661.
- (3) Norrish, R. G. W.; Porter, G. Chemical Reactions Produced by Very High Light Intensities. *Nature* **1949**, *164*, 658.
- (4) Turro, N. J.; Ramamurthy, V.; Scaiano, J. C. *Modern Molecular Photochemistry of Organic Molecules*; University Science Books: Sausalito, CA, 2010.
- (5) Castner, E. W.; Margulis, C. J.; Maroncelli, M.; Wishart, J. F. Ionic Liquids: Structure and Photochemical Reactions. *Annu. Rev. Phys. Chem.* **2011**, *62*, 85–105.
- (6) Barthel, J.; Bachhuber, K.; Buchner, R.; Hetzenauer, H. Dielectric Spectra of Some Common Solvents in the Microwave Region. Water and Lower Alcohols. *Chem. Phys. Lett.* **1990**, *165*, 369–373.
- (7) Böttcher, C. J. F.; Bordewijk, P. *Theory of Electric Polarization, Vol. II: Dielectrics in Time-Dependent Fields*; Elsevier: Amsterdam, 1978.
- (8) Kivelson, D.; Friedman, H. Longitudinal Dielectric Relaxation. *J. Phys. Chem.* **1989**, *93*, 7026–7031.
- (9) Barthel, J.; Kleebauer, M.; Buchner, R. Dielectric Relaxation of Electrolyte Solutions in Acetonitrile. *J. Solution Chem.* **1995**, *24*, 1–17.
- (10) Bakhshiev, N. G. Universal Intermolecular Interactions and Their Effect on the Position of the Electronic Spectra of Molecules in Two-Component Solutions. VII. Theory (General Case of an Isotropic Solution). *Opt. Spektrosk.* **1964**, *16*, 821–832.
- (11) Ware, W. R.; Chow, P.; Lee, S. K. Time-Resolved Nanosecond Emission Spectroscopy: Spectral Shift Due to Solvent-Solute Relaxation. *Chem. Phys. Lett.* **1968**, *2*, 356–358.
- (12) Seliskar, C. J.; Brand, L. Solvent Dependence of the Luminescence of N-Arylamino-naphthalenesulfonates. *Science* **1971**, *171*, 799–800.
- (13) Kahlow, M. A.; Kang, T. J.; Barbara, P. F. Transient Solvation of Polar Dye Molecules in Polar Aprotic Solvents. *J. Chem. Phys.* **1988**, *88*, 2372–2378.
- (14) Simon, J. D. Time-Resolved Studies of Solvation in Polar Media. *Acc. Chem. Res.* **1988**, *21*, 128–134.
- (15) Maroncelli, M., Jr.; Castner, E. W.; Bagchi, B.; Fleming, G. R. Dipolar Solvation Dynamics. *Faraday Discuss. Chem. Soc.* **1988**, *85*, 199–210.
- (16) Castner, E. W.; Maroncelli, M.; Fleming, G. R. Subpicosecond Resolution Studies of Solvation Dynamics in Polar Aprotic and Alcohol Solvents. *J. Chem. Phys.* **1987**, *86*, 1090–1097.
- (17) Maroncelli, M.; Fleming, G. R. Picosecond Solvation Dynamics of Coumarin 153: The Importance of Molecular Aspects of Solvation. *J. Chem. Phys.* **1987**, *86*, 6221–6239.
- (18) Maroncelli, M.; Fleming, G. R. Computer Simulation of the Dynamics of Aqueous Solvation. *J. Chem. Phys.* **1988**, *89*, 5044–5069.
- (19) Bader, J. S.; Chandler, D. Computer Simulation of Photochemically Induced Electron Transfer. *Chem. Phys. Lett.* **1989**, *157*, 501–504.
- (20) Rosenthal, S. J.; Xie, X.; Du, M.; Fleming, G. R. Femtosecond Solvation Dynamics in Acetonitrile: Observation of the Inertial Contribution to the Solvent Response. *J. Chem. Phys.* **1991**, *95*, 4715–4718.
- (21) Jimenez, R.; Fleming, G. R.; Kumar, P. V.; Maroncelli, M. Femtosecond Solvation Dynamics of Water. *Nature* **1994**, *369*, 471–473.
- (22) Horng, M. L.; Gardecki, J. A.; Papazyan, A.; Maroncelli, M. Subpicosecond Measurements of Polar Solvation Dynamics: Coumarin 153 Revisited. *J. Phys. Chem.* **1995**, *99*, 17311–17337.
- (23) Stratt, R. M.; Maroncelli, M. Nonreactive Dynamics in Solution: The Emerging Molecular View of Solvation Dynamics and Vibrational Relaxation. *J. Phys. Chem.* **1996**, *100*, 12981–12996.
- (24) Castner, E. W., Jr.; Maroncelli, M. Solvent Dynamics Derived from Optical Kerr Effect, Dielectric Dispersion, and Time-Resolved Stokes Shift Measurements: An Empirical Comparison. *J. Mol. Liq.* **1998**, *77*, 1–36.
- (25) de Boeij, W. P.; Pshenichnikov, M. S.; Wiersma, D. A. Phase-Locked Heterodyned Detected Stimulated Photon Echo. A Unique Tool to Study Solute-Solvent Interaction. *Chem. Phys. Lett.* **1995**, *238*, 1–8.
- (26) Passino, S. A.; Nagasawa, Y.; Joo, T.; Fleming, G. R. Three Pulse Echo Peak Shift Studies of Polar Solvation Dynamics. *J. Phys. Chem. A* **1997**, *101*, 725–731.
- (27) de Boeij, W. P.; Pshenichnikov, M. S.; Wiersma, D. A. Ultrafast Solvation Dynamics Explored by Femtosecond Photon Echo Spectroscopies. *Annu. Rev. Phys. Chem.* **1998**, *49*, 99–123.
- (28) Cho, M.; Fleming, G. R. The Integrated Photon Echo and Solvation Dynamics. II. Peak Shifts and Two-Dimensional Photon Echo of a Coupled Chromophore System. *J. Chem. Phys.* **2005**, *123*, 114506.
- (29) Gummy, J. C.; Nicolet, O.; Vauthey, E. Investigation of the Solvation Dynamics of an Organic Dye in Polar Solvents Using the Femtosecond Transient Grating Technique. *J. Phys. Chem. A* **1999**, *103*, 10737–10743.
- (30) Bredenbeck, J.; Helbing, J.; Hamm, P. Solvation Beyond the Linear Response Regime. *Phys. Rev. Lett.* **2005**, *95*, 083201.
- (31) Kwak, K.; Park, S.; Fayer, M. D. Dynamics around Solutes and Solute-Solvent Complexes in Mixed Solvents. *Proc. Natl. Acad. Sci. U. S. A.* **2007**, *104*, 14221–14226.
- (32) Dunbar, J. A.; Arthur, E. J.; White, A. M.; Kubarych, K. J. Ultrafast 2D-IR and Simulation Investigations of Preferential Solvation and Cosolvent Exchange Dynamics. *J. Phys. Chem. B* **2015**, *119*, 6271–6279.
- (33) Giraud, G.; Gordon, C. M.; Dunkin, I. R.; Wynne, K. The Effects of Anion and Cation Substitution on the Ultrafast Solvent Dynamics of Ionic Liquids: A Time-Resolved Optical Kerr-Effect Spectroscopic Study. *J. Chem. Phys.* **2003**, *119*, 464–477.
- (34) Smith, N. A.; Lin, S.; Meech, S. R.; Shirota, H.; Yoshihara, K. Ultrafast Dynamics of Liquid Anilines Studied by the Optical Kerr Effect. *J. Phys. Chem. A* **1997**, *101*, 9578–9586.
- (35) Smith, N. A.; Meech, S. R. Ultrafast Dynamics of Polar Monosubstituted Benzene Liquids Studied by the Femtosecond Optical Kerr Effect. *J. Phys. Chem. A* **2000**, *104*, 4223–4235.
- (36) Bragg, A. E.; Cavanagh, M. C.; Schwartz, B. J. Linear Response Breakdown in Solvation Dynamics Induced by Atomic Electron-Transfer Reactions. *Science* **2008**, *321*, 1817–1822.
- (37) Vuilleumier, R.; Tay, K. A.; Jeanmairet, G.; Borgis, D.; Boutin, A. Extension of Marcus Picture for Electron Transfer Reactions with Large Solvation Changes. *J. Am. Chem. Soc.* **2012**, *134*, 2067–2074.
- (38) Chapman, C. F.; Fee, R. S.; Maroncelli, M. Measurements of the Solute Dependence of Solvation Dynamics in 1-Propanol: The Role of Specific Hydrogen-Bonding Interactions. *J. Phys. Chem.* **1995**, *99*, 4811–4819.
- (39) Sajadi, M.; Weinberger, M.; Wagenknecht, H.-A.; Ernsting, N. P. Polar Solvation Dynamics in Water and Methanol: Search for Molecularity. *Phys. Chem. Chem. Phys.* **2011**, *13*, 17768–17774.
- (40) Zhang, X.-X.; Breffke, J.; Ernsting, N. P.; Maroncelli, M. Observations of Probe Dependence of the Solvation Dynamics in Ionic Liquids. *Phys. Chem. Chem. Phys.* **2015**, *17*, 12949–12956.
- (41) Zhang, X.-X.; Würth, C.; Zhao, L.; Resch-Genger, U.; Ernsting, N. P.; Sajadi, M. Femtosecond Broadband Fluorescence Upconversion Spectroscopy: Improved Setup and Photometric Correction. *Rev. Sci. Instrum.* **2011**, *82*, 063108.
- (42) Sajadi, M.; Quick, M.; Ernsting, N. P. Femtosecond Broadband Fluorescence Spectroscopy by Down- and up-Conversion in  $\beta$ -Barium Borate Crystals. *Appl. Phys. Lett.* **2013**, *103*, 173514.
- (43) Hill, T. L. *An Introduction to Statistical Thermodynamics*; Dover: New York, 1986.
- (44) Pigliucci, A.; Duvanel, G.; Daku, L. M. L.; Vauthey, E. Investigation of the Influence of Solute-Solvent Interactions on the Vibrational Energy Relaxation Dynamics of Large Molecules in Liquids. *J. Phys. Chem. A* **2007**, *111*, 6135–6145.
- (45) Elles, C. G.; Crim, F. F. Connecting Chemical Dynamics in Gases and Liquids. *Annu. Rev. Phys. Chem.* **2006**, *57*, 273–302.
- (46) Nesbitt, D. J.; Field, R. W. Vibrational Energy Flow in Highly Excited Molecules: Role of Intramolecular Vibrational Redistribution. *J. Phys. Chem.* **1996**, *100*, 12735–12756.

- (47) von Bente, R.; Link, O.; Abel, B.; Schwarzer, D. The Impact of a Solvent and a Methyl Rotor on Timescales of Intramolecular Vibrational Energy Redistribution in Aromatic Molecules. *J. Phys. Chem. A* **2004**, *108*, 363–367.
- (48) Yoo, H. S.; DeWitt, M. J.; Pate, B. H. Vibrational Dynamics of Terminal Acetylenes: I. Comparison of the Intramolecular Vibrational Energy Redistribution Rate of Gases and the Total Relaxation Rate of Dilute Solutions at Room Temperature. *J. Phys. Chem. A* **2004**, *108*, 1348–1364.
- (49) Elles, C. G.; Cox, M. J.; Crim, F. F. Vibrational Relaxation of  $\text{CH}_3\text{I}$  in the Gas Phase and in Solution. *J. Chem. Phys.* **2004**, *120*, 6973–6979.
- (50) Weiner, A. M.; Ippen, E. P. Femtosecond Excited State Relaxation of Dye Molecules in Solution. *Chem. Phys. Lett.* **1985**, *114*, 456–460.
- (51) Elsaesser, T.; Kaiser, W. Vibrational and Vibronic Relaxation of Large Polyatomic Molecules in Liquids. *Annu. Rev. Phys. Chem.* **1991**, *42*, 83–107.
- (52) Kovalenko, S. A.; Schanz, R.; Hennig, H.; Ernsting, N. P. Cooling Dynamics of an Optically Excited Molecular Probe in Solution from Femtosecond Broadband Transient Absorption Spectroscopy. *J. Chem. Phys.* **2001**, *115*, 3256–3274.
- (53) Schwarzer, D.; Hanisch, C.; Kutne, P.; Troe, J. Vibrational Energy Transfer in Highly Excited Bridged Azulene-Aryl Compounds: Direct Observation of Energy Flow through Aliphatic Chains and into the Solvent. *J. Phys. Chem. A* **2002**, *106*, 8019–8028.
- (54) Braem, O.; Penfold, T. J.; Cannizzo, A.; Chergui, M. A. Femtosecond Fluorescence Study of Vibrational Relaxation and Cooling Dynamics of UV Dyes. *Phys. Chem. Chem. Phys.* **2012**, *14*, 3513–3519.
- (55) Laerner, F.; Elsaesser, T.; Kaiser, W. Ultrashort Vibronic and Thermal Relaxation of Dye Molecules after Femtosecond Ultraviolet Excitation. *Chem. Phys. Lett.* **1989**, *156*, 381–386.
- (56) Sension, R. J.; Repinec, S. T.; Hochstrasser, R. M. Femtosecond Laser Study of Energy Disposal in the Solution Phase Isomerization of Stilbene. *J. Chem. Phys.* **1990**, *93*, 9185–9188.
- (57) Iwata, K.; Hamaguchi, H.-o. Microscopic Mechanism of Solute–Solvent Energy Dissipation Probed by Picosecond Time-Resolved Raman Spectroscopy. *J. Phys. Chem. A* **1997**, *101*, 632–637.
- (58) Pecourt, J.-M. L.; Peon, J.; Kohler, B. DNA Excited-State Dynamics: Ultrafast Internal Conversion and Vibrational Cooling in a Series of Nucleosides. *J. Am. Chem. Soc.* **2001**, *123*, 10370–10378.
- (59) Benniston, A. C.; Matousek, P.; McCulloch, I. E.; Parker, A. W.; Towrie, M. Detailed Picosecond Kerr-Gated Time-Resolved Resonance Raman Spectroscopy and Time-Resolved Emission Studies of Merocyanine 540 in Various Solvents. *J. Phys. Chem. A* **2003**, *107*, 4347–4353.
- (60) Kiba, T.; Sato, S.-i.; Akomoto, S.; Kajasima, T.; Yamazaki, I. Solvent-Assisted Intramolecular Vibrational Energy Redistribution of S1 Perylene in Ketone Solvents. *J. Photochem. Photobiol., A* **2006**, *178*, 201–207.
- (61) Middleton, C. T.; Cohen, B.; Kohler, B. Solvent and Solvent Isotope Effects on the Vibrational Cooling Dynamics of a DNA Base Derivative. *J. Phys. Chem. A* **2007**, *111*, 10460–10467.
- (62) Nakamura, R.; Hamada, N. Vibrational Energy Flow in Photoactive Yellow Protein Revealed by Infrared Pump–Visible Probe Spectroscopy. *J. Phys. Chem. B* **2015**, *119*, 5957–5961.
- (63) Nibbering, E. T. J.; Fidler, H.; Pines, E. Ultrafast Chemistry: Using Time-Resolved Vibrational Spectroscopy for Interrogation of Structural Dynamics. *Annu. Rev. Phys. Chem.* **2005**, *56*, 337–367.
- (64) Iwata, K.; Hamaguchi, H. Vibrational Cooling Process in Solution Probed by Picosecond Time-Resolved Raman Spectroscopy. Analysis of the Cooling Kinetics. *J. Mol. Liq.* **1995**, *65*, 417–420.
- (65) Grilj, J.; Laricheva, E. N.; Olivucci, M.; Vauthey, E. Fluorescence of Radical Ions in Liquid Solution: Wurster's Blue as a Case Study. *Angew. Chem., Int. Ed.* **2011**, *50*, 4496–4498.
- (66) Zhang, Y.; Chen, J.; Kohler, B. Hydrogen Bond Donors Accelerate Vibrational Cooling of Hot Purine Derivatives in Heavy Water. *J. Phys. Chem. A* **2013**, *117*, 6771–6780.
- (67) Ulstrup, J. *Charge Transfer Processes in Condensed Media*; Springer: Berlin, 1979.
- (68) Devault, D. Quantum Mechanical Tunnelling in Biological Systems. *Q. Rev. Biophys.* **1980**, *13*, 387–564.
- (69) Newton, N. D.; Sutin, N. Electron Transfer Reactions in Condensed Phases. *Annu. Rev. Phys. Chem.* **1984**, *35*, 437.
- (70) Marcus, R. A.; Sutin, N. Electron Transfer in Chemistry and Biology. *Biochim. Biophys. Acta, Rev. Bioenerg.* **1985**, *811*, 265–322.
- (71) Bolton, J. R.; Archer, M. D. Basic Electron-Transfer Theory. *Adv. Chem. Ser.* **1991**, *228*, 7–23.
- (72) Heitele, H. Dynamic Solvent Effects on Electron Transfer Reactions. *Angew. Chem., Int. Ed. Engl.* **1993**, *32*, 359–377.
- (73) Pollard, W. T.; Felts, A. K.; Friesner, R. A. The Redfield Equation in Condensed-Phase Quantum Dynamics. *Adv. Chem. Phys.* **1996**, *93*, 77–134.
- (74) Barbara, P. F.; Meyer, T. J.; Ratner, M. A. Contemporary Issues in Electron Transfer Research. *J. Phys. Chem.* **1996**, *100*, 13148.
- (75) Kuznetsov, A. M.; Ulstrup, J. *Electron Transfer in Chemistry and Biology*; Wiley: Chichester, U.K., 1999.
- (76) Bagchi, B.; Gayathri, N. Interplay between Ultrafast Polar Solvation and Vibrational Dynamics in Electron Transfer Reactions: Role of High-Frequency Vibrational Modes. *Adv. Chem. Phys.* **1999**, *107*, 1–80.
- (77) Bixon, M.; Jortner, J. Electron Transfer—from Isolated Molecules to Biomolecules. *Adv. Chem. Phys.* **1999**, *106*, 35–202.
- (78) Raineri, F. O.; Friedman, H. L. Solvent Control of Electron Transfer Reactions. *Adv. Chem. Phys.* **1999**, *107*, 81–189.
- (79) Barzykin, A. V.; Frantsuzov, P. A.; Seki, K.; Tachiya, M. Solvent Effects in Nonadiabatic Electron-Transfer Reactions: Theoretical Aspects. *Adv. Chem. Phys.* **2002**, *123*, 511–616.
- (80) Nitzan, A. *Chemical Dynamics in Condensed Phases*; Oxford University Press: Oxford, 2006; pp 483–535.
- (81) Ivanov, A. I.; Mikhailova, V. A. Kinetics of Fast Photochemical Charge Separation and Charge Recombination Reactions. *Russ. Chem. Rev.* **2011**, *79*, 1047–1070.
- (82) Gurney, R. W. The Quantum Mechanics of Electrolysis. *Proc. R. Soc. London, Ser. A* **1931**, *134*, 137–154.
- (83) Marcus, R. A. On the Theory of Red-Ox. Reactions Involving Electron Transfer. I. *J. Chem. Phys.* **1956**, *24*, 966.
- (84) Marcus, R. A. On the Theory of Ox-Red Reactions Involving Electron Transfer. V. Unified Treatment for Homogeneous and Electrode Reactions. *J. Chem. Phys.* **1965**, *43*, 679.
- (85) Weller, A. Photoinduced Electron Transfer in Solutions: Exciplex and Radical Ion Pair Formation Free Enthalpies and Their Solvent Dependence. *Z. Phys. Chem.* **1982**, *133*, 93–98.
- (86) Levich, V. G.; Dogonadze, R. R. Theory of Nonradiation Electron Transitions from Ion to Ion Solns. *Dokl. Akad. Nauk SSSR* **1959**, *124*, 123–126.
- (87) Kestner, N. R.; Logan, J.; Jortner, J. Thermal Electron Transfer Reactions in Polar Solvents. *J. Phys. Chem.* **1974**, *78*, 2148–2166.
- (88) Ulstrup, J.; Jortner, J. The Effect of Intramolecular Quantum Modes on Free Energy Relationships for Electron Transfer Reactions. *J. Chem. Phys.* **1975**, *63*, 4358–4368.
- (89) Siders, P.; Marcus, R. A. Quantum Effects for Electron-Transfer Reactions in the "Inverted Region". *J. Am. Chem. Soc.* **1981**, *103*, 748–752.
- (90) Englman, R.; Jortner, J. The Energy Gap Law for Radiationless Transitions in Large Molecules. *Mol. Phys.* **1970**, *18*, 145–164.
- (91) Kramers, H. A. Brownian Motion in a Field of Force and the Diffusion Model of Chemical Reactions. *Physica* **1940**, *7*, 284–304.
- (92) Zusman, L. D. Outer-Sphere Electron Transfer in Polar Solvents. *Chem. Phys.* **1980**, *49*, 295–304.
- (93) Zusman, L. D. The Theory of Electron Transfer Reactions in Solvents with Two Characteristic Relaxation Times. *Chem. Phys.* **1988**, *119*, 51–61.
- (94) Rips, I.; Jortner, J. Dynamic Solvent Effects on Outer-Sphere Electron Transfer. *J. Chem. Phys.* **1987**, *87*, 2090–2104.



- (95) Garg, A.; Onuchic, J. N.; Ambegaokar, V. Effect of Friction on Electron Transfer in Biomolecules. *J. Chem. Phys.* **1985**, *83*, 4491–4503.
- (96) Jortner, J.; Bixon, M. Intramolecular Vibrational Excitations Accompanying Solvent Controlled Electron Transfer Reactions. *J. Chem. Phys.* **1988**, *88*, 167.
- (97) Marcus, R. A.; Sumi, H. Solvent Dynamics and Vibrational Effects in Electron Transfer Reactions. *J. Electroanal. Chem. Interfacial Electrochem.* **1986**, *204*, 59–67.
- (98) Sumi, H.; Marcus, R. A. Dynamical Effects in Electron Transfer Reactions. *J. Chem. Phys.* **1986**, *84*, 4894–4914.
- (99) Nadler, W.; Marcus, R. A. Dynamical Effects in Electron Transfer Reactions. II. Numerical Solution. *J. Chem. Phys.* **1987**, *86*, 3906–3924.
- (100) Walker, G. C.; Aakesson, E.; Johnson, A. E.; Levinger, N. E.; Barbara, P. F. Interplay of Solvent Motion and Vibrational Excitation in Electron-Transfer Kinetics: Experiment and Theory. *J. Phys. Chem.* **1992**, *96*, 3728–3736.
- (101) Najbar, J.; Dorfman, R. C.; Fayer, M. D. Solvent Relaxation Effects on the Kinetics of Photoinduced Electron Transfer Reactions. *J. Chem. Phys.* **1991**, *94*, 1081–1092.
- (102) Tachiya, M.; Murata, S. Non-Marcus Energy Gap Dependence of Back Electron Transfer in Contact Ion Pairs. *J. Am. Chem. Soc.* **1994**, *116*, 2434–2436.
- (103) Gayathri, N.; Bagchi, B. Quantum and Non-Markovian Effects in the Electron Transfer Reaction Dynamics in the Marcus Inverted Region. *J. Phys. Chem.* **1996**, *100*, 3056–3062.
- (104) Ivanov, A. I.; Potovoi, V. V. Theory of Non-Thermal Electron Transfer. *Chem. Phys.* **1999**, *247*, 245–259.
- (105) Feskov, S. V.; Ionkin, V. N.; Ivanov, A. I. Effect of High-Frequency Modes and Hot Transitions on Free Energy Gap Dependence of Charge Recombination Rate. *J. Phys. Chem. A* **2006**, *110*, 11919–11925.
- (106) Nazarov, A. E.; Barykov, V. Y.; Ivanov, A. I. Effect of Intramolecular High-Frequency Vibrational Mode Excitation on Ultrafast Photoinduced Charge Transfer and Charge Recombination Kinetics. *J. Phys. Chem. B* **2016**, *120*, 3196–3205.
- (107) Wasielewski, M. R.; Niemczyk, M. P.; Svec, W. A.; Pewitt, E. B. Dependence of Rate Constants for the Photoinduced Charge Separation and Dark Charge Recombination on Free Energy of Reaction in Restricted Distance Porphyrin Quinone Molecules. *J. Am. Chem. Soc.* **1985**, *107*, 1080–1082.
- (108) Closs, G. L.; Miller, J. R. Intramolecular Long Distance Electron Transfer in Organic Molecules. *Science* **1988**, *240*, 440.
- (109) Piotrowski, P. Photoinduced Electron Transfer in Molecular Systems: Recent Developments. *Chem. Soc. Rev.* **1999**, *28*, 143–150.
- (110) Verhoeven, J. W. From Close Contact to Long-Range Intramolecular Electron Transfer. *Adv. Chem. Phys.* **1999**, *106*, 603–644.
- (111) Mataga, N.; Chosrowjan, H.; Shibata, Y.; Yoshida, N.; Osuka, A.; Kikuzawa, T.; Okada, T. First Unequivocal Observation of the Whole Bell-Shaped Energy Gap Law in Intramolecular Charge Separation from S<sub>2</sub> Excited State of Directly Linked Porphyrin-Imide Dyads and Its Solvent-Polarity Dependencies. *J. Am. Chem. Soc.* **2001**, *123*, 12422–12423.
- (112) Napper, A. M.; Head, N. J.; Oliver, A. M.; Shephard, M. J.; Paddon-Row, M. N.; Read, I.; Waldeck, D. H. Use of U-Shaped Donor-Bridge-Acceptor Molecules to Study Electron Tunneling through Nonbonded Contacts. *J. Am. Chem. Soc.* **2002**, *124*, 10171–10181.
- (113) Adams, D. M.; Brus, L.; Chidsey, C. E. D.; Creager, S.; Creutz, C.; Kagan, C. R.; Kamat, P. V.; Lieberman, M.; Lindsay, S.; Marcus, R. A.; et al. Charge Transfer in the Nanoscale: Current Status. *J. Phys. Chem. B* **2003**, *107*, 6668–6697.
- (114) Albinsson, B.; Mårtensson, J. Long-Range Electron and Excitation Energy Transfer in Donor-Bridge-Acceptor Systems. *J. Photochem. Photobiol., C* **2008**, *9*, 138–155.
- (115) Song, H.-e.; Kirmaier, C.; Taniguchi, M.; Diers, J. R.; Bocian, D. F.; Lindsey, J. S.; Holten, D. Determination of Ground-State Hole Transfer Rates between Equivalent Sites in Oxidized Multiporphyrin Arrays Using Time-Resolved Optical Spectroscopy. *J. Am. Chem. Soc.* **2008**, *130*, 15636–15648.
- (116) Lemmetyinen, H.; Tkachenko, N. V.; Efimov, A.; Niemi, M. Photoinduced Intra- and Intermolecular Electron Transfer in Solutions and in Solid Organized Molecular Assemblies. *Phys. Chem. Chem. Phys.* **2011**, *13*, 397–412.
- (117) Wenger, O. S. How Donor-Bridge-Acceptor Energetics Influence Electron Tunneling Dynamics and Their Distance Dependences. *Acc. Chem. Res.* **2011**, *44*, 25–35.
- (118) Natali, M.; Campagna, S.; Scandola, F. Photoinduced Electron Transfer across Molecular Bridges: Electron- and Hole-Transfer Superexchange Pathways. *Chem. Soc. Rev.* **2014**, *43*, 4005–4018.
- (119) Delor, M.; Sazanovich, I. V.; Towrie, M.; Weinstein, J. A. Probing and Exploiting the Interplay between Nuclear and Electronic Motion in Charge Transfer Processes. *Acc. Chem. Res.* **2015**, *48*, 1131–1139.
- (120) Hung, S.-C.; Macpherson, A. N.; Lin, S.; Liddell, P. A.; Seely, G. R.; Moore, A. L.; Moore, T. A.; Gust, D. Photoinduced Electron and Proton Transfer in a Molecular Triad. *Adv. Chem. Ser.* **1998**, *254*, 177–218.
- (121) Guldi, D. M. Fullerene-Porphyrin Architecture; Photosynthetic Antenna and Reaction Center Model. *Chem. Soc. Rev.* **2002**, *31*, 22–36.
- (122) Holten, D.; Bocian, D. F.; Lindsey, J. S. Probing Electronic Communication in Covalently Linked Multiporphyrin Arrays. A Guide to the Rational Design of Molecular Photonics Devices. *Acc. Chem. Res.* **2002**, *35*, 57–69.
- (123) Wasielewski, M. R. Energy, Charge, and Spin Transport in Molecules and Self-Assembled Nanostructures Inspired by Photosynthesis. *J. Org. Chem.* **2006**, *71*, 5051–5066.
- (124) Balzani, V.; Credi, A.; Venturi, M. Light Powered Molecular Machines. *Chem. Soc. Rev.* **2009**, *38*, 1542–1550.
- (125) Bottari, G.; de la Torre, G.; Guldi, D. M.; Torres, T. Covalent and Noncovalent Phthalocyanine–Carbon Nanostructure Systems: Synthesis, Photoinduced Electron Transfer, and Application to Molecular Photovoltaics. *Chem. Rev.* **2010**, *110*, 6768–6816.
- (126) Gust, D.; Moore, T. A.; Moore, A. L. Solar Fuels via Artificial Photosynthesis. *Acc. Chem. Res.* **2009**, *42*, 1890–1898.
- (127) Wasielewski, M. R. M. Self-Assembly Strategies for Integrating Light Harvesting and Charge Separation in Artificial Photosynthetic Systems. *Acc. Chem. Res.* **2009**, *42*, 1910–1921.
- (128) D'Souza, F.; Ito, O. Supramolecular Donor-Acceptor Hybrids of Porphyrins/Phthalocyanines with Fullerenes/Carbon Nanotubes: Electron Transfer, Sensing, Switching, and Catalytic Applications. *Chem. Commun.* **2009**, 4913–4928.
- (129) Bottari, G.; Trukhina, O.; Ince, M.; Torres, T. Towards Artificial Photosynthesis: Supramolecular, Donor-Acceptor, Porphyrin- and Phthalocyanine/Carbon Nanostructure Ensembles. *Coord. Chem. Rev.* **2012**, *256*, 2453–2477.
- (130) Karlsson, S.; Boixel, J.; Pellegrin, Y.; Blart, E.; Becker, H.-C.; Odobel, F.; Hammarström, L. Accumulative Electron Transfer: Multiple Charge Separation in Artificial Photosynthesis. *Faraday Discuss.* **2012**, *155*, 233–252.
- (131) Fukuzumi, S.; Ohkubo, K. Assemblies of Artificial Photosynthetic Reaction Centers. *J. Mater. Chem.* **2012**, *22*, 4575–4587.
- (132) Fukuzumi, S.; Ohkubo, K.; Suenobu, T. Long-Lived Charge Separation and Applications in Artificial Photosynthesis. *Acc. Chem. Res.* **2014**, *47*, 1455–1464.
- (133) Hush, N. S. Homogeneous and Heterogeneous Optical and Thermal Electron Transfer. *Electrochim. Acta* **1968**, *13*, 1005–1023.
- (134) Creutz, C. Mixed Valence Complexes of d<sub>5</sub>-d<sub>6</sub> Metal Centers. *Prog. Inorg. Chem.* **1983**, *30*, 1–73.
- (135) Brunschwig, B. S.; Creutz, C.; Sutin, N. Optical Transitions of Symmetrical Mixed-Valence Systems in the Class II-III Transition Regime. *Chem. Soc. Rev.* **2002**, *31*, 168–184.
- (136) Cave, R. J.; Castner, E. W., Jr. Time-Dependent DFT Investigation of the Ground and Excited States of Coumarins 102, 152, 153 and 343. *J. Phys. Chem. A* **2002**, *106*, 12117–12123.



- (137) Samanta, A.; Fessenden, R. W. Excited-State Dipole Moment of 7-Aminocoumarins as Determined from Time-Resolved Microwave Dielectric Absorption Measurements. *J. Phys. Chem. A* **2000**, *104*, 8577–8582.
- (138) Maroncelli, M. The Dynamics of Solvation in Polar Liquids. *J. Mol. Liq.* **1993**, *57*, 1–37.
- (139) Fleming, G. R.; Cho, M. Chromophore-Solvent Dynamics. *Annu. Rev. Phys. Chem.* **1996**, *47*, 109–134.
- (140) Glasbeek, M.; Zhang, H. Femtosecond Studies of Solvation and Intramolecular Configurational Dynamics of Fluorophores in Liquid Solution. *Chem. Rev.* **2004**, *104*, 1929–1954.
- (141) Bagchi, B.; Jana, B. Solvation Dynamics in Dipolar Liquids. *Chem. Soc. Rev.* **2010**, *39*, 1936–1954.
- (142) Reichardt, C. Solvatochromic Dyes as Solvent Polarity Indicators. *Chem. Rev.* **1994**, *94*, 2319–2358.
- (143) Machado, V. G.; Stock, R. I.; Reichardt, C. Pyridinium N-Phenolate Betaine Dyes. *Chem. Rev.* **2014**, *114*, 10429–10475.
- (144) Mente, S. R.; Maroncelli, M. Computer Simulations of the Solvatochromism of Betaine-30. *J. Phys. Chem. B* **1999**, *103*, 7704–7719.
- (145) Åkesson, E.; Walker, G. C.; Barbara, P. F. Dynamic Solvent Effects on Electron Transfer Rates in the Inverted Regime: Ultrafast Studies on the Betaines. *J. Chem. Phys.* **1991**, *95*, 4188–4194.
- (146) Barbara, P. F.; Walker, G. C.; Smith, T. P. Vibrational Modes and the Dynamic Solvent Effect in Electron and Proton Transfer. *Science* **1992**, *256*, 975–981.
- (147) Johnson, A. E.; Levinger, N. E.; Jarzeba, W.; Schlieff, R. E.; Kliner, D. A. V.; Barbara, P. F. Experimental and Theoretical Study of Inhomogeneous Electron Transfer in Betaine: Comparison of Measured and Predicted Spectral Dynamics. *Chem. Phys.* **1993**, *176*, 555–574.
- (148) Reid, P. J.; Barbara, P. F. Dynamic Solvent Effect on Betaine-30 Electron Transfer Kinetics in Alcohols. *J. Phys. Chem.* **1995**, *99*, 3554–3565.
- (149) Hogiu, S.; Werncke, W.; Pfeiffer, M.; Elsaesser, T. Mode Specific Vibrational Kinetics after Intermolecular Electron Transfer Studied by Picosecond Anti-Stokes Raman Spectroscopy. *Chem. Phys. Lett.* **1999**, *312*, 407.
- (150) Hogiu, S.; Werncke, W.; Pfeiffer, M.; Dreyer, J.; Elsaesser, T. Mode-Specific Vibrational Excitation and Energy Redistribution after Ultrafast Intramolecular Electron Transfer. *J. Chem. Phys.* **2000**, *113*, 1587–1594.
- (151) Werncke, W.; Wachsmann-Hogiu, S.; Dreyer, J.; Vodchits, A. I.; Elsaesser, T. Ultrafast Intramolecular Electron Transfer Studied by Picosecond and Stationary Raman Spectroscopy. *Bull. Chem. Soc. Jpn.* **2002**, *75*, 1049–1055.
- (152) McHale, J. L. Subpicosecond Solvent Dynamics in Charge-Transfer Transitions: Challenges and Opportunities in Resonance Raman Spectroscopy. *Acc. Chem. Res.* **2001**, *34*, 265–272.
- (153) Zhao, X.; Burt, J. A.; McHale, J. L. Resonance Raman Analysis of Nonlinear Solvent Dynamics: Betaine-30 in Ethanol. *J. Chem. Phys.* **2004**, *121*, 11195–11201.
- (154) Chen, H. Functional Mode Electron-Transfer Theory. *J. Phys. Chem. B* **2014**, *118*, 7586–7593.
- (155) Beard, M. C.; Turner, G. M.; Schmittenmaier, C. A. Measurement of Electromagnetic Radiation Emitted During Rapid Intramolecular Electron Transfer. *J. Am. Chem. Soc.* **2000**, *122*, 11541–11542.
- (156) Beard, M. C.; Turner, G. M.; Schmittenmaier, C. A. Measuring Intramolecular Charge Transfer via Coherent Generation of THz Radiation. *J. Phys. Chem. A* **2002**, *106*, 878–883.
- (157) Beard, M. C.; Turner, G. M.; Schmittenmaier, C. A. Transient Photoconductivity in GaAs as Measured by Time-Resolved Terahertz Spectroscopy. *Phys. Rev. B: Condens. Matter Mater. Phys.* **2000**, *62*, 15764–15777.
- (158) Baiz, C. R.; Kubarych, K. J. Ultrafast Vibrational Stark-Effect Spectroscopy: Exploring Charge-Transfer Reactions by Directly Monitoring the Solvation Shell Response. *J. Am. Chem. Soc.* **2010**, *132*, 12784–12785.
- (159) Kovalenko, S. A.; Eilers-König, N.; Senyushkina, T.; Ernsting, N. P. Charge Transfer and Solvation of Betaine-30 in Polar Solvents: A Femtosecond Broadband Transient Absorption Study. *J. Phys. Chem. A* **2001**, *105*, 4834–4843.
- (160) Lobaugh, J.; Rossky, P. J. Computer Simulation of the Excited State Dynamics of Betaine-30 in Acetonitrile. *J. Phys. Chem. A* **1999**, *103*, 9432–9447.
- (161) Ishida, T.; Rossky, P. J. Consequences of Strong Coupling between Solvation and Electronic Structure in the Excited State of a Betaine Dye. *J. Phys. Chem. B* **2008**, *112*, 11353–11360.
- (162) Kharlanov, V.; Rettig, W. Experimental and Theoretical Study of Excited-State Structure and Relaxation Processes of Betaine-30 and of Pyridinium Model Compounds. *J. Phys. Chem. A* **2009**, *113*, 10693–10703.
- (163) Ruchira Silva, W.; Frontiera, R. R. Excited State Structural Evolution During Charge-Transfer Reactions in Betaine-30. *Phys. Chem. Chem. Phys.* **2016**, *18*, 20290–20297.
- (164) Duvanel, G.; Grilj, J.; Chaumeil, H.; Jacques, P.; Vauthey, E. Ultrafast Excited-State Dynamics of a Series of Zwitterionic Pyridinium Phenoxides with Increasing Sterical Hindering. *Photochem. Photobiol. Sci.* **2010**, *9*, 908–915.
- (165) Boeglin, A.; Barsella, A.; Fort, A.; Mançois, F.; Rodriguez, V.; Diemer, V.; Chaumeil, H.; Defoin, A.; Jacques, P.; Carré, C. Optical Properties and Progressive Sterical Hindering in Pyridinium Phenoxides. *Chem. Phys. Lett.* **2007**, *442*, 298–301.
- (166) Letrun, R.; Koch, M.; Dekhtyar, M. L.; Kurdyukov, V. V.; Tolmachev, A. I.; Rettig, W.; Vauthey, E. Ultrafast Excited-State Dynamics of Donor–Acceptor Biaryls: Comparison between Pyridinium and Pyrilyum Phenolates. *J. Phys. Chem. A* **2013**, *117*, 13112–13126.
- (167) Mataga, N.; Yao, H.; Okada, T.; Rettig, W. Charge-Transfer Rates in Symmetric and Symmetry-Disturbed Derivatives of 9,9'-Bianthryl. *J. Phys. Chem.* **1989**, *93*, 3383–3386.
- (168) Grabner, G.; Rechthaler, K.; Köhler, G. Two-State Model for the Photophysics of 9,9'-Bianthryl. Fluorescence, Transient-Absorption, and Semiempirical Studies. *J. Phys. Chem. A* **1998**, *102*, 689–696.
- (169) Herbich, J.; Kapturkiewicz, A. Electronic Structure and Molecular Conformation in the Excited Charge Transfer Singlet States of 9-Acrydyl and Other Aryl Derivatives of Aromatic Amines. *J. Am. Chem. Soc.* **1998**, *120*, 1014–1029.
- (170) Piet, J. J.; Taylor, P. N.; Wegewijs, B. R.; Anderson, H. L.; Osuka, A.; Warman, J. M. Photoexcitations of Covalently Bridged Zinc Porphyrin Oligomers: Frenkel Versus Wannier-Mott Type Excitons. *J. Phys. Chem. B* **2001**, *105*, 97–104.
- (171) Grabowski, Z. R.; Rotkiewicz, K.; Rettig, W. Structural Changes Accompanying Intramolecular Electron Transfer: Focus on Twisted Intramolecular Charge-Transfer States and Structures. *Chem. Rev.* **2003**, *103*, 3899–4031.
- (172) Mohammed, O. F.; Vauthey, E. Ultrafast Excited-State Dynamics of Aminoperylene and of Its Protonated Form Observed by Femtosecond Absorption Spectroscopy. *Chem. Phys. Lett.* **2010**, *487*, 246–250.
- (173) Carlotti, B.; Kikaš, I.; Škorić, I.; Spalletti, A.; Elisei, F. Photophysics of Push–Pull Distyrylfurans, Thiophenes and Pyridines by Fast and Ultrafast Techniques. *ChemPhysChem* **2013**, *14*, 970–981.
- (174) López-Arteaga, R.; Stephansen, A. B.; Guarin, C. A.; Solling, T. I.; Peon, J. The Influence of Push–Pull States on the Ultrafast Intersystem Crossing in Nitroaromatics. *J. Phys. Chem. B* **2013**, *117*, 9947–9955.
- (175) Carlotti, B.; Benassi, E.; Cesaretti, A.; Fortuna, C. G.; Spalletti, A.; Barone, V.; Elisei, F. An Ultrafast Spectroscopic and Quantum Mechanical Investigation of Multiple Emissions in Push–Pull Pyridinium Derivatives Bearing Different Electron Donors. *Phys. Chem. Chem. Phys.* **2015**, *17*, 20981–20989.
- (176) Ghosh, R.; Nandi, A.; Palit, D. K. Solvent Sensitive Intramolecular Charge Transfer Dynamics in the Excited States of 4-N,N-Dimethylamino-4'-Nitrophenyl. *Phys. Chem. Chem. Phys.* **2016**, *18*, 7661–7671.

- (177) Safarzadeh-Amiri, A. A Time-Resolved Fluorescence Study of the Dynamic Stokes Shift of trans-4-Dimethylamino-4'-Cyanostilbene. *Chem. Phys. Lett.* **1986**, *125*, 272–278.
- (178) Gilabert, E.; Lapouyade, R.; Rullière, C. Dual Fluorescence in trans-4-Dimethylamino-4'-Cyanostilbene Revealed by Picosecond Time-Resolved Spectroscopy: A Possible New "Tict" Compound. *Chem. Phys. Lett.* **1988**, *145*, 262–268.
- (179) Gilabert, E.; Lapouyade, R.; Rullière, C. Time-Resolved Dual Fluorescence of Push–Pull Stilbenes at High Solute Concentration and Excitation Intensity: Evidence for an Emitting Bimer. *Chem. Phys. Lett.* **1991**, *185*, 82–87.
- (180) Lapouyade, R.; Czeschka, K.; Majenz, W.; Rettig, W.; Gilabert, E.; Rullière, C. Photophysics of Donor-Acceptor Substituted Stilbenes. A Time-Resolved Fluorescence Study Using Selectively Bridged Dimethylamino Cyano Model Compounds. *J. Phys. Chem.* **1992**, *96*, 9643–9650.
- (181) Abraham, E.; Oberlé, J.; Jonusauskas, G.; Lapouyade, R.; Minoshima, K.; Rullière, C. Picosecond Time-Resolved Dual Fluorescence, Transient Absorption and Reorientation Time Measurements of Push-Pull Diphenyl-Polyenes: Evidence for 'Loose' Complex and 'Bimer' Species. *Chem. Phys.* **1997**, *219*, 73–89.
- (182) Eilers-König, N.; Kühne, T.; Schwarzer, D.; Vöhringer, P.; Schroeder, J. Femtosecond Dynamics of Intramolecular Charge Transfer in 4-Dimethylamino-4'-Cyanostilbene in Polar Solvents. *Chem. Phys. Lett.* **1996**, *253*, 69–76.
- (183) Kovalenko, S. A.; Schanz, R.; Senyushkina, T. A.; Ernstring, N. P. Femtosecond Spectroscopy of p-Dimethylaminocyanostilbene in Solution—No Evidence for Dual Fluorescence. *Phys. Chem. Chem. Phys.* **2002**, *4*, 703–707.
- (184) Arzhantsev, S.; Zachariasse, K. A.; Maroncelli, M. Photophysics of trans-4-(Dimethylamino)-4'-Cyanostilbene and Its Use as a Solvation Probe. *J. Phys. Chem. A* **2006**, *110*, 3454–3470.
- (185) Meyer, M.; Mialocq, J. C. Ground State and Singlet Excited State of Laser Dye DCM: Dipole Moments and Solvent Induced Spectral Shifts. *Opt. Commun.* **1987**, *64*, 264–268.
- (186) Easter, D. C.; Baranavski, A. P. Ultrafast Relaxation in the Fluorescent State of the Laser Dye DCM. *Chem. Phys. Lett.* **1993**, *201*, 153–158.
- (187) Martin, M. M.; Plaza, P.; Meyer, Y. H. Ultrafast Intramolecular Charge Transfer in the Merocyanine Dye DCM. *Chem. Phys.* **1995**, *192*, 367–377.
- (188) Rettig, W.; Majenz, W. Competing Adiabatic Photoreaction Channels in Stilbene Derivatives. *Chem. Phys. Lett.* **1989**, *154*, 335–341.
- (189) Gustavsson, T.; Baldacchino, G.; Mialocq, J. C.; Pommeret, S. A Femtosecond Fluorescence up-Conversion Study of the Dynamic Stokes Shift of the DCM Dye Molecule in Polar and Non-Polar Solvents. *Chem. Phys. Lett.* **1995**, *236*, 587–594.
- (190) van der Meulen, P.; Zhang, H.; Jonkman, A. M.; Glasbeek, M. Subpicosecond Solvation Relaxation of 4-(Dicyanomethylene)-2-Methyl-6-(p-(Dimethylamino)Styryl)-4h-Pyran in Polar Liquids. *J. Phys. Chem.* **1996**, *100*, 5367–5373.
- (191) Kovalenko, S. A.; Ernstring, N. P.; Ruthmann, J. Femtosecond Hole-Burning Spectroscopy of the Dye DCM in Solution: The Transition from the Locally Excited to a Charge-Transfer State. *Chem. Phys. Lett.* **1996**, *258*, 445–454.
- (192) Boldrini, B.; Cavalli, E.; Painelli, A.; Terenziani, F. Polar Dyes in Solution: A Joint Experimental and Theoretical Study of Absorption and Emission Band Shapes. *J. Phys. Chem. A* **2002**, *106*, 6286–6294.
- (193) Van Tassel, A. J.; Prantl, M. A.; Fleming, G. R. Investigation of the Excited State Structure of DCM via Ultrafast Electronic Pump/Vibrational Probe. *J. Phys. Chem. B* **2006**, *110*, 18989–18995.
- (194) Petsalakis, I. D.; Georgiadou, D. G.; Vasilopoulou, M.; Pistolis, G.; Dimotikali, D.; Argitis, P.; Theodorakopoulos, G. Theoretical Investigation on the Effect of Protonation on the Absorption and Emission Spectra of Two Amine-Group-Bearing, Red "Push–Pull" Emitters, 4-Dimethylamino-4'-Nitrostilbene and 4-(Dicyanomethylene)-2-Methyl-6-P-(Dimethylamino) Styryl-4h-Pyran, by DFT and TDDFT Calculations. *J. Phys. Chem. A* **2010**, *114*, 5580–5587.
- (195) Lewis, N. H. C.; Dong, H.; Oliver, T. A. A.; Fleming, G. R. Measuring Correlated Electronic and Vibrational Spectral Dynamics Using Line Shapes in Two-Dimensional Electronic-Vibrational Spectroscopy. *J. Chem. Phys.* **2015**, *142*, 174202.
- (196) Terenziani, F.; Painelli, A. Two-Dimensional Electronic-Vibrational Spectra: Modeling Correlated Electronic and Nuclear Motion. *Phys. Chem. Chem. Phys.* **2015**, *17*, 13074–13081.
- (197) Oliver, T. A. A.; Lewis, N. H. C.; Fleming, G. R. Correlating the Motion of Electrons and Nuclei with Two-Dimensional Electronic-Vibrational Spectroscopy. *Proc. Natl. Acad. Sci. U. S. A.* **2014**, *111*, 10061–10066.
- (198) Oliver, T. A. A.; Lewis, N. H. C.; Fleming, G. R. Correction for Oliver Et Al., Correlating the Motion of Electrons and Nuclei with Two-Dimensional Electronic-Vibrational Spectroscopy. *Proc. Natl. Acad. Sci. U. S. A.* **2014**, *111*, 16628–16628.
- (199) Lippert, E.; Lüder, W.; Moll, F.; Nägele, W.; Boos, H.; Prigge, H.; Seibold-Blankenstein, I. Umwandlung von Elektronenanregungsenergie. *Angew. Chem.* **1961**, *73*, 695–706.
- (200) Rotkiewicz, K.; Grellmann, K. H.; Grabowski, Z. R. Reinterpretation of the Anomalous Fluorescence of p,N,N-Dimethylamino-Benzointrile. *Chem. Phys. Lett.* **1973**, *19*, 315–318.
- (201) Leinhos, U.; Kuehnle, W.; Zachariasse, K. A. Intramolecular Charge Transfer and Thermal Exciplex Dissociation with p-Aminobenzonitriles in Toluene. *J. Phys. Chem.* **1991**, *95*, 2013–2021.
- (202) Zachariasse, K. A. Comment on 'Pseudo-Jahn-Teller and Tict-Models: A Photophysical Comparison of Meta- and Para-DMABN Derivatives' [Chem. Phys. Lett. 305 (1999) 8]: The PICT Model for Dual Fluorescence of Aminobenzonitriles. *Chem. Phys. Lett.* **2000**, *320*, 8–13.
- (203) Yoshihara, T.; Druzhinin, S. I.; Zachariasse, K. A. Fast Intramolecular Charge Transfer with a Planar Rigidized Electron Donor/Acceptor Molecule. *J. Am. Chem. Soc.* **2004**, *126*, 8535–8539.
- (204) Schuddeboom, W.; Jonker, S. A.; Warman, J. M.; Leinhos, U.; Kuehnle, W.; Zachariasse, K. A. Excited-State Dipole Moments of Dual Fluorescent 4-(Dialkylamino)Benzonitriles: Influence of Alkyl Chain Length and Effective Solvent Polarity. *J. Phys. Chem.* **1992**, *96*, 10809–10819.
- (205) Gorse, A.-D.; Pesquer, M. Intramolecular Charge Transfer Excited State Relaxation Processes in Para-Substituted N,N-Dimethylaniline: A Theoretical Study Including Solvent Effects. *J. Phys. Chem.* **1995**, *99*, 4039–4049.
- (206) Sobolewski, A. L.; Domcke, W. Charge Transfer in Aminobenzonitriles: Do They Twist? *Chem. Phys. Lett.* **1996**, *250*, 428–436.
- (207) Sobolewski, A. L.; Sudholt, W.; Domcke, W. Ab Initio Investigation of Reaction Pathways for Intramolecular Charge Transfer in Dimethylanilino Derivatives. *J. Phys. Chem. A* **1998**, *102*, 2716–2722.
- (208) Chudoba, C.; Kummrow, A.; Dreyer, J.; Stenger, J.; Nibbering, E. T. J.; Elsaesser, T.; Zachariasse, K. A. Excited State Structure of 4-(Dimethylamino)Benzonitrile Studied by Femtosecond Mid-Infrared Spectroscopy and Ab Initio Calculations. *Chem. Phys. Lett.* **1999**, *309*, 357–363.
- (209) Druzhinin, S. I.; Ernstring, N. P.; Kovalenko, S. A.; Lustres, L. P.; Senyushkina, T. A.; Zachariasse, K. A. Dynamics of Ultrafast Intramolecular Charge Transfer with 4-(Dimethylamino)Benzonitrile in Acetonitrile. *J. Phys. Chem. A* **2006**, *110*, 2955–2969.
- (210) Galievsky, V. A.; Druzhinin, S.; Demeter, A.; Jiang, Y.-B.; Kovalenko, S. A.; Lustres, J. L. P.; Venugopal, K.; Ernstring, N. P.; Allonas, X.; Noltemeyer, M.; et al. Ultrafast Intramolecular Charge Transfer and Internal Conversion with Tetrafluoro-Aminobenzonitriles. *ChemPhysChem* **2005**, *6*, 2307–2323.
- (211) Rhinehart, J. M.; Challa, J. R.; McCamant, D. W. Multimode Charge-Transfer Dynamics of 4-(Dimethylamino)Benzonitrile Probed with Ultraviolet Femtosecond Stimulated Raman Spectroscopy. *J. Phys. Chem. B* **2012**, *116*, 10522–10534.
- (212) Park, M.; Kim, C. H.; Joo, T. Multifaceted Ultrafast Intramolecular Charge Transfer Dynamics of 4-(Dimethylamino)-Benzonitrile (DMABN). *J. Phys. Chem. A* **2013**, *117*, 370–377.

- (213) Pigliucci, A.; Vauthey, E.; Rettig, W. Entropic Effects in Excited State CT Reactions. *Chem. Phys. Lett.* **2009**, *469*, 115–120.
- (214) Gomez, I.; Reguero, M.; Boggio-Pasqua, M.; Robb, M. A. Intramolecular Charge Transfer in 4-Aminobenzonitriles Does Not Necessarily Need the Twist. *J. Am. Chem. Soc.* **2005**, *127*, 7119–7129.
- (215) Park, M.; Im, D.; Rhee, Y. H.; Joo, T. Coherent and Homogeneous Intramolecular Charge-Transfer Dynamics of 1-Tert-Butyl-6-Cyano-1,2,3,4-Tetrahydroquinoline (NTC6), a Rigid Analogue of DMABN. *J. Phys. Chem. A* **2014**, *118*, 5125–5134.
- (216) Perveaux, A.; Castro, P. J.; Lauvergnat, D.; Reguero, M.; Lasorne, B. Intramolecular Charge Transfer in 4-Aminobenzonitrile Does Not Need the Twist and May Not Need the Bend. *J. Phys. Chem. Lett.* **2015**, *6*, 1316–1320.
- (217) Kosower, E. M. Intramolecular Donor-Acceptor Systems. 9. Photophysics of (Phenylamino)Naphthalenesulfonates: A Paradigm for Excited-State Intramolecular Charge Transfer. *Acc. Chem. Res.* **1982**, *15*, 259–266.
- (218) Kosower, E. M.; Huppert, D. Solvent Motion Controls the Rate of Intramolecular Electron Transfer in Solution. *Chem. Phys. Lett.* **1983**, *96*, 433–435.
- (219) Heitele, H.; Michel-Beyerle, M. E.; Finckh, P. The Influence of Dielectric Relaxation on Intramolecular Electron Transfer. *Chem. Phys. Lett.* **1987**, *138*, 237–243.
- (220) Masad, A.; Huppert, D.; Kosower, E. M. The Transition from Non-Adiabatic to Solvent Controlled Adiabatic Electron Transfer Kinetics. *Chem. Phys.* **1990**, *144*, 391–400.
- (221) Huppert, D.; Ittah, V.; Masad, A.; Kosower, E. M. Fast Non-Exponential Intramolecular Electron Transfer Reactions in Pentanediol Solutions. *Chem. Phys. Lett.* **1988**, *150*, 349–356.
- (222) Su, S. G.; Simon, J. D. Non-Equilibrium and Non-Adiabatic Effects on Excited State Electron Transfer Reactions in Solutions. *Chem. Phys. Lett.* **1989**, *158*, 423–428.
- (223) Simon, J. D.; Su, S. G. Effect of Viscosity and Rotor Size on the Dynamics of Twisted Intramolecular Charge Transfer. *J. Phys. Chem.* **1990**, *94*, 3656–3660.
- (224) Schneider, F.; Lippert, E. Electron Spectra and Electron Structure of 9,9'-Bianthryl. *Ber. Bunsenges. Phys. Chem.* **1968**, *72*, 1155–1160.
- (225) Kahlow, M. A.; Kang, T. J.; Barbara, P. F. Electron-Transfer Times Are Not Equal to Longitudinal Relaxation Times in Polar Aprotic Solvents. *J. Phys. Chem.* **1987**, *91*, 6452–6455.
- (226) Kang, T. J.; Kahlow, M. A.; Giser, D.; Swallen, S.; Nagarajan, V.; Jarzeba, W.; Barbara, P. F. Dynamic Solvent Effects in the Electron Transfer Kinetics of S<sub>1</sub> Bianthryl. *J. Phys. Chem.* **1988**, *92*, 6800–6807.
- (227) Horng, M. L.; Gardecki, J. A.; Maroncelli, M. Rotational Dynamics of Coumarin 153: Time Dependent Friction, Dielectric Friction and Other Non-Hydrodynamic Effects. *J. Phys. Chem. A* **1997**, *101*, 1030.
- (228) Kang, T. J.; Jarzeba, W.; Barbara, P. F.; Fonseca, T. A. Photodynamical Model for the Excited State Electron Transfer of Bianthryl and Related Molecules. *Chem. Phys.* **1990**, *149*, 81–95.
- (229) Mataga, N.; Nishikawa, S.; Okada, T. Torsional Relaxation from Perpendicular and Tilted Configurations in the Intramolecular Charge Transfer of Excited 9,9'-Bianthryl as Studied by fs-ps Time Resolved Absorption Spectral Measurements in Solution. *Chem. Phys. Lett.* **1996**, *257*, 327–332.
- (230) Jurczok, M.; Plaza, P.; Rettig, W.; Martin, M. M. Ultrafast Electron Transfer in Acceptor Substituted Bianthryl Derivatives. *Chem. Phys.* **2000**, *256*, 137–148.
- (231) Jurczok, M.; Gustavsson, T.; Mialocq, J.-C.; Rettig, W. Electron Transfer and Solvation in 9,9'-Bianthryl and Derivatives: A Sub-ps Fluorescence Upconversion Study. *Chem. Phys. Lett.* **2001**, *344*, 357–366.
- (232) Kovalenko, S. A.; Lustres, J. L. P.; Ernstring, N. P.; Rettig, W. Photoinduced Electron Transfer in Bianthryl and Cyanobianthryl in Solution: The Case for a High-Frequency Intramolecular Reaction Coordinate. *J. Phys. Chem. A* **2003**, *107*, 10228–10232.
- (233) Takaya, T.; Hamaguchi, H.-o.; Kuroda, H.; Iwata, K. Femtosecond Electron Transfer Dynamics of 9,9'-Bianthryl in Acetonitrile as Studied by Time-Resolved near-Infrared Absorption Spectroscopy. *Chem. Phys. Lett.* **2004**, *399*, 210–214.
- (234) Takaya, T.; Saha, S.; Hamaguchi, H.; Sarkar, M.; Samanta, A.; Iwata, K. Charge Resonance Character in the Charge Transfer State of Bianthryls: Effect of Symmetry Breaking on Time-Resolved near-IR Absorption Spectra. *J. Phys. Chem. A* **2006**, *110*, 4291–4295.
- (235) Takaya, T.; Hamaguchi, H.; Iwata, K. Femtosecond Time-Resolved Absorption Anisotropy Spectroscopy on 9, 9'-Bianthryl: Detection of Partial Intramolecular Charge Transfer in Polar and Nonpolar Solvents. *J. Chem. Phys.* **2009**, *130*, 014501.
- (236) van Duijnen, P. T.; Zijlstra, R. W. J.; Grozema, F. C.; Swart, M.; Feringa, B. L. Solvent Induced Charge Separation in the Excited States of Symmetrical Ethylene: A Direct Reaction Field Study. *J. Phys. Chem. A* **2001**, *105*, 3583–3590.
- (237) Giaimo, J. M.; Gusev, A. V.; Wasielewski, M. R. Excited-State Symmetry Breaking in Cofacial and Linear Dimers of a Green Perylenediimide Chlorophyll Analogue Leading to Ultrafast Charge Separation. *J. Am. Chem. Soc.* **2002**, *124*, 8530–8531.
- (238) Fuller, M. J.; Gusev, A. V.; Wasielewski, M. R. Ultrafast Charge Separation Due to Excited State Symmetry Breaking in Dimers of Push-Pull Perylenes. *Isr. J. Chem.* **2004**, *44*, 101–108.
- (239) Holman, M. W.; Yan, P.; Adams, D. M.; Westenhoff, S.; Silva, C. Ultrafast Spectroscopy of the Solvent Dependence of Electron Transfer in a Perylenebisimide Dimer. *J. Phys. Chem. A* **2005**, *109*, 8548–8552.
- (240) Markovic, V.; Villamaina, D.; Barabanov, I.; Daku, L. M. L.; Vauthey, E. Photoinduced Symmetry-Breaking Charge Separation: The Direction of the Charge Transfer. *Angew. Chem., Int. Ed.* **2011**, *50*, 7596–7598.
- (241) Lindquist, R. J.; Lefler, K. M.; Brown, K. E.; Dyar, S. M.; Margulies, E. A.; Young, R. M.; Wasielewski, M. R. Energy Flow Dynamics within Cofacial and Slip-Stacked Perylene-3,4-Dicarboximide Dimer Models of  $\Pi$ -Aggregates. *J. Am. Chem. Soc.* **2014**, *136*, 14912–14923.
- (242) Vauthey, E. Photoinduced Symmetry-Breaking Charge Separation. *ChemPhysChem* **2012**, *13*, 2001–2011.
- (243) Okada, T.; Kawai, M.; Ikemachi, T.; Mataga, N.; Sakata, Y.; Misumi, S.; Shionoya, S. Picosecond Laser Spectroscopy of Dual Excited Electronic States of 4-(9-Anthryl)-N,N-Dimethylaniline. *J. Phys. Chem.* **1984**, *88*, 1976–1981.
- (244) Siemiarz, A.; Grabowski, Z. R.; Krówczyński, A.; Asher, M.; Ottolenghi, M. Two Emitting States of Excited Pp-(9-Anthryl)-N,N-Dimethylaniline Derivatives in Polar Solvents. *Chem. Phys. Lett.* **1977**, *51*, 315–320.
- (245) Huppert, D.; Rentzepis, P. M. Pressure Dependence on Excited State Intramolecular Electron Transfer Dynamics in Polar Solvents. *J. Phys. Chem.* **1988**, *92*, 5466–5469.
- (246) Tominaga, K.; Walker, G. C.; Jarzeba, W.; Barbara, P. F. Ultrafast Charge Separation in ADMA: Experiment, Simulation, and Theoretical Issues. *J. Phys. Chem.* **1991**, *95*, 10475–10485.
- (247) Tominaga, K.; Walker, G. C.; Kang, T. J.; Barbara, P. F.; Fonseca, T. Reaction Rates in the Phenomenological Adiabatic Excited-State Electron-Transfer Theory. *J. Phys. Chem.* **1991**, *95*, 10485–10492.
- (248) Techert, S.; Schmatz, S.; Wiessner, A.; Staerk, H. Photo-physical Characteristics of Directly Linked Pyrene-Dimethylaniline Derivatives. *J. Phys. Chem. A* **2000**, *104*, 5700–5710.
- (249) Banerji, N.; Angulo, G.; Barabanov, I. I.; Vauthey, E. Intramolecular Charge-Transfer Dynamics in Covalently Linked Perylene-Dimethylaniline and Cyanoperylene-Dimethylaniline. *J. Phys. Chem. A* **2008**, *112*, 9665–9674.
- (250) Martin, M. M.; Plaza, P.; Chagnenet-Barret, P.; Siemiarz, A. UV-Vis Subpicosecond Spectroscopy of 4-(9-Anthryl)-N,N'-Dimethylaniline in Polar and Nonpolar Solvents: A Two-Dimensional View of the Photodynamics. *J. Phys. Chem. A* **2002**, *106*, 2351–2358.
- (251) Baigar, E.; Gilch, P.; Zinth, W.; Stöckl, M.; Härter, P.; von Feilitzsch, T.; Michel-Beyerle, M. E. Ultrafast Intramolecular Electron Transfer from a Ferrocene Donor Moiety to a Nile Blue Acceptor. *Chem. Phys. Lett.* **2002**, *352*, 176.



- (252) Kubo, M.; Mori, Y.; Otani, M.; Murakami, M.; Ishibashi, Y.; Yasuda, M.; Hosomizu, K.; Miyasaka, H.; Imahori, H.; Nakashima, S. Coherent Nuclear Dynamics in Ultrafast Electron Transfer in a Porphyrin-Ferrocene Dyad. *Chem. Phys. Lett.* **2006**, *429*, 91–96.
- (253) Bizjak, T.; Karpiuk, J.; Lochbrunner, S.; Riedle, E. 50-fs Photoinduced Intramolecular Charge Separation in Triphenylmethane Lactones. *J. Phys. Chem. A* **2004**, *108*, 10763–10769.
- (254) Tkachenko, N. V.; Lemmetyinen, H.; Sonoda, J.; Ohkubo, K.; Sato, T.; Imahori, H.; Fukuzumi, S. Ultrafast Photodynamics of Exciplex Formation and Photoinduced Electron Transfer in Porphyrin-Fullerene Dyads Linked at Close Proximity. *J. Phys. Chem. A* **2003**, *107*, 8834–8844.
- (255) Oseki, Y.; Fujitsuka, M.; Cho, D. W.; Sugimoto, A.; Tojo, S.; Majima, T. Ultrafast Photoinduced Intramolecular Charge Separation and Recombination Processes in the Oligothiophene-Substituted Benzene Dyads with an Amide Spacer. *J. Phys. Chem. B* **2005**, *109*, 19257–19262.
- (256) Sartin, M. M.; Huang, C.; Marshall, A. S.; Makarov, N.; Barlow, S.; Marder, S. R.; Perry, J. W. Nonlinear Optical Pulse Suppression via Ultrafast Photoinduced Electron Transfer in an Aggregated Perylene Diimide/Oligothiophene Molecular Triad. *J. Phys. Chem. A* **2014**, *118*, 110–121.
- (257) Dyar, S. M.; Smeigh, A. L.; Karlen, S. D.; Young, R. M.; Wasielewski, M. R. Photo-Initiated Multi-Step Electron Transfer in Donor-Acceptor Systems Using a Novel Bi-Functionalized Perylene Chromophore. *Chem. Phys. Lett.* **2015**, *629*, 23–28.
- (258) Bandi, V.; Gobeze, H. B.; D'Souza, F. Ultrafast Photoinduced Electron Transfer and Charge Stabilization in Donor-Acceptor Dyads Capable of Harvesting near-Infrared Light. *Chem. - Eur. J.* **2015**, *21*, 11483–11494.
- (259) Okada, T.; Migita, M.; Mataga, N.; Sakata, Y.; Misumi, S. Picosecond Laser Spectroscopy of Intramolecular Heteroexcimer Systems. Time-Resolved Absorption Studies of p-(CH<sub>3</sub>NC<sub>6</sub>H<sub>4</sub>(CH<sub>2</sub>), (1-Pyrenyl) and -(9-Anthryl) Systems. *J. Am. Chem. Soc.* **1981**, *103*, 4715–4720.
- (260) Swinnen, A. M.; Van der Auweraer, M.; de Schryver, F. C.; Makatani, K.; Okada, T.; Mataga, M. Photophysics of the Intramolecular Exciplex Formation in W-(1-Pyrenyl)-Alpha,N,N-Dimethylaminoalkanes. *J. Am. Chem. Soc.* **1987**, *109*, 321–330.
- (261) Banerji, N.; Fürstenberg, A.; Bhosale, S.; Sisson, A. L.; Sakai, N.; Matile, S.; Vauthey, E. Ultrafast Photoinduced Charge Separation in Naphthalene Diimide Based Multichromophoric Systems in Liquid Solutions and in a Lipid Membrane. *J. Phys. Chem. B* **2008**, *112*, 8912–8922.
- (262) Banerji, N.; Duvanel, G.; Perez-Velasco, A.; Maity, S.; Sakai, N.; Matile, S.; Vauthey, E. Excited-State Dynamics of Hybrid Multichromophoric Systems: Toward an Excitation Wavelength Control of the Charge Separation Pathways. *J. Phys. Chem. A* **2009**, *113*, 8202–8212.
- (263) Yushchenko, O.; Villamaina, D.; Sakai, N.; Matile, S.; Vauthey, E. Comparison of Charge-Transfer Dynamics of Naphthalenediimide Triads in Solution and II-Stack Architectures on Solid Surfaces. *J. Phys. Chem. C* **2015**, *119*, 14999–15008.
- (264) Siemiarczuk, A.; Wagner, B. D.; Ware, W. R. Comparison of the Maximum Entropy and Exponential Series Methods for the Recovery of Distributions of Lifetimes from Fluorescence Lifetime Data. *J. Phys. Chem.* **1990**, *94*, 1661–1666.
- (265) Włodarczyk, J.; Kierdaszuk, B. Interpretation of Fluorescence Decays Using a Power-Like Model. *Biophys. J.* **2003**, *85*, 589–598.
- (266) Edholm, O.; Blomberg, C. Stretched Exponentials and Barrier Distributions. *Chem. Phys.* **2000**, *252*, 221–225.
- (267) Kao, Y.-T.; Guo, X.; Yang, Y.; Liu, Z.; Hassanali, A.; Song, Q.-H.; Wang, L.; Zhong, D. Ultrafast Dynamics of Nonequilibrium Electron Transfer in Photoinduced Redox Cycle: Solvent Mediation and Conformation Flexibility. *J. Phys. Chem. B* **2012**, *116*, 9130–9140.
- (268) Rubtsov, I. V.; Redmore, N. P.; Hochstrasser, R. M.; Therien, M. J. Interrogating Conformationally Dependent Electron-Transfer Dynamics via Ultrafast Visible Pump/IR Probe Spectroscopy. *J. Am. Chem. Soc.* **2004**, *126*, 2684–2685.
- (269) Duvanel, G.; Banerji, N.; Vauthey, E. Excited-State Dynamics of Donor-Acceptor Bridged Systems Containing a Boron-Dipyrromethene Chromophore: Interplay between Charge Separation and Reorientational Motion. *J. Phys. Chem. A* **2007**, *111*, 5361–5369.
- (270) Wiederrecht, G. P.; Watanabe, S.; Wasielewski, M. R. Solvent Effects on the Energetics and Dynamics of Ultrafast Electron Transfer in Chlorophyll-Porphyrin-Acceptor Triads. *Chem. Phys.* **1993**, *176*, 601–614.
- (271) Macpherson, A. N.; Liddell, P. A.; Lin, S.; Noss, L.; Seely, G. R.; DeGraziano, J. M.; Moore, A. L.; Moore, T. A.; Gust, D. Ultrafast Photoinduced Electron Transfer in Rigid Porphyrin-Quinone Dyads. *J. Am. Chem. Soc.* **1995**, *117*, 7202–7212.
- (272) Wiederrecht, G. P.; Niemczyk, M. P.; Svec, W. A.; Wasielewski, M. R. Ultrafast Photoinduced Electron Transfer in a Chlorophyll-Based Triad: Vibrationally Hot Ion Pair Intermediates and Dynamic Solvent Effect. *J. Am. Chem. Soc.* **1996**, *118*, 81–88.
- (273) Longuet-Higgins, H. C.; Beer, M. Anomalous Light Emission of Azulene. *J. Chem. Phys.* **1955**, *23*, 1390–1391.
- (274) Birks, J. B. The Photophysics of Azulene. *Chem. Phys. Lett.* **1972**, *17*, 370–372.
- (275) Gurzadyan, G. G.; Tran-Thi, T.-H.; Gustavsson, T. Time-Resolved Fluorescence Spectroscopy of High-Lying Electronic States of Zn-Tetraphenylporphyrin. *J. Chem. Phys.* **1998**, *108*, 385–388.
- (276) Yu, H.-Z.; Baskin, J. S.; Zewail, A. H. Ultrafast Dynamics of Porphyrins in the Condensed Phase: II. Zinc Tetraphenylporphyrin. *J. Phys. Chem. A* **2002**, *106*, 9845–9854.
- (277) Mataga, N.; Chosrowjan, H.; Taniguchi, S.; Shibata, Y. Ultrafast Charge Separation from the S<sub>2</sub> Excited State of Directly Linked Porphyrin-Imide Dyads: First Unequivocal Observation of the Whole Bell-Shaped Energy-Gap Law and Its Solvent Dependencies. *J. Phys. Chem. A* **2002**, *106*, 12191–12201.
- (278) Mataga, N.; Taniguchi, S.; Chosrowjan, H.; Osuka, A.; Kurotoby, K. Observations of the Whole Bell-Shaped Energy Gap Law in the Intra-Molecular Charge Separation (CS) from S<sub>2</sub> State of Directly Linked Zn-Porphyrin-Imide Dyads: Examinations of Wider Range of Energy Gap for the Cs Rates in Normal Regions. *Chem. Phys. Lett.* **2005**, *403*, 163–168.
- (279) Wallin, S.; Monnereau, C.; Blart, E.; Gankou, J.-R.; Odobel, F.; Hammarström, L. State-Selective Electron Transfer in an Unsymmetric Acceptor–Zn(II)Porphyrin–Acceptor Triad: Toward a Controlled Directionality of Electron Transfer from the Porphyrin S<sub>2</sub> and S<sub>1</sub> States as a Basis for a Molecular Switch. *J. Phys. Chem. A* **2010**, *114*, 1709–1721.
- (280) Ionkin, V. N.; Ivanov, A. I. Numerical Simulations of Ultrafast Charge Separation Dynamics from Second Excited State of Directly Linked Zinc–Porphyrin–Imide Dyads and Ensuing Hot Charge Recombination into the First Excited State. *J. Phys. Chem. A* **2009**, *113*, 103–107.
- (281) Rogozina, M. V.; Ionkin, V. N.; Ivanov, A. I. What Factors Control Product Yield in Charge Separation Reaction from Second Excited State in Zinc-Porphyrin Derivatives? *J. Phys. Chem. A* **2012**, *116*, 1159–1167.
- (282) Feskov, S. V.; Ivanov, A. I. Efficiency of Intramolecular Charge Separation from the Second Excited State: Suppression of the Hot Charge Recombination by Electron Transfer to the Secondary Acceptor. *J. Phys. Chem. A* **2013**, *117*, 11479–11489.
- (283) Rogozina, M. V.; Ionkin, V. N.; Ivanov, A. I. Dynamics of Charge Separation from Second Excited State and Following Charge Recombination in Zinc-Porphyrin–Acceptor Dyads. *J. Phys. Chem. A* **2013**, *117*, 4564–4573.
- (284) Rogozina, M. V.; Ionkin, V. N.; Ivanov, A. I. Kinetics of Charge Separated State Population Produced by Intramolecular Electron Transfer Quenching of Second Excited State. *J. Photochem. Photobiol., A* **2015**, *301*, 55–61.
- (285) Cho, H. S.; Jeong, D. H.; Yoon, M.-C.; Kim, Y. H.; Kim, Y.-R.; Kim, D.; Jeoung, S. C.; Kim, S. K.; Aratani, N.; Shinmori, H.; et al. Excited-State Energy Transfer Processes in Phenylene- and Biphenylene-Linked and Directly-Linked Zinc(II) and Free-Base Hybrid Diporphyrins. *J. Phys. Chem. A* **2001**, *105*, 4200–4210.

- (286) Liu, X.; Tripathy, U.; Bhosale, S. V.; Langford, S. J.; Steer, R. P. Photophysics of Soret-Excited Tetrapyrroles in Solution. II. Effects of Perdeuteration, Substituent Nature and Position, and Macrocyclic Structure and Conformation in Zinc(II) Porphyrins. *J. Phys. Chem. A* **2008**, *112*, 8986–8998.
- (287) Villamaina, D.; Bhosale, S.; Langford, S. J.; Vauthey, E. Excited-State Dynamics of Porphyrin-Naphthalenediimide-Porphyrin Triads. *Phys. Chem. Chem. Phys.* **2013**, *15*, 1177–1187.
- (288) Gouterman, M. Optical Spectra and Electronic Structure of Porphyrins and Related Rings. In *The Porphyrins Vol. III*; Dolphin, D., Ed.; Academic Press: New York, 1978; pp 1–165.
- (289) Galli, C.; Wynne, K.; LeCours, S. M.; Therien, M. J.; Hochstrasser, R. M. Direct Measurement of Electronic Dephasing Using Anisotropy. *Chem. Phys. Lett.* **1993**, *206*, 493–499.
- (290) Wynne, K.; LeCours, S. M.; Galli, C.; Therien, M. J.; Hochstrasser, R. M. Porphyrin-Quinone Electron Transfer Revisited. The Role of Excited-State Degeneracy in Ultrafast Charge Transfer Reactions. *J. Am. Chem. Soc.* **1995**, *117*, 3749–3753.
- (291) Pillai, S.; Ravensbergen, J.; Antoniuk-Pablant, A.; Sherman, B. D.; van Grondelle, R.; Frese, R. N.; Moore, T. A.; Gust, D.; Moore, A. L.; Kennis, J. T. M. Carotenoids as Electron or Excited-State Energy Donors in Artificial Photosynthesis: An Ultrafast Investigation of a Carotenoporphyrin and a Carotenofullerene Dyad. *Phys. Chem. Chem. Phys.* **2013**, *15*, 4775–4784.
- (292) Kee, T. W. Femtosecond Pump–Push–Probe and Pump–Dump–Probe Spectroscopy of Conjugated Polymers: New Insight and Opportunities. *J. Phys. Chem. Lett.* **2014**, *5*, 3231–3240.
- (293) Debreczeny, M. P.; Svec, W. A.; Marsch, E. M.; Wasielewski, M. R. Femtosecond Optical Control of Charge Shift within Electron Donor-Acceptor Arrays: An Approach to Molecular Switches. *J. Am. Chem. Soc.* **1996**, *118*, 8174–8175.
- (294) Wan, C.; Xia, T.; Becker, H.-C.; Zewail, A. H. Ultrafast Unequilibrated Charge Transfer: A New Channel in the Quenching of Fluorescent Biological Probes. *Chem. Phys. Lett.* **2005**, *412*, 158–163.
- (295) Kang, Y. K.; Duncan, T. V.; Therien, M. J. Temperature-Dependent Mechanistic Transition for Photoinduced Electron Transfer Modulated by Excited-State Vibrational Relaxation Dynamics. *J. Phys. Chem. B* **2007**, *111*, 6829–6838.
- (296) Kichigina, A. O.; Ionkin, V. N.; Ivanov, A. I. U-Shaped Temperature Dependence of Rate Constant of Intramolecular Photoinduced Charge Separation in Zinc–Porphyrin–Bridge–Quinone Compounds. *J. Phys. Chem. B* **2013**, *117*, 7426–7435.
- (297) Villamaina, D.; Kelson, M. M. A.; Bhosale, S. V.; Vauthey, E. Excitation Wavelength Dependence of the Charge Separation Pathways in Tetraporphyrin-Naphthalene Diimide Pentads. *Phys. Chem. Chem. Phys.* **2014**, *16*, 5188–5200.
- (298) Rozzi, C. A.; Falke, S. M.; Spallanzani, N.; Rubio, A.; Molinari, E.; Brida, D.; Maiuri, M.; Cerullo, G.; Schramm, H.; Christoffers, J.; et al. Quantum Coherence Controls the Charge Separation in a Prototypical Artificial Light-Harvesting System. *Nat. Commun.* **2013**, *4*, 1602.
- (299) Delor, M.; Scattergood, P. A.; Sazanovich, I. V.; Parker, A. W.; Greetham, G. M.; Meijer, A. J. H. M.; Towrie, M.; Weinstein, J. A. Toward Control of Electron Transfer in Donor-Acceptor Molecules by Bond-Specific Infrared Excitation. *Science* **2014**, *346*, 1492–1495.
- (300) Wilemski, G.; Fixman, M. General Theory of Diffusion-Controlled Reactions. *J. Chem. Phys.* **1973**, *58*, 4009–4019.
- (301) Burshtein, A. I. Non-Markovian Theories of Transfer Reactions in Luminescence and Chemiluminescence and Photo- and Electrochemistry. *Adv. Chem. Phys.* **2004**, *129*, 105–418.
- (302) Smoluchowski, M. v. Versuch Einer Mathematischen Theorie der Koagulationskinetik Kolloider Lösungen. *Z. Phys. Chem.* **1917**, *92*, 129–168.
- (303) Collins, F. C.; Kimball, G. E. Diffusion-Controlled Reaction Rates. *J. Colloid Sci.* **1949**, *4*, 425–437.
- (304) Murata, S.; Tachiya, M. Transient Effect in Fluorescence Quenching by Electron Transfer. 3. Distribution of Electron Transfer Distance in Liquid and Solid Solutions. *J. Phys. Chem.* **1996**, *100*, 4064–4070.
- (305) Weidemaier, K.; Tavernier, H. L.; Swallen, S. F.; Fayer, M. D. Photoinduced Electron Transfer and Geminate Recombination in Liquids. *J. Phys. Chem. A* **1997**, *101*, 1887–1902.
- (306) Rice, S. A. *Comprehensive Chemical Kinetics: Diffusion-Limited Reactions V. 25*; Elsevier Science Ltd: Amsterdam, 1985.
- (307) Keizer, J. Diffusion Effects on Rapid Bimolecular Chemical Reactions. *Chem. Rev.* **1987**, *87*, 167–180.
- (308) Szabo, A. Theory of Diffusion-Influenced Fluorescence Quenching. *J. Phys. Chem.* **1989**, *93*, 6929–6939.
- (309) Sikorski, M.; Krystkowiak, E.; Steer, R. P. The Kinetics of Fast Fluorescence Quenching Processes. *J. Photochem. Photobiol., A* **1998**, *117*, 1–16.
- (310) Burshtein, A. I. Unified Theory of Photochemical Charge Separation. In *Adv. Chem. Phys.*; Prigogine, I., Rice, S. A., Eds.; John Wiley & Sons, Inc.: New York, 2000; pp 419–587.
- (311) Burshtein, A. I. Contact and Distant Luminescence Quenching in Solutions. *Adv. Phys. Chem.* **2009**, *2009*.110.1155/2009/214219
- (312) Mulliken, R. S. Molecular Compounds and Their Spectra. II. *J. Am. Chem. Soc.* **1952**, *74*, 811–824.
- (313) Gasparri, G. F.; Mangia, A.; Musatti, A.; Nardelli, M. The Crystal and Molecular Structure of Monothiosemicarbazide Silver(I) Chloride. *Acta Crystallogr., Sect. B: Struct. Crystallogr. Cryst. Chem.* **1968**, *24*, 367–374.
- (314) Larsen, F. K.; Little, R. G.; Coppens, P. A Liquid-Nitrogen Temperature Study of the Pyrene-d8-Tetracyanoethylene Charge-Transfer Complex. *Acta Crystallogr., Sect. B: Struct. Crystallogr. Cryst. Chem.* **1975**, *31*, 430–440.
- (315) Kuroda, H.; Amano, T.; Ikemoto, I.; Akamatu, H. Charge-Transfer Interaction in Tetracyanoethylene Complexes of Pyrene and Naphthalene. *J. Am. Chem. Soc.* **1967**, *89*, 6056–6063.
- (316) Bender, C. J. Theoretical Models of Charge-Transfer Complexes. *Chem. Soc. Rev.* **1986**, *15*, 475–502.
- (317) Voigt, E.-M. Multiple Charge-Transfer Bands in Complexes Involving Aromatic Donors. *J. Am. Chem. Soc.* **1964**, *86*, 3611–3617.
- (318) Rossi, M.; Buser, U.; Haselbach, E. Multiple Charge Transfer Transitions in Alkylbenzene-TCNE Complexes. *Helv. Chim. Acta* **1976**, *59*, 1039–1053.
- (319) Smith, M. L.; McHale, J. L. Optical and Resonance Raman Studies of the 1:1 and 2:1 Complexes of Hexamethylbenzene with Tetracyanoethylene. *J. Phys. Chem.* **1985**, *89*, 4002–4007.
- (320) Hayashi, M.; Yang, T.-S.; Yu, J.; Mebel, A.; Lin, S. H. On the Theoretical Investigation on Spectroscopy of the Electron Donor-Acceptor Complex TCNE-HMB. *J. Phys. Chem. A* **1997**, *101*, 4156–4162.
- (321) Klessinger, M. Ionization Potentials of Substituted Benzenes. *Angew. Chem., Int. Ed. Engl.* **1972**, *11*, 525–526.
- (322) Michaelian, K. H.; Rieckhoff, K. E.; Voigt, E.-M. Raman Resonance of Electron Donor/Acceptor Complexes. *Proc. Natl. Acad. Sci. U. S. A.* **1975**, *72*, 4196–4199.
- (323) Itoh, M.; Mimura, T. Fluorescent States of Exciplex and Charge Transfer Complexes: Experimental Evidence for an Identical Fluorescent State. *Chem. Phys. Lett.* **1974**, *24*, 551–554.
- (324) Mataga, N.; Shioyama, H.; Kanda, Y. Dynamics of Charge Recombination Processes in the Singlet Electron-Transfer State of Pyrene-Pyromellitic Dianhydride Systems in Various Solvents. Picosecond Laser Photolysis Studies. *J. Phys. Chem.* **1987**, *91*, 314–317.
- (325) Ojima, S.; Miyasaka, H.; Mataga, N. Femtosecond-Picosecond Laser Photolysis Studies on the Dynamics of Excited Charge-Transfer Complexes in Solution. 1. Charge Separation Processes in the Course of the Relaxation from the Excited Franck-Condon State of 1,2,4,5-Tetracyanobenzene in Benzene and Methyl-Substituted Benzene Solutions. *J. Phys. Chem.* **1990**, *94*, 4147–4152.
- (326) Asahi, T.; Mataga, N. Charge Recombination Process of Ion Pair State Produced by Excitation of Charge-Transfer Complex in Acetonitrile Solution. Essentially Different Character of Its Energy Gap Dependence from That of Geminate Ion Pair Formed by Encounter between Fluorescer and Quencher. *J. Phys. Chem.* **1989**, *93*, 6575–6578.



- (327) Asahi, T.; Mataga, N.; Takahashi, Y.; Miyashi, T. Energy Gap Dependence of the Charge Recombination Process of Ion Pairs Produced by Excitation of 2,6,9,10-Tetracyanoanthracene-Methyl Substituted Benzene Charge Transfer Complexes in Acetonitrile. *Chem. Phys. Lett.* **1990**, *171*, 309–313.
- (328) Asahi, T.; Mataga, N. fs-ps Laser Photolysis Studies on the Dynamics of Excited Charge Transfer Complexes: Aromatic Hydrocarbons-Acid Anhydride, Tetracyanoethylene and Tetracyanoquinodimethane Systems in Acetonitrile Solutions. *J. Phys. Chem.* **1991**, *95*, 1956–1963.
- (329) Asahi, T.; Ohkohchi, M.; Mataga, N. Energy Gap Dependences of Charge Recombination Processes of Ion Pairs Produced by Excitation of Charge-Transfer Complexes: Solvent Polarity Effects. *J. Phys. Chem.* **1993**, *97*, 13132–13137.
- (330) Jarzeba, W.; Schlieff, R. E.; Barbara, P. F. The Role of Solute/Solvent Electronic Interaction in the Femtosecond Dynamics of the Bromide/Benzene Cation Contact Ion Pair in Benzene Solution. *J. Phys. Chem.* **1994**, *98*, 9102–9105.
- (331) Jarzeba, W.; Thakur, K.; Hoermann, A.; Barbara, P. F. Ultrafast Electron Transfer in Optically Prepared "Simple" Ion Pairs: The Mechanism at High Donor Concentration. *J. Phys. Chem.* **1995**, *99*, 2016–2023.
- (332) Jarzeba, W.; Pommeret, S.; Mialocq, J.-C. Ultrafast Dynamics of the Excited Methyl-Viologen-Iodide Charge Transfer Complex. *Chem. Phys. Lett.* **2001**, *333*, 419–426.
- (333) Mohammed, O. F.; Vauthey, E. Simultaneous Generation of Different Types of Ion Pairs Upon Charge-Transfer Excitation of a Donor-Acceptor Complex Revealed by Ultrafast Transient Absorption Spectroscopy. *J. Phys. Chem. A* **2008**, *112*, 5804–5809.
- (334) Zhou, J.; Findley, B. R.; Teslja, A.; Braun, C. L.; Sutin, N. Ion Pairs from Photoexcited, 'Random' Electron Donors and Acceptors: Alkylbenzenes and Tetracyanoethylene. *J. Phys. Chem. A* **2000**, *104*, 11512.
- (335) Zhou, J.; Findley, B. R.; Braun, C. L.; Sutin, N. The Separation Distance Distribution in Electron-Donor-Acceptor Systems and the Wavelength Dependence of Free Ion Yields. *J. Chem. Phys.* **2001**, *114*, 10448–10456.
- (336) Kimura, Y.; Takebayashi, Y.; Hirota, N. Electron Transfer Rate in the Hexamethyl-Tetracyanoethylene Charge Transfer Complex in Carbon Dioxide. *Chem. Phys. Lett.* **1996**, *257*, 429–433.
- (337) Jarzeba, W.; Murata, S.; Tachiya, M. Ultrafast Dynamics of the Excited Tetracyanoethylene-Toluene Electron Donor-Acceptor Complex. *Chem. Phys. Lett.* **1999**, *301*, 347–355.
- (338) Wynne, K.; Galli, C.; Hochstrasser, R. M. Ultrafast Charge Transfer in an Electron Donor-Acceptor Complex. *J. Chem. Phys.* **1994**, *100*, 4797–4810.
- (339) Nicolet, O.; Vauthey, E. Ultrafast Nonequilibrium Charge Recombination Dynamics of Excited Donor-Acceptor Complexes. *J. Phys. Chem. A* **2002**, *106*, 5553–5562.
- (340) Frantsuzov, P. A.; Tachiya, M. Charge Recombination in Contact Ion Pairs. *J. Chem. Phys.* **2000**, *112*, 4216–4220.
- (341) Yudanov, V. V.; Mikhailova, V. A.; Ivanov, A. I. Non-equilibrium Phenomena in Charge Recombination of Excited Donor-Acceptor Complexes and Free Energy Gap Law. *J. Phys. Chem. A* **2010**, *114*, 12998–13004.
- (342) Ushakov, E. N.; Nadtochenko, V. A.; Gromov, S. P.; Vedernikov, A. I.; Lobova, N. A.; Alifimov, M. V.; Gostev, F. E.; Petrukhin, A. N.; Sarkisov, O. M. Ultrafast Excited State Dynamics of the Bi- and Termolecular Stilbene-Viologen Charge-Transfer Complexes Assembled via Host-Guest Interactions. *Chem. Phys.* **2004**, *298*, 251–261.
- (343) Ivanov, A. I.; Belikeev, F. N.; Fedunov, R. G.; Vauthey, E. The Effect of Excitation Pulse Carrier Frequency on Ultrafast Charge Recombination Dynamics of Excited Donor-Acceptor Complexes. *Chem. Phys. Lett.* **2003**, *372*, 73–81.
- (344) Fedunov, R. G.; Feskov, S. V.; Ivanov, A. I.; Nicolet, O.; Pagès, S.; Vauthey, E. Effect of the Excitation Pulse Carrier Frequency on the Ultrafast Charge Recombination Dynamics of Donor-Acceptor Complexes: Stochastic Simulations and Experiments. *J. Chem. Phys.* **2004**, *121*, 3643–3656.
- (345) Nicolet, O.; Banerji, N.; Pages, S.; Vauthey, E. Effect of the Excitation. *J. Phys. Chem. A* **2005**, *109*, 8236–8245.
- (346) Wynne, K.; Reid, G. D.; Hochstrasser, R. M. Vibrational Coherence in Electron Transfer: The Tetracyanoethylene-Pyrene Complex. *J. Chem. Phys.* **1996**, *105*, 2287–2298.
- (347) Wynne, K.; Hochstrasser, R. M. Coherence and Adiabaticity in Ultrafast Electron Transfer. *Adv. Chem. Phys.* **1999**, *107*, 263–310.
- (348) Rubtsov, I. V.; Yoshihara, K. Oscillatory Fluorescence Decay of an Electron Donor-Acceptor Complex. *J. Phys. Chem. A* **1997**, *101*, 6138–6140.
- (349) Hayashi, M.; Yang, T.-S.; Yu, J.; Mebel, A.; Chang, R.; Lin, S. H.; Rubtsov, I. V.; Yoshihara, K. Vibronic and Vibrational Coherence and Relaxation Dynamics in the Tcne-Hmb Complex. *J. Phys. Chem. A* **1998**, *102*, 4256–4265.
- (350) Rubtsov, I. V.; Yoshihara, K. Vibrational Coherence in Electron Donor-Acceptor Complexes. *J. Phys. Chem. A* **1999**, *103*, 10202–10212.
- (351) Kemnitz, K. Diffusionless Homogeneous Electron Transfer. Determination of the through-Space Electron-Exchange Matrix Element of Aromatic Donor-Acceptor Pairs. *Chem. Phys. Lett.* **1988**, *152*, 305–310.
- (352) Kemnitz, K.; Yoshihara, K. Diffusionless Electron Transfer of Xanthene Dyes in Nonpolar and Weakly Polar Donor- and Acceptor-Solvents. *Chem. Lett.* **1991**, *20*, 645–648.
- (353) Kandori, H.; Kemnitz, K.; Yoshihara, K. Subpicosecond Transient Absorption Study of Intermolecular Electron Transfer between Solute and Electron-Donating Solvents. *J. Phys. Chem.* **1992**, *96*, 8042–8048.
- (354) Nagasawa, Y.; Yartsev, A. P.; Tominaga, K.; Johnson, A. E.; Yoshihara, K. Substituent Effects on Intermolecular Electron Transfer: Coumarins in Electron-Donating Solvents. *J. Am. Chem. Soc.* **1993**, *115*, 7922–7923.
- (355) Ghosh, H. N.; Verma, S.; Nibbering, E. T. J. Ultrafast Forward and Backward Electron Transfer Dynamics of Coumarin 337 in Hydrogen-Bonded Anilines as Studied with Femtosecond UV-Pump/IR-Probe Spectroscopy. *J. Phys. Chem. A* **2011**, *115*, 664–670.
- (356) Xu, Q.-H.; Scholes, G. D.; Yang, M.; Fleming, G. R. Probing Solvation and Reaction Coordinates of Ultrafast Photoinduced Electron-Transfer Reactions Using Nonlinear Spectroscopies: Rhodamine 6G in Electron-Donating Solvents. *J. Phys. Chem. A* **1999**, *103*, 10348–10358.
- (357) Saik, V. O.; Goun, A. A.; Fayer, M. D. Photoinduced Electron Transfer and Geminate Recombination for Photoexcited Acceptors in a Pure Donor Solvent. *J. Chem. Phys.* **2004**, *120*, 9601–9611.
- (358) Jiang, L.; Liu, W.; Song, Y.; He, X.; Wang, Y.; Yang, Y. Photoinduced Electron Transfer of Rhodamine 6g/N,N-Diethylaniline Revealed by Multiplex Transient Grating and Transient Absorption Spectroscopies. *Appl. Phys. B: Lasers Opt.* **2014**, *116*, 271–277.
- (359) Jiang, L.-l.; Liu, W.-l.; Song, Y.-f.; He, X.; Wang, Y.; Wang, C.; Wu, H.-l.; Yang, F.; Yang, Y.-q. Photoinduced Intermolecular Electron Transfer and Off-Resonance Raman Characteristics of Rhodamine 101/N,N-Diethylaniline. *Chem. Phys.* **2014**, *429*, 12–19.
- (360) Iwai, S.; Murata, S.; Katoh, R.; Tachiya, M.; Kikuchi, K.; Takahashi, Y. Ultrafast Charge Separation and Exciplex Formation Induced by Strong Interaction between Electron Donor and Acceptor at Short Distances. *J. Chem. Phys.* **2000**, *112*, 7111–7117.
- (361) Asahi, T.; Mataga, N. Femtosecond-Picosecond Laser Photolysis Studies on the Dynamics of Excited Charge-Transfer Complexes: Aromatic Hydrocarbon-Acid Anhydride, -Tetracyanoethylene, and -Tetracyanoquinodimethane Systems in Acetonitrile Solutions. *J. Phys. Chem.* **1991**, *95*, 1956–1963.
- (362) Seel, M.; Engleitner, S.; Zinth, W. Wavepacket Motion and Ultrafast Electron Transfer in the System Oxazine 1 in N,N-Dimethylaniline. *Chem. Phys. Lett.* **1997**, *275*, 363–369.
- (363) Wolfseder, B.; Seidner, L.; Domcke, W.; Stock, G.; Seel, M.; Engleitner, S.; Zinth, W. Vibrational Coherence in Ultrafast Electron-Transfer Dynamics of Oxazine 1 in N,N-Dimethylaniline: Simulation



of a Femtosecond Pump-Probe Experiment. *Chem. Phys.* **1998**, *233*, 323–334.

(364) Engleitner, S.; Seel, M.; Zinth, W. Nonexponentialities in the Ultrafast Electron-Transfer Dynamics in the System Oxazine 1 in N,N-Dimethylaniline. *J. Phys. Chem. A* **1999**, *103*, 3013–3019.

(365) Nagasawa, Y.; Yoneda, Y.; Nambu, S.; Muramatsu, M.; Takeuchi, E.; Tsumori, H.; Miyasaka, H. Femtosecond Degenerate Four-Wave-Mixing Measurements of Coherent Intramolecular Vibrations in an Ultrafast Electron Transfer System. *Vib. Spectrosc.* **2014**, *70*, 58–62.

(366) Nagasawa, Y.; Yoneda, Y.; Nambu, S.; Muramatsu, M.; Takeuchi, E.; Tsumori, H.; Morikawa, S.; Katayama, T.; Miyasaka, H. Coherent Wavepacket Motion in an Ultrafast Electron Transfer System Monitored by Femtosecond Degenerate Four-Wave-Mixing and Pump-Probe Spectroscopy. *Chem. Phys.* **2014**, *442*, 68–76.

(367) Rafiq, S.; Dean, J. C.; Scholes, G. D. Observing Vibrational Wavepackets During an Ultrafast Electron Transfer Reaction. *J. Phys. Chem. A* **2015**, *119*, 11837–11846.

(368) Pal, H.; Nagasawa, Y.; Tominaga, K.; Yoshihara, K. Deuterium Isotope Effect on Ultrafast Intermolecular Electron Transfer. *J. Phys. Chem.* **1996**, *100*, 11964–11974.

(369) Shirota, H.; Pal, H.; Tominaga, K.; Yoshihara, K. Substituent Effect and Deuterium Isotope Effect of Ultrafast Intermolecular Electron Transfer: Coumarin in Electron-Donating Solvent. *J. Phys. Chem. A* **1998**, *102*, 3089–3102.

(370) Yoshihara, K.; Nagasawa, Y.; Yartsev, A.; Johnson, A. E.; Tominaga, K. Solvent and Nuclear Dynamic Effects on Intermolecular Electron Transfer. *J. Mol. Liq.* **1995**, *65–66*, 59–64.

(371) Nagasawa, Y.; Yartsev, A. P.; Tominaga, K.; Bisht, P. B.; Johnson, A. E.; Yoshihara, K. Dynamic Aspects of Ultrafast Intermolecular Electron Transfer Faster Than Solvation Process: Substituent Effects and Energy Gap Dependence. *J. Phys. Chem.* **1995**, *99*, 653–662.

(372) Shirota, H.; Pal, H.; Tominaga, K.; Yoshihara, K. Ultrafast Intermolecular Electron Transfer in Coumarin-Hydrazine System. *Chem. Phys.* **1998**, *236*, 355–364.

(373) Kobayashi, T.; Takagi, Y.; Kandori, H.; Kemnitz, K.; Yoshihara, K. Femtosecond Intermolecular Electron Transfer in Diffusionless, Weakly Polar Systems: Nile Blue in Aniline and N,N-Dimethylaniline. *Chem. Phys. Lett.* **1991**, *180*, 416–422.

(374) Yartsev, A.; Nagasawa, Y.; Douhal, A.; Yoshihara, K. Solvent and Nuclear Dynamics in Ultrafast Intermolecular Electron Transfer in a Diffusionless, Weakly Polar System. *Chem. Phys. Lett.* **1993**, *207*, 546–550.

(375) Yoshihara, K.; Nagasawa, Y.; Yartsev, A.; Kumazaki, S.; Kandori, H.; Johnson, A. E.; Tominaga, K. Femtosecond Intermolecular Electron Transfer in Condensed Systems. *J. Photochem. Photobiol., A* **1994**, *80*, 169–175.

(376) Nagasawa, Y.; Yartsev, A. P.; Tominaga, K.; Johnson, A. E.; Yoshihara, K. Temperature Dependence of Ultrafast Intermolecular Electron Transfer Faster Than Solvation Process. *J. Chem. Phys.* **1994**, *101*, 5717.

(377) Rubtsov, I. V.; Shirota, H.; Yoshihara, K. Ultrafast Photoinduced Solute–Solvent Electron Transfer: Configuration Dependence. *J. Phys. Chem. A* **1999**, *103*, 1801–1808.

(378) Andrews, D. P.; McFadyen, G. G.; Beddard, G. S. Ultrafast Electron Transfer between Methylene Blue and Liquid Anilines. *Chem. Phys. Lett.* **1998**, *293*, 343–351.

(379) Wang, C.; Akhremitchev, B.; Walker, G. C. Femtosecond Infrared and Visible Spectroscopy of Photoinduced Intermolecular Electron Transfer Dynamics and Solvent–Solute Reaction Geometries: Coumarin 337 in Dimethylaniline. *J. Phys. Chem. A* **1997**, *101*, 2735–2738.

(380) Castner, E. W.; Kennedy, D.; Cave, R. J. Solvent as Electron Donor: Donor/Acceptor Electronic Coupling Is a Dynamical Variable. *J. Phys. Chem. A* **2000**, *104*, 2869–2885.

(381) Morandeira, A.; Fürstenberg, A.; Gumy, J.-C.; Vauthey, E. Fluorescence Quenching in Electron-Donating Solvents. 1. Influence

of the Solute–Solvent Interactions on the Dynamics. *J. Phys. Chem. A* **2003**, *107*, 5375–5383.

(382) Morandeira, A.; Fürstenberg, A.; Vauthey, E. Fluorescence Quenching in Electron-Donating Solvents. 2. Solvent Dependence and Product Dynamics. *J. Phys. Chem. A* **2004**, *108*, 8190–8200.

(383) Singh, P. K.; Nath, S.; Bhasikuttan, A. C.; Kumbhakar, M.; Mohanty, J.; Sarkar, S. K.; Mukherjee, T.; Pal, H. Effect of Donor Orientation on Ultrafast Intermolecular Electron Transfer in Coumarin-Amine Systems. *J. Chem. Phys.* **2008**, *129*, 114504.

(384) Letrun, R.; Vauthey, E. Excitation Wavelength Dependence of the Dynamics of Bimolecular Photoinduced Electron Transfer Reactions. *J. Phys. Chem. Lett.* **2014**, *5*, 1685–1690.

(385) Angulo, G.; Cuertos, A.; Rosspeintner, A.; Vauthey, E. Experimental Evidence of the Relevance of Orientational Correlations in Photoinduced Bimolecular Reactions in Solution. *J. Phys. Chem. A* **2013**, *117*, 8814–8825.

(386) Swallen, S. F.; Weidemaier, K.; Fayer, M. D. Solvent Structure and Hydrodynamic Effects in Photoinduced Electron Transfer. *J. Chem. Phys.* **1996**, *104*, 2976–2986.

(387) Song, L.; Swallen, S. F.; Dorfman, R. C.; Weidemaier, K.; Fayer, M. D. Photoinduced Electron Transfer and Geminate Recombination in Solution. *J. Phys. Chem.* **1993**, *97*, 1374–1382.

(388) Rosspeintner, A.; Angulo, G.; Vauthey, E. Bimolecular Photoinduced Electron Transfer Beyond the Diffusion Limit: The Rehm–Weller Experiment Revisited with Femtosecond Time Resolution. *J. Am. Chem. Soc.* **2014**, *136*, 2026–2032.

(389) Nemzek, T. L.; Ware, W. R. Kinetics of Diffusion-Controlled Reactions: Transient Effects in Fluorescence Quenching. *J. Chem. Phys.* **1975**, *62*, 477–489.

(390) Joshi, N.; Johnson, M. L.; Gryczynski, I.; Lakowicz, J. R. Radiation Boundary Conditions in Collisional Quenching of Fluorescence; Determination by Frequency-Domain Fluorometry. *Chem. Phys. Lett.* **1987**, *135*, 200–207.

(391) Lakowicz, J. R.; Johnson, M. L.; Gryczynski, I.; Joshi, N.; Laczo, G. Transient Effects in Fluorescence Quenching Measured by 2-GHz Frequency-Domain Fluorometry. *J. Phys. Chem.* **1987**, *91*, 3277–3285.

(392) Periasamy, N.; Doraiswamy, S.; Maiya, G. B.; Venkataraman, B. Diffusion Controlled Reactions: Fluorescence Quenching of Cationic Dyes by Charged Quenchers. *J. Chem. Phys.* **1988**, *88*, 1638–1651.

(393) Periasamy, N.; Doraiswamy, S.; Venkataraman, B.; Fleming, G. R. Diffusion Controlled Reactions: Experimental Verification of the Time-Dependent Rate Equation. *J. Chem. Phys.* **1988**, *89*, 4799–4806.

(394) Eads, D. D.; Periasamy, N.; Fleming, G. R. Diffusion Influenced Reactions at Short Times: Breakdown of the Debye–Smoluchowski Description. *J. Chem. Phys.* **1989**, *90*, 3876–3878.

(395) Eads, D. D.; Dismar, B. G.; Fleming, G. R. A Subpicosecond, Subnanosecond and Steady-State Study of Diffusion Influenced Fluorescence Quenching. *J. Chem. Phys.* **1990**, *93*, 1136–1148.

(396) Song, L.; Dorfman, R. C.; Swallen, S. F.; Fayer, M. D. Influence of Diffusion on Photoinduced Electron Transfer. *J. Phys. Chem.* **1991**, *95*, 3454–3457.

(397) Lakowicz, J. R.; Kuśba, J.; Szmajnski, H.; Johnson, M. L.; Gryczynski, I. Distance-Dependent Fluorescence Quenching Observed by Frequency-Domain Fluorometry. *Chem. Phys. Lett.* **1993**, *206*, 455–463.

(398) Lakowicz, J. R.; Zelent, B.; Gryczynski, I.; Kuba, J.; Johnson, M. L. Distance-Dependent Fluorescence Quenching of Tryptophan by Acrylamide. *Photochem. Photobiol.* **1994**, *60*, 205–214.

(399) Zelent, B.; Kuśba, J.; Gryczynski, I.; Lakowicz, J. R. Distance-Dependent Quenching of Anthracene Fluorescence by N, N-Diethylaniline Observed by Frequency-Domain Fluorometry. *Appl. Spectrosc.* **1995**, *49*, 43–50.

(400) Zelent, B.; Kuśba, J.; Gryczynski, I.; Johnson, M. L.; Lakowicz, J. R. Distance-Dependent Fluorescence Quenching of P-Bis[2-(5-Phenylloxazolyl)]Benzene by Various Quenchers. *J. Phys. Chem.* **1996**, *100*, 18592–18602.

(401) Lakowicz, J. R.; Zelent, B.; Kuśba, J.; Gryczynski, I. Distance-Dependent Quenching of Nile Blue Fluorescence by N,N-Diethylaniline

- line Observed by Frequency-Domain Fluorometry. *J. Fluoresc.* **1996**, *6*, 187–194.
- (402) Zelent, B.; Kušba, J.; Gryczynski, I.; Johnson, M. L.; Lakowicz, J. R. Time-Resolved and Steady-State Fluorescence Quenching of N-Acetyl-L-Tryptophanamide by Acrylamide and Iodide. *Biophys. Chem.* **1998**, *73*, 53–75.
- (403) Shannon, C. F.; Eads, D. D. Diffusion-Controlled Electron Transfer Reactions: Subpicosecond Fluorescence Measurements of Coumarin 1 Quenched by Aniline and N,N-Dimethylaniline. *J. Chem. Phys.* **1995**, *103*, S208–S223.
- (404) Swallen, S. F.; Weidemaier, K.; Tavernier, H. L.; Fayer, M. D. Experimental and Theoretical Analysis of Photoinduced Electron Transfer: Including the Role of Liquid Structure. *J. Phys. Chem.* **1996**, *100*, 8106–8117.
- (405) Tavernier, H. L.; Fayer, M. D. Solute–Solute Spatial Distribution in Hydrogen Bonding Liquids Probed with Time-Dependent Intermolecular Electron Transfer. *J. Chem. Phys.* **2001**, *114*, 4552–4564.
- (406) Yabe, T.; Chosrowjan, H.; Yamada, K.; Hirata, Y.; Okada, T. Effects of Quencher Concentration on Biomolecular Reaction Rate in Solution. *J. Photochem. Photobiol., A* **1997**, *109*, 15–20.
- (407) Gladkikh, V.; Burshtein, A. I.; Angulo, G.; Pagès, S.; Lang, B.; Vauthey, E. Kinetics and Yields of Electron Transfer in the Inverted Region. *J. Phys. Chem. A* **2004**, *108*, 6667–6678.
- (408) Rosspeintner, A.; Kattinig, D. R.; Angulo, G.; Landgraf, S.; Grampp, G.; Cuetos, A. On the Coherent Description of Diffusion-Influenced Fluorescence Quenching Experiments. *Chem. - Eur. J.* **2007**, *13*, 6474–6483.
- (409) Angulo, G.; Kattinig, D. R.; Rosspeintner, A.; Grampp, G.; Vauthey, E. On the Coherent Description of Diffusion-Influenced Fluorescence Quenching Experiments II: Early Events. *Chem. - Eur. J.* **2010**, *16*, 2291–2299.
- (410) Gladkikh, V. S.; Burshtein, A. I.; Tavernier, H. L.; Fayer, M. D. Influence of Diffusion on the Kinetics of Donor–Acceptor Electron Transfer Monitored by the Quenching of Donor Fluorescence. *J. Phys. Chem. A* **2002**, *106*, 6982–6990.
- (411) Murata, S.; Nishimura, M.; Matsuzaki, S. Y.; Tachiya, M. Transient Effect in Fluorescence Quenching Induced by Electron Transfer. I. Analysis by the Collins–Kimball Model of Diffusion-Controlled Reactions. *Chem. Phys. Lett.* **1994**, *219*, 200–206.
- (412) Burel, L.; Mostafavi, M.; Murata, S.; Tachiya, M. Transient Effect in Fluorescence Quenching by Electron Transfer. 4. Long-Range Electron Transfer in a Nonpolar Solvent. *J. Phys. Chem. A* **1999**, *103*, 5882–5888.
- (413) Scully, A. D.; Takeda, T.; Okamoto, M.; Hirayama, S. Evidence for Long-Range Electron Transfer in a Diffusion-Influenced Bimolecular Reaction from Fluorescence Decay Measurements. *Chem. Phys. Lett.* **1994**, *228*, 32–40.
- (414) Scully, A. D.; Ohtaka, H.; Takezaki, M.; Tominaga, T. Diffusion-Facilitated Direct Determination of Intrinsic Parameters for Rapid Photoinduced Bimolecular Electron-Transfer Reactions in Nonpolar Solvents. *J. Phys. Chem. A* **2015**, *119*, 2770–2779.
- (415) Rehm, D.; Weller, A. Kinetik Und Mechanismus der Elektronenübertragung bei der Fluoreszenzlöschung in Acetonitril. *Ber. Bunsen-Ges.* **1969**, *73*, 834–839.
- (416) Rehm, D.; Weller, A. Kinetics of Fluorescence Quenching by Electron and H-Atom Transfer. *Isr. J. Chem.* **1970**, *8*, 259–271.
- (417) Nishikawa, S.; Asahi, T.; Okada, T.; Mataga, N.; Kakitani, T. Determination of the Bimolecular Rate Constant of Photoinduced Charge Separation in the Energy Gap Region Where the Reaction Is Diffusion Controlled – Analysis of the Transient Effect in the Course of Fluorescence Quenching Reaction. *Chem. Phys. Lett.* **1991**, *185*, 237–243.
- (418) Matsuda, N.; Kakitani, T.; Denda, T.; Mataga, N. Examination of the Viability of the Collins–Kimball Model and Numerical Calculation of the Time-Dependent Energy Gap Law of Photoinduced Charge Separation in Polar Solution. *Chem. Phys.* **1995**, *190*, 83–95.
- (419) Angel, S. A.; Peters, K. S. Free Energy Dependence of the Intrinsic Rate of Electron Transfer in Diffusional Quenching of trans-Stilbene S1 by Electron-Deficient Olefins. *J. Phys. Chem.* **1991**, *95*, 3606–3612.
- (420) Venkataraman, B.; Periasamy, N.; Modi, S.; Dutt, G. B.; Doraiswamy, S. Intermolecular Electron Transfer Rate in Diffusion Limited Region: Picosecond Fluorescence Studies. *Spectrochim. Acta, Part A* **1992**, *48*, 1707–1713.
- (421) Murata, S.; Matsuzaki, S. Y.; Tachiya, M. Transient Effect in Fluorescence Quenching by Electron Transfer. 2. Determination of the Rate Parameters Involved in the Marcus Equation. *J. Phys. Chem.* **1995**, *99*, S354–S358.
- (422) Iwai, S.; Murata, S.; Tachiya, M. Ultrafast Fluorescence Quenching by Electron Transfer and Fluorescence from the Second Excited State of a Charge Transfer Complex as Studied by Femtosecond up-Conversion Spectroscopy. *J. Chem. Phys.* **1998**, *109*, S963–S970.
- (423) Iwai, S.; Murata, S.; Tachiya, M. Contribution of the Ultrafast, Short-Distance Intermolecular Electron Transfer to the Fluorescence Quenching Rate in Solution. *J. Chem. Phys.* **2001**, *114*, 1312–1318.
- (424) Liang, M.; Kaintz, A.; Baker, G. A.; Maroncelli, M. Bimolecular Electron Transfer in Ionic Liquids: Are Reaction Rates Anomalously High? *J. Phys. Chem. B* **2012**, *116*, 1370–1384.
- (425) Koch, M.; Rosspeintner, A.; Angulo, G.; Vauthey, E. Bimolecular Photoinduced Electron Transfer in Imidazolium-Based Room-Temperature Ionic Liquids Is Not Faster Than in Conventional Solvents. *J. Am. Chem. Soc.* **2012**, *134*, 3729–3736.
- (426) Rosspeintner, A.; Koch, M.; Angulo, G.; Vauthey, E. Spurious Observation of the Marcus Inverted Region in Bimolecular Photoinduced Electron Transfer. *J. Am. Chem. Soc.* **2012**, *134*, 11396–11399.
- (427) Mohammed, O. F.; Adamczyk, K.; Banerji, N.; Dreyer, J.; Lang, B.; Nibbering, E. T. J.; Vauthey, E. Direct Femtosecond Observation of Tight and Loose Ion Pairs Upon Photoinduced Bimolecular Electron Transfer. *Angew. Chem., Int. Ed.* **2008**, *47*, 9044–9048.
- (428) Gould, I. R.; Ege, D.; Mattes, S. L.; Farid, S. Return Electron Transfer within Geminate Radical Ion Pairs. Observation of the Marcus Inverted Region. *J. Am. Chem. Soc.* **1987**, *109*, 3794–3796.
- (429) Mataga, N.; Asahi, T.; Kanda, Y.; Okada, T.; Kakitani, T. The Bell-Shaped Energy Gap Dependence of the Charge Recombination Reaction of Geminate Radical Ion Pairs Produced by Fluorescence Quenching Reaction in Acetonitrile Solution. *Chem. Phys.* **1988**, *127*, 249–261.
- (430) Kikuchi, K.; Takahashi, Y.; Koike, K.; Wakamatsu, K.; Ikeda, H.; Miyashi, T. The Free Enthalpy Dependence of Rate Constants of Return Electron Transfer within Photoproduced Geminate Radical Ion Pairs. *Z. Phys. Chem.* **1990**, *167*, 27–39.
- (431) Jayanthi, S. S.; Ramamurthy, P. Excited Singlet State Reactions of Triphenylpyrylium Ion with Electron Donors: Evidence for Electron Transfer and the Observation of Marcus Inverted Region for the Charge Shift in the Radical Pair. *J. Phys. Chem. A* **1997**, *101*, 2016–2022.
- (432) Kircher, T.; Löhmansröben, H. G. Photoinduced Charge Recombination Reactions of a Perylene Dye in Acetonitrile. *Phys. Chem. Chem. Phys.* **1999**, *1*, 3987–3992.
- (433) Vauthey, E. Direct Measurements of the Charge-Recombination Dynamics of Geminate Ion Pairs Formed Upon Electron-Transfer Quenching at High Donor Concentration. *J. Phys. Chem. A* **2001**, *105*, 340–348.
- (434) Gould, I. R.; Farid, S. Dynamics of Bimolecular Photoinduced Electron-Transfer Reactions. *Acc. Chem. Res.* **1996**, *29*, S22–S28.
- (435) Pagès, S.; Lang, B.; Vauthey, E. Ultrafast Spectroscopic Investigation of the Charge Recombination Dynamics of Ion Pairs Formed Upon Highly Exergonic Bimolecular Electron-Transfer Quenching: Looking for the Normal Region. *J. Phys. Chem. A* **2004**, *108*, 549–555.
- (436) Petersson, J.; Eklund, M.; Davidsson, J.; Hammarström, L. Ultrafast Electron Transfer Dynamics of a Zn(II)Porphyrin–Viologen Complex Revisited: S2 vs S1 Reactions and Survival of Excess Excitation Energy. *J. Phys. Chem. B* **2010**, *114*, 14329–14338.
- (437) Petersson, J.; Hammarström, L. Ultrafast Electron Transfer Dynamics in a Series of Porphyrin/Viologen Complexes: Involvement

of Electronically Excited Radical Pair Products. *J. Phys. Chem. B* **2015**, *119*, 7531–7540.

(438) Muller, P.-A.; Vauthey, E. Charge Recombination Dynamics of Geminate Ion Pairs Formed by Electron Transfer Quenching of Molecules in an Upper Excited State. *J. Phys. Chem. A* **2001**, *105*, 5994–6000.

(439) Morandeira, A.; Engeli, L.; Vauthey, E. Ultrafast Charge Recombination of Photogenerated Ion Pairs to an Electronic Excited State. *J. Phys. Chem. A* **2002**, *106*, 4833–4837.

(440) Koch, M.; Rosspeintner, A.; Adamczyk, K.; Lang, B.; Dreyer, J.; Nibbering, E. T. J.; Vauthey, E. Real-Time Observation of the Formation of Excited Radical Ions in Bimolecular Photoinduced Charge Separation: Absence of the Marcus Inverted Region Explained. *J. Am. Chem. Soc.* **2013**, *135*, 9843–9848.

(441) Goun, A.; Glusac, K.; Fayer, M. D. Photoinduced Electron Transfer and Geminate Recombination in Liquids on Short Time Scales: Experiments and Theory. *J. Chem. Phys.* **2006**, *124*, 084504.

(442) Dorfman, R. C.; Fayer, M. D. The Influence of Diffusion on Photoinduced Electron Transfer and Geminate Recombination. *J. Chem. Phys.* **1992**, *96*, 7410–7422.

(443) Gladkikh, V.; Burshtein, A. I.; Feskov, S. V.; Ivanov, A. I.; Vauthey, E. Hot Recombination of Photogenerated Ion Pairs. *J. Chem. Phys.* **2005**, *123*, 244510.

(444) Rosspeintner, A.; Angulo, G.; Vauthey, E. Driving Force Dependence of Charge Recombination in Reactive and Nonreactive Solvents. *J. Phys. Chem. A* **2012**, *116*, 9473–9483.

(445) Waluk, J. *Conformational Analysis of Molecules in Excited States*; Wiley-VCH: New York, 2000.

(446) Elsaesser, T.; Bakker, H. J. *Ultrafast Hydrogen Bonding Dynamics and Proton Transfer Processes in the Condensed Phase*; Springer: Dordrecht, 2002.

(447) Hynes, J. T.; Klinman, J. P.; Limbach, H.-H.; Schowen, R. L. *Hydrogen-Transfer Reactions*; Wiley-VCH: Weinheim, 2007.

(448) Han, K.-L.; Zhao, G.-J. *Hydrogen Bonding and Transfer in the Excited State*; John Wiley & Sons: West Sussex, 2011.

(449) Marcus, R. A. Theoretical Relations among Rate Constants, Barriers, and Brønsted Slopes of Chemical Reactions. *J. Phys. Chem.* **1968**, *72*, 891–899.

(450) Cohen, A. O.; Marcus, R. A. Slope of Free Energy Plots in Chemical Kinetics. *J. Phys. Chem.* **1968**, *72*, 4249–4256.

(451) Marcus, R. A. Energetic and Dynamical Aspects of Proton Transfer Reactions in Solution. *Faraday Symp. Chem. Soc.* **1975**, *10*, 60–68.

(452) Agmon, N.; Levine, R. D. Energy, Entropy and the Reaction Coordinate: Thermodynamic-Like Relations in Chemical Kinetics. *Chem. Phys. Lett.* **1977**, *52*, 197–201.

(453) Agmon, N.; Levine, R. D. Empirical Triatomic Potential Energy Surfaces Defined over Orthogonal Bond Order Coordinates. *J. Chem. Phys.* **1979**, *71*, 3034–3041.

(454) Agmon, N.; Levine, R. D. Structural Considerations in Chemical Kinetics: Gas Phase H-Atom Transfer Reaction Series. *Isr. J. Chem.* **1980**, *19*, 330–336.

(455) Agmon, N. From Energy Profiles to Structure-Reactivity Correlations. *Int. J. Chem. Kinet.* **1981**, *13*, 333–365.

(456) Barroso, M.; Arnaut, L. G.; Formosinho, S. J. Intersecting-State Model Calculations on Fast and Ultrafast Excited-State Proton Transfers in Naphthols and Substituted Naphthols. *J. Photochem. Photobiol., A* **2002**, *154*, 13–21.

(457) Barroso, M.; Arnaut, L. G.; Formosinho, S. J. Absolute Rate Calculations. Proton Transfers in Solution. *J. Phys. Chem. A* **2007**, *111*, 591–602.

(458) Pauling, L. Atomic Radii and Interatomic Distances in Metals. *J. Am. Chem. Soc.* **1947**, *69*, 542–553.

(459) Borgis, D.; Hynes, J. T. Curve Crossing Formulation for Proton Transfer Reactions in Solution. *J. Phys. Chem.* **1996**, *100*, 1118–1128.

(460) Kiefer, P. M.; Hynes, J. T. Nonlinear Free Energy Relations for Adiabatic Proton Transfer Reactions in a Polar Environment. II.

Inclusion of the Hydrogen Bond Vibration. *J. Phys. Chem. A* **2002**, *106*, 1850–1861.

(461) Kiefer, P. M.; Hynes, J. T. Nonlinear Free Energy Relations for Adiabatic Proton Transfer Reactions in a Polar Environment. I. Fixed Proton Donor–Acceptor Separation. *J. Phys. Chem. A* **2002**, *106*, 1834–1849.

(462) Kiefer, P. M.; Hynes, J. T. Kinetic Isotope Effects for Nonadiabatic Proton Transfer Reactions in a Polar Environment. I. Interpretation of Tunneling Kinetic Isotopic Effects. *J. Phys. Chem. A* **2004**, *108*, 11793–11808.

(463) Kiefer, P. M.; Hynes, J. T. Adiabatic and Nonadiabatic Proton Transfer Rate Constants in Solution. *Solid State Ionics* **2004**, *168*, 219–224.

(464) Kiefer, P. M.; Hynes, J. T. Theoretical Aspects of Proton Transfer Reactions in a Polar Environment. In *Hydrogen-Transfer Reactions*; Wiley-VCH: Weinheim, 2007; pp 303–348.

(465) Kiefer, P. M.; Hynes, J. T. Theoretical Aspects of Tunneling Proton Transfer Reactions in a Polar Environment. *J. Phys. Org. Chem.* **2010**, *23*, 632–646.

(466) Weber, K. The Close Relationship of Fluorescence Obliteration to the Inhibition of Photochemical Reactions. *Z. Phys. Chem., Abt. B* **1931**, *15*, 18–44.

(467) Förster, T. Die pH-Abhängigkeit der Fluoreszenz von Naphthalinderivaten. *Z. Elektrochem. Angew. Phys. Chem.* **1950**, *54*, 531–535.

(468) Förster, T. Elektrolytische Dissoziation Angeregter Moleküle. *Z. Elektrochem. Angew. Phys. Chem.* **1950**, *54*, 42–46.

(469) Grabowski, Z. R.; Grabowska, A. The Förster Cycle Reconsidered. *Z. Phys. Chem.* **1976**, *101*, 197–208.

(470) Weller, A. Quantitative Untersuchungen der Fluoreszenzwandlung bei Naphtholen. *Z. Elektrochem. Ber. Bunsenges. Phys. Chem.* **1952**, *56*, 662–668.

(471) Weller, A. Allgemeine Basenkatalyse bei der Elektrolytischen Dissoziation Angeregter Naphthole. *Z. Elektrochem. Ber. Bunsenges. Phys. Chem.* **1954**, *58*, 849–853.

(472) Eigen, M. Proton Transfer, Acid-Base Catalysis, and Enzymatic Hydrolysis. Part I: Elementary Processes. *Angew. Chem., Int. Ed. Engl.* **1964**, *3*, 1–19.

(473) Klöpffer, W. Intramolecular Proton Transfer in Electronically Excited Molecules. In *Adv. Photochem.*; John Wiley & Sons: New York, 1977; pp 311–358.

(474) Martynov, I. Y.; Demyashkevich, A. B.; Uzhinov, B. M.; Kuzmin, M. G. Proton Transfer Reactions in the Excited Electronic States of Aromatic Molecules. *Russ. Chem. Rev.* **1977**, *46*, 1–15.

(475) Kasha, M. Proton-Transfer Spectroscopy. Perturbation of the Tautomerization Potential. *J. Chem. Soc., Faraday Trans. 2* **1986**, *82*, 2379–2392.

(476) Barbara, P. F.; Walsh, P. K.; Brus, L. E. Picosecond Kinetic and Vibrationally Resolved Spectroscopic Studies of Intramolecular Excited-State Hydrogen Atom Transfer. *J. Phys. Chem.* **1989**, *93*, 29–34.

(477) Formosinho, S. J.; Arnaut, L. G. Excited-State Proton Transfer Reactions II. Intramolecular Reactions. *J. Photochem. Photobiol., A* **1993**, *75*, 21–48.

(478) Ormson, S. M.; Brown, R. G. Excited State Intramolecular Proton Transfer. Part 1: ESIPT to Nitrogen. *Prog. React. Kinet.* **1994**, *19*, 45–91.

(479) LeGourrière, D.; Ormson, S. M.; Brown, R. G. Excited State Intramolecular Proton Transfer. Part 2. ESIPT to Oxygen. *Prog. React. Kinet.* **1994**, *19*, 211–275.

(480) Douhal, A.; Lahmani, F.; Zewail, A. H. Proton-Transfer Reaction Dynamics. *Chem. Phys.* **1996**, *207*, 477–498.

(481) Uzhinov, B. M.; Khimich, M. N. Conformational Effects in Excited State Intramolecular Proton Transfer of Organic Compounds. *Russ. Chem. Rev.* **2011**, *80*, 553–577.

(482) Demchenko, A. P. Visualization and Sensing of Intermolecular Interactions with Two-Color Fluorescent Probes. *FEBS Lett.* **2006**, *580*, 2951–2957.



- (483) Kwon, J. E.; Park, S. Y. Advanced Organic Optoelectronic Materials: Harnessing Excited-State Intramolecular Proton Transfer (ESIPT) Process. *Adv. Mater.* **2011**, *23*, 3615–3642.
- (484) Zhao, J.; Ji, S.; Chen, Y.; Guo, H.; Yang, P. Excited State Intramolecular Proton Transfer (ESIPT): From Principal Photo-physics to the Development of New Chromophores and Applications in Fluorescent Molecular Probes and Luminescent Materials. *Phys. Chem. Chem. Phys.* **2012**, *14*, 8803–8817.
- (485) Arzhantsev, S. Y.; Takeuchi, S.; Tahara, T. Ultrafast Excited-State Proton Transfer Dynamics of 1,8-Dihydroxyanthraquinone (Chrysazin) Studied by Femtosecond Time-Resolved Fluorescence Spectroscopy. *Chem. Phys. Lett.* **2000**, *330*, 83–90.
- (486) Choi, J. R.; Jeoung, S. C.; Cho, D. W. Two-Photon-Induced Excited-State Intramolecular Proton Transfer Process in 1-Hydroxyanthraquinone. *Chem. Phys. Lett.* **2004**, *385*, 384–388.
- (487) Jethwa, J.; Ou, D.; Winkler, K.; Hartmann, N.; Vöhringer, P. Ultrafast Proton-Transfer and Coherent Wavepacket Motion of Electronically Excited 1,8-Dihydroxyanthraquinone in Liquid Benzyl Alcohol Solution. *Z. Phys. Chem.* **2000**, *214*, 1367–1381.
- (488) Manna, A.; Sayed, M.; Kumar, A.; Pal, H. Atypical Energetic and Kinetic Course of Excited-State Intramolecular Proton Transfer (ESIPT) in Room-Temperature Protic Ionic Liquids. *J. Phys. Chem. B* **2014**, *118*, 2487–2498.
- (489) Mohammed, O. F.; Xiao, D.; Batista, V. S.; Nibbering, E. T. Excited-State Intramolecular Hydrogen Transfer (ESIHT) of 1,8-Dihydroxy-9,10-anthraquinone (DHAQ) Characterized by Ultrafast Electronic and Vibrational Spectroscopy and Computational Modeling. *J. Phys. Chem. A* **2014**, *118*, 3090–3099.
- (490) Neuwahl, F. V. R.; Bussotti, L.; Righini, R.; Buntinx, G. Ultrafast Proton Transfer in the  $S_1$  State of 1-Chloroacetylaminanthraquinone. *Phys. Chem. Chem. Phys.* **2001**, *3*, 1277–1283.
- (491) Schmidtke, S. J.; Underwood, D. F.; Blank, D. A. Following the Solvent Directly During Ultrafast Excited State Proton Transfer. *J. Am. Chem. Soc.* **2004**, *126*, 8620–8621.
- (492) Smith, T. P.; Zaklika, K. A.; Thakur, K.; Barbara, P. F. Excited State Intramolecular Proton Transfer in 1-(Acylamino)-anthraquinones. *J. Am. Chem. Soc.* **1991**, *113*, 4035–4036.
- (493) Smith, T. P.; Zaklika, K. A.; Thakur, K.; Walker, G. C.; Tominaga, K.; Barbara, P. F. Spectroscopic Studies of Excited-State Intramolecular Proton Transfer in 1-(Acylamino)anthraquinones. *J. Phys. Chem.* **1991**, *95*, 10465–10475.
- (494) Ryu, J.; Kim, H. W.; Kim, M. S.; Joo, T. Ultrafast Excited State Intramolecular Proton Transfer Dynamics of 1-Hydroxyanthraquinone in Solution. *Bull. Korean Chem. Soc.* **2013**, *34*, 465–469.
- (495) Marks, D.; Prosposito, P.; Zhang, H.; Glasbeek, M. Femtosecond Laser Selective Intramolecular Double-Proton Transfer in [2,2'-Bipyridyl]-3,3'-diol. *Chem. Phys. Lett.* **1998**, *289*, 535–540.
- (496) Marks, D.; Zhang, H.; Glasbeek, M.; Borowicz, P.; Grabowska, A. Solvent Dependence of (Sub)Picosecond Proton Transfer in Photo-Excited [2,2'-Bipyridyl]-3,3'-diol. *Chem. Phys. Lett.* **1997**, *275*, 370–376.
- (497) Neuwahl, F. V. R.; Foggi, P.; Brown, R. G. Sub-picosecond and Picosecond Dynamics in the  $S_1$  State of [2,2'-Bipyridyl]-3,3'-diol Investigated by UV-Visible Transient Absorption Spectroscopy. *Chem. Phys. Lett.* **2000**, *319*, 157–163.
- (498) Stock, K.; Schrieffer, C.; Lochbrunner, S.; Riedle, E. Reaction Path Dependent Coherent Wavepacket Dynamics in Excited State Intramolecular Double Proton Transfer. *Chem. Phys.* **2008**, *349*, 197–203.
- (499) Toebe, P.; Glasbeek, M. Ultrafast Excited-State Intramolecular Double Proton Transfer Dynamics of [2,2'-Bipyridyl]-3,3'-diamine. *Chem. Phys. Lett.* **2005**, *407*, 487–492.
- (500) Zhang, H.; van der Meulen, P.; Glasbeek, M. Ultrafast Single and Double Proton Transfer in Photo-Excited [2,2'-Bipyridyl]-3,3'-diol. *Chem. Phys. Lett.* **1996**, *253*, 97–102.
- (501) Brenlla, A.; Veiga, M.; Perez Lustres, J. L.; Rios Rodriguez, M. C.; Rodriguez-Prieto, F.; Mosquera, M. Photoinduced Proton and Charge Transfer in 2-(2'-Hydroxyphenyl)imidazo[4,5-*b*]pyridine. *J. Phys. Chem. B* **2013**, *117*, 884–896.
- (502) Chudoba, C.; Lutgen, S.; Jentzsch, T.; Riedle, E.; Woerner, M.; Elsaesser, T. Femtosecond Studies of Vibrationally Hot Molecules Produced by Intramolecular Proton Transfer in the Excited State. *Chem. Phys. Lett.* **1995**, *240*, 35–41.
- (503) Douhal, A.; Kim, S. K.; Zewail, A. H. Femtosecond Molecular Dynamics of Tautomerization in Model Base Pairs. *Nature* **1995**, *378*, 260–263.
- (504) Driscoll, E.; Sorenson, S.; Dawlaty, J. M. Ultrafast Intramolecular Electron and Proton Transfer in Bis(imino)isoindole Derivatives. *J. Phys. Chem. A* **2015**, *119*, 5618–5625.
- (505) Fita, P.; Luzina, E.; Dziembowska, T.; Radzewicz, C.; Grabowska, A. Chemistry, Photophysics, and Ultrafast Kinetics of Two Structurally Related Schiff Bases Containing the Naphthalene or Quinoline Ring. *J. Chem. Phys.* **2006**, *125*, 184508.
- (506) Fuke, K.; Ishikawa, H. Dynamics of Proton Transfer Reactions of Model Base Pairs in the Ground and Excited States: Revisited. *Chem. Phys. Lett.* **2015**, *623*, 117–129.
- (507) Marks, D.; Zhang, H.; Borowicz, P.; Waluk, J.; Glasbeek, M. (Sub)Picosecond Fluorescence Upconversion Studies of Intermolecular Proton Transfer of Dipyrro[2,3-*a*:3',2'-*i*]carbazole and Related Compounds. *J. Phys. Chem. A* **2000**, *104*, 7167–7175.
- (508) Peng, C. Y.; Shen, J. Y.; Chen, Y. T.; Wu, P. J.; Hung, W. Y.; Hu, W. P.; Chou, P. T. Optically Triggered Stepwise Double-Proton Transfer in an Intramolecular Proton Relay: A Case Study of 1,8-Dihydroxy-2-naphthaldehyde. *J. Am. Chem. Soc.* **2015**, *137*, 14349–14357.
- (509) Takeuchi, S.; Tahara, T. The Answer to Concerted Versus Step-Wise Controversy for the Double Proton Transfer Mechanism of 7-Azaindole Dimer in Solution. *Proc. Natl. Acad. Sci. U. S. A.* **2007**, *104*, 5285–5290.
- (510) Verma, P. K.; Steinbacher, A.; Koch, F.; Nuernberger, P.; Brixner, T. Monitoring Ultrafast Intramolecular Proton Transfer Processes in an Unsymmetric  $\beta$ -Diketone. *Phys. Chem. Chem. Phys.* **2015**, *17*, 8459–8466.
- (511) Verma, P. K.; Steinbacher, A.; Schmiedel, A.; Nuernberger, P.; Brixner, T. Excited-State Intramolecular Proton Transfer of 2-Acetylindan-1,3-dione Studied by Ultrafast Absorption and Fluorescence Spectroscopy. *Struct. Dyn.* **2016**, *3*, 023606.
- (512) Waluk, J. Hydrogen-Bonding-Induced Phenomena in Bifunctional Heteroazaaromatics. *Acc. Chem. Res.* **2003**, *36*, 832–838.
- (513) Marsh, J. K. XLIX.—Studies in Fluorescence Spectra. Part II. Phenol and Phenolic Ether Vapours. *J. Chem. Soc., Trans.* **1924**, *125*, 418–423.
- (514) Weller, A. Innermolekularer Protonenübergang im Angeregten Zustand. *Z. Elektrochem. Ber. Bunsenges. Phys. Chem.* **1956**, *60*, 1144–1147.
- (515) Sandros, K. Hydrogen Bonding Effects on the Fluorescence of Methyl Salicylate. *Acta Chem. Scand.* **1976**, *30A*, 761–763.
- (516) Klöpffer, W.; Naundorf, G. On the Fluorescence of Methyl Salicylate in Hydrogen Bonding Solvents. *J. Lumin.* **1974**, *8*, 457–461.
- (517) Lopez-Delgado, R.; Lazare, S. Fluorescence Properties of Methyl Salicylate in Vapor, Liquid, and Solution. *J. Phys. Chem.* **1981**, *85*, 763–768.
- (518) Kosower, E. M.; Dodiuk, H. Multiple Fluorescences III. Methyl 2,6-Dihydroxybenzoate and Methyl Salicylate. *J. Lumin.* **1975**, *11*, 249–254.
- (519) Felker, P. M.; Lambert, W. R.; Zewail, A. H. Picosecond Excitation of Jet-Cooled Hydrogen-Bonded Systems: Dispersed Fluorescence and Time-Resolved Studies of Methyl Salicylate. *J. Chem. Phys.* **1982**, *77*, 1603–1605.
- (520) Smith, K. K.; Kaufmann, K. J. Picosecond Studies of Intramolecular Proton Transfer. *J. Phys. Chem.* **1978**, *82*, 2286–2291.
- (521) Goodman, J.; Brus, L. E. Proton Transfer and Tautomerism in an Excited State of Methyl Salicylate. *J. Am. Chem. Soc.* **1978**, *100*, 7472–7474.
- (522) Herek, J. L.; Pedersen, S.; Bañares, L.; Zewail, A. H. Femtosecond Real-Time Probing of Reactions. IX. Hydrogen-Atom Transfer. *J. Chem. Phys.* **1992**, *97*, 9046–9061.

- (523) Nagaoka, S.; Hirota, N.; Sumitani, M.; Yoshihara, K. Investigation of the Dynamic Processes of the Excited States of *o*-Hydroxybenzaldehyde and *o*-Hydroxyacetophenone by Emission and Picosecond Spectroscopy. *J. Am. Chem. Soc.* **1983**, *105*, 4220–4226.
- (524) Stock, K.; Bizjak, T.; Lochbrunner, S. Proton Transfer and Internal Conversion of *o*-Hydroxybenzaldehyde: Coherent Versus Statistical Excited-State Dynamics. *Chem. Phys. Lett.* **2002**, *354*, 409–416.
- (525) Lochbrunner, S.; Schultz, T.; Schmitt, M.; Shaffer, J. P.; Zgierski, M. Z.; Stolow, A. Dynamics of Excited-State Proton Transfer Systems via Time-Resolved Photoelectron Spectroscopy. *J. Chem. Phys.* **2001**, *114*, 2519–2522.
- (526) Douhal, A.; Lahmani, F.; Zehnacker-Rentien, A. Excited-State Intramolecular Proton Transfer in Jet-Cooled 1-Hydroxy-2-acetonaphthone. *Chem. Phys.* **1993**, *178*, 493–504.
- (527) Organero, J. A.; Tormo, L.; Douhal, A. Caging Ultrafast Proton Transfer and Twisting Motion of 1-Hydroxy-2-acetonaphthone. *Chem. Phys. Lett.* **2002**, *363*, 409–414.
- (528) Organero, J. A.; Douhal, A. Temperature and Solvent Effects on the Photodynamics of 1'-Hydroxy-2'-acetonaphthone. *Chem. Phys. Lett.* **2003**, *381*, 759–765.
- (529) Organero, J. A.; Douhal, A. Confinement Effects on the Photorelaxation of a Proton-Transfer Phototautomer. *Chem. Phys. Lett.* **2003**, *373*, 426–431.
- (530) Douhal, A. Breaking, Making, and Twisting of Chemical Bonds in Gas, Liquid, and Nanocavities. *Acc. Chem. Res.* **2004**, *37*, 349–355.
- (531) Lochbrunner, S.; Szeghalmi, A.; Stock, K.; Schmitt, M. Ultrafast Proton Transfer of 1-Hydroxy-2-acetonaphthone: Reaction Path from Resonance Raman and Transient Absorption Studies. *J. Chem. Phys.* **2005**, *122*, 244315.
- (532) Ortiz-Sanchez, J. M.; Gelabert, R.; Moreno, M.; Lluch, J. M. Electronic and Quantum Dynamical Insight into the Ultrafast Proton Transfer of 1-Hydroxy-2-acetonaphthone. *J. Chem. Phys.* **2007**, *127*, 084318.
- (533) Thistlethwaite, P. J.; Woolfe, G. J. Kinetic Evidence for Excited State Proton Transfer in Salicylamide. *Chem. Phys. Lett.* **1979**, *63*, 401–405.
- (534) Woolfe, G. J.; Thistlethwaite, P. J. Excited-State Prototropic Reactivity in Salicylamide and Salicylanilide. *J. Am. Chem. Soc.* **1980**, *102*, 6917–6923.
- (535) Barbara, P. F.; Rentzepis, P. M.; Brus, L. E. Photochemical Kinetics of Salicylidenaniline. *J. Am. Chem. Soc.* **1980**, *102*, 2786–2791.
- (536) Mitra, S.; Tamai, N. Femtosecond Spectroscopic Study on Photochromic Salicylideneaniline. *Chem. Phys. Lett.* **1998**, *282*, 391–397.
- (537) Sengupta, P. K.; Kasha, M. Excited State Proton-Transfer Spectroscopy of 3-Hydroxyflavone and Quercetin. *Chem. Phys. Lett.* **1979**, *68*, 382–385.
- (538) Woolfe, G. J.; Thistlethwaite, P. J. Direct Observation of Excited State Intramolecular Proton Transfer Kinetics in 3-Hydroxyflavone. *J. Am. Chem. Soc.* **1981**, *103*, 6916–6923.
- (539) Itoh, M.; Tokumura, K.; Tanimoto, Y.; Okada, Y.; Takeuchi, H.; Obi, K.; Tanaka, I. Time-Resolved and Steady-State Fluorescence Studies of the Excited-State Proton Transfer in 3-Hydroxyflavone and 3-Hydroxychromone. *J. Am. Chem. Soc.* **1982**, *104*, 4146–4150.
- (540) Strandjord, A. J. G.; Barbara, P. F. Hydrogen/Deuterium Isotope Effects on the Excited-State Proton Transfer Kinetics of 3-Hydroxyflavone. *Chem. Phys. Lett.* **1983**, *98*, 21–26.
- (541) McMorro, D.; Kasha, M. Intramolecular Excited-State Proton Transfer in 3-Hydroxyflavone. Hydrogen-Bonding Solvent Perturbations. *J. Phys. Chem.* **1984**, *88*, 2235–2243.
- (542) Brucker, G. A.; Kelley, D. F.; Swinney, T. C. Proton-Transfer and Solvent Polarization Dynamics in 3-Hydroxyflavone. *J. Phys. Chem.* **1991**, *95*, 3190–3195.
- (543) Strandjord, A. J. G.; Barbara, P. F. The Proton-Transfer Kinetics of 3-Hydroxyflavone: Solvent Effects. *J. Phys. Chem.* **1985**, *89*, 2355–2361.
- (544) Swinney, T. C.; Kelley, D. F. Proton-Transfer and Solvent Polarization Dynamics in 3-Hydroxyflavone. 2. Mixed Solvents. *J. Phys. Chem.* **1991**, *95*, 10369–10373.
- (545) McMorro, D.; Dzuga, T. P.; Aartsma, T. J. Excited-State Dynamics of the Intramolecular Proton Transfer of 3-Hydroxyflavone in the Absence of External Hydrogen-Bonding Interactions. *Chem. Phys. Lett.* **1984**, *103*, 492–496.
- (546) Strandjord, A. J. G.; Courtney, S. H.; Friedrich, D. M.; Barbara, P. F. Excited-State Dynamics of 3-Hydroxyflavone. *J. Phys. Chem.* **1983**, *87*, 1125–1133.
- (547) Brucker, G. A.; Kelley, D. F. Role of Phenyl Torsion in the Excited-State Dynamics of 3-Hydroxyflavone. *J. Phys. Chem.* **1988**, *92*, 3805–3809.
- (548) Schwartz, B. J.; Peteanu, L. A.; Harris, C. B. Direct Observation of Fast Proton Transfer: Femtosecond Photophysics of 3-Hydroxyflavone. *J. Phys. Chem.* **1992**, *96*, 3591–3598.
- (549) Ormson, S. M.; LeGourri  rec, D.; Brown, R. G.; Foggi, P. Sub-picosecond Pump-Probe Spectroscopy of ESIPT in 3-Hydroxyflavone. *J. Chem. Soc., Chem. Commun.* **1995**, 2133–2130.
- (550) Ameer-Beg, S.; Ormson, S. M.; Brown, R. G.; Matousek, P.; Towrie, M.; Nibbering, E. T. J.; Foggi, P.; Neuwahl, F. V. R. Ultrafast Measurements of Excited State Intramolecular Proton Transfer (ESIPT) in Room Temperature Solutions of 3-Hydroxyflavone and Derivatives. *J. Phys. Chem. A* **2001**, *105*, 3709–3718.
- (551) Dzuga, T. P.; Schmidt, J.; Aartsma, T. J. On the Ground-State Tautomerization of 3-Hydroxyflavone. *Chem. Phys. Lett.* **1986**, *127*, 336–342.
- (552) Rulli  re, C.; Decl  my, A. A Picosecond Transient Absorption Study of the Intramolecular Excited State Proton Transfer in 3-Hydroxyflavone: Assignment of the Observed Bands. *Chem. Phys. Lett.* **1987**, *134*, 64–69.
- (553) Hsieh, C.-C.; Jiang, C.-M.; Chou, P.-T. Recent Experimental Advances on Excited-State Intramolecular Proton Coupled Electron Transfer Reaction. *Acc. Chem. Res.* **2010**, *43*, 1364–1374.
- (554) Swinney, T. C.; Kelley, D. F. Proton Transfer Dynamics in Substituted 3-Hydroxyflavones: Solvent Polarization Effects. *J. Chem. Phys.* **1993**, *99*, 211–221.
- (555) Chou, P.-T.; Martinez, M. L.; Clements, J. H. Reversal of Excitation Behavior of Proton-Transfer vs. Charge-Transfer by Dielectric Perturbation of Electronic Manifolds. *J. Phys. Chem.* **1993**, *97*, 2618–2622.
- (556) Shynkar, V. V.; M  ly, Y.; Duportail, G.; Pi  mont, E.; Klymchenko, A. S.; Demchenko, A. P. Picosecond Time-Resolved Fluorescence Studies Are Consistent with Reversible Excited-State Intramolecular Proton Transfer in 4'-(Dialkylamino)-3-hydroxyflavones. *J. Phys. Chem. A* **2003**, *107*, 9522–9529.
- (557) Ameer-Beg, S.; Ormson, S. M.; Poteau, X.; Brown, R. G.; Foggi, P.; Bussotti, L.; Neuwahl, F. V. R. Ultrafast Measurements of Charge and Excited-State Intramolecular Proton Transfer in Solutions of 4'-(*N,N*-Dimethylamino) Derivatives of 3-Hydroxyflavone. *J. Phys. Chem. A* **2004**, *108*, 6938–6943.
- (558) Douhal, A.; Sanz, M.; Carranza, M. A.; Organero, J. A.; Santos, L. Femtosecond Observation of Intramolecular Charge- and Proton-Transfer Reactions in a Hydroxyflavone Derivative. *Chem. Phys. Lett.* **2004**, *394*, 54–60.
- (559) Chou, P.-T.; Huang, C.-H.; Pu, S.-C.; Cheng, Y.-M.; Liu, Y.-H.; Wang, Y.; Chen, C.-T. Tuning Excited-State Charge/Proton Transfer Coupled Reaction via the Dipolar Functionality. *J. Phys. Chem. A* **2004**, *108*, 6452–6454.
- (560) Chou, P.-T.; Pu, S.-C.; Cheng, Y.-M.; Yu, W.-S.; Yu, Y.-C.; Hung, F.-T.; Hu, W.-P. Femtosecond Dynamics on Excited-State Proton/Charge-Transfer Reaction in 4'-*N,N*-Diethylamino-3-hydroxyflavone. The Role of Dipolar Vectors in Constructing a Rational Mechanism. *J. Phys. Chem. A* **2005**, *109*, 3777–3787.
- (561) Cheng, Y.-M.; Pu, S.-C.; Yu, Y.-C.; Chou, P.-T.; Huang, C.-H.; Chen, C.-T.; Li, T.-H.; Hu, W.-P. Spectroscopy and Femtosecond Dynamics of 7-*N,N*-Diethylamino-3-hydroxyflavone. The Correlation of Dipole Moments among Various States to Rationalize the Excited-



- State Proton Transfer Reaction. *J. Phys. Chem. A* **2005**, *109*, 11696–11706.
- (562) Demchenko, A. P.; Tang, K. C.; Chou, P.-T. Excited-State Proton Coupled Charge Transfer Modulated by Molecular Structure and Media Polarization. *Chem. Soc. Rev.* **2013**, *42*, 1379–1408.
- (563) Tomin, V. I.; Demchenko, A. P.; Chou, P.-T. Thermodynamic vs. Kinetic Control of Excited-State Proton Transfer Reactions. *J. Photochem. Photobiol., C* **2015**, *22*, 1–18.
- (564) Fukuda, M.; Terazima, M.; Kimura, Y. Study on the Excited State Intramolecular Proton Transfer of 4'-N,N-Diethylamino-3-hydroxyflavone in Imidazolium-Based Room Temperature Ionic Liquids. *Chem. Phys. Lett.* **2008**, *463*, 364–368.
- (565) Kimura, Y.; Fukuda, M.; Suda, K.; Terazima, M. Excited State Intramolecular Proton Transfer Reaction of 4'-N,N-Diethylamino-3-hydroxyflavone and Solvation Dynamics in Room Temperature Ionic Liquids Studied by Optical Kerr Gate Fluorescence Measurement. *J. Phys. Chem. B* **2010**, *114*, 11847–11858.
- (566) Suda, K.; Terazima, M.; Kimura, Y. Excitation Wavelength Dependence of Photo-Induced Intramolecular Proton Transfer Reaction of 4'-N,N-Diethylamino-3-hydroxyflavone in Various Liquids. *Chem. Phys. Lett.* **2012**, *531*, 70–74.
- (567) Suda, K.; Terazima, M.; Sato, H.; Kimura, Y. Excitation Wavelength Dependence of Excited State Intramolecular Proton Transfer Reaction of 4'-N,N-Diethylamino-3-hydroxyflavone in Room Temperature Ionic Liquids Studied by Optical Kerr Gate Fluorescence Measurement. *J. Phys. Chem. B* **2013**, *117*, 12567–12582.
- (568) Nakagaki, R.; Kobayashi, T.; Nagakura, S. Luminescence Properties and the Primary Process of Photochromism of 2-(2'-Hydroxyphenyl)benzothiazole. *Bull. Chem. Soc. Jpn.* **1978**, *51*, 1671–1675.
- (569) Barbara, P. F.; Brus, L. E.; Rentzepis, P. M. Intramolecular Proton Transfer and Excited-State Relaxation in 2-(2'-Hydroxyphenyl)-benzothiazole. *J. Am. Chem. Soc.* **1980**, *102*, 5631–5635.
- (570) Woolfe, G. J.; Melzig, M.; Schneider, S.; Dörr, F. The Role of Tautomeric and Rotameric Species in the Photophysics of 2-(2'-Hydroxyphenyl)benzoxazole. *Chem. Phys.* **1983**, *77*, 213–221.
- (571) Elsaesser, T.; Kaiser, W. Visible and Infrared Spectroscopy of Intramolecular Proton Transfer Using Picosecond Laser Pulses. *Chem. Phys. Lett.* **1986**, *128*, 231–237.
- (572) Laerner, F.; Elsaesser, T.; Kaiser, W. Femtosecond Spectroscopy of Excited-State Proton Transfer in 2-(2'-Hydroxyphenyl)-benzothiazole. *Chem. Phys. Lett.* **1988**, *148*, 119–124.
- (573) Frey, W.; Laerner, F.; Elsaesser, T. Femtosecond Studies of Excited-State Proton and Deuterium Transfer in Benzothiazole Compounds. *J. Phys. Chem.* **1991**, *95*, 10391–10395.
- (574) Lochbrunner, S.; Wurzer, A. J.; Riedle, E. Microscopic Mechanism of Ultrafast Excited-State Intramolecular Proton Transfer: A 30-fs Study of 2-(2'-Hydroxyphenyl)benzothiazole. *J. Phys. Chem. A* **2003**, *107*, 10580–10590.
- (575) Lochbrunner, S.; Wurzer, A. J.; Riedle, E. Ultrafast Excited-State Proton Transfer and Subsequent Coherent Skeletal Motion of 2-(2'-Hydroxyphenyl)benzothiazole. *J. Chem. Phys.* **2000**, *112*, 10699–10702.
- (576) Lochbrunner, S.; Stock, K.; Riedle, E. Direct Observation of the Nuclear Motion During Ultrafast Intramolecular Proton Transfer. *J. Mol. Struct.* **2004**, *700*, 13–18.
- (577) Schrieffer, C.; Lochbrunner, S.; Ofial, A. R.; Riedle, E. The Origin of Ultrafast Proton Transfer: Multidimensional Wave Packet Motion vs. Tunneling. *Chem. Phys. Lett.* **2011**, *503*, 61–65.
- (578) de Vivie-Riedle, R.; De Waele, V.; Kurtz, L.; Riedle, E. Ultrafast Excited-State Proton Transfer of 2-(2'-Hydroxyphenyl)benzothiazole: Theoretical Analysis of the Skeletal Deformations and the Active Vibrational Modes. *J. Phys. Chem. A* **2003**, *107*, 10591–10599.
- (579) Pfeiffer, M.; Lenz, K.; Lau, A.; Elsaesser, T. Resonance Raman Studies of Heterocyclic Aromatic Compounds Showing Ultrafast Intramolecular Proton Transfer. *J. Raman Spectrosc.* **1995**, *26*, 607–615.
- (580) Rini, M.; Kummrow, A.; Dreyer, J.; Nibbering, E. T. J.; Elsaesser, T. Femtosecond Mid-Infrared Spectroscopy of Condensed Phase Hydrogen-Bonded Systems as a Probe of Structural Dynamics. *Faraday Discuss.* **2003**, *122*, 27–40.
- (581) Luber, S.; Adamczyk, K.; Nibbering, E. T. J.; Batista, V. S. Photoinduced Proton Coupled Electron Transfer in 2-(2'-Hydroxyphenyl)-Benzothiazole. *J. Phys. Chem. A* **2013**, *117*, 5269–5279.
- (582) Arthen-Engeland, T.; Bultmann, T.; Ernsting, N. P.; Rodriguez, M. A.; Thiel, W. Singlet Excited-State Intramolecular Proton Transfer in 2-(2'-Hydroxyphenyl)benzoxazole: Spectroscopy at Low Temperatures, Femtosecond Transient Absorption, and MNDO Calculations. *Chem. Phys.* **1992**, *163*, 43–53.
- (583) Abou-Zied, O. K.; Jimenez, R.; Thompson, E. H. Z.; Millar, D. P.; Romesberg, F. E. Solvent-Dependent Photoinduced Tautomerization of 2-(2'-Hydroxyphenyl)benzoxazole. *J. Phys. Chem. A* **2002**, *106*, 3665–3672.
- (584) Ernsting, N. P.; Kovalenko, S. A.; Senyushkina, T.; Saam, J.; Farztdinov, V. Wave-Packet-Assisted Decomposition of Femtosecond Transient Ultraviolet–Visible Absorption Spectra: Application to Excited-State Intramolecular Proton Transfer in Solution. *J. Phys. Chem. A* **2001**, *105*, 3443–3453.
- (585) Wnuk, P.; Burdzinski, G.; Sliwa, M.; Kijak, M.; Grabowska, A.; Sepiol, J.; Kubicki, J. From Ultrafast Events to Equilibrium—Uncovering the Unusual Dynamics of ESIPT Reaction: The Case of Dually Fluorescent Diethyl-2,5-(dibenzoxazolyl)-hydroquinone. *Phys. Chem. Chem. Phys.* **2014**, *16*, 2542–2552.
- (586) Cheng, Y.-M.; Pu, S.-C.; Hsu, C.-J.; Lai, C.-H.; Chou, P.-T. Femtosecond Dynamics on 2-(2'-Hydroxy-4'-diethylaminophenyl)-benzothiazole: Solvent Polarity in the Excited-State Proton Transfer. *ChemPhysChem* **2006**, *7*, 1372–1381.
- (587) Hsieh, C.-C.; Cheng, Y.-M.; Hsu, C.-J.; Chen, K.-Y.; Chou, P.-T. Spectroscopy and Femtosecond Dynamics of Excited-State Proton Transfer Induced Charge Transfer Reaction. *J. Phys. Chem. A* **2008**, *112*, 8323–8332.
- (588) Gutierrez, M.; Alarcos, N.; Liras, M.; Sanchez, F.; Douhal, A. Switching to a Reversible Proton Motion in a Charge-Transferred Dye. *J. Phys. Chem. B* **2015**, *119*, 552–562.
- (589) Alarcos, N.; Gutierrez, M.; Liras, M.; Sanchez, F.; Douhal, A. An Abnormally Slow Proton Transfer Reaction in a Simple HBO Derivative Due to Ultrafast Intramolecular-Charge Transfer Events. *Phys. Chem. Chem. Phys.* **2015**, *17*, 16257–16269.
- (590) Kim, C. H.; Park, J.; Seo, J.; Park, S. Y.; Joo, T. Excited State Intramolecular Proton Transfer and Charge Transfer Dynamics of a 2-(2'-Hydroxyphenyl)benzoxazole Derivative in Solution. *J. Phys. Chem. A* **2010**, *114*, 5618–5629.
- (591) Martinez, M. L.; Cooper, W. C.; Chou, P.-T. A Novel Excited-State Intramolecular Proton Transfer Molecule, 10-Hydroxybenzo[h]-quinoline. *Chem. Phys. Lett.* **1992**, *193*, 151–154.
- (592) Chou, P.-T.; Chen, Y.-C.; Yu, W.-S.; Chou, Y.-H.; Wei, C.-Y.; Cheng, Y.-M. Excited-State Intramolecular Proton Transfer in 10-Hydroxybenzo[h]quinoline. *J. Phys. Chem. A* **2001**, *105*, 1731–1740.
- (593) Takeuchi, S.; Tahara, T. Coherent Nuclear Wavepacket Motions in Ultrafast Excited-State Intramolecular Proton Transfer: Sub-30-fs Resolved Pump-Probe Absorption Spectroscopy of 10-Hydroxybenzo[h]quinoline in Solution. *J. Phys. Chem. A* **2005**, *109*, 10199–10207.
- (594) Schrieffer, C.; Barbatti, M.; Stock, K.; Aquino, A. J. A.; Tunega, D.; Lochbrunner, S.; Riedle, E.; de Vivie-Riedle, R.; Lischka, H. The Interplay of Skeletal Deformations and Ultrafast Excited-State Intramolecular Proton Transfer: Experimental and Theoretical Investigation of 10-Hydroxybenzo[h]quinoline. *Chem. Phys.* **2008**, *347*, 446–461.
- (595) Kim, C. H.; Joo, T. Coherent Excited State Intramolecular Proton Transfer Probed by Time-Resolved Fluorescence. *Phys. Chem. Chem. Phys.* **2009**, *11*, 10266–10269.
- (596) Lee, J.; Kim, C. H.; Joo, T. Active Role of Proton in Excited State Intramolecular Proton Transfer Reaction. *J. Phys. Chem. A* **2013**, *117*, 1400–1405.
- (597) Hammes-Schiffer, S. Theoretical Perspectives on Proton-Coupled Electron Transfer Reactions. *Acc. Chem. Res.* **2001**, *34*, 273–281.



- (598) Weinberg, D. R.; Gagliardi, C. J.; Hull, J. F.; Murphy, C. F.; Kent, C. A.; Westlake, B. C.; Paul, A.; Ess, D. H.; McCafferty, D. G.; Meyer, T. J. Proton-Coupled Electron Transfer. *Chem. Rev.* **2012**, *112*, 4016–4093.
- (599) Weller, A. Fast Reactions of Excited Molecules. *Prog. React. Kinet.* **1961**, *1*, 187–214.
- (600) Ireland, J. F.; Wyatt, P. A. H. Acid-Base Properties of Electronically Excited States of Organic Molecules. *Adv. Phys. Org. Chem.* **1976**, *12*, 131–221.
- (601) Kosower, E. M.; Huppert, D. Excited State Electron and Proton Transfers. *Annu. Rev. Phys. Chem.* **1986**, *37*, 127–156.
- (602) Shizuka, H. Excited-State Proton-Transfer Reactions and Proton-Induced Quenching of Aromatic Compounds. *Acc. Chem. Res.* **1985**, *18*, 141–147.
- (603) Gutman, M.; Nachliel, E. The Dynamic Aspects of Proton Transfer Processes. *Biochim. Biophys. Acta, Bioenerg.* **1990**, *1015*, 391–414.
- (604) Arnaut, L. G.; Formosinho, S. J. Excited-State Proton Transfer Reactions I. Fundamentals and Intermolecular Reactions. *J. Photochem. Photobiol., A* **1993**, *75*, 1–20.
- (605) Tolbert, L. M.; Solntsev, K. M. Excited-State Proton Transfer: From Constrained Systems to “Super” Photoacids to Superfast Proton Transfer. *Acc. Chem. Res.* **2002**, *35*, 19–27.
- (606) Agmon, N. Elementary Steps in Excited-State Proton Transfer. *J. Phys. Chem. A* **2005**, *109*, 13–35.
- (607) Pines, E.; Huppert, D. Observation of Geminate Recombination in Excited State Proton Transfer. *J. Chem. Phys.* **1986**, *84*, 3576–3577.
- (608) Pines, E.; Huppert, D. Geminate Recombination Proton-Transfer Reactions. *Chem. Phys. Lett.* **1986**, *126*, 88–91.
- (609) Pines, E.; Huppert, D. Salt Effect in Photoacid Quantum Yield Measurements: A Demonstration of the Geminate Recombination Role in Deprotonation Reactions. *J. Am. Chem. Soc.* **1989**, *111*, 4096–4097.
- (610) Agmon, N.; Huppert, D.; Masad, A.; Pines, E. Excited-State Proton Transfer to Methanol-Water Mixtures. *J. Phys. Chem.* **1991**, *95*, 10407–10413.
- (611) von Smoluchowski, M. Versuch Einer Mathematischen Theorie der Koagulationskinetik Kolloider Lösungen. *Z. Phys. Chem. (Leipzig)* **1917**, *92*, 129–168.
- (612) Debye, P. Reaction Rates in Ionic Solutions. *Trans. Electrochem. Soc.* **1942**, *82*, 265–272.
- (613) Pines, E.; Huppert, D.; Agmon, N. Geminate Recombination in Excited-State Proton-Transfer Reactions: Numerical Solution of the Debye–Smoluchowski Equation with Backreaction and Comparison with Experimental Results. *J. Chem. Phys.* **1988**, *88*, 5620–5630.
- (614) Agmon, N.; Pines, E.; Huppert, D. Geminate Recombination in Proton-Transfer Reactions. II. Comparison of Diffusional and Kinetic Schemes. *J. Chem. Phys.* **1988**, *88*, 5631–5638.
- (615) Agmon, N.; Szabo, A. Theory of Reversible Diffusion-Influenced Reactions. *J. Chem. Phys.* **1990**, *92*, 5270–5284.
- (616) Huppert, D.; Agmon, N.; Pines, E. Long-Time Behavior of Reversible Geminate Recombination Reactions. *J. Opt. Soc. Am. B* **1990**, *7*, 1545–1550.
- (617) Agmon, N.; Gopich, I. V. Kinetic Transition in Excited-State Reversible Reactions. *Chem. Phys. Lett.* **1999**, *302*, 399–404.
- (618) Solntsev, K. M.; Huppert, D.; Agmon, N. Photochemistry of “Super”-Photoacids. *J. Phys. Chem. A* **1999**, *103*, 6984–6997.
- (619) Agmon, N. Excited-State Reversible Geminate Reaction. II. Contact Geminate Quenching. *J. Chem. Phys.* **1999**, *110*, 2175–2180.
- (620) Krissinel, E. B.; Agmon, N. Spherical Symmetric Diffusion Problem. *J. Comput. Chem.* **1996**, *17*, 1085–1098.
- (621) Pines, E.; Fleming, G. R. Self Quenching of 1-Naphthol. Connection between Time-Resolved and Steady-State Measurements. *Chem. Phys.* **1994**, *183*, 393–402.
- (622) Solntsev, K. M.; Huppert, D.; Agmon, N.; Tolbert, L. M. Photochemistry of “Super” Photoacids. 2. Excited-State Proton Transfer in Methanol/Water Mixtures. *J. Phys. Chem. A* **2000**, *104*, 4658–4669.
- (623) Solntsev, K. M.; Huppert, D.; Agmon, N. Experimental Evidence for a Kinetic Transition in Reversible Reactions. *Phys. Rev. Lett.* **2001**, *86*, 3427–3430.
- (624) Solntsev, K. M.; Huppert, D.; Agmon, N. Solvatochromism of  $\beta$ -Naphthol. *J. Phys. Chem. A* **1998**, *102*, 9599–9606.
- (625) Solntsev, K. M.; Huppert, D.; Tolbert, L. M.; Agmon, N. Solvatochromic Shifts of “Super” Photoacids. *J. Am. Chem. Soc.* **1998**, *120*, 7981–7982.
- (626) Spies, C.; Finkler, B.; Acar, N.; Jung, G. Solvatochromism of Pyranine-Derived Photoacids. *Phys. Chem. Chem. Phys.* **2013**, *15*, 19893–19905.
- (627) Knochenmuss, R.; Leutwyler, S. Proton Transfer from 1-Naphthol to Water: Small Clusters to the Bulk. *J. Chem. Phys.* **1989**, *91*, 1268–1278.
- (628) Soumillion, J. P.; Vandereecken, P.; Van der Auwerdaer, M.; De Schryver, F. C.; Schanck, A. Photophysical Analysis of Ion Pairing of  $\beta$ -Naphtholate in Medium Polarity Solvents: Mixtures of Contact and Solvent-Separated Ion Pairs. *J. Am. Chem. Soc.* **1989**, *111*, 2217–2225.
- (629) Perez-Lustres, J. L.; Rodriguez-Prieto, F.; Mosquera, M.; Senyushkina, T. A.; Ernsting, N. P.; Kovalenko, S. A. Ultrafast Proton Transfer to Solvent: Molecular and Intermediates from Solvation- and Diffusion-Controlled Regimes. *J. Am. Chem. Soc.* **2007**, *129*, 5408–5418.
- (630) Biczok, L.; Valat, P.; Wintgens, V. Solvent and Temperature Effects on the Deactivation Pathways of Excited Ion Pairs Produced via Photoinduced Proton Transfer. *Photochem. Photobiol. Sci.* **2003**, *2*, 230–235.
- (631) Premont-Schwarz, M.; Barak, T.; Pines, D.; Nibbering, E. T.; Pines, E. Ultrafast Excited-State Proton-Transfer Reaction of 1-Naphthol-3,6-disulfonate and Several 5-Substituted 1-Naphthol Derivatives. *J. Phys. Chem. B* **2013**, *117*, 4594–4603.
- (632) Tolbert, L. M.; Haubrich, J. E. Photoexcited Proton Transfer from Enhanced Photoacids. *J. Am. Chem. Soc.* **1994**, *116*, 10593–10600.
- (633) Weller, A. Protolytische Reaktionen Angeregter Oxyverbindungen. *Z. Phys. Chem.* **1958**, *17*, 224–245.
- (634) Harris, C. M.; Selinger, B. K. Proton-Induced Fluorescence Quenching of 2-Naphthol. *J. Phys. Chem.* **1980**, *84*, 891–898.
- (635) Harris, C. M.; Selinger, B. K. Acid-Base Properties of 1-Naphthol. Proton-Induced Fluorescence Quenching. *J. Phys. Chem.* **1980**, *84*, 1366–1371.
- (636) Webb, S. P.; Yeh, S. W.; Philips, L. A.; Tolbert, M. A.; Clark, J. H. Ultrafast Excited-State Proton Transfer in 1-Naphthol. *J. Am. Chem. Soc.* **1984**, *106*, 7286–7288.
- (637) Webb, S. P.; Philips, L. A.; Yeh, S. W.; Tolbert, L. M.; Clark, J. H. Picosecond Kinetics of the Excited-State, Proton-Transfer Reaction of 1-Naphthol in Water. *J. Phys. Chem.* **1986**, *90*, 5154–5164.
- (638) Magnes, B.-Z.; Strashnikova, N. V.; Pines, E. Evidence for  $^1L_a$ ,  $^1L_b$  Dual State Emission in 1-Naphthol and 1-Methoxynaphthalene Fluorescence in Liquid Solutions. *Isr. J. Chem.* **1999**, *39*, 361–373.
- (639) Pines, E.; Tepper, D.; Magnes, B.-Z.; Pines, D.; Barak, T. Competitive Geminate Quenching and Geminate Recombination Reactions of 1-Naphthol. *Ber. Bunsen-Ges.* **1998**, *102*, 504–510.
- (640) Tolbert, L. M.; Haubrich, J. E. Enhanced Photoacidities of Cyanonaphthols. *J. Am. Chem. Soc.* **1990**, *112*, 8163–8165.
- (641) Lee, J.; Griffin, R. D.; Robinson, G. W. 2-Naphthol: A Simple Example of Proton Transfer Effected by Water Structure. *J. Chem. Phys.* **1985**, *82*, 4920–4925.
- (642) Lee, J.; Robinson, G. W.; Webb, S. P.; Philips, L. A.; Clark, J. H. Hydration Dynamics of Protons from Photon Initiated Acids. *J. Am. Chem. Soc.* **1986**, *108*, 6538–6542.
- (643) Krishnan, R.; Fillingim, T. G.; Lee, J.; Robinson, G. W. Solvent Structural Effects on Proton Dissociation. *J. Am. Chem. Soc.* **1990**, *112*, 1353–1357.
- (644) Huppert, D.; Tolbert, L. M.; Linares-Samaniego, S. Ultrafast Excited-State Proton Transfer from Cyano-Substituted 2-Naphthols. *J. Phys. Chem. A* **1997**, *101*, 4602–4605.
- (645) Pines, E.; Pines, D.; Barak, T.; Magnes, B.-Z.; Tolbert, L. M.; Haubrich, J. E. Isotope and Temperature Effects in Ultrafast Proton-

Transfer from a Strong Excited-State Acid. *Ber. Bunsen-Ges.* **1998**, *102*, 511–517.

(646) Carmeli, I.; Huppert, D.; Tolbert, L. M.; Haubrich, J. E. Ultrafast Excited-State Proton Transfer from Dicyano-Naphthol. *Chem. Phys. Lett.* **1996**, *260*, 109–114.

(647) Landau, L. D. Zur Theorie der Energieübertragung II. *Phys. Z. Sowjetunion* **1932**, *2*, 46–51.

(648) Zener, C. Non-Adiabatic Crossing of Energy Levels. *Proc. R. Soc. London, Ser. A* **1932**, *137*, 696–702.

(649) Cohen, B.; Segal, J.; Huppert, D. Proton Transfer from Photoacid to Solvent. *J. Phys. Chem. A* **2002**, *106*, 7462–7467.

(650) Cohen, B.; Huppert, D. Evidence for a Continuous Transition from Nonadiabatic to Adiabatic Proton Transfer Dynamics in Protic Liquids. *J. Phys. Chem. A* **2001**, *105*, 2980–2988.

(651) Cohen, B.; Leiderman, P.; Huppert, D. Unusual Temperature Dependence of Proton Transfer. 2. Excited-State Proton Transfer from Photoacids to Water. *J. Phys. Chem. A* **2002**, *106*, 11115–11122.

(652) Smith, K. K.; Kaufmann, K. J.; Huppert, D.; Gutman, M. Picosecond Proton Ejection: An Ultrafast pH Jump. *Chem. Phys. Lett.* **1979**, *64*, 522–527.

(653) Förster, T.; Völker, S. Kinetics of Proton Transfer Reactions Involving Hydroxypyrene-trisulphonate in Aqueous Solution by Nanosecond Laser Absorption Spectroscopy. *Chem. Phys. Lett.* **1975**, *34*, 1–6.

(654) Haar, H. P.; Klein, U. K. A.; Hauser, M. The Coulomb Cage Pair. *Chem. Phys. Lett.* **1978**, *58*, 525–530.

(655) Hauser, M.; Haar, H. P.; Klein, U. K. A. Indirect Demonstration of the Coulomb Cage for Prototropic Dissociation. *Ber. Bunsen-Ges.* **1977**, *81*, 27–30.

(656) Gutman, M.; Huppert, D.; Pines, E. The pH Jump: A Rapid Modulation of pH of Aqueous Solutions by a Laser Pulse. *J. Am. Chem. Soc.* **1981**, *103*, 3709–3713.

(657) Pines, E.; Huppert, D. pH Jump: A Relaxational Approach. *J. Phys. Chem.* **1983**, *87*, 4471–4478.

(658) Pines, E.; Pines, D.; Ma, Y. Z.; Fleming, G. R. Femtosecond Pump-Probe Measurements of Solvation by Hydrogen-Bonding Interactions. *ChemPhysChem* **2004**, *5*, 1315–1327.

(659) Finkler, B.; Spies, C.; Vester, M.; Walte, F.; Omlor, K.; Riemann, I.; Zimmer, M.; Stracke, F.; Gerhards, M.; Jung, G. Highly Photostable "Super"-Photoacids for Ultrasensitive Fluorescence Spectroscopy. *Photochem. Photobiol. Sci.* **2014**, *13*, 548–562.

(660) Prayer, C.; Gustavsson, T.; Tran-Thi, T. H. What's New in the Proton Transfer Reaction from Pyranine to Water? A Femtosecond Study of the Proton Transfer Dynamics. *AIP Conf. Proc.* **1995**, *364*, 333–339.

(661) Tran-Thi, T. H.; Gustavsson, T.; Prayer, C.; Pommeret, S.; Hynes, J. T. Primary Ultrafast Events Preceding the Photoinduced Proton Transfer from Pyranine to Water. *Chem. Phys. Lett.* **2000**, *329*, 421–430.

(662) Tran-Thi, T. H.; Prayer, C.; Millié, P.; Uznanski, P.; Hynes, J. T. Substituent and Solvent Effects on the Nature of the Transitions of Pyrenol and Pyranine. Identification of an Intermediate in the Excited-State Proton-Transfer Reaction. *J. Phys. Chem. A* **2002**, *106*, 2244–2255.

(663) Hynes, J. T.; Tran-Thi, T.-H.; Granucci, G. Intermolecular Photochemical Proton Transfer in Solution: New Insights and Perspectives. *J. Photochem. Photobiol. A* **2002**, *154*, 3–11.

(664) Mohammed, O. F.; Dreyer, J.; Magnes, B. Z.; Pines, E.; Nibbering, E. T. Solvent-Dependent Photoacidity State of Pyranine Monitored by Transient Mid-Infrared Spectroscopy. *ChemPhysChem* **2005**, *6*, 625–636.

(665) Mohammed, O. F.; Pines, D.; Dreyer, J.; Pines, E.; Nibbering, E. T. Sequential Proton Transfer through Water Bridges in Acid-Base Reactions. *Science* **2005**, *310*, 83–86.

(666) Leiderman, P.; Genosar, L.; Huppert, D. Excited-State Proton Transfer: Indication of Three Steps in the Dissociation and Recombination Process. *J. Phys. Chem. A* **2005**, *109*, 5965–5977.

(667) Gepshtein, R.; Leiderman, P.; Genosar, L.; Huppert, D. Testing the Three Step Excited State Proton Transfer Model by the Effect of an Excess Proton. *J. Phys. Chem. A* **2005**, *109*, 9674–9684.

(668) Spry, D. B.; Goun, A.; Bell, C. B., 3rd; Fayer, M. D. Identification and Properties of the  $^1\text{L}_a$  and  $^1\text{L}_b$  States of Pyranine. *J. Chem. Phys.* **2006**, *125*, 144514.

(669) Spry, D. B.; Goun, A.; Fayer, M. D. Deprotonation Dynamics and Stokes Shift of Pyranine (HPTS). *J. Phys. Chem. A* **2007**, *111*, 230–237.

(670) Spry, D. B.; Fayer, M. D. Observation of Slow Charge Redistribution Preceding Excited-State Proton Transfer. *J. Chem. Phys.* **2007**, *127*, 204501.

(671) Spry, D. B.; Fayer, M. D. Charge Redistribution and Photoacidity: Neutral Versus Cationic Photoacids. *J. Chem. Phys.* **2008**, *128*, 084508.

(672) Brenlla, A.; Veiga Gutierrez, M.; Rios Rodriguez, M. C.; Rodriguez-Prieto, F.; Mosquera, M.; Perez Lustres, J. L. Moderately Strong Photoacid Dissociates in Alcohols with High Transient Concentration of the Proton-Transfer Contact Pair. *J. Phys. Chem. Lett.* **2014**, *5*, 989–994.

(673) Kumpulainen, T.; Bakker, B. H.; Brouwer, A. M. Complexes of a Naphthalimide Photoacid with Organic Bases, and Their Excited-State Dynamics in Polar Aprotic Organic Solvents. *Phys. Chem. Chem. Phys.* **2015**, *17*, 20715–20724.

(674) Simkovitch, R.; Akulov, K.; Shomer, S.; Roth, M. E.; Shabat, D.; Schwartz, T.; Huppert, D. Comprehensive Study of Ultrafast Excited-State Proton Transfer in Water and  $\text{D}_2\text{O}$  Providing the Missing  $\text{RO}^-\cdots\text{H}^+$  Ion-Pair Fingerprint. *J. Phys. Chem. A* **2014**, *118*, 4425–4443.

(675) Veiga-Gutierrez, M.; Brenlla, A.; Carreira Blanco, C.; Fernandez, B.; Kovalenko, S. A.; Rodriguez-Prieto, F.; Mosquera, M.; Lustres, J. L. Dissociation of a Strong Acid in Neat Solvents: Diffusion Is Observed after Reversible Proton Ejection inside the Solvent Shell. *J. Phys. Chem. B* **2013**, *117*, 14065–14078.

(676) Spies, C.; Shomer, S.; Finkler, B.; Pines, D.; Pines, E.; Jung, G.; Huppert, D. Solvent Dependence of Excited-State Proton Transfer from Pyranine-Derived Photoacids. *Phys. Chem. Chem. Phys.* **2014**, *16*, 9104–9114.

(677) Genosar, L.; Cohen, B.; Huppert, D. Ultrafast Direct Photoacid–Base Reaction. *J. Phys. Chem. A* **2000**, *104*, 6689–6698.

(678) Rini, M.; Magnes, B. Z.; Pines, E.; Nibbering, E. T. Real-Time Observation of Bimodal Proton Transfer in Acid-Base Pairs in Water. *Science* **2003**, *301*, 349–352.

(679) Rini, M.; Pines, D.; Magnes, B. Z.; Pines, E.; Nibbering, E. T. Bimodal Proton Transfer in Acid-Base Reactions in Water. *J. Chem. Phys.* **2004**, *121*, 9593–9610.

(680) Mohammed, O. F.; Pines, D.; Nibbering, E. T.; Pines, E. Base-Induced Solvent Switches in Acid-Base Reactions. *Angew. Chem., Int. Ed.* **2007**, *46*, 1458–1461.

(681) Mohammed, O. F.; Pines, D.; Pines, E.; Nibbering, E. T. J. Aqueous Bimolecular Proton Transfer in Acid–Base Neutralization. *Chem. Phys.* **2007**, *341*, 240–257.

(682) Agmon, N. The Grotthuss Mechanism. *Chem. Phys. Lett.* **1995**, *244*, 456–462.

(683) de Grotthuss, C. J. T. Memoir on the Decomposition of Water and of the Bodies That It Holds in Solution by Means of Galvanic Electricity. *Biochim. Biophys. Acta, Bioenerg.* **2006**, *1757*, 871–875.

(684) Siwick, B. J.; Bakker, H. J. On the Role of Water in Intermolecular Proton-Transfer Reactions. *J. Am. Chem. Soc.* **2007**, *129*, 13412–13420.

(685) Siwick, B. J.; Cox, M. J.; Bakker, H. J. Long-Range Proton Transfer in Aqueous Acid-Base Reactions. *J. Phys. Chem. B* **2008**, *112*, 378–389.

(686) Cox, M. J.; Bakker, H. J. Parallel Proton Transfer Pathways in Aqueous Acid-Base Reactions. *J. Chem. Phys.* **2008**, *128*, 174501.

(687) Cox, M. J.; Siwick, B. J.; Bakker, H. J. Influence of Ions on Aqueous Acid-Base Reactions. *ChemPhysChem* **2009**, *10*, 236–244.

- (688) Cox, M. J.; Timmer, R. L.; Bakker, H. J.; Park, S.; Agmon, N. Distance-Dependent Proton Transfer Along Water Wires Connecting Acid-Base Pairs. *J. Phys. Chem. A* **2009**, *113*, 6599–6606.
- (689) Cox, M. J.; Bakker, H. J. Femtosecond Study of the Deuteron-Transfer Dynamics of Naphtol Salts in Water. *J. Phys. Chem. A* **2010**, *114*, 10523–10530.
- (690) Mason, S. F.; Philp, J.; Smith, B. E. Prototropic Equilibria of Electronically Excited Molecules. Part II. 3-, 6-, and 7-Hydroxyquinoline. *J. Chem. Soc. A* **1968**, 3051–3056.
- (691) Bardez, E.; Chatelain, A.; Larrey, B.; Valeur, B. Photoinduced Coupled Proton and Electron Transfers. 1. 6-Hydroxyquinoline. *J. Phys. Chem.* **1994**, *98*, 2357–2366.
- (692) Schulman, S.; Fernando, Q. Excited State Prototropic Equilibria of Some Quinolins. *Tetrahedron* **1968**, *24*, 1777–1783.
- (693) Thistlethwaite, P. J.; Corkill, P. J. Direct Observation of Photoautomerism Kinetics in 7-Quinolinsol by Picosecond Spectroscopy. *Chem. Phys. Lett.* **1982**, *85*, 317–321.
- (694) Thistlethwaite, P. J. Solvation Effects in the Phototautomerization of 7-Quinolinsol. *Chem. Phys. Lett.* **1983**, *96*, 509–512.
- (695) Itoh, M.; Adachi, T.; Tokumura, K. Time-Resolved Fluorescence and Absorption Spectra and Two-Step Laser Excitation Fluorescence of the Excited-State Proton Transfer in the Methanol Solution of 7-Hydroxyquinoline. *J. Am. Chem. Soc.* **1984**, *106*, 850–855.
- (696) Konijnenberg, J.; Ekemans, G. B.; Huizer, A. H.; Varma, C. A. G. O. Mechanism and Solvent Dependence of the Solvent-Catalysed Pseudo-Intramolecular Proton Transfer of 7-Hydroxyquinoline in the First Electronically Excited Singlet State and in the Ground State of Its Tautomer. *J. Chem. Soc., Faraday Trans. 2* **1989**, *85*, 39–51.
- (697) Bohra, A.; Lavin, A.; Collins, S. Ground-State Triple Proton Transfer in 7-Hydroxyquinoline. 4. Observation in Room-Temperature Methanol and Aqueous Solutions. *J. Phys. Chem.* **1994**, *98*, 11424–11427.
- (698) Kim, T.-G.; Lee, S.-I.; Jang, D.-J.; Kim, Y. Unusually Large Tunneling Effect on the Proton Transfer of Aqueous 7-Hydroxyquinoline. *J. Phys. Chem.* **1995**, *99*, 12698–12700.
- (699) Nakagawa, T.; Kohtani, S.; Itoh, M. Picosecond Fluorescence and Two-Step LIF Studies of the Excited-State Proton Transfer in Methanol Solutions of 7-Hydroxyquinoline and Methyl-Substituted 7-Hydroxyquinolines. *J. Am. Chem. Soc.* **1995**, *117*, 7952–7957.
- (700) Tokumura, K.; Natsume, M.; Nakagawa, T.; Hashimoto, M.; Yuzawa, T.; Hamaguchi, H.-o.; Itoh, M. Time-Resolved Infrared Study of Ground-State Phototautomer Formed in the Excited-State Proton Transfer of 7-Hydroxyquinoline in Methanol. *Chem. Phys. Lett.* **1997**, *271*, 320–326.
- (701) Yu, H.; Kwon, H. J.; Jang, D. J. Excited State Proton Transfers and Subsequent Electron Rearrangement of Aqueous 6-Hydroxyquinoline. *Bull. Korean Chem. Soc.* **1997**, *18*, 156–161.
- (702) Bardez, E.; Fedorov, A.; Berberan-Santos, M. N.; Martinho, J. M. G. Photoinduced Coupled Proton and Electron Transfers. 2. 7-Hydroxyquinolinium Ion. *J. Phys. Chem. A* **1999**, *103*, 4131–4136.
- (703) Bardez, E. Excited-State Proton Transfer in Bifunctional Compounds. *Isr. J. Chem.* **1999**, *39*, 319–332.
- (704) Chou, P.-T.; Martinez, S. S. Reinvestigation of Solvent Catalyzed Ground-State Reverse Proton Transfer in 7-Hydroxyquinoline. *Chem. Phys. Lett.* **1995**, *235*, 463–470.
- (705) Presiado, I.; Erez, Y.; Gepshtein, R.; Huppert, D. Excited-State Proton Transfer and Proton Reactions of 6-Hydroxyquinoline and 7-Hydroxyquinoline in Water and Ice. *J. Phys. Chem. C* **2009**, *113*, 20066–20075.
- (706) Kim, T. G.; Kim, Y.; Jang, D.-J. Catalytic Roles of Water Prototropic Species in the Tautomerization of Excited 6-Hydroxyquinoline: Migration of Hydrated Proton Clusters. *J. Phys. Chem. A* **2001**, *105*, 4328–4332.
- (707) Poizat, O.; Bardez, E.; Buntinx, G.; Alain, V. Picosecond Dynamics of the Photoexcited 6-Methoxyquinoline and 6-Hydroxyquinoline Molecules in Solution. *J. Phys. Chem. A* **2004**, *108*, 1873–1880.
- (708) Lee, S.-I.; Jang, D.-J. Proton Transfers of Aqueous 7-Hydroxyquinoline in the First Excited Singlet, Lowest Triplet, and Ground States. *J. Phys. Chem.* **1995**, *99*, 7537–7541.
- (709) Garcia-Ochoa, I.; Bisht, P. B.; Sanchez, F.; Martinez-Ataz, E.; Santos, L.; Tripathi, H. B.; Douhal, A. Experimental and Theoretical Studies of the Proton-Hopping Reaction of 7-Hydroxyquinoline in Viscous Hydroxylic Media. *J. Phys. Chem. A* **1998**, *102*, 8871–8880.
- (710) Chou, P.-T.; Wei, C.-Y.; Chris Wang, C.-R.; Hung, F.-T.; Chang, C.-P. Proton-Transfer Tautomerism of 7-Hydroxyquinolines Mediated by Hydrogen-Bonded Complexes. *J. Phys. Chem. A* **1999**, *103*, 1939–1949.
- (711) Kohtani, S.; Tagami, A.; Nakagaki, R. Excited-State Proton Transfer of 7-Hydroxyquinoline in a Non-Polar Medium: Mechanism of Triple Proton Transfer in the Hydrogen-Bonded System. *Chem. Phys. Lett.* **2000**, *316*, 88–93.
- (712) Park, H. J.; Kwon, O.-H.; Ah, C. S.; Jang, D.-J. Excited-State Tautomerization Dynamics of 7-Hydroxyquinoline in  $\beta$ -Cyclodextrin. *J. Phys. Chem. B* **2005**, *109*, 3938–3943.
- (713) Kwon, O.-H.; Lee, Y.-S.; Yoo, B. K.; Jang, D.-J. Excited-State Triple Proton Transfer of 7-Hydroxyquinoline Along a Hydrogen-Bonded Alcohol Chain: Vibrationally Assisted Proton Tunneling. *Angew. Chem., Int. Ed.* **2006**, *45*, 415–419.
- (714) Park, S.-Y.; Kim, B.; Lee, Y.-S.; Kwon, O.-H.; Jang, D.-J. Triple Proton Transfer of Excited 7-Hydroxyquinoline Along a Hydrogen-Bonded Water Chain in Ethers: Secondary Solvent Effect on the Reaction Rate. *Photochem. Photobiol. Sci.* **2009**, *8*, 1611–1617.
- (715) Park, S.-Y.; Lee, Y.-S.; Kwon, O.-H.; Jang, D.-J. Proton Transport of Water in Acid-Base Reactions of 7-Hydroxyquinoline. *Chem. Commun.* **2009**, 926–928.
- (716) Park, S.-Y.; Jang, D.-J. Accumulated Proton-Donating Ability of Solvent Molecules in Proton Transfer. *J. Am. Chem. Soc.* **2010**, *132*, 297–302.
- (717) Kang, B.; Ko, K. C.; Park, S. Y.; Jang, D. J.; Lee, J. Y. Solvent Effect on the Excited-State Proton Transfer of 7-Hydroxyquinoline Along a Hydrogen-Bonded Ethanol Dimer. *Phys. Chem. Chem. Phys.* **2011**, *13*, 6332–6339.
- (718) Al-Lawatia, N.; Husband, J.; Steinbrecher, T.; Abou-Zied, O. K. Tautomerism in 7-Hydroxyquinoline: A Combined Experimental and Theoretical Study in Water. *J. Phys. Chem. A* **2011**, *115*, 4195–4201.
- (719) Park, S.-Y.; Jang, D.-J. Excited-State Hydrogen Relay Along a Blended-Alcohol Chain as a Model System of a Proton Wire: Deuterium Effect on the Reaction Dynamics. *Phys. Chem. Chem. Phys.* **2012**, *14*, 8885–8891.
- (720) Park, S.-Y.; Kim, H.-B.; Yoo, B. K.; Jang, D.-J. Direct Observation of Conformation-Dependent Pathways in the Excited-State Proton Transfer of 7-Hydroxyquinoline in Bulk Alcohols. *J. Phys. Chem. B* **2012**, *116*, 14153–14158.
- (721) Kwon, O.-H.; Mohammed, O. F. Water-Wire Catalysis in Photoinduced Acid-Base Reactions. *Phys. Chem. Chem. Phys.* **2012**, *14*, 8974–8980.
- (722) Mehata, M. S. Photoinduced Excited State Proton Rearrangement of 6-Hydroxyquinoline Along a Hydrogen-Bonded Acetic Acid Wire. *Chem. Phys. Lett.* **2007**, *436*, 357–361.
- (723) Mehata, M. S. Proton Translocation and Electronic Relaxation Along a Hydrogen-Bonded Molecular Wire in a 6-Hydroxyquinoline/Acetic Acid Complex. *J. Phys. Chem. B* **2008**, *112*, 8383–8386.
- (724) Kim, T. G.; Topp, M. R. Ultrafast Excited-State Deprotonation and Electron Transfer in Hydroxyquinoline Derivatives. *J. Phys. Chem. A* **2004**, *108*, 10060–10065.
- (725) Perez Lustres, J. L.; Kovalenko, S. A.; Mosquera, M.; Senyushkina, T.; Flasche, W.; Ernstring, N. P. Ultrafast Solvation of N-Methyl-6-quinolone Probes Local IR Spectrum. *Angew. Chem., Int. Ed.* **2005**, *44*, 5635–5639.
- (726) Lee, Y. M.; Park, S.-Y.; Kim, H.; Kim, T. G.; Kwon, O.-H. Photoinduced Strong Acid–Weak Base Reactions in a Polar Aprotic Solvent. *Methods Appl. Fluoresc.* **2016**, *4*, 024004.
- (727) Gould, E. A.; Popov, A. V.; Tolbert, L. M.; Presiado, I.; Erez, Y.; Huppert, D.; Solntsev, K. M. Excited-State Proton Transfer in N-



Methyl-6-hydroxyquinolinium Salts: Solvent and Temperature Effects. *Phys. Chem. Chem. Phys.* **2012**, *14*, 8964–8973.

(728) Popov, A. V.; Gould, E. A.; Salvitti, M. A.; Hernandez, R.; Solntsev, K. M. Diffusional Effects on the Reversible Excited-State Proton Transfer. From Experiments to Brownian Dynamics Simulations. *Phys. Chem. Chem. Phys.* **2011**, *13*, 14914–14927.

(729) Karton-Lifshin, N.; Presiado, I.; Erez, Y.; Gepshtein, R.; Shabat, D.; Huppert, D. Ultrafast Excited-State Intermolecular Proton Transfer of Cyanine Fluorochrome Dyes. *J. Phys. Chem. A* **2012**, *116*, 85–92.

(730) Simkovitch, R.; Karton-Lifshin, N.; Shomer, S.; Shabat, D.; Huppert, D. Ultrafast Excited-State Proton Transfer to the Solvent Occurs on a Hundred-Femtosecond Time-Scale. *J. Phys. Chem. A* **2013**, *117*, 3405–3413.

(731) Presiado, I.; Karton-Lifshin, N.; Erez, Y.; Gepshtein, R.; Shabat, D.; Huppert, D. Ultrafast Proton Transfer of Three Novel Quinone Cyanine Photoacids. *J. Phys. Chem. A* **2012**, *116*, 7353–7363.

(732) Simkovitch, R.; Shomer, S.; Gepshtein, R.; Roth, M. E.; Shabat, D.; Huppert, D. Comparison of the Rate of Excited-State Proton Transfer from Photoacids to Alcohols and Water. *J. Photochem. Photobiol., A* **2014**, *277*, 90–101.

(733) Simkovitch, R.; Shomer, S.; Gepshtein, R.; Shabat, D.; Huppert, D. Excited-State Proton Transfer from Quinone-Cyanine 9 to Protic Polar-Solvent Mixtures. *J. Phys. Chem. A* **2014**, *118*, 1832–1840.

(734) Simkovitch, R.; Shomer, S.; Gepshtein, R.; Huppert, D. How Fast Can a Proton-Transfer Reaction Be Beyond the Solvent-Control Limit? *J. Phys. Chem. B* **2015**, *119*, 2253–2262.

(735) Simkovitch, R.; Shomer, S.; Gepshtein, R.; Shabat, D.; Huppert, D. Temperature Dependence of the Excited-State Proton-Transfer Reaction of Quinone-Cyanine-7. *J. Phys. Chem. A* **2013**, *117*, 3925–3934.

(736) Walrafen, G. E. Raman Spectral Studies of the Effects of Temperature on Water Structure. *J. Chem. Phys.* **1967**, *47*, 114–126.

(737) Addison, K.; Conyard, J.; Dixon, T.; Bulman Page, P. C.; Solntsev, K. M.; Meech, S. R. Ultrafast Studies of the Photophysics of Cis and Trans States of the Green Fluorescent Protein Chromophore. *J. Phys. Chem. Lett.* **2012**, *3*, 2298–2302.

(738) Briand, J.; Léonard, J.; Haacke, S. Ultrafast Photo-Induced Reaction Dynamics in Bacteriorhodopsin and Its Trp Mutants. *J. Opt.* **2010**, *12*, 084004.

(739) Malhado, J. P.; Hynes, J. T. Photoisomerization for a Model Protonated Schiff Base in Solution: Sloped/Peaked Conical Intersection Perspective. *J. Chem. Phys.* **2012**, *137*, 22A543.

(740) Buhl, E.; Braun, M.; Lakatos, A.; Glaubitz, C.; Wachtveitl, J. Fluorescence and Excited State Dynamics of the Deprotonated Schiff Base Retinal in Proteorhodopsin. *Biol. Chem.* **2015**, *396*, 1109–1115.

(741) Mathies, R. A.; Cruz, C. H. B.; Pollard, W. T.; Shank, C. V. Direct Observation of the Femtosecond Excited-State *cis-trans* Isomerization in Bacteriorhodopsin. *Science* **1988**, *240*, 777–779.

(742) Atkinson, G. H.; Brack, T. L.; Blanchard, D.; Rumbles, G. Picosecond Time-Resolved Resonance Raman Spectroscopy of the Initial trans to cis Isomerization in the Bacteriorhodopsin Photocycle. *Chem. Phys.* **1989**, *131*, 1.

(743) Diller, R.; Maiti, S.; Walker, G. C.; Cowen, B. R.; Pippenger, R.; Bogolni, R. A.; Hochstrasser, R. M. Femtosecond Time-Resolved Infrared Laser Study of the J-K Transition of Bacteriorhodopsin. *Chem. Phys. Lett.* **1995**, *241*, 109.

(744) Kobayashi, T.; Saito, T.; Ohtani, H. Real-Time Spectroscopy of Transition States in Bacteriorhodopsin During Retinal Isomerization. *Nature* **2001**, *414*, 531–534.

(745) Kukura, P.; McCamant, D. W.; Yoon, S.; Wandschneider, D. B.; Mathies, R. A. Structural Observation of the Primary Isomerization in Vision with Femtosecond-Stimulated Raman. *Science* **2005**, *310*, 1006–1009.

(746) Quick, M.; Dobryakov, A. L.; Gerecke, M.; Richter, C.; Berndt, F.; Ioffe, I. N.; Granovsky, A. A.; Mahrwald, R.; Ernsting, N. P.; Kovalenko, S. A. Photoisomerization Dynamics and Pathways of *trans*- and *cis*-Azobenzene in Solution from Broadband Femtosecond

Spectroscopies and Calculations. *J. Phys. Chem. B* **2014**, *118*, 8756–8771.

(747) Liu, R. S.; Asato, A. E. The Primary Process of Vision and the Structure of Bathorhodopsin: A Mechanism for Photoisomerization of Polyenes. *Proc. Natl. Acad. Sci. U. S. A.* **1985**, *82*, 259–263.

(748) Quick, M.; Berndt, F.; Dobryakov, A. L.; Ioffe, I. N.; Granovsky, A. A.; Knie, C.; Mahrwald, R.; Lenoir, D.; Ernsting, N. P.; Kovalenko, S. A. Photoisomerization Dynamics of Stiff-Stilbene in Solution. *J. Phys. Chem. B* **2014**, *118*, 1389–1402.

(749) Michl, J.; Bonačić-Koutecký, V. *Electronic Aspects of Organic Photochemistry*; Wiley: New York, 1990.

(750) Klessinger, M. Conical Intersections and the Mechanism of Singlet Photoreactions. *Angew. Chem., Int. Ed. Engl.* **1995**, *34*, 549–551.

(751) Bernardi, F.; Olivucci, M.; Robb, M. A. Potential Energy Surface Crossings in Organic Photochemistry. *Chem. Soc. Rev.* **1996**, *25*, 321–328.

(752) Domcke, W.; Yarkony, D. R.; Köppel, H. *Conical Intersections*; World Scientific: London, 2004; Vol. 15.

(753) Domcke, W.; Yarkony, D. R.; Köppel, H. *Conical Intersections*; World Scientific: London, 2011; Vol. 17.

(754) Yarkony, D. R. Nonadiabatic Quantum Chemistry—Past, Present, and Future. *Chem. Rev.* **2012**, *112*, 481–498.

(755) Malhado, J. P.; Spezia, R.; Hynes, J. T. Conical Intersection Structure and Dynamics for a Model Protonated Schiff Base Photoisomerization in Solution. *Int. J. Quantum Chem.* **2013**, *113*, 296–305.

(756) Sajadi, M.; Dobryakov, A. L.; Garbin, E.; Ernsting, N. P.; Kovalenko, S. A. Time-Resolved Fluorescence Spectra of *cis*-Stilbene in Hexane and Acetonitrile. *Chem. Phys. Lett.* **2010**, *489*, 44–47.

(757) Kovalenko, S. A.; Dobryakov, A. L.; Ioffe, I.; Ernsting, N. P. Evidence for the Phantom State in Photoinduced *cis-trans* Isomerization of Stilbene. *Chem. Phys. Lett.* **2010**, *493*, 255–258.

(758) Dobryakov, A. L.; Ioffe, I.; Granovsky, A. A.; Ernsting, N. P.; Kovalenko, S. A. Femtosecond Raman Spectra of *cis*-Stilbene and *trans*-Stilbene with Isotopomers in Solution. *J. Chem. Phys.* **2012**, *137*, 244505.

(759) Berndt, F.; Dobryakov, A. L.; Quick, M.; Mahrwald, R.; Ernsting, N. P.; Lenoir, D.; Kovalenko, S. A. Long-Lived Perpendicular Conformation in the Photoisomerization Path of 1,1'-Dimethylstilbene and 1,1'-Diethylstilbene. *Chem. Phys. Lett.* **2012**, *544*, 39–42.

(760) Kovalenko, S. A.; Dobryakov, A. L. On the Excitation Wavelength Dependence and Arrhenius Behavior of Stilbene Isomerization Rates in Solution. *Chem. Phys. Lett.* **2013**, *570*, 56–60.

(761) Waldeck, D. H. Photoisomerization Dynamics of Stilbenes. *Chem. Rev.* **1991**, *91*, 415–436.

(762) Görner, H.; Kuhn, H. J. *Cis-Trans* Photoisomerization of Stilbenes and Stilbene-Like Molecules. In *Adv. Photochem.*; John Wiley & Sons, Inc.: NJ, 1995; Vol. 19, pp 1–117.

(763) Saltiel, J. Perdeuteriostilbene. The Role of Phantom States in the *cis-trans* Photoisomerization of Stilbenes. *J. Am. Chem. Soc.* **1967**, *89*, 1036–1037.

(764) Saltiel, J. Perdeuteriostilbene. The Triplet and Singlet Paths for Stilbene Photoisomerization. *J. Am. Chem. Soc.* **1968**, *90*, 6394–6400.

(765) Saltiel, J.; D'Agostino, J. T. Separation of Viscosity and Temperature Effects on the Singlet Pathway to Stilbene Photoisomerization. *J. Am. Chem. Soc.* **1972**, *94*, 6445–6456.

(766) Orlandi, G.; Siebrand, W. Model for the Direct Photoisomerization of Stilbene. *Chem. Phys. Lett.* **1975**, *30*, 352–354.

(767) Greene, B. I.; Farrow, R. C. Subpicosecond Time Resolved Multiphoton Ionization: Excited State Dynamics of *cis*-Stilbene under Collision Free Conditions. *J. Chem. Phys.* **1983**, *78*, 3336–3338.

(768) Doany, F.; Heilweil, E.; Moore, R.; Hochstrasser, R. Picosecond Study of an Intermediate in the *trans* to *cis* Isomerization Pathway of Stiff Stilbene. *J. Chem. Phys.* **1984**, *80*, 201–206.

(769) Lee, M.; Bain, A. J.; McCarthy, P. J.; Han, C. H.; Haseltine, J. N.; Smith, A. B.; Hochstrasser, R. M. Picosecond Photoisomerization and Rotational Reorientation Dynamics in Solution. *J. Chem. Phys.* **1986**, *85*, 4341–4348.

- (770) Rothenberger, G.; Negus, D. K.; Hochstrasser, R. M. Solvent Influence on Photoisomerization Dynamics. *J. Chem. Phys.* **1983**, *79*, 5360–5367.
- (771) Grote, R. F.; Hynes, J. T. The Stable States Picture of Chemical Reactions. II. Rate Constants for Condensed and Gas Phase Reaction Models. *J. Chem. Phys.* **1980**, *73*, 2715–2733.
- (772) Grote, R. F.; Hynes, J. T. Reactive Modes in Condensed Phase Reactions. *J. Chem. Phys.* **1981**, *74*, 4465–4476.
- (773) van der Zwan, G.; Hynes, J. T. Reactive Paths in the Diffusion Limit. *J. Chem. Phys.* **1982**, *77*, 1295–1302.
- (774) Fleming, G. R.; Courtney, S. H.; Balk, M. W. Activated Barrier Crossing: Comparison of Experiment and Theory. *J. Stat. Phys.* **1986**, *42*, 83–104.
- (775) Kim, S. K.; Fleming, G. R. Reorientation and Isomerization of *trans*-Stilbene in Alkane Solutions. *J. Phys. Chem.* **1988**, *92*, 2168–2172.
- (776) Todd, D. C.; Jean, J. M.; Rosenthal, S. J.; Ruggiero, A. J.; Yang, D.; Fleming, G. R. Fluorescence Upconversion Study of *cis*-Stilbene Isomerization. *J. Chem. Phys.* **1990**, *93*, 8658–8668.
- (777) Todd, D. C.; Fleming, G. R. *Cis*-Stilbene Isomerization: Temperature Dependence and the Role of Mechanical Friction. *J. Chem. Phys.* **1993**, *98*, 269–279.
- (778) Takeuchi, S.; Tahara, T. Vibrational Coherence of  $S_1$  *trans*-Stilbene in Solution Observed by 40-fs-Resolved Absorption Spectroscopy: Comparison of the Low-Frequency Vibration Appearing in the Frequency-Domain and Time-Domain Spectroscopies. *Chem. Phys. Lett.* **2000**, *326*, 430–438.
- (779) Ishii, K.; Takeuchi, S.; Tahara, T. A 40-fs Time-Resolved Absorption Study on *cis*-Stilbene in Solution: Observation of Wavepacket Motion on the Reactive Excited State. *Chem. Phys. Lett.* **2004**, *398*, 400–406.
- (780) Szarka, A. Z.; Pugliano, N.; Palit, D. K.; Hochstrasser, R. M. Vibrational Coherence in the Solution Phase Photoisomerization Reaction of *cis*-Stilbene. *Chem. Phys. Lett.* **1995**, *240*, 25–30.
- (781) Fuß, W.; Kosmidis, C.; Schmid, W. E.; Trushin, S. A. The Photochemical *cis*–*trans* Isomerization of Free Stilbene Molecules Follows a Hula-Twist Pathway. *Angew. Chem., Int. Ed.* **2004**, *43*, 4178–4182.
- (782) Fuß, W.; Kosmidis, C.; Schmid, W. E.; Trushin, S. A. The Lifetime of the Perpendicular Minimum of *cis*-Stilbene Observed by Dissociative Intense-Laser Field Ionization. *Chem. Phys. Lett.* **2004**, *385*, 423–430.
- (783) Rau, H.; Lueddecke, E. On the Rotation-Inversion Controversy on Photoisomerization of Azobenzenes. Experimental Proof of Inversion. *J. Am. Chem. Soc.* **1982**, *104*, 1616–1620.
- (784) Rau, H.; Yu-Quan, S. Photoisomerization of Sterically Hindered Azobenzenes. *J. Photochem. Photobiol., A* **1988**, *42*, 321–327.
- (785) Siewertsen, R.; Neumann, H.; Buchheim-Stehn, B.; Herges, R.; Näther, C.; Renth, F.; Temps, F. Highly Efficient Reversible *Z*–*E* Photoisomerization of a Bridged Azobenzene with Visible Light through Resolved  $S_1(n\pi^*)$  Absorption Bands. *J. Am. Chem. Soc.* **2009**, *131*, 15594–15595.
- (786) Dhammika Bandara, H. M.; Burdette, S. C. Photoisomerization in Different Classes of Azobenzene. *Chem. Soc. Rev.* **2012**, *41*, 1809–1825.
- (787) Yager, K. G.; Barrett, C. J. Novel Photo-Switching Using Azobenzene Functional Materials. *J. Photochem. Photobiol., A* **2006**, *182*, 250–261.
- (788) Böckmann, M.; Doltsinis, N. L.; Marx, D. Nonadiabatic Hybrid Quantum and Molecular Mechanic Simulations of Azobenzene Photoswitching in Bulk Liquid Environment. *J. Phys. Chem. A* **2010**, *114*, 745–754.
- (789) Böckmann, M.; Doltsinis, N. L.; Marx, D. Enhanced Photoswitching of Bridged Azobenzene Studied by Nonadiabatic Ab Initio Simulation. *J. Chem. Phys.* **2012**, *137*, 22A505.
- (790) Khan, A.; Kaiser, C.; Hecht, S. Prototype of a Photoswitchable Foldamer. *Angew. Chem., Int. Ed.* **2006**, *45*, 1878–1881.
- (791) Bléger, D.; Liebig, T.; Thiermann, R.; Maskos, M.; Rabe, J. P.; Hecht, S. Light-Orchestrated Macromolecular “Accordions”: Reversible Photoinduced Shrinking of Rigid-Rod Polymers. *Angew. Chem., Int. Ed.* **2011**, *50*, 12559–12563.
- (792) Bortolus, P.; Monti, S. *Cis*-*Trans* Photoisomerization of Azobenzenes. Solvent and Triplet Donor Effects. *J. Phys. Chem.* **1979**, *83*, 648–652.
- (793) Lednev, I. K.; Ye, T. Q.; Hester, R. E.; Moore, J. N. Femtosecond Time-Resolved UV–Visible Absorption Spectroscopy of *trans*-Azobenzene in Solution. *J. Phys. Chem.* **1996**, *100*, 13338.
- (794) Lednev, I. K.; Ye, T. Q.; Matousek, P.; Towrie, M.; Fogg, P.; Neuwahl, F. V. R.; Umapathy, S.; Hester, R. E.; Moore, J. N. Femtosecond Time-Resolved UV-Visible Absorption Spectroscopy of *trans*-Azobenzene: Dependence on Excitation Wavelength. *Chem. Phys. Lett.* **1998**, *290*, 68–74.
- (795) Nagele, T.; Hoche, R.; Zinth, W.; Wachtveitl, J. Femtosecond Photoisomerization of *cis*-Azobenzene. *Chem. Phys. Lett.* **1997**, *272*, 489–495.
- (796) Wachtveitl, J.; Nagele, T.; Puell, B.; Zinth, W.; Kruger, M.; RudolphBohner, S.; Oesterhelt, D.; Moroder, L. Ultrafast Photoisomerization of Azobenzene Compounds. *J. Photochem. Photobiol., A* **1997**, *105*, 283–288.
- (797) Satzger, H.; Spörlein, S.; Root, C.; Wachtveitl, J.; Zinth, W.; Gilch, P. Fluorescence Spectra of *trans*- and *cis*-Azobenzene – Emission from the Franck–Condon State. *Chem. Phys. Lett.* **2003**, *372*, 216–223.
- (798) Satzger, H.; Root, C.; Braun, M. Excited-State Dynamics of *trans*- and *cis*-Azobenzene after UV Excitation in the  $\pi\pi^*$  Band. *J. Phys. Chem. A* **2004**, *108*, 6265–6271.
- (799) Monti, S.; Orlandi, G.; Palmieri, P. Features of the Photochemically Active State Surfaces of Azobenzene. *Chem. Phys.* **1982**, *71*, 87–99.
- (800) Hamm, P.; Ohline, S. M.; Zinth, W. Vibrational Cooling after Ultrafast Photoisomerization of Azobenzene Measured by Femtosecond Infrared Spectroscopy. *J. Chem. Phys.* **1997**, *106*, 519–529.
- (801) Hamm, P.; Ohline, S.; Zurek, M.; Roschinger, T. Vibrational Cooling after Photo Isomerisation: First Application of a Novel Intramolecular Thermometer. *Laser Chem.* **1999**, *19*, 45–49.
- (802) Fujino, T.; Tahara, T. Picosecond Time-Resolved Raman Study of *trans*-Azobenzene. *J. Phys. Chem. A* **2000**, *104*, 4203–4210.
- (803) Fujino, T.; Arzhantsev, S. Y.; Tahara, T. Femtosecond Time-Resolved Fluorescence Study of Photoisomerization of *trans*-Azobenzene. *J. Phys. Chem. A* **2001**, *105*, 8123–8129.
- (804) Pancur, T.; Renth, F.; Temps, F.; Harbaum, B.; Krüger, A.; Herges, R.; Näther, C. Femtosecond Fluorescence Up-Conversion Spectroscopy of a Rotation-Restricted Azobenzene after Excitation to the  $S_1$  State. *Phys. Chem. Chem. Phys.* **2005**, *7*, 1985–1989.
- (805) Chang, C.-W.; Lu, Y.-C.; Wang, T.-T.; Diao, E. W.-G. Photoisomerization Dynamics of Azobenzene in Solution with  $S_1$  Excitation: A Femtosecond Fluorescence Anisotropy Study. *J. Am. Chem. Soc.* **2004**, *126*, 10109–10118.
- (806) Schmidt, B.; Sobotta, C.; Malkmus, S.; Laimgruber, S.; Braun, M.; Zinth, W.; Gilch, P. Femtosecond Fluorescence and Absorption Dynamics of an Azobenzene with a Strong Push-Pull Substitution. *J. Phys. Chem. A* **2004**, *108*, 4399–4404.
- (807) Fliegl, H.; Köhn, A.; Hättig, C.; Ahlrichs, R. Ab Initio Calculation of the Vibrational and Electronic Spectra of *trans*- and *cis*-Azobenzene. *J. Am. Chem. Soc.* **2003**, *125*, 9821–9827.
- (808) Diao, E. W. G. A New *Trans*-to-*Cis* Photoisomerization Mechanism of Azobenzene on the  $S_1(n,\pi^*)$  Surface. *J. Phys. Chem. A* **2004**, *108*, 950–956.
- (809) Cembran, A.; Bernardi, F.; Garavelli, M.; Gagliardi, L.; Orlandi, G. On the Mechanism of the *cis*–*trans* Isomerization in the Lowest Electronic States of Azobenzene:  $S_0$ ,  $S_1$ , and  $T_1$ . *J. Am. Chem. Soc.* **2004**, *126*, 3234–3243.
- (810) Crecca, C. R.; Roitberg, A. E. Theoretical Study of the Isomerization Mechanism of Azobenzene and Disubstituted Azobenzene Derivatives. *J. Phys. Chem. A* **2006**, *110*, 8188–8203.
- (811) Granucci, G.; Persico, M. Excited State Dynamics with the Direct Trajectory Surface Hopping Method: Azobenzene and Its Derivatives as a Case Study. *Theor. Chem. Acc.* **2007**, *117*, 1131–1143.

- (812) Harabuchi, Y.; Ishii, M.; Nakayama, A.; Noro, T.; Taketsugu, T. A Multireference Perturbation Study of the Nn Stretching Frequency of *trans*-Azobenzene in  $n\pi^*$  Excitation and an Implication for the Photoisomerization Mechanism. *J. Chem. Phys.* **2013**, *138*, 064305.
- (813) Sampedro Ruiz, D.; Cembran, A.; Garavelli, M.; Olivucci, M.; Fuß, W. Structure of the Conical Intersections Driving the *cis*–*trans* Photoisomerization of Conjugated Molecules. *Photochem. Photobiol.* **2002**, *76*, 622–633.
- (814) Yuan, S.; Dou, Y.; Wu, W.; Hu, Y.; Zhao, J. Why Does *trans*-Azobenzene Have a Smaller Isomerization Yield for  $\pi\pi^*$  Excitation Than for  $n\pi^*$  Excitation? *J. Phys. Chem. A* **2008**, *112*, 13326–13334.
- (815) Jiang, C.-W.; Xie, R.-H.; Li, F.-L.; Allen, R. E. Comparative Studies of the *trans*–*cis* Photoisomerizations of Azobenzene and a Bridged Azobenzene. *J. Phys. Chem. A* **2011**, *115*, 244–249.
- (816) Sharkov, A. V.; Pakulev, A. V.; Chekalin, S. V.; Matveet, Y. A. Primary Events in Bacteriorhodopsin Probed by Subpicosecond Spectroscopy. *Biochim. Biophys. Acta, Bioenerg.* **1985**, *808*, 94–102.
- (817) Nuss, M. C.; Zinth, W.; Kaiser, W.; Koelling, E.; Oesterheld, D. Femtosecond Spectroscopy of the First Events of the Photochemical Cycle in Bacteriorhodopsin. *Chem. Phys. Lett.* **1985**, *117*, 1–7.
- (818) Polland, H. J.; Franz, M. A.; Zinth, W.; Kaiser, W.; Kölling, E.; Oesterheld, D. Early Picosecond Events in the Photocycle of Bacteriorhodopsin. *Biophys. J.* **1986**, *49*, 651–662.
- (819) Dobler, J.; Zinth, W.; Kaiser, W. Excited-State Reaction Dynamics of Bacteriorhodopsin Studied by Femtosecond Spectroscopy. *Chem. Phys. Lett.* **1988**, *144*, 215–220.
- (820) Warshel, A. Bicycle-Pedal Model for the First Step in the Vision Process. *Nature* **1976**, *260*, 679–683.
- (821) Mishra, A.; Behera, R. K.; Behera, P. K.; Mishra, B. K.; Behera, G. B. Cyanines During the 1990s: A Review. *Chem. Rev.* **2000**, *100*, 1973–2012.
- (822) Bagchi, B.; Fleming, G. R.; Oxtoby, D. W. Theory of Electronic Relaxation in Solution in the Absence of an Activation Barrier. *J. Chem. Phys.* **1983**, *78*, 7375–7385.
- (823) Velsko, S.; Waldeck, D.; Fleming, G. Breakdown of Kramer Theory Description of Photochemical Isomerization and the Possible Involvement of Frequency-Dependent Friction. *J. Chem. Phys.* **1983**, *78*, 249–258.
- (824) Sundström, V.; Gillbro, T. Viscosity Dependent Radiationless Relaxation Rate of Cyanine Dyes. A Picosecond Laser Spectroscopy Study. *Chem. Phys.* **1981**, *61*, 257–269.
- (825) Akesson, E.; Sundstrom, V.; Gillbro, T. Solvnt Dependent Barrier Heights of Excited-State Photoisomerization Reactions. *Chem. Phys. Lett.* **1985**, *121*, 513–522.
- (826) Akesson, E.; Bergstrom, H.; Sundstrom, V.; Gillbro, T. Photochemical Isomerization in the Absence of a Potential Barrier. *Chem. Phys. Lett.* **1986**, *126*, 385–393.
- (827) Yartsev, A.; Alvarez, J.; Aberg, U.; Sundstrom, V. Overdamped Wavepacket Motion Along a Barrierless Potential-Energy Surface in Excited-State Isomerization. *Chem. Phys. Lett.* **1995**, *243*, 281–289.
- (828) Vauthy, E. Isomerization Dynamics of a Thiacyanine Dye in Different Electronic States and in Different Classes of Solvents. *Chem. Phys.* **1995**, *196*, 569–582.
- (829) Bagchi, B.; Oxtoby, D. W.; Fleming, G. R. Theory of Electronic Relaxation in Solution in the Absence of an Activation Barrier. *J. Chem. Phys.* **1983**, *78*, 7375–7385.
- (830) Xu, Q.-H.; Fleming, G. R. Isomerization Dynamics of 1,1'-Diethyl-4,4'-Cyanine (1144C) Studied by Different Third-Order Nonlinear Spectroscopic Measurements. *J. Phys. Chem. A* **2001**, *105*, 10187–10195.
- (831) Sanchez-Galvez, A.; Hunt, P.; Robb, M. A.; Olivucci, M.; Vreven, T.; Schlegel, H. B. Ultrafast Radiationless Deactivation of Organic Dyes: Evidence for a Two-State Two-Mode Pathway in Polymethine Cyanines. *J. Am. Chem. Soc.* **2000**, *122*, 2911–2924.
- (832) Nuernberger, P.; Vogt, G.; Gerber, G.; Improta, R.; Santoro, F. Femtosecond Study on the Isomerization Dynamics of NK88. I. Ground-State Dynamics after Photoexcitation. *J. Chem. Phys.* **2006**, *125*, 044512.
- (833) Vogt, G.; Nuernberger, P.; Gerber, G.; Improta, R.; Santoro, F. Femtosecond Study on the Isomerization Dynamics of NK88. II. Excited-State Dynamics. *J. Chem. Phys.* **2006**, *125*, 044513.
- (834) Vogt, G.; Krampert, G.; Niklaus, P.; Nuernberger, P.; Gerber, G. Optimal Control of Photoisomerization. *Phys. Rev. Lett.* **2005**, *94*, 068305.
- (835) Dietzek, B.; Pascher, T.; Yartsev, A. Tracking Ultrafast Excited-State Bond-Twisting Motion in Solution Close to the Franck–Condon Point. *J. Phys. Chem. B* **2007**, *111*, 6034–6041.
- (836) Dietzek, B.; Brüggemann, B.; Pascher, T.; Yartsev, A. Mechanisms of Molecular Response in the Optimal Control of Photoisomerization. *Phys. Rev. Lett.* **2006**, *97*, 258301.
- (837) Dietzek, B.; Yartsev, A.; Tarnovsky, A. N. Watching Ultrafast Barrierless Excited-State Isomerization of Pseudocyanine in Real Time. *J. Phys. Chem. B* **2007**, *111*, 4520–4526.
- (838) Dietzek, B.; Tarnovsky, A. N.; Yartsev, A. Visualizing Overdamped Wavepacket Motion: Excited-State Isomerization of Pseudocyanine in Viscous Solvents. *Chem. Phys.* **2009**, *357*, 54–62.
- (839) Wei, Z.; Nakamura, T.; Takeuchi, S.; Tahara, T. Tracking of the Nuclear Wavepacket Motion in Cyanine Photoisomerization by Ultrafast Pump-Dump-Probe Spectroscopy. *J. Am. Chem. Soc.* **2011**, *133*, 8205–8210.
- (840) Weigel, A.; Pfaffe, M.; Sajadi, M.; Mahrwald, R.; Improta, R.; Barone, V.; Polli, D.; Cerullo, G.; Ernsting, N. P.; Santoro, F. Barrierless Photoisomerisation of the "Simplest Cyanine": Joining Computational and Femtosecond Optical Spectroscopies to Trace the Full Reaction Path. *Phys. Chem. Chem. Phys.* **2012**, *14*, 13350–13364.
- (841) Kahan, A.; Wand, A.; Ruhman, S.; Zilberg, S.; Haas, Y. Solvent Tuning of a Conical Intersection: Direct Experimental Verification of a Theoretical Prediction. *J. Phys. Chem. A* **2011**, *115*, 10854–10861.
- (842) Xu, X. F.; Kahan, A.; Zilberg, S.; Haas, Y. Photoreactivity of a Push–Pull Merocyanine in Static Electric Fields: A Three-State Model of Isomerization Reactions Involving Conical Intersections. *J. Phys. Chem. A* **2009**, *113*, 9779–9791.
- (843) Malhado, J. P.; Bearpark, M. J.; Hynes, J. T. Non-Adiabatic Dynamics Close to Conical Intersections and the Surface Hopping Perspective. *Front. Chem. (Lausanne, Switz.)* **2014**, *2*, 97–117.
- (844) Yonehara, T.; Hanasaki, K.; Takatsuka, K. Fundamental Approaches to Nonadiabaticity: Toward a Chemical Theory Beyond the Born–Oppenheimer Paradigm. *Chem. Rev.* **2012**, *112*, 499–542.
- (845) Bixon, M. Intramolecular Radiationless Transitions. *J. Chem. Phys.* **1968**, *48*, 715–726.
- (846) Freed, K. F. Multiphonon Processes in the Nonradiative Decay of Large Molecules. *J. Chem. Phys.* **1970**, *52*, 6272–6271.
- (847) Freed, K. F. Radiationless Transitions in Molecules. *Acc. Chem. Res.* **1978**, *11*, 74–80.
- (848) Levine, B. G.; Martínez, T. J. Isomerization through Conical Intersections. *Annu. Rev. Phys. Chem.* **2007**, *58*, 613–634.
- (849) Schoenlein, R. W.; Peteanu, L. A.; Mathies, R. A.; Shank, C. V. The First Step in Vision: Femtosecond Isomerization of Rhodopsin. *Science* **1991**, *254*, 412–415.
- (850) Sension, R.; Repinec, S.; Szarka, A.; Hochstrasser, R. Femtosecond Laser Studies of the *cis*-Stilbene Photoisomerization Reactions. *J. Chem. Phys.* **1993**, *98*, 6291–6315.
- (851) Qing, W.; Schoenlein, R. W.; Peteanu, L.; Mathies, R. A.; Shank, C. V. Vibrationally Coherent Photochemistry in the Femtosecond Primary Event of Vision. *Science* **1994**, *266*, 422–424.
- (852) Yarkony, D. R. Conical Intersections: Diabolical and Often Misunderstood. *Acc. Chem. Res.* **1998**, *31*, 511–518.
- (853) Robb, M. A.; Bernardi, F.; Olivucci, M. Conical Intersections as a Mechanistic Feature of Organic Photochemistry. *Pure Appl. Chem.* **1995**, *67*, 783–789.
- (854) Atchity, G. J.; Xantheas, S. S.; Ruedenberg, K. Potential Energy Surfaces near Intersections. *J. Chem. Phys.* **1991**, *95*, 1862–1876.
- (855) Yarkony, D. R. Nuclear Dynamics near Conical Intersections in the Adiabatic Representation: I. The Effects of Local Topography on Interstate Transitions. *J. Chem. Phys.* **2001**, *114*, 2601–2614.
- (856) Ben-Nun, M.; Molnar, F.; Schulten, K.; Martínez, T. J. The Role of Intersection Topography in Bond Selectivity of *cis*–*trans*



Photoisomerization. *Proc. Natl. Acad. Sci. U. S. A.* **2002**, *99*, 1769–1773.

(857) Malhado, J. P.; Hynes, J. T. Photoisomerization for a Model Protonated Schiff Base in Solution: Sloped/Peaked Conical Intersection Perspective. *J. Chem. Phys.* **2012**, *137*, 22A543.

(858) Blancafort, L. Photochemistry and Photophysics at Extended Seams of Conical Intersection. *ChemPhysChem* **2014**, *15*, 3166–3181.

(859) Malhado, J. P.; Spezia, R.; Hynes, J. T. Dynamical Friction Effects on the Photoisomerization of a Model Protonated Schiff Base in Solution. *J. Phys. Chem. A* **2011**, *115*, 3720–3735.

(860) Crespo-Hernandez, C. E.; Cohen, B.; Hare, P. M.; Kohler, B. Ultrafast Excited-State Dynamics in Nucleic Acids. *Chem. Rev.* **2004**, *104*, 1977–2019.

(861) Ippen, E. P.; Shank, C. V.; Woerner, R. L. Picosecond Dynamics of Azulene. *Chem. Phys. Lett.* **1977**, *46*, 20–23.

(862) Palmer, I. J.; Ragazos, I. N.; Bernardi, F.; Olivucci, M.; Robb, M. A. An MC-SCF Study of the  $S_1$  and  $S_2$  Photochemical Reactions of Benzene. *J. Am. Chem. Soc.* **1993**, *115*, 673–682.

(863) Kummer, A. D.; Kompa, C.; Niwa, H.; Hirano, T.; Kojima, S.; Michel-Beyerle, M. E. Viscosity-Dependent Fluorescence Decay of the GFP Chromophore in Solution Due to Fast Internal Conversion. *J. Phys. Chem. B* **2002**, *106*, 7554–7559.

(864) Litvinenko, K. L.; Webber, N. M.; Meech, S. R. Internal Conversion in the Chromophore of the Green Fluorescent Protein: Temperature Dependence and Isoviscosity Analysis. *J. Phys. Chem. A* **2003**, *107*, 2616–2623.

(865) van der Meer, M. J.; Zhang, H.; Glasbeek, M. Femtosecond Fluorescence Upconversion Studies of Barrierless Bond Twisting of Auramine in Solution. *J. Chem. Phys.* **2000**, *112*, 2878.

(866) Ippen, E. P.; Shank, C. V.; Bergman, A. Picosecond Recovery Dynamics of Malachite Green. *Chem. Phys. Lett.* **1976**, *38*, 611–614.

(867) Gottfried, N. H.; Roither, B.; Scherer, P. O. J. New Aspects of the Ultrafast Electronic Decay of Malachite Green in Solution. *Opt. Commun.* **1997**, *143*, 261–264.

(868) Nagasawa, Y.; Ando, Y.; Okada, T. Solvent Dependent Ultrafast Ground State Recovery Dynamics of Triphenylmethane Dyes. *J. Chin. Chem. Soc.* **2000**, *47*, 699–704.

(869) Nagasawa, Y.; Ando, Y.; Kataoka, D.; Matsuda, H.; Miyasaka, H.; Okada, T. Ultrafast Excited State Deactivation of Triphenylmethane Dyes. *J. Phys. Chem. A* **2002**, *106*, 2024–2035.

(870) Miyata, R.; Kimura, Y.; Terazima, M. Intermolecular Energy Transfer from the Photo-Excited Molecule to Solvent: Malachite Green. *Chem. Phys. Lett.* **2002**, *365*, 406–412.

(871) Bhasikuttan, A. C.; Sapre, A. V.; Okada, T. Ultrafast Relaxation Dynamics from the  $S_2$  State of Malachite Green Studied with Femtosecond Upconversion Spectroscopy. *J. Phys. Chem. A* **2003**, *107*, 3030–3035.

(872) Fita, P.; Punzi, A.; Vauthey, E. Local Viscosity of Binary Water + Glycerol Mixtures at Liquid/Liquid Interfaces Probed by Time-Resolved Surface Second Harmonic Generation. *J. Phys. Chem. C* **2009**, *113*, 20705–20712.

(873) Nakayama, A.; Taketsugu, T. Ultrafast Nonradiative Decay of Electronically Excited States of Malachite Green: Ab Initio Calculations. *J. Phys. Chem. A* **2011**, *115*, 8808–8815.

(874) Morgenthaler, M. J. E.; Meech, S. R. Picosecond Dynamics of Torsional Motion in Malachite Green Adsorbed on Silica. A Time-Resolved Surface Second Harmonic Generation Study. *Chem. Phys. Lett.* **1993**, *202*, 57–64.

(875) Shi, X.; Borguet, E.; Tarnovsky, A. N.; Eienthal, K. B. Ultrafast Dynamics and Structure at Aqueous Interfaces by Second Harmonic Generation. *Chem. Phys.* **1996**, *205*, 167–178.

(876) Sen, P.; Yamaguchi, S.; Tahara, T. Ultrafast Dynamics of Malachite Green at the Air-Water Interface Studied by Femtosecond Time-Resolved Electronic Sum Frequency Generation (TR-ESFG): An Indicator for Local Viscosity. *Faraday Discuss.* **2010**, *145*, 411–428.

(877) Gumy, J.-C.; Vauthey, E. Investigation of the Excited State Dynamics of Radical Ions in the Condensed Phase Using the Picosecond Transient Grating Technique. *J. Phys. Chem. A* **1997**, *101*, 8575–8580.

(878) Brodard, P.; Sarbach, A.; Gumy, J.-C.; Bally, T.; Vauthey, E. Excited State Dynamics of Organic Radical Ions in Liquids and in Low-Temperature Matrices. *J. Phys. Chem. A* **2001**, *105*, 6594–6601.

(879) Zhao, L.; Lian, R.; Shkrob, I. A.; Crowell, R. A.; Pommeret, S.; Chronister, E. L.; Liu, A. D.; Trifunac, A. D. Ultrafast Studies on the Photophysics of Matrix-Isolated Radical Cations of Polycyclic Aromatic Hydrocarbons. *J. Phys. Chem. A* **2004**, *108*, 25–31.

(880) Hall, K. F.; Boggio-Pasqua, M.; Bearpark, M. J.; Robb, M. A. Photostability Via Sloped Conical Intersections: A Computational Study of the Excited States of the Naphthalene Radical Cation. *J. Phys. Chem. A* **2006**, *110*, 13591–13599.

(881) Tokmachev, A. M.; Boggio-Pasqua, M.; Bearpark, M. J.; Robb, M. A. Photostability via Sloped Conical Intersections: A Computational Study of the Pyrene Radical Cation. *J. Phys. Chem. A* **2008**, *112*, 10881–10886.

(882) Tokmachev, A. M.; Boggio-Pasqua, M.; Mendive-Tapia, D.; Bearpark, M. J.; Robb, M. A. Fluorescence of the Perylene Radical Cation and an Inaccessible  $D_0/D_1$  Conical Intersection: An MMVB, RASSCF, and TD-DFT Computational Study. *J. Chem. Phys.* **2010**, *132*, 044306.

(883) Häupl, T.; Lomoth, R.; Hammarström, L. Femtosecond Dynamics of the Photoexcited Methyl Viologen Radical Cation. *J. Phys. Chem. A* **2003**, *107*, 435–438.

(884) Hope, M. J.; Higglet, M. P.; Andrews, D. L.; Meech, S. R.; Hands, I. D.; Dunn, J. L.; Bates, C. A. Observation of Ultrafast Internal Conversion in Fullerene Anions in Solution. *Chem. Phys. Lett.* **2009**, *474*, 112–114.

(885) Grilj, J.; Todorova, T. K.; Yi, C.; Liu, S.-X.; Vauthey, E.; Decurtins, S. A Spectroscopic and Computational Study of a Photoinduced Cross-Dehydrogenative Coupling Reaction of a Stable Semiquinone Radical. *Chem. - Eur. J.* **2012**, *18*, 13605–13608.

(886) Tamai, N.; Miyasaka, H. Ultrafast Dynamics of Photochromic Systems. *Chem. Rev.* **2000**, *100*, 1875–1890.

(887) Deb, S.; Weber, P. M. The Ultrafast Pathway of Photon-Induced Electrocyclic Ring-Opening Reactions: The Case of 1,3-Cyclohexadiene. *Annu. Rev. Phys. Chem.* **2011**, *62*, 19–39.

(888) Arruda, B. C.; Sension, R. J. Ultrafast Polyene Dynamics: The Ring Opening of 1,3-Cyclohexadiene Derivatives. *Phys. Chem. Chem. Phys.* **2014**, *16*, 4439–4455.

(889) Irie, M. Diarylethenes for Memories and Switches. *Chem. Rev.* **2000**, *100*, 1685–1716.

(890) Irie, M.; Fukaminato, T.; Matsuda, K.; Kobatake, S. Photochromism of Diarylethene Molecules and Crystals: Memories, Switches, and Actuators. *Chem. Rev.* **2014**, *114*, 12174–12277.

(891) Dürr, H.; Bouas-Laurent, H. *Photochromism: Molecules and Systems*; Elsevier: Amsterdam, 2003.

(892) Woodward, R. B.; Hoffmann, R. The Conservation of Orbital Symmetry. *Angew. Chem., Int. Ed. Engl.* **1969**, *8*, 781–853.

(893) Miyasaka, H.; Araki, S.; Tabata, A.; Nobuto, T.; Malaga, N.; Irie, M. Picosecond Laser Photolysis Studies on Photochromic Reactions of 1,2-Bis(2,4,5-Trimethyl-3-Thienyl)Maleic Anhydride in Solutions. *Chem. Phys. Lett.* **1994**, *230*, 249–254.

(894) Tamai, N.; Saika, T.; Shimidzu, T.; Irie, M. Femtosecond Dynamics of a Thiophene Oligomer with a Photoswitch by Transient Absorption Spectroscopy. *J. Phys. Chem.* **1996**, *100*, 4689–4692.

(895) Miyasaka, H.; Nobuto, T.; Itaya, A.; Tamai, N.; Irie, M. Picosecond Laser Photolysis Studies on a Photochromic Dithienylethene in Solution and in Crystalline Phases. *Chem. Phys. Lett.* **1997**, *269*, 281–285.

(896) Ern, J.; Bens, A. T.; Bock, A.; Martin, H. D.; Kryschi, C. Femtosecond Transient Absorption Studies on Photochromism of Dithienylethene Derivates. *J. Lumin.* **1998**, *76–77*, 90–94.

(897) Ern, J.; Bens, A. T.; Martin, H. D.; Mukamel, S.; Schmid, D.; Tretiak, S.; Tsiper, E.; Kryschi, C. Reaction Dynamics of Photochromic Dithienylethene Derivatives. *Chem. Phys.* **1999**, *246*, 115–125.

(898) Ern, J.; Bens, A.; Martin, H. D.; Mukamel, S.; Schmid, D.; Tretiak, S.; Tsiper, E.; Kryschi, C. Femtosecond Reaction Dynamics of

- a Photochromic Dithienylethene Derivative. *J. Lumin.* **2000**, 87–89, 742–744.
- (899) Ern, J.; Bens, A. T.; Martin, H. D.; Mukamel, S.; Tretiak, S.; Tsyganenko, K.; Kuldova, K.; Trommsdorff, H. P.; Kryschi, C. Reaction Dynamics of a Photochromic Fluorescing Dithienylethene. *J. Phys. Chem. A* **2001**, 105, 1741–1749.
- (900) Miyasaka, H.; Murakami, M.; Itaya, A.; Guillaumont, D.; Nakamura, S.; Irie, M. Multiphoton Gated Photochromic Reaction in a Diarylethene Derivative. *J. Am. Chem. Soc.* **2001**, 123, 753–754.
- (901) Bertarelli, C.; Gallazzi, M. C.; Stellacci, F.; Zerbi, G.; Stagira, S.; Nisoli, M.; De Silvestri, S. Ultrafast Photoinduced Ring-Closure Dynamics of a Diarylethene Polymer. *Chem. Phys. Lett.* **2002**, 359, 278–282.
- (902) Ern, J.; Bens, A. T.; Martin, H.-D.; Kuldova, K.; Trommsdorff, H. P.; Kryschi, C. Ring-Opening and -Closure Reaction Dynamics of a Photochromic Dithienylethene Derivative. *J. Phys. Chem. A* **2002**, 106, 1654–1660.
- (903) Hania, P. R.; Telesca, R.; Lucas, L. N.; Pugzlys, A.; Van Esch, J.; Feringa, B. L.; Snijders, J. G.; Duppen, K. An Optical and Theoretical Investigation of the Ultrafast Dynamics of a Bisthiénylene-Based Photochromic Switch. *J. Phys. Chem. A* **2002**, 106, 8498–8507.
- (904) Miyasaka, H.; Nobuto, T.; Murakami, M.; Itaya, A.; Tamai, N.; Irie, M. Solvent Viscosity Effects on Photochromic Reactions of a Diarylethene Derivative as Revealed by Picosecond Laser Spectroscopy. *J. Phys. Chem. A* **2002**, 106, 8096–8102.
- (905) Okabe, C.; Tanaka, N.; Fukaminato, T.; Kawai, T.; Irie, M.; Nibu, Y.; Shimada, H.; Goldberg, A.; Nakamura, S.; Sekiya, H. Raman Spectroscopic Study on Photochromic Reaction of a Diarylethene Derivative. *Chem. Phys. Lett.* **2002**, 357, 113–118.
- (906) Miyasaka, H.; Murakami, M.; Okada, T.; Nagata, Y.; Itaya, A.; Kobatake, S.; Irie, M. Picosecond and Femtosecond Laser Photolysis Studies of a Photochromic Diarylethene Derivative: Multiphoton Gated Reaction. *Chem. Phys. Lett.* **2003**, 371, 40–48.
- (907) Okabe, C.; Nakabayashi, T.; Nishi, N.; Fukaminato, T.; Kawai, T.; Irie, M.; Sekiya, H. Picosecond Time-Resolved Stokes and Anti-Stokes Raman Studies on the Photochromic Reactions of Diarylethene Derivatives. *J. Phys. Chem. A* **2003**, 107, 5384–5390.
- (908) Shim, S.; Joo, T.; Bae, S. C.; Kim, K. S.; Kim, E. Ring Opening Dynamics of a Photochromic Diarylethene Derivative in Solution. *J. Phys. Chem. A* **2003**, 107, 8106–8110.
- (909) Murakami, M.; Miyasaka, H.; Okada, T.; Kobatake, S.; Irie, M. Dynamics and Mechanisms of the Multiphoton Gated Photochromic Reaction of Diarylethene Derivatives. *J. Am. Chem. Soc.* **2004**, 126, 14764–14772.
- (910) Hania, P. R.; Pugzlys, A.; Lucas, L. N.; de Jong, J. J. D.; Feringa, B. L.; van Esch, J. H.; Jonkman, H. T.; Duppen, K. Ring Closure Dynamics of Bte-Based Photochromic Switches: Perfluoro- Versus Perhydrocyclopentene Derivatives. *J. Phys. Chem. A* **2005**, 109, 9437–9442.
- (911) Shim, S.; Eom, I.; Joo, T.; Kim, E.; Kim, K. S. Ring Closure Reaction Dynamics of Diarylethene Derivatives in Solution. *J. Phys. Chem. A* **2007**, 111, 8910–8917.
- (912) Elsner, C.; Cordes, T.; Dietrich, P.; Zastrow, M.; Herzog, T. T.; Ruck-Braun, K.; Zinth, W. Photochromic Bis(Thiophen-3-Yl)Maleimides Studied with Time-Resolved Spectroscopy. *J. Phys. Chem. A* **2009**, 113, 1033–1039.
- (913) Ishibashi, Y.; Mukaida, M.; Falkenström, M.; Miyasaka, H.; Kobatake, S.; Irie, M. One- and Multi-Photon Cycloreversion Reaction Dynamics of Diarylethene Derivative with Asymmetrical Structure, as Revealed by Ultrafast Laser Spectroscopy. *Phys. Chem. Chem. Phys.* **2009**, 11, 2640–2648.
- (914) Aloise, S.; Sliwa, M.; Pawlowska, Z.; Réhault, J.; Dubois, J.; Poizat, O.; Buntinx, G.; Perrier, A.; Maurel, F.; Yamaguchi, S.; et al. Bridged Photochromic Diarylethenes Investigated by Ultrafast Absorption Spectroscopy: Evidence for Two Distinct Photocyclization Pathways. *J. Am. Chem. Soc.* **2010**, 132, 7379–7390.
- (915) Ishibashi, Y.; Fujiwara, M.; Umesato, T.; Saito, H.; Kobatake, S.; Irie, M.; Miyasaka, H. Cyclization Reaction Dynamics of a Photochromic Diarylethene Derivative as Revealed by Femtosecond to Microsecond Time-Resolved Spectroscopy. *J. Phys. Chem. C* **2011**, 115, 4265–4272.
- (916) Ishibashi, Y.; Umesato, T.; Kobatake, S.; Irie, M.; Miyasaka, H. Femtosecond Laser Photolysis Studies on Temperature Dependence of Cyclization and Cycloreversion Reactions of a Photochromic Diarylethene Derivative. *J. Phys. Chem. C* **2012**, 116, 4862–4869.
- (917) Ward, C. L.; Elles, C. G. Controlling the Excited-State Reaction Dynamics of a Photochromic Molecular Switch with Sequential Two-Photon Excitation. *J. Phys. Chem. Lett.* **2012**, 3, 2995–3000.
- (918) Molloy, M. S.; Snyder, J. A.; Bragg, A. E. Structural and Solvent Control of Nonadiabatic Photochemical Bond Formation: Photocyclization of o-Terphenyl in Solution. *J. Phys. Chem. A* **2014**, 118, 3913–3925.
- (919) Pontecorvo, E.; Ferrante, C.; Elles, C. G.; Scopigno, T. Structural Rearrangement Accompanying the Ultrafast Electrocyclization Reaction of a Photochromic Molecular Switch. *J. Phys. Chem. B* **2014**, 118, 6915–6921.
- (920) Ward, C. L.; Elles, C. G. Cycloreversion Dynamics of a Photochromic Molecular Switch via One-Photon and Sequential Two-Photon Excitation. *J. Phys. Chem. A* **2014**, 118, 10011–10019.
- (921) Buckup, T.; Sarter, C.; Volpp, H.-R.; Jäschke, A.; Motzkus, M. Ultrafast Time-Resolved Spectroscopy of Diarylethene-Based Photo-switchable Deoxyuridine Nucleosides. *J. Phys. Chem. Lett.* **2015**, 6, 4717–4721.
- (922) Valley, D. T.; Hoffman, D. P.; Mathies, R. A. Reactive and Unreactive Pathways in a Photochemical Ring Opening Reaction from 2d Femtosecond Stimulated Raman. *Phys. Chem. Chem. Phys.* **2015**, 17, 9231–9240.
- (923) Ishibashi, Y.; Umesato, T.; Fujiwara, M.; Une, K.; Yoneda, Y.; Sotome, H.; Katayama, T.; Kobatake, S.; Asahi, T.; Irie, M.; et al. Solvent Polarity Dependence of Photochromic Reactions of a Diarylethene Derivative as Revealed by Steady-State and Transient Spectroscopies. *J. Phys. Chem. C* **2016**, 120, 1170–1177.
- (924) Wang, Y.; Yan, Y.; Liu, D.; Liu, S.; Wang, G.; Pu, S. Different Ultrafast Dynamics of Several Dithienylethene Photochromism Derivatives: Under Parallel and Perpendicular Polarization Configurations. *Optik (Munich, Ger.)* **2016**, 127, 5285–5288.
- (925) Ishibashi, Y.; Tani, K.; Miyasaka, H.; Kobatake, S.; Irie, M. Picosecond Laser Photolysis Study of Cycloreversion Reaction of a Diarylethene Derivative in Polycrystals: Multiphoton-Gated Reaction. *Chem. Phys. Lett.* **2007**, 437, 243–247.
- (926) Tani, K.; Ishibashi, Y.; Miyasaka, H.; Kobatake, S.; Irie, M. Dynamics of Cyclization, Cycloreversion, and Multiphoton-Gated Reaction of a Photochromic Diarylethene Derivative in Crystalline Phase. *J. Phys. Chem. C* **2008**, 112, 11150–11157.
- (927) Jean-Ruel, H.; Cooney, R. R.; Gao, M.; Lu, C.; Kochman, M. A.; Morrison, C. A.; Miller, R. J. D. Femtosecond Dynamics of the Ring Closing Process of Diarylethene: A Case Study of Electrocyclic Reactions in Photochromic Single Crystals. *J. Phys. Chem. A* **2011**, 115, 13158–13168.
- (928) Jean-Ruel, H.; Gao, M.; Kochman, M. A.; Lu, C.; Liu, L. C.; Cooney, R. R.; Morrison, C. A.; Miller, R. J. D. Ring-Closing Reaction in Diarylethene Captured by Femtosecond Electron Crystallography. *J. Phys. Chem. B* **2013**, 117, 15894–15902.
- (929) Miller, R. J. D. Femtosecond Crystallography with Ultrabright Electrons and X-Rays: Capturing Chemistry in Action. *Science* **2014**, 343, 1108–1116.
- (930) Chernyak, V.; Mukamel, S. Size-Consistent Quasiparticle Representation of Nonlinear Optical Susceptibilities in Many-Electron Systems. *J. Chem. Phys.* **1996**, 104, 444–459.
- (931) Mukamel, S.; Tretiak, S.; Wagersreiter, T.; Chernyak, V. Electronic Coherence and Collective Optical Excitations of Conjugated Molecules. *Science* **1997**, 277, 781–787.
- (932) Ishibashi, Y.; Katayama, T.; Ota, C.; Kobatake, S.; Irie, M.; Yokoyama, Y.; Miyasaka, H. Ultrafast Laser Spectroscopic Study on Photochromic Cycloreversion Dynamics in Fulgide Derivatives: One-



Photon and Multiphoton-Gated Reactions. *New J. Chem.* **2009**, *33*, 1409–1419.

(933) Ishibashi, Y.; Okuno, K.; Ota, C.; Umesato, T.; Katayama, T.; Murakami, M.; Kobatake, S.; Irie, M.; Miyasaka, H. Multiphoton-Gated Cycloreversion Reactions of Photochromic Diarylethene Derivatives with Low Reaction Yields Upon One-Photon Visible Excitation. *Photochem. Photobiol. Sci.* **2010**, *9*, 172–180.

(934) Smith, M. C.; Snyder, J. A.; Streifel, B. C.; Bragg, A. E. Ultrafast Excited-State Dynamics of Ortho-Terphenyl and 1,2-Diphenylcyclohexene: The Role of “Ethylene Twisting” in the Nonadiabatic Photocyclization of Stilbene Analogs. *J. Phys. Chem. Lett.* **2013**, *4*, 1895–1900.

(935) Yokoyama, Y. Fulgides for Memories and Switches. *Chem. Rev.* **2000**, *100*, 1717–1740.

(936) Liang, Y. C.; Dvornikov, A. S.; Rentzepis, P. M. Nonvolatile Read-out Molecular Memory. *Proc. Natl. Acad. Sci. U. S. A.* **2003**, *100*, 8109–8112.

(937) Malkmus, S.; Koller, F. O.; Draxler, S.; Schrader, T. E.; Schreier, W. J.; Brust, T.; DiGirolamo, J. A.; Lees, W. J.; Zinth, W.; Braun, M. All-Optical Operation Cycle on Molecular Bits with 250-GHz Clock-Rate Based on Photochromic Fulgides. *Adv. Funct. Mater.* **2007**, *17*, 3657–3662.

(938) Willner, I.; Rubin, S. Control of the Structure and Functions of Biomaterials by Light. *Angew. Chem., Int. Ed. Engl.* **1996**, *35*, 367–385.

(939) Willner, I.; Willner, B. Photochemical Biomolecular Switches: The Route to Optobioelectronics. In *Molecular Switches*; Feringa, B. L., Ed.; Wiley-VCH Verlag GmbH: Berlin, 2001; pp 165–218.

(940) Raymo, F. M.; Tomasulo, M. Electron and Energy Transfer Modulation with Photochromic Switches. *Chem. Soc. Rev.* **2005**, *34*, 327–336.

(941) Renth, F.; Siewertsen, R.; Temps, F. Enhanced Photoswitching and Ultrafast Dynamics in Structurally Modified Photochromic Fulgides. *Int. Rev. Phys. Chem.* **2013**, *32*, 1–38.

(942) Heinz, B.; Malkmus, S.; Laimgruber, S.; Dietrich, S.; Schulz, C.; Rück-Braun, K.; Braun, M.; Zinth, W.; Gilch, P. Comparing a Photoinduced Pericyclic Ring Opening and Closure: Differences in the Excited State Pathways. *J. Am. Chem. Soc.* **2007**, *129*, 8577–8584.

(943) Koller, F. O.; Schreier, W. J.; Schrader, T. E.; Malkmus, S.; Schulz, C.; Dietrich, S.; Rueck-Braun, K.; Braun, M. Ultrafast Ring-Closure Reaction of Photochromic Indolylfulgimides Studied with UV-Pump-IR-Probe Spectroscopy. *J. Phys. Chem. A* **2008**, *112*, 210–214.

(944) Draxler, S.; Brust, T.; Malkmus, S.; Koller, F. O.; Heinz, B.; Laimgruber, S.; Schulz, C.; Dietrich, S.; Rueck-Braun, K.; Zinth, W.; et al. Ultrafast Reaction Dynamics of the Complete Photo Cycle of an Indolylfulgimide Studied by Absorption, Fluorescence and Vibrational Spectroscopy. *J. Mol. Liq.* **2008**, *141*, 130–136.

(945) Cordes, T.; Herzog, T. T.; Malkmus, S.; Draxler, S.; Brust, T.; DiGirolamo, J. A.; Lees, W. J.; Braun, M. Wavelength and Solvent Independent Photochemistry: The Electrocyclic Ring-Closure of Indolylfulgides. *Photochem. Photobiol. Sci.* **2009**, *8*, 528–534.

(946) Nenov, A.; Schreier, W. J.; Koller, F. O.; Braun, M.; de Vivie-Riedle, R.; Zinth, W.; Pugliesi, I. Molecular Model of the Ring-Opening and Ring-Closure Reaction of a Fluorinated Indolylfulgide. *J. Phys. Chem. A* **2012**, *116*, 10518–10528.

(947) Slavov, C.; Bellakbil, N.; Wahl, J.; Mayer, K.; Rück-Braun, K.; Burghardt, I.; Wachtveitl, J.; Braun, M. Ultrafast Coherent Oscillations Reveal a Reactive Mode in the Ring-Opening Reaction of Fulgides. *Phys. Chem. Chem. Phys.* **2015**, *17*, 14045–14053.

(948) Slavov, C.; Boumrifak, C.; Hammer, C. A.; Trojanowski, P.; Chen, X.; Lees, W. J.; Wachtveitl, J.; Braun, M. The Ultrafast Reactions in the Photochromic Cycle of Water-Soluble Fulgimide Photoswitches. *Phys. Chem. Chem. Phys.* **2016**, *18*, 10289–10296.

(949) Siewertsen, R.; Renth, F.; Temps, F.; Sönnichsen, F. Parallel Ultrafast E-C Ring Closure and E-Z Isomerisation in a Photochromic Furfylfulgide Studied by Femtosecond Time-Resolved Spectroscopy. *Phys. Chem. Chem. Phys.* **2009**, *11*, 5952–5961.

(950) Siewertsen, R.; Strübe, F.; Mattay, J.; Renth, F.; Temps, F. Tuning of Switching Properties and Excited-State Dynamics of

Fulgides by Structural Modifications. *Phys. Chem. Chem. Phys.* **2011**, *13*, 3800–3808.

(951) Malkmus, S.; Koller, F. O.; Heinz, B.; Schreier, W. J.; Schrader, T. E.; Zinth, W.; Schulz, C.; Dietrich, S.; Rueck-Braun, K.; Braun, M. Ultrafast Ring Opening Reaction of a Photochromic Indolylfulgimide. *Chem. Phys. Lett.* **2006**, *417*, 266–271.

(952) Koller, F. O.; Schreier, W. J.; Schrader, T. E.; Sieg, A.; Malkmus, S.; Schulz, C.; Dietrich, S.; Rueck-Braun, K.; Zinth, W.; Braun, M. Ultrafast Structural Dynamics of Photochromic Indolylfulgimides Studied by Vibrational Spectroscopy and DFT Calculations. *J. Phys. Chem. A* **2006**, *110*, 12769–12776.

(953) Brust, T.; Draxler, S.; Malkmus, S.; Schulz, C.; Zastrow, M.; Rück-Braun, K.; Zinth, W.; Braun, M. Ultrafast Dynamics and Temperature Effects on the Quantum Efficiency of the Ring-Opening Reaction of a Photochromic Indolylfulgide. *J. Mol. Liq.* **2008**, *141*, 137–139.

(954) Brust, T.; Malkmus, S.; Draxler, S.; Ahmed, S. A.; Rück-Braun, K.; Zinth, W.; Braun, M. Photochemistry with Thermal Versus Optical Excess Energy: Ultrafast Cycloreversion of Indolylfulgides and Indolylfulgimides. *J. Photochem. Photobiol., A* **2009**, *207*, 209–216.

(955) Cordes, T.; Malkmus, S.; DiGirolamo, J. A.; Lees, W. J.; Nenov, A.; Vivie-Riedle, R. d.; Braun, M.; Zinth, W. Accelerated and Efficient Photochemistry from Higher Excited Electronic States in Fulgide Molecules. *J. Phys. Chem. A* **2008**, *112*, 13364–13371.

(956) Ishibashi, Y.; Murakami, M.; Miyasaka, H.; Kobatake, S.; Irie, M.; Yokoyama, Y. Laser Multiphoton-Gated Photochromic Reaction of a Fulgide Derivative. *J. Phys. Chem. C* **2007**, *111*, 2730–2737.

(957) Siewertsen, R.; Strübe, F.; Mattay, J.; Renth, F.; Temps, F. Electronic and Steric Effects on the Photo-Induced C–E Ring-Opening of Structurally Modified Furfylfulgides. *Phys. Chem. Chem. Phys.* **2011**, *13*, 15699–15707.

(958) Draxler, S.; Brust, T.; Malkmus, S.; DiGirolamo, J. A.; Lees, W. J.; Zinth, W.; Braun, M. Ring-Opening Reaction of a Trifluorinated Indolylfulgide: Mode-Specific Photochemistry after Pre-Excitation. *Phys. Chem. Chem. Phys.* **2009**, *11*, 5019–5027.

(959) Uhlmann, E.; Gauglitz, G. New Aspects in the Photokinetics of Aberchrome 540. *J. Photochem. Photobiol., A* **1996**, *98*, 45–49.

(960) Renth, F.; Foca, M.; Petter, A.; Temps, F. Ultrafast Transient Absorption Spectroscopy of the Photo-Induced Z–E Isomerization of a Photochromic Furfylfulgide. *Chem. Phys. Lett.* **2006**, *428*, 62–67.

(961) Minkin, V. I. Photo-, Thermo-, Solvato-, and Electrochromic Spiroheterocyclic Compounds. *Chem. Rev.* **2004**, *104*, 2751–2776.

(962) Feringa, B. L.; Browne, W. R. *Molecular Switches*; Wiley-VCH Verlag GmbH & Co. KGaA: Berlin, 2011.

(963) Berkovic, G.; Krongauz, V.; Weiss, V. Spiropyran and Spirooxazines for Memories and Switches. *Chem. Rev.* **2000**, *100*, 1741–1754.

(964) Saragi, T. P. I.; Spehr, T.; Siebert, A.; Fuhrmann-Lieker, T.; Salbeck, J. Spiro Compounds for Organic Optoelectronics. *Chem. Rev.* **2007**, *107*, 1011–1065.

(965) Szymanski, W.; Beierle, J. M.; Kistemaker, H. A.; Velema, W. A.; Feringa, B. L. Reversible Photocontrol of Biological Systems by the Incorporation of Molecular Photoswitches. *Chem. Rev.* **2013**, *113*, 6114–6178.

(966) Rini, M.; Holm, A.-K.; Nibbering, E. T. J.; Fidler, H. Ultrafast UV-Mid-IR Investigation of the Ring Opening Reaction of a Photochromic Spiropyran. *J. Am. Chem. Soc.* **2003**, *125*, 3028–3034.

(967) Holm, A.-K.; Rini, M.; Nibbering, E. T. J.; Fidler, H. Femtosecond UV/Mid-IR Study of Photochromism of the Spiropyran 1',3'-Dihydro-1',3',3'-Trimethyl-6-Nitrospiro[2h-1-Benzopyran-2,2'-(2h)-Indole] in Solution. *Chem. Phys. Lett.* **2003**, *376*, 214–219.

(968) Holm, A.-K.; Mohammed, O. F.; Rini, M.; Mukhtar, E.; Nibbering, E. T. J.; Fidler, H. Sequential Merocyanine Product Isomerization Following Femtosecond UV Excitation of a Spiropyran. *J. Phys. Chem. A* **2005**, *109*, 8962–8968.

(969) Fidler, H.; Rini, M.; Nibbering, E. T. J. The Role of Large Conformational Changes in Efficient Ultrafast Internal Conversion: Deviations from the Energy Gap Law. *J. Am. Chem. Soc.* **2004**, *126*, 3789–3794.



(970) Ernsting, N. P.; Arthen-Engeland, T. Photochemical Ring-Opening Reaction of Indolinespiroopyrans Studied by Subpicosecond Transient Absorption. *J. Phys. Chem.* **1991**, *95*, 5502–5509.

(971) Buback, J.; Kullmann, M.; Langhojer, F.; Nuernberger, P.; Schmidt, R.; Würthner, F.; Brixner, T. Ultrafast Bidirectional Photoswitching of a Spiropyran. *J. Am. Chem. Soc.* **2010**, *132*, 16510–16519.

(972) Buback, J.; Nuernberger, P.; Kullmann, M.; Langhojer, F.; Schmidt, R.; Würthner, F.; Brixner, T. Ring-Closure and Isomerization Capabilities of Spiropyran-Derived Merocyanine Isomers. *J. Phys. Chem. A* **2011**, *115*, 3924–3935.

(973) Hobley, J.; Pfeifer-Fukumura, U.; Bletz, M.; Asahi, T.; Masuhara, H.; Fukumura, H. Ultrafast Photo-Dynamics of a Reversible Photochromic Spiropyran. *J. Phys. Chem. A* **2002**, *106*, 2265–2270.

(974) Kohl-Landgraf, J.; Braun, M.; Özçoban, C.; Gonçalves, D. P. N.; Heckel, A.; Wachtveitl, J. Ultrafast Dynamics of a Spiropyran in Water. *J. Am. Chem. Soc.* **2012**, *134*, 14070–14077.

(975) di Nunzio, M. R.; Danilov, E. O.; Rodgers, M. A. J.; Favaro, G. Ultrafast Excited-State Dynamics in Some Spirooxazines and Chromenes. Evidence for a Dual Relaxation Pathway. *Photochem. Photobiol. Sci.* **2010**, *9*, 1391–1391.

(976) Kumar, R. S. S.; Luer, L.; Polli, D.; Garbugli, M.; Lanzani, G. Primary Photoevents in a Metastable Photomerocyanine of Spirooxazines. *Opt. Mater. Express* **2011**, *1*, 293–304.

(977) Herzog, T. T.; Ryseck, G.; Ploetz, E.; Cordes, T. The Photochemical Ring Opening Reaction of Chromene as Seen by Transient Absorption and Fluorescence Spectroscopy. *Photochem. Photobiol. Sci.* **2013**, *12*, 1202–1209.

(978) Aubard, J.; Maurel, F.; Buntinx, G.; Poizat, O.; Levi, G.; Guglielmetti, R.; Samat, A. Femto/Picosecond Transient Absorption Spectroscopy of Photochromic 3,3-Diphenylnaphtho[2,1-B]Pyran. *Mol. Cryst. Liq. Cryst. Sci. Technol., Sect. A* **2000**, *345*, 215–220.

(979) Gentili, P. L.; Danilov, E.; Ortica, F.; Rodgers, M. A. J.; Favaro, G. Dynamics of the Excited States of Chromenes Studied by Fast and Ultrafast Spectroscopies. *Photochem. Photobiol. Sci.* **2004**, *3*, 886–891.

(980) Moine, B.; Buntinx, G.; Poizat, O.; Rehault, J.; Moustrou, C.; Samat, A. Transient Absorption Investigation of the Photophysical Properties of New Photochromic 3h-Naphtho[2,1-B]Pyran. *J. Phys. Org. Chem.* **2007**, *20*, 936–943.

(981) Moine, B.; Réhault, J.; Aloïse, S.; Micheau, J.-C.; Moustrou, C.; Samat, A.; Poizat, O.; Buntinx, G. Transient Absorption Studies of the Photochromic Behavior of 3h-Naphtho[2,1-B]Pyrans Linked to Thiophene Oligomers via an Acetylenic Junction. *J. Phys. Chem. A* **2008**, *112*, 4719–4726.